Minimisation Techniques of Multiple Antennas in Mobile Phones and Effect of the Capacity of Multielement Antenna System

Thaysen, Jesper

Publication date:
2005

Document Version
Publisher's PDF, also known as Version of record

Minimisation techniques of multiple antennas in mobile phones and effect of the capacity on multielement antenna system

Jesper Thaysen

April 2005

The present work was carried out at Ørsted•DTU in partial fulfillment of the requirements for the Ph.D. degree from Technical University of Denmark.

Supervisor:	Associate Professor Kaj B. Jakobsen, Ph. D.
Co-supervisors:	Jens Troelsen, Nokia Denmark, M. Sc. Hans-Erik Gram, Nokia Denmark, M. Sc.
ISBN:	87-911-84-51-7

Preface

This thesis is submitted in partial fulfillment of the Ph.D degree from the Section of Electromagnetic, Ørsted•DTU at Technical University of Denmark. The work was performed from May 2001 to July 2002, and from August 2003 to April 2005 partly at the Section of electromagnetic, Ørsted•DTU and partly at the Antenna Group at Nokia Denmark.

Throughout this Ph.D. study Associate Professor Kaj B. Jakobsen from Technical University of Denmark has been the supervisor. Hans Erik Gram and Jens Troelsen have been appointed as co-supervisors from Nokia Denmark A/S.

This work was fully founded by Nokia Denmark A/S. Thanks to Thomas Olsgaard, Aleksis Anterow, and Ole Feddersen all from Nokia Denmark A/S for initiating and supporting this project.

Special thanks go to my supervisor Associate Professor Kaj B. Jakobsen from Technical University of Denmark, especially for always taking your time for me. Also, for your openness for contact to the research life outside the university walls.

Also, I would like to express my sincere gratitude to my family, friends and colleagues without whom this thesis would never have been completed.

Finally this project would never have been realized without the ever support and patience from Emma and Mette.

Ringsted, April 2005.

Jesper Thaysen

Abstract

With the recent progress and rapid size decrease of mobile phones, the design of antennas for small mobile phones is acquiring great importance. In view of this situation, the design concept of antenna systems for small mobile phones are discussed, referring to the trends in modern mobile communications and the demands for future antenna systems such as Multiple-Input Multi-output (MIMO) systems.

MIMO systems use multiple antenna elements at both the transmitter and receiver to improve the capacity over single antenna topologies in multipath environment. In such systems, the antenna properties as well as the multipath channel characteristics play key roles in determining communication performance. Despite the overwhelming amount of papers published in the area of MIMO systems during the past years, the mechanisms for successful implementation of multiple antennas in a mobile phone are largely unstudied, and how their performance can be optimised is not fully explored. Therefore, there is a need for new methods from which the antenna designer can evaluate the MIMO performance of mobile phone antennas and use the results to determine how they are performing. Issues considered include channel capacity, capacity versus signal to noise ratio, and capacity for MIMO systems with unequal numbers of antennas in link ends, and the impact of antenna element properties on the MIMO system performance.

A simple closed formed equation to calculate the envelope correlation between any two antennas in a MIMO system of an arbitrary number of antenna elements is derived. The equation uses the scattering parameters obtained at the antenna feed point to calculate the envelope correlation coefficient. This approach has the advantage that it does not require knowledge of the antenna radiation pattern. Numerical data are shown to validate the approach. It is found that choosing configurations that maximise the distances between the open ends of the Planar Inverted-F Antennas (PIFAs) yields the lowest mutual coupling as well as the lowest envelope correlations.

When a small antenna is attached to a small metal object, like the metal chassis of a mobile phone, the size and shape of the object and the position of the antenna on it can have a strong effect on the antenna performance. It is shown that the optimal location of a camera or a loudspeaker could be determined directly from the raw unprocessed electric near-field distribution. The result is that metallic objects should be located in areas below local minima in the electric field amplitude of the total field.

Finally, the thesis demonstrates a 30% size reduction by inductive or capacitive loading of the PIFA.

Resume

Mobiltelefonteknologien er i hastig udvikling, en udvikling, der går i retning af mindre telefoner med stadig flere applikationer. For at opfylde kravene til den hastige reduktion i størrelse er det vigtigt at kunne designe små mobiltelefonantenner. I nærværende Ph.D. afhandling diskuteres designkoncepter for små mobiltelefonantenner, specielt med henblik på de tendenser og krav, der er til fremtidige mobiltelefonsystemer, for eksempel Multiple-Input Multi-output (MIMO) systemer.

MIMO systemer benytter flere antenner (både på sende- og modtagesiden) til at forøge kapaciteten. For at et MIMO system skal fungere optimalt, kræves det, at sender og modtager befinder sig i såkaldt spredende omgivelser. Kapaciteten og dermed fordelen ved MIMO kan beregnes udfra kendskab til antennens egenskaber samt kendskab til transmissionskanalen. Til trods for, at der er offentliggjort et overvældende antal artikler de seneste år om MIMO systemer, er mekanismerne for, hvordan antennerne kan implementeres i mobiltelefonerne stort set ikke belyst. Ligeledes er antenneegenskabernes betydning for et MIMO system ikke udforsket tilstrækkeligt. Dette understreger behovet for metoder til at evaluere MIMO systemets egenskaber udfra mobiltelefonantennernes egenskaber. I afhandlingen studeres MIMO systemer med forskellige antal antenner på sende- og modtagesiden.

Der er udledt en ligning til at beregne korrelationen imellem to antenner i et MIMO system med et vilkårligt antal antenneelementer. Den udledte ligning har den fordel, at den bruger spredningsparametrene målt ved antennefødepunktet til at beregne korrelationen og ikke fjernfeltets udstrålingsegenskaber, hvilket giver en tidsmæssig gevinst. Formlen er eftervist med numeriske data. Det vises, at konfigurationer, der maksimerer afstanden imellem den åbne ende af de designede ”Planar Inverted F- Antennas” (PIFA), giver den laveste indbyrdes kobling og ligeledes den laveste korrelation.

Hvis en lille antenne er placeret i nærheden af et lille metalobjekt, for eksempel metalliske dele af mobiltelefonkabinettet, højtalere eller et kamera, vil formen og placeringen af dette object have en kraftig indflydelse på antennens egenskaber. Det vises, at den optimale placering af et metallisk objekt, såsom et kamera eller en højttaler, kan findes direkte udfra de ubehandlede nærfeltsmålinger af det elektriske felt. Heraf følger det, at metalliske objekter påvirker det elektriske felts fordeling mindst, hvis de metalliske objekter er placeret over arealer, hvor der er et lokalt minimum i det elektriske felts fordeling.

Til sidst demonstreres det i denne afhandling, at en PIFA kan reduceres med 30% ved at erstatte en del af antennen med en spole eller en kondensator.

List of papers

This thesis is primarily based on the work contained in the following papers, referred to in the text by their Roman numerals. Paper [I]-[X] are attached immediately after the conclusion of this thesis.

I. J. Thaysen and K. B. Jakobsen, "Reduction of Antenna Correlation and Bandwidth Optimisation for Improved MIMO Performance," submitted 2005.

II. J. Thaysen and K. B. Jakobsen, "Infinite MIMO Antenna array performance from scattering parameters," accepted in *Microwave Opt Technol. Lett.*, 2005.

III. J. Thaysen and K. B. Jakobsen, "Design considerations for low antenna correlation and mutual coupling reduction in multi antenna terminals," accepted in *ETT-European Transactions on Telecommunications,* 2005.

IV. J. Thaysen and K. B. Jakobsen, "An experimental evaluation of the capacity, correlation, efficiency, and mutual coupling of three MIMO designs for mobile phones," accepted in *IEEE transaction of vehicular communication*, 2005.

V. J. Thaysen and K. B. Jakobsen, "Estimation of the Optimal Location of Metallic Objects Inside a Mobile Phone," accepted in *Microwave journal,* 2005.

VI. J. Thaysen and K. B. Jakobsen, "Mutual Coupling between Identical Planar Inverted-F Antennas," accepted to *International Journal of Electronics and Communications (AEU),* 2005.

VII. J. Thaysen and K. B. Jakobsen, "Coupling reduction by lumped components," *Jina'04, Internationales de Nice sur les Antennas,* p. 4, 2004.

VIII. J. Thaysen and K. B. Jakobsen, "Size reduction techniques for mobile phone antennas using lumped inductors," accepted in *Microwave journal*, 2005.

IX. J. Thaysen and K. B. Jakobsen, "Mobile phone antennas reduction techniques by capacitive top loading," accepted in *Microwaves and RF,* 2005.

X. J. Thaysen and K. B. Jakobsen, "One turn stub loaded loop patch antenna on a small ground plane," *Microwave Opt Technol. Lett.,* vol. 45 (2), pp. 126-128, 2005.

In addition, the two review chapters in this thesis are submitted.

XI. J. Thaysen and K. B. Jakobsen, "A review of the MIMO system in an antenna perspective," *Chapter 2 in this thesis, submitted*, 2005.

XII. J. Thaysen and K. B. Jakobsen, "Antenna and antenna system minimisation for mobile phones – an overview," *Chapter 3 in this thesis, submitted*, 2005.

Other publications

The following publications are further outcome of the work carried out during this Ph. D. study. The papers are not attached.

- J. Thaysen, K. B. Jakobsen, and H-R. Lenler-Eriksen, "Wideband Cavity Backed Spiral Antenna for Stepped Frequency Ground Penetrating Radar," to appear at *IEEE APS symposium*, Washington D.C., USA, July 2005.
- J. Thaysen and K. B. Jakobsen, "MIMO channel capacity versus mutual coupling in multi antenna element system," *AMTA 2004, Antenna Measurement Techniques Association, 26th Annual Meeting & Symposium*, Atlanta, GA, USA, pp 124-129, 2004.
- J. Thaysen and K. B. Jakobsen, "Small inductor Loaded mobile phone Antenna," *JINA 2004*, *International Symposium on Antennas*, p. 4*,* 2004.
- J. Thaysen and K. B. Jakobsen, "Capacitive loaded mobile phone Antenna," *JINA 2004*, *International Symposium on Antennas,* p. 4*,* 2004.
- J. Thaysen and K. B. Jakobsen, "Stub Loaded Low profile loop patch Antenna on a Finite Ground Plane," *Proceedings of 2004 URSI International Symposium on Electromagnetic Theory*, Pisa, Italy, 2004.
- J. Thaysen and K. B. Jakobsen, "Near field Distribution from a Planar Inverted-F Antenna," *Proc. of Twelfth International Conference on Antennas & Propagation*, Univ. of Exeter, UK, p. 4, 2003.
- J. Thaysen, K. B. Jakobsen, and J. Appel-Hansen, "A Wideband Balun - How Does it Work?," *A Collection from Applied Microwave & Wireless (More Practical Filters and Couplers)*, Noble Publishing Corporation, ISBN 1-884932-31-2 pp. 77-82, 2002.
- J. Thaysen, "Mutual Coupling Between Two Identical Planar Inverted-F Antennas," *Proc. IEEE Antennas and Propagation Society International Symposium*, vol. 4, pp. 504-507, 2002.
- J. Thaysen, K. B. Jakobsen, and E. K. Miller, "Modeling of a Frequency Independent Antenna," *Proceedings of USNC/URSI National Radio Science Meeting*, p. 1, 2002.
- J. Thaysen, J. Appel-Hansen, and K. B. Jakobsen, "The radiation pattern of a logarithmic spiral antenna," *Proc. 2001 URSI International Symposium on Electromagnetic Theory*, Victoria, British Columbia, Canada, pp. 19-21, May 2001.

Contents

1 Introduction and motivation

This present thesis addresses the aspects of using multiple antennas inside a mobile phone. Issues related to the practical implementation of the proposed antennas on a ground plane that has a size, which is comparable to modern mobile phones, are discussed.

Minimising the volume of an antenna system is an essential step for reducing the overall size of a mobile phone. Using more than one antenna inside a mobile phone, which is less than one wavelength, inevitably affects the performances of the antennas.

The research is made as general as possible heading for the four following applications: Separate receiver (RX) and transmitter (TX) antennas, separate antennas for different frequency protocols, diversity gain and Multi-Input Multi-Output (MIMO) system. Therefore, the aim of this work was to investigate the possibilities to implement more than one antenna in a mobile phone, where the antennas of interests has the same resonant frequency with reference to the MIMO principle or two separate antennas with slightly different resonant frequency together covering one single frequency protocol, i.e., one receiver and one transmitter antenna.

However, issues related to any other hardware or software implementation related to the actual implementation and technical requirements are not included. Also, diversity is treated as part of MIMO, only.

To achieve these aims, the following objectives were formulated:

- Reduction of the mutual coupling between antennas, in order to locate these within a smaller volume.
- Reduction of the size of the antennas, e.g. using lumped or distributed inductors and capacitors.
- Investigating the optimum location and mutual orientation between two antennas in order to reduce the mutual coupling and to reduce the envelope correlation.
- Investigation of the relation between the mutual coupling and the envelope correlation of a MIMO antenna system.
- Investigation of the relation between the scattering parameters and the envelope correlation in MIMO systems consisting of three or more antennas.
- Investigation of the electric near-field of the antenna including the ground plane for determining the optimal location of external components, such as loud speakers and cameras with respect to the antennas.
- Investigation of the MIMO performance of different prototypes mounted in realistic environment, i.e., beside artificial hand and head.

The introduction part of this thesis is divided into two chapters. Chapter 2 acts as a review of the MIMO system in an antennas perspective. An overview of the antenna and antenna system minimisation for mobile phones are given in Chapter 3. Issues discussed are in particular size reduction techniques, mutual orientation of the antennas and location of the antennas with respect to the remaining component inside the mobile phone. This is primarily discussed with respect to the Planar Inverted-F antenna, with some proposals for a one turn loop antenna. The conclusions are drawn in Chapter 4.

Hereafter follows the ten primary articles described on page *xi* in this thesis.

2 A review of the MIMO system in an antenna perspective

2.1 Introduction

When a mobile and wireless terminal is moved in multipath environments, strong fading occurs inevitably due to multipath propagation. Diversity is a technique to overcome the effects of multipath fading [1]. In a receiver diversity system, the basic concept is that the receiver should have more than one version of the transmitted signal available, each received through a distinct channel. In the channel, the fading properties are most likely independent, i.e., simultaneously deep fade in all channels are seldom [1]. Thus, the performance of the terminals in such environments can be significantly improved by making use of spatial, polarization or pattern diversity. This means that the signals on the two antennas (with different position, polarization or radiation patterns) are combined such that fading is avoided in the combined signal. This corresponds to an increase in the signal to noise ratio (*SNR*) in the fading dips, and hence the fading margins in the system link budget can be reduced. Alternatively, the increased *SNR* can be used to increase the capacity of the communication channel. Therefore, a trade-off between *SNR* and capacity exists. If we make use of two or more antennas on both the transmitter and the receiver side, and if we make use of the improved *SNR* to increase the capacity of the communication system, we obtain a Multiple-Input Multiple-Output (MIMO) system [2].

In the next section the principles of MIMO systems are discussed referring to a MIMO system with three antennas on both the transmitter and the receiver end. Section 2.3 includes details regarding the derivation of the envelope correlation [I, II, III]. Section 2.4 deals with the two- and three-antenna MIMO systems, and in Section 2.5 the capacity of different sized antenna systems are discussed as well as a discussion regarding MIMO systems with antenna selection is provided [IV]. The conclusions are drawn in Section 2.6.

2.2 MIMO system principles

The idea behind MIMO is that the signals on the transmitter (TX) antennas at one end and the receiver (RX) antennas at the other end are “combined” in such a way that the quality in terms of the bit-error rate (*BER*) or the data rate (bits/sec) for each of the MIMO user can be improved [2]. A MIMO-system transmits data over a matrix channel rather than just over a single radio channel. This requires signal processing over both time and space as illustrated in Figure 1 [3].

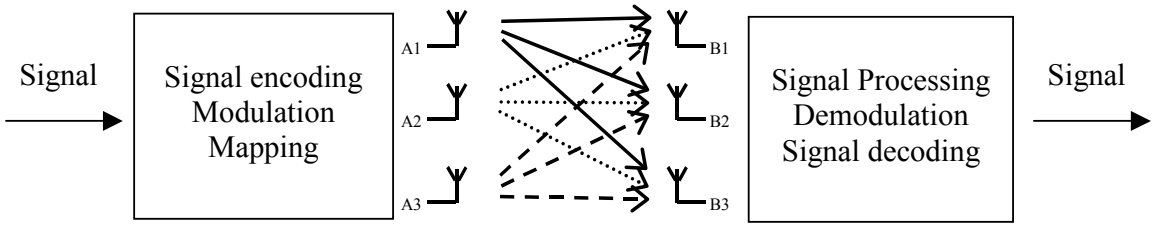

Figure 1. Illustration of the MIMO system with 3 transmitter and 3 receiver antennas.

The signal to be transmitted is fed to a simplified transmitting block in which proper error correction coding is added, filtering and amplification are performed. Hereafter, the three different signals are transmitted simultaneously from antenna element A1, A2, and A3. At the

receiver each of the antenna element B1-B3 receives a signal from each of the transmitting antennas.

If the received signals at each of the antenna element B1-B3 are sufficiently independent, as typically the case in the presence of rich multipath environment, it is possible to re-establish the original transmitted signal. The relationship between A (A1, A2, A3) and B (B1, B2, B3) is $B(t) = H(t)\,A(t)$. Each matrix H represents the transmission at a certain time (t) and spatial location of the antennas in the multipath environment. Hence, a (3, 3) MIMO system has a potential capacity increase of three as compared to the single element. In theory this gives an upper speed limit that is limited only by the hardware cost and the requirement of a rich multi path environment. Therefore, MIMO systems are very attractive in order to boost the capacity of a wireless communication system that operates in a rich multipath environment.

Since the early pioneering work by Winters [4], Foschini [5], and Telatar [6], MIMO systems have received considerable attention due to the potential increase in capacity. It has been shown that MIMO systems have the potential for large capacities, since the system can provide several independent communication channels between the transmitter and receiver [5]. In an ideal multipath channel, the theoretical MIMO capacity increases linearly by m times the capacity of a single-antenna system SISO (Single-Input Single-Output), where m is the smallest of the number of transmit or receive antenna elements [5]. The theoretical capacity increases linearly with the number of antenna elements N in a (N, N) MIMO system [1].

However, in a more practical MIMO system the capacity is reduced due to correlation between the signals in the receiver [7], this effect has been investigated both theoretically [8], [9], and experimentally [10]. Therefore the correlation between the signals that are received from the different antenna elements is an important parameter in a MIMO system, due to the increased capacity for decreased correlation [3]. As long as the envelope correlation is less than $\rho_e < 0.5$ diversity gain could be obtained in a mobile phone [1]. Even though, this motivates for low correlation, it is not a guarantee for high capacity, since in some special propagation scenarios, the MIMO channel capacity can be low (i.e., comparable to the SISO capacity) even though the signals at the antenna elements are uncorrelated [13]. This effect that has been denoted ”keyhole” leading to a drop in the capacity [14]. It is related to scenarios where rich scattering around the transmitter and receiver leads to low correlation of the signals, while other propagation effects, like diffraction or waveguiding, lead to a rank reduction of the transfer function matrix. This gives rise to significant local scattering around both the transmitter and the receiver unit causing uncorrelated fading at each end of the MIMO link. However, the channels still have poor rank properties and hence low capacity. See for example Jensen et al. [15] for a thorough description of the “keyholes”. The rank of the MIMO channel is defined as the number of independent equations offered by the MIMO system (the algebraic rank) [5]. The rank is always less than both the number of TX antennas and the number of RX antennas.

Recently, Oestges et al. [16] have published that high correlation not necessarily results in low capacity. In Schumacher et al. [17] the physical channel is related to the observed correlations. In both cases it is the cross correlation that is investigated, and not as in this paper the correlation between the interelements. The results obtained in [16, 17] are therefore not directly adaptable to the results discussed by Thaysen et al. [I].

Moreover in the case of non-richness of the scattering environment that could be line-of-sight properties the simple receiver diversity system yields full transmission. However, for the MIMO system line-of-sight properties cause increased correlation at the receiver, and hence the principle behind the MIMO system collapses since three unknowns must be resolved from

a linear system of one equation. By proper handshaking between the receiver and the transmitter, the potential collapse of the MIMO principle could be avoided [5].

The expected linear capacity enhancement for increasing the number of antennas motivates the increase of antenna elements. However, mutual coupling between the antenna elements affects the correlation [18-22], [44]. For a finite size mobile phone this causes inevitably higher mutual coupling due to the smaller distances between the antennas [23], [24]. Therefore, knowledge regarding how these antennas should be oriented in order to minimise the coupling [24], [VI] and the correlation is needed [III]. The increased mutual coupling results in higher spatial correlation [III] which in many case leads to a lower MIMO gain as compared to fully uncorrelated antenna signals [3].

2.3 Correlation between the MIMO antenna elements

So far, the correlation between signals received from different antenna elements is an important parameter in a multi-input multi-output (MIMO) system due to the increased capacity for decreased correlation.

Derivation of the Envelope correlation

There are two forms of antenna correlation: Signal correlation and envelope correlation. Signal correlation refers to the correlation between the complex signals of two different antennas, while envelope correlation refers to the correlation between signal amplitudes of two different antennas. Envelope correlation is often the parameter measured in antenna experiments (phase less) and is in most cases approximately equal to the square of the complex magnitude of the signal correlation [26]. In Vaughan et al. [26] the maximum relative error is computed to being less than 10%. In this thesis, unless otherwise mentioned, it is the correlation that is calculated using the complex value of the signals that is referred to.

The calculation of the antenna correlation can be approached in different ways, one is based on the far-field pattern [1], and another is based directly on the scattering parameters at the antenna terminals [27]. A third method based on Clarke's formula [28], has recently been used by Boyle [29] and Hui et al. [30]. Correlation calculation using the radiation pattern principle is a time consuming process, independently of whether it is done using numerical or experimental data. However, it is an often used method (see for example Leather et al. [31]). Blanch et al. [27] proposes a formula for calculating the correlation between antennas in a two antenna system using the scattering parameters. The results coincide with that obtained from the radiation pattern measurement of each of the elements. The correlation between two antennas can be calculated using the impedance matrix as well [32].

Thaysen et al. [I] propose a novel closed formed expression to calculate the envelope correlation coefficient from the scattering parameters between any two antennas in a (*3, 3*) MIMO antenna array system. The expression gives knowledge of where the effort could be placed doing design and optimisation of the antennas in a diversity or MIMO system.

In Thaysen et al. [I], a (3, 3) MIMO system is created, thus the correlation between any two antennas in this three-antenna system is required. The formula has been derived using the law of energy conservation [34], which also is the case in the work by Blanch et al. [27] and Salonen et al. [33].

The envelope correlation for a two-antenna system can be calculated using Equation 1 [1, 26, 27], where $\vec{\mathbf{F}}_i(\theta,\phi)$ is the field radiation pattern of the antenna system when port *i* is excited (all

other ports are terminated with loads representing the source impedance on their ports), and • denotes the Hermitian product.

$$\rho_e = \frac{\left| \iint_{4\pi} \left[\vec{F}_1(\theta,\phi) \bullet \vec{F}_2^*(\theta,\phi) \right] d\Omega \right|^2}{\iint_{4\pi} \left| \vec{F}_1(\theta,\phi) \right|^2 d\Omega \iint_{4\pi} \left| \vec{F}_2(\theta,\phi) \right|^2 d\Omega} \tag{1}$$

In the case of a (3, 3) MIMO system, with N=3 antennas in both ends, the envelope correlation between antenna i=1 and j=2 could be calculated using Equation 2. For the correlation in a two-antenna diversity scheme, i.e., N=2, see Blanch et al. [27].

$$\rho_e(1,2,3) = \frac{\left| S_{11}^* S_{12} + S_{12}^* S_{22} + S_{13}^* S_{32} \right|^2}{\left(1 - \left(\left|S_{11}\right|^2 + \left|S_{21}\right|^2 + \left|S_{31}\right|^2 \right)\right)\left(1 - \left(\left|S_{12}\right|^2 + \left|S_{22}\right|^2 + \left|S_{32}\right|^2 \right)\right)} \tag{2}$$

Further details regarding the derivation is given by Thaysen et al. [I].

Thaysen et al. [II] have extended the envelope correlation formula to the general (N, N) case (also valid for the two and three antenna systems, i.e., N = 2 and 3). Hence, a closed formed equation for the magnitude square of the complex correlation (which is the same as the power correlation) and approximately equal to the envelope correlation [26] between any two antennas in a MIMO system consisting of N antennas is derived as:

$$\rho_e(i,j,N) = \frac{\left| \sum_{n=1}^{N} S_{i,n}^* S_{n,j} \right|^2}{\prod_{k=i,j} \left[1 - \sum_{n=1}^{N} S_{k,n}^* S_{n,k} \right]}. \tag{3}$$

The envelope correlation is determined from the distribution of the external sources and the radiation pattern from the antennas. Only by assuming omni-directional source distribution one can relate the mutual impedances (or scattering parameters) to the correlation [26]. This means that the envelope correlations estimated based on S-parameters (Equation 3) correspond to that given by Equation 1 only if a uniform distribution of the sources is assumed. Given that the investigation is to design practical antenna system for MIMO (e.g. in a mobile phone), the uniform distribution of the sources assumed in the envelope correlation expression may be inadequate. Therefore, it should be clearly pointed out that this formulation cannot completely replace the correlation, calculated using Equation 1 (as a quality criterion) in the case of small terminal antennas. This is mainly due to the fact that the mutual coupling is a near-field effect, whereas the pattern correlation is a pure far-field effect. The radiation pattern based method gives us the possibility to include a better description of the radio channel in the evaluation, although it makes the evaluation more cumbersome.

Thaysen et al. [II] validate the proposed formula in the special case of a (3, 3) MIMO system by comparing the envelope correlation obtained using Equation 1 to that based on Equation 3 see Figure 2. In the frequency range from 1.4 GHz to 2.4 GHz the envelope correlation that is based on the envelope correlations formula given by Equation 1, yields slightly lower values as compared to the radiation pattern based method given by Equation 3. Parts of the difference could be caused by the measurement facility, primary due to the dips in the ϕ = 180° ± 12°, (see e.g. Thaysen et al. [I]) which are caused by the antenna mounting and positioning system [25]. The discrepancies are also related to the fact that the scattering parameters are measured in the laboratory, a scattering environment, whereas the radiation patterns are measured in an

anechoic environment. The maximum absolute difference between the envelope correlations calculated using Equation 1 and that based on Equation 3 are 0.04.

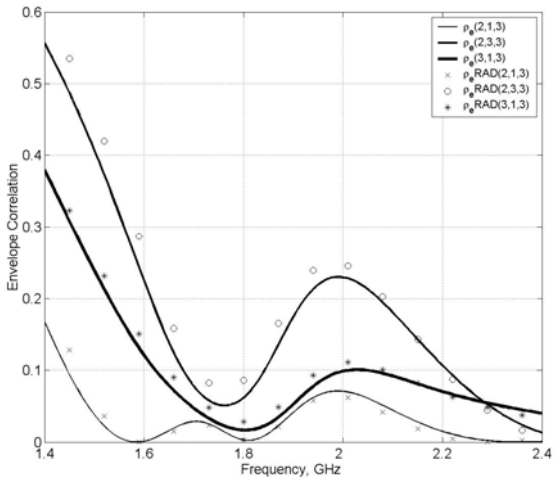

Figure 2. Simulated envelope correlation versus frequency for a three-antenna configuration [II]. Calculated using the scattering parameter formula (Equation 2) (solid lines) and the radiation pattern formula (Equation 1) (○, *, ×).

Thaysen et al. [III] relate the mutual orientations, the location, and the mutual coupling to the envelope correlation between two identical antennas. Symmetrical as well as asymmetrical coupling scenarios using two identical PIFAs located close to each other on the same ground plane are investigated, in order to determine the envelope correlation versus distance for fixed orientations, and mutual coupling versus rotation of the antennas for fixed distance. The results (simulated using IE3D [12]) illustrate how to orientate and locate the antennas in order to minimise the envelope correlation. Two different cases are investigated; one with parallel PIFAs another with orthogonal orientation illustrated in Figure 3 (with a horizontal distance, *d,* defined so that *d* is positive in the case illustrated in Figure 3a). For the parallel (see Figure 2a) case with 10 mm separation, it is found that the envelope correlation is $\rho_e = 0.8$ and simply by rotation of one the antennas 180 degrees, the envelope correlation decreases to $\rho_e = 0.4$. Similar for the orthogonal antennas set-up (see Figure 3b), here the envelope correlation decreases from $\rho_e = 0.5$ to $\rho_e = 0.25$. For the orthogonal set-ups the highest envelope correlation is obtained when the open end and the feed line are vertically on line.

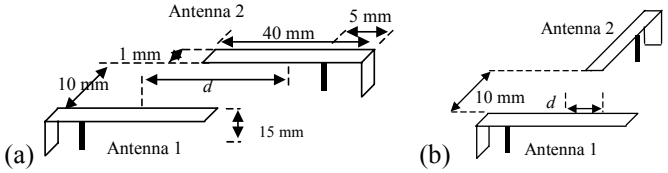

Figure 3. Illustration of the parallel (a) and orthogonal (b) configurations that are investigated.

In Thaysen et al. [III] it is found that the deviation in the centre frequency (min. $|S_{11}|$) is most affected in the case of parallel antennas, each having the feed point in the same end, here a change of 12% is observed. In the other scenarios (the two orthogonal cases) the change is below 2%, as compared to a single PIFA. Maximum envelope correlation of $\rho_e = 0.8$ is obtained for the parallel set-up, when the antennas are vertically overlapping each other, and highest for the set-up having the feed line in same ends.

An almost exponential relation between the mutual coupling and the envelope correlation is found [III]. A certain limit of the mutual coupling of –10 dB is found. Below the limit the envelope correlation is almost constant, being $\rho_e = 0.15$, and therefore effort in decreasing the mutual coupling could be limited to this level.

Thaysen et al. [I] have investigated several configurations (see Figure 4), each including a number of completely identical antennas and applied some performance metrics (correlation and bandwidth) to choose the best antenna configuration. At a later stage in the design of the MIMO antennas one should optimise the input impedance and bandwidth of the PIFA (e.g., by changing the distance between feed and ground contact) within each location on the board and then do the comparison again. Also, the proximity effect by the mobile phone cover and by the artificial hand and head should be included [IV]. The results concerning the optimal configurations might differ somewhat.

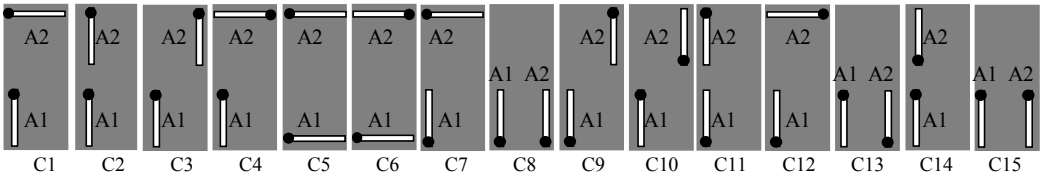

Figure 4. Layouts of the fifteen different two-antenna configurations (C1 - C15) located on the same finite ground plane. The matchsticks symbolise the PIFAs (A1 and A2), and the dot on the matchstick denotes the location of the shorting pin.

For MIMO application, where low envelope correlation is essential, one should bear in mind that the location and orientation of the antennas should be optimised not only with respect to envelope correlation but also with respect to the bandwidth. It is found that for the two-antenna configuration optimal locations and orientation with respect to the MIMO performance, i.e., bandwidth and envelope correlation between the antennas are not necessarily the ones with the lowest envelope correlation [I]. A certain bandwidth is required as well.

Thaysen et al. [I] have found that configurations C7 and C8 (see Figure 4) yield the best performance when taking the envelope correlation and bandwidth into account. Configuration C7 includes two orthogonal PIFAs, one located parallel to the long edge (40 mm x 100 mm ground plane) of the ground plane, having the shorting pin located parallel to the short edge. The other antenna is located parallel to the short edge, with the short pin inline with the other antenna. Configuration C8 contains two PIFAs located parallel to the long edge (40 mm × 100 mm ground plane) of the ground plane, both having the shorting pin located parallel to the short edge.

From the 15 different two-antenna configurations investigated by Thaysen et al. [I], the relation between the envelope correlation and the mutual coupling indicates that low mutual coupling leads to low envelope correlation. However, low envelope correlation does not necessarily come from low mutual coupling. Also, observed is that low mutual coupling leads to low bandwidth, this is primary caused by poor impedance match (high reflection coefficient) of the antennas, in these particular configurations. A high bandwidth occurs in the configurations that also yield a high mutual coupling. Thaysen et al. [I] conclude that high mutual coupling reduces the freedom in choosing an optimal configuration.

Taking the increased complexity into account it might be that careful optimisation of a given number of antenna elements is preferred as compared to the scenario when an extra antenna element has been added. In Thaysen et al. [I], the evaluation of the MIMO system is based on the antenna performance, such as envelope correlation, mutual coupling, resonance frequency, bandwidth, and radiation efficiency of the interelements, especially with focus on the envelope correlation and the bandwidth. However, the capacity should be evaluated in a multipath environment in order to determine this fully [IV].

Thaysen et al. [I] propose a three-antenna configuration that has a maximum envelope correlation of $\rho_e = 0.24$ in the frequency band of interest, i.e., from 1.7 GHz to 1.9 GHz. This number is approximately half of the "rule of thumb" number ($\rho_e < 0.5$) for diversity gain stated in [1].

2.4 MIMO channel measurement and modelling

In order to calculate the capacity of MIMO systems information of both the propagation environment and the antenna configurations is required.

MIMO channel

Realistic evaluation of MIMO antenna structures requires multi element propagation measurements with MIMO antenna configurations.

One way to obtain these multi element propagation measurements is to measure the actual prototype in real scattering environment. This, however is a very time consuming process. Moreover, the entire measurement must be repeated for all MIMO antenna proposals.

Another way to obtain these multielement propagation measurements is to combine the measured or simulated propagation paths with the radiation pattern of the antenna elements. This leads to a MIMO coupling matrix between the antenna elements. This requires the extraction of the full double-directional propagation channel parameters and has been done experimentally; see for example [35, 36]. The results of the radio channel measurement system equipped with a channel sounder for measuring the spatial and temporal characteristics of the radiowave channel, a linear transmitting (TX) antenna array, and a spherical receiving (RX) antenna array both employing dual polarised patch antennas are used [37, 38]. The linear antenna array consists of eight directive and dual polarised antenna elements from which different numbers of elements were selected in the post processing of the measurement data [36, 39]. The spherical receiving antenna array is formed by 32 directive and dual-polarised elements, similar to the elements of the TX array. The elements that are located on the sphere were used at the receiving mobile station (MS). One dual polarised element consists of two orthogonal channels, i.e., θ- and φ-polarised feeds [36, 39].

In Thaysen et al. [IV], the used MIMO coupling matrix between the antenna elements represents a small macrocell MIMO environment measured in downtown Helsinki (see for example [35] for maps). The measured MIMO coupling matrix used in this thesis was performed by Dr. Vainikainens group at Helsinki University of Technologi, HUT (see e.g. [35, 40]). This coupling matrix is then combined with the complex radiation pattern of the antennas under test.

Channel transfer function

The signal at the base station is related to the signal at the receiving signal mobile station through the matrix H that represents the transmission at a certain time and spatial location of the antennas in the multipath environment via

$$y(t) = H(t)s(t), \tag{4}$$

where *y(t) i*s the TX signal at the base station

$$y(t) = [y_1(t), y_2(t), \cdots, y_m(t)]^T, \tag{5}$$

and *s(t)* is the signal at the RX signal at the mobile station

$$s(t) = [s_1(t), s_2(t), \cdots, s_n(t)]^T. \tag{6}$$

The matrix *H* that represents the transmission at a certain time and spatial location of the antennas in the multipath environment is

$$H = \begin{bmatrix} \alpha_{1,1} & \alpha_{1,2} & \cdots & \alpha_{1,n} \\ \alpha_{1,1} & \alpha_{1,1} & \cdots & \alpha_{1,n} \\ \vdots & \vdots & \ddots & \vdots \\ \alpha_{m,1} & \alpha_{m,1} & \cdots & \alpha_{m,n} \end{bmatrix}, \tag{7}$$

where $\alpha_{i,j}$ is the complex transmission coefficient from antenna *i* to antenna *j*.

These results are restricted to frequency flat fading channels, and therefore the corresponding input – output relation simplifies to $B = H A$, where *H* is the narrow band matrix that describes the channel from the *m*th transmit antenna to the *n*th receive antenna in a (*m, n*) MIMO antenna system. The capacity of the MIMO system could then be calculated with a combination of the measured radiation patterns of the antennas and the measured MIMO channel.

For calculating the capacity it is the radiation pattern of a single element when all the other elements are present (but terminated with loads representing the source impedance on their ports) that must be measured. In Thaysen et al. [IV], the complex radiation patterns are measured in a radio-anechoic chamber. Both in free space and in more realistic environments, i.e., where the antennas are mounted next to an artificial hand and head are measured in order to determine the proximity effect by an artificial human hand and head.

2.5 Capacity of different MIMO systems

In order to obtain as realistic results as possible for the MIMO evaluation, it is the measured macrocell MIMO environment combined with the radiation pattern from the proposed MIMO system antennas that are used in the following.

Fundamental Capacity Results

In a traditional channel with only one transmission channel used for data transmission the Single-Input Single-Output (SISO) system capacity becomes [41]

$$\mathrm{C} = \log_2(1 + SNR) \quad [\mathrm{bit/s/Hz}], \tag{8}$$

where *SNR* is the signal to noise ratio.

Without any knowledge of the channel characteristics, the only way to distribute the transmit power is to share it equally on all the transmit antenna elements [5]. The capacity of such MIMO system with unknown channel and equal power distribution is defined as [4]-[6]

$$C = \log_2\left[\det\left(I + \frac{SNR}{m}\overline{H}\ \overline{H}^*\right)\right] \quad [\text{bit/s/Hz}] \tag{9}$$

with I as the identity matrix, (*) means transpose conjugate and H is the MIMO system channel matrix. It has been demonstrated that the capacity in Equation 9 grows linearly with $m = \min(M, N)$, rather than logarithmically as in the diversity case [5], [6].

This capacity formula is valid under narrow band assumptions, i.e., a frequency-flat fading MIMO channel [5]. If the channel were frequency selective the matrices H depends on the frequency as well. In such case one should integrate over the transmitted bandwidth, for calculating the capacity in such case see for example Vaughan et al. [26].

Assuming that the channel is known at the transmitter, the signal transmission is divided over the transmit antennas in such a way as to optimise the channel capacity. The total transmit power is divided such that a greater portion goes to the channels with higher gain, and lesser or even none to the channels with smaller gains [5]. This technique is known as water filling [5].

For a transmitter that has a perfect knowledge of the MIMO channel, the maximum achievable capacity corresponds to the water filling solution. In practice, the available knowledge may only be partial, due to the time selectivity of the channel, and delay or absence of the feedback from the receiver. However, exploiting the partial knowledge leads to a significant improvement when compared to the capacity without any channel knowledge [2]. Water filling has a significant advantage over equal power schemes at low *SNR*. At low *SNR* the Water filling technique finds the largest eigenvalues to H and send the entire power trough one single mode (channel). At intermediate *SNR* the water-filling still improves the capacity over the equal power schemes. However this advantage decreases with increasing *SNR*. At intermediate *SNR* the water-filling technique uses L number of antennas where $1<L<\min(N, M)$. At high *SNR*, the water filling schemes functions almost as equal power schemes and the advantage over the equal power scheme decreases [2].

Capacity in multipath environments

Thaysen et al. [IV] show experimental results of the capacity and the diversity gain for three simple yet realistic two- and three-antenna configurations as illustrated in Figure 5. The channel data used are measured in a small macro cell environment, in downtown Helsinki. The provided results are for both the free space radiation pattern as well as the talk position radiation pattern, i.e., beside an artificial hand and head. In Thaysen et al. [IV] the channel is unknown at the transmitter, and hence the capacity is calculated using equal power allocation, i.e., using Equation 9.

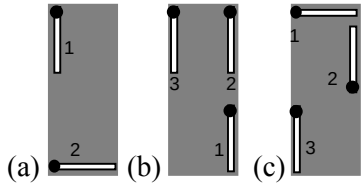

Figure 5. Antenna models (a) – (c). The matchsticks symbolises the PIFAs and the dots denote the location of the shorting pins on antenna 1,2, and 3.

The proposed two-antenna configuration (see Figure 5a) yields a 50% outage channel capacity $C_{0.5}$ in the (2, 2) MIMO system of 4.9 bit/s/Hz in talk position. This is a capacity decrease of 0.1 bit/s/Hz as compared to the capacity obtained using the free-space radiation patterns, see Figure 6a. This rather small difference in the capacity is obtained even though that the measured talk position radiation efficiency is reduced to one fourth of the corresponding free-space radiation efficiency. This comes from the rather unchanged ratio between the peak total efficiencies measured in free space.

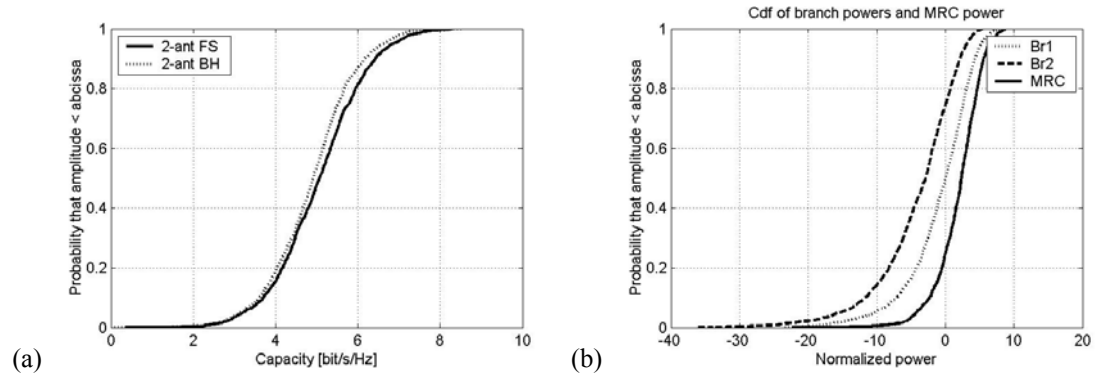

Figure 6. Capacity results for the two-antenna configuration in the macro environment. The antenna patterns are measured in free space (FS) and beside head (BH) (a). Cumulative distribution functions of the branch power (Br) Br1, Br2, and MRC power (b).

The gain of using more than one antenna is calculated as the difference between the power after maximum ratio combining (*MRC*) and the stronger branch power (Br1 are related to antenna 1 and Br2 are related to antenna 2) at the level that 90 % of the signals exceed [40]. This result is strongly affected by branch power difference and envelope correlation. As shown in Figure 6b, the *MRC* is 4.8 dB higher than Br1. At the probability level *p* of 50% the difference between Br1 and Br2, $\Delta_{Br2\text{-}Br1}$ is 2.8 dB [IV]. The fact that the branch power of antenna 1 is the highest seems reasonably when taking the measured radiation efficiency into account; since antenna 1 has the highest radiation efficiency.

The three antenna configuration, (3, 3) MIMO system, has a 50% outage channel capacity $C_{0.5}$ of 7.1 bit/s/Hz and 6.4 bit/s/Hz using the free-space and beside head radiation patterns, respectively (see illustration in Figure 5b). In spite of the fact that the capacity is decreased in talk position, the third antenna still results in a 1.5 bit/s/Hz as compared to the (2, 2) MIMO configuration.

The *MRC* is 5.5 dB higher than Br3, which has the highest value of the three antennas. At the probability level *p* of 50% the $\Delta_{Br3\text{-}Br1}$ is 2.7 dB, and $\Delta_{Br3\text{-}Br2}$ is 11.3 dB. This indicates that antenna 2 contributes the least to the total capacity. Bearing in mind that the talk position radiation efficiency of antenna 2 is a few percent, primarily due to the fact that one of the artificial fingers has direct contact to the radiating element of antenna 2, it is an advantages to have three antennas instead of two, seen from a capacity point of view.

Thaysen et al. [IV] evaluate a three-antenna MIMO system mounted in a mobile phone (see illustration in Figure 5c). The fact that the measured free-space radiation efficiency is approximately 20 percent point lower when incorporating the antennas into a mobile phone does not affect the free-space capacity, which is unchanged 7.1 bit/s/Hz. Placed beside an artificial hand and head, the capacity is 6.9 bit/s/Hz. This is 0.5 bit/s/Hz above the three-antenna configuration which is not incorporated into a phone. For all three antennas the measured radiation efficiency, when placed next to an artificial hand and head, is between 4%

and 14% in the frequency range from 1.7 GHz to 1.9 GHz. In average this is lower than the three-antenna configuration mounted on a ground plane (and not in a mobile phone cover), however, the high radiation efficiency (above 20%) of antenna 3 can not make it up for the extremely low radiation efficiency of antenna 2 (below 2%).

For three-antenna configuration mounted in a mobile phone the power after maximum ratio combining is 7.9 dB higher than Br3. At the probability level p of 50% the $\Delta_{Br1\text{-}Br3}$ is 1.7 dB, and $\Delta_{Br1\text{-}Br2}$ is 3.7 dB. The branch power difference between the two extra antennas, antenna 2 and antenna 3, $\Delta_{Br2\text{-}Br3}$ is 2 dB. This indicates that both antenna 2 and antenna 3 contributes to the total capacity, antenna 3 contributes the most.

Capacity versus signal to noise ratio

Thaysen et al. [IV] show that the capacity increases with increased signal to noise ratio (*SNR*) see Figure 7. At low *SNR*, i.e., below 5 dB the difference in using 3 antennas instead of 2 antennas is low. At *SNR* = 0 dB the difference is 0.5 bit/s/Hz, the talk position capacity of 1.6 bit/s/Hz being the lowest. The gain by using an extra antenna having a *SNR* of 50 dB is a talk position capacity of 43 bit/s/Hz, being 14 bit/s/Hz higher that the capacity obtained using the two-antenna configuration. The Shannon limit of the capacity of the SISO system at a signal to noise ration of 50 dB is 16.6 bit/s/Hz. This is approximately half the (2, 2) capacity and a third of that obtained using a (3, 3) MIMO system. Similar trends could be found in for example [2, 3, 5].

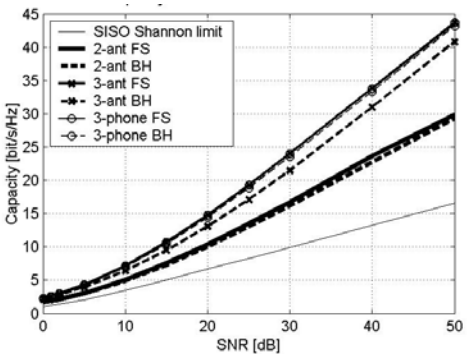

Figure 7. Mean capacity, with the outage rate of 50% at varying SNR for the three configurations. The antenna patterns are measured in free space (FS) and beside head (BH). Notice that the SISO capacity is based on the Shannon limit.

Capacity versus antenna elements

The MIMO system is based on two or more subchannels transferring data simultaneously at the same bandwidth. The effect of increasing the number of TX elements on the average capacity for the three different configuration used here are discussed by Thaysen et al. [IV]. Simply by adding more elements at the TX antenna configuration the capacity could be increased. For the two-antenna configuration proposed by Thaysen et al. [IV], the talk position capacity is increased from 4.1 bit/s/Hz for the simple diversity setup (1, 2) to 4.9 bit/s/Hz for the full (2, 2) MIMO system. The capacity reaches 5.2 bit/s/Hz in the case of three TX elements and two RX elements (3, 2). Meaning that the extra TX antenna yields an extra 0.3 bit/s/Hz. For the three-antenna configuration mounted inside a mobile phone the talk position capacity increases from 4.7 bit/s/Hz to 8.2 bit/s/Hz, when increasing the numbers of TX elements from one to seven. Above four TX elements the capacity increase is less per TX element as the capacity increase per TX element below three. From one to four the talk position capacity increases from 4.7 bit/s/Hz to 7.4 bit/s/Hz, as compared to an increase of 0.8

bit/s/Hz for the last three antennas. The most significant improvement is for an increase from one to two TX elements, i.e., from a (1, 3) to a (2, 3) MIMO system. Bearing in mind the capacity grows linearly with $m = \min(M, N)$ and logarithmically in the diversity case this is in accordance with theory [5], [6]. Sulonen et al. [39] have obtained similar trends.

MIMO system with diversity

Recently, Molisch et al. [42] have shown a MIMO system, which takes simple diversity into account, i.e. in either one or both of the link ends. This setup uses L antenna elements from the (N, N) MIMO system, in this way a reduced MIMO system is created which has a reduced complexity as compared to the full (N, N) MIMO system. Among others, Vaughan has shown that transmit or receive diversity can improve the link quality [11]. Lebrun et al. [43] suggest two methods for complexity reduction; one based on the signal to noise ratio, and another based on the signal strength. The results presented by Lebrun et al. [43] are based on a known channel with the water filling. In Thaysen et al. [IV] the capacity results are calculated under the assumption that the channel is unknown at the transmitter, and that the power are distributed equally. Adding an extra antenna increases the capacity [IV], [39], however, this decreases the interelement performance due to the reduced space between the antenna elements [I]. Thus the benefit by the extra antenna might be reduced as compared to the theoretical expected capacity increase. Therefore, a trade-off between the capacity and the increased complexity of the MIMO antenna system when an extra antenna element has been added exists. Taking the increased complexity into account it might be that careful optimisation of a given number of antenna elements is preferred as compared to the scenario when an extra antenna element has been added. The capacity for different numbers of TX elements for the two and three antenna configurations is shown in Figure 8.

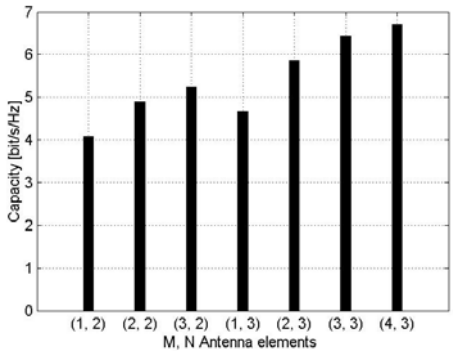

Figure 8. Capacity, with the outage rate of 50% as a function of number of antenna element at the sphere in macro environment. The antenna patterns are measured beside head (BH).

Thaysen et al. [IV] study the effect of a reduced MIMO system with an unequal number of antennas in the receiver and transmitter as well. Here it is concluded that, from a capacity point of view, it is better to have a full (2, 2) MIMO system ($C_{0.5}$ of 4.9 bit/s/Hz) than a TX diversity system of (1, 3) ($C_{0.5}$ of 4.7 bit/s/Hz). It is found that it is better to have an extra RX antenna, i.e., (TX, RX) = (2, 3) rather than an extra TX antenna (3, 2). The RX diversity setup has a capacity of 5.8 bit/s/Hz which is 0.6 bit/s/Hz higher than the TX diversity setup. This is in accordance with the results described by Foschini et al. [5]. For a known channel the RX diversity setup yields the same capacity as the TX diversity setup [2]. Bearing in mind that the hardware complexity of a MIMO system increased with the number of antennas, antenna selection could be used as a simple method to increase the capacity of a MIMO antenna configuration with minimal added hardware complexity.

2.6 Conclusion

The increasing demand for wireless communication systems having high data rate transmission could to some extent be accomplished using MIMO. The basic idea behind MIMO system architecture is that the signals on the transmitter (TX) antennas at one end and the receiver (RX) antennas at the other end are "combined" in such a way that the quality in terms of the bit-error rate (*BER*) or the data rate (bits/sec) for each of the MIMO user can be improved. A MIMO-system transmits data over a matrix channel rather than just over single radio channel, with significant increased capacity or higher link reliability using the same bandwidth and transmitter power as today.

The correlation between the interelement in a MIMO system affect the capacity. Here, it is the envelope correlation that is investigated. A closed formed expression used to calculate the envelope correlation coefficient from the scattering parameters between any two antennas in an infinite MIMO antenna array system is discussed. The expression gives a knowledge of where the effort could be placed doing design and optimisation of the antennas in a diversity or MIMO system. The formula can be applied to space, polarisation and pattern diversity as well.

An almost exponential relation between the mutual coupling and the envelope correlation is found by Thaysen et al. [III]. A certain limit of the mutual coupling of –10 dB is found, below the limit the envelope correlation is almost constant, being $\rho_e = 0.15$, and therefore effort in decreasing the mutual coupling should be limited to this level. As long as the envelope correlation is less than $\rho_e < 0.5$ diversity gain could be obtained in a mobile phone [1].

Thaysen et al. [I] have investigated 15 different two-antenna configurations (each on a finite ground plane). The relation between the envelope correlation and the mutual coupling indicates that low mutual coupling leads to low envelope correlation. However, low envelope correlation does not necessarily come from low mutual coupling. Also, observed is that low mutual coupling leads to low bandwidth, this is primarily caused by poor impedance match (high reflection coefficient) of the antennas, in these particular configurations. A high mutual coupling follows a high bandwidth. The conclusion is that high mutual coupling reduces the freedom in choosing an optimal configuration.

The MIMO capacity formula was briefly explained which showed the increased capacity as compared to conventional SISO systems.

From our study and overview of the MIMO principle, it is clear that MIMO systems offer significant gain in performance over traditional wireless communication systems. Measurements were presented to show the capability for several potential MIMO antenna configurations.

2.7 References

The references referred to in the text by their Roman numerals are found on page v in the beginning of this thesis.

[1] R. G. Vaughan and J. Bach Andersen, "Antenna diversity in mobile communication," *IEEE Trans. Veh. J1 Technol*., 36, pp. 149−172, 1987.

[2] D. Gesbert, M. Shafi, D. S. Shiu, P. J. Smith, and A. Naguib, "From theory to practice: An overview of MIMO space-time coded wireless systems,"*IEEE J. Select. Areas in Commun.,* vol. 21 (3), 2003.

[3] A. Goldsmith, S. Jafar, N. Jindal, and S. Vishwanath, "Capacity limis of MIMO channels,"

IEEE J. Select. Areas Commun., vol. 21, no. 5, pp. 684−702, 2003.

[4] J. H. Winters, "On the capacity of radio communication systems with diversity in a Rayleigh fading environment," *IEEE J. Select Areas Commun.*, vol. SAC-5, pp. 871–878, 1987.

[5] G. J. Foschini and M. J. Gans, "On limits of wireless communications in a fading environment when using multiple antennas," *Wireless Pers. Commun.*, vol. 6, pp. 311–335, 1998.

[6] I. E. Telatar, "Capacity of multi-antenna Gaussian channels," *Eur. Trans. Telecommun. Related Technol.*, vol. 10, pp. 585–595, 1999.

[7] R. Janaswamy, "Effect of Element Mutual Coupling on the Capacity of Fixed Length Linear Arrays," *IEEE Antennas and Wireless Propagat. Lett*, vol. 1, pp. 157−160, 2002.

[8] D. Shiu, G. J. Foschini, M. J. Gans, and J. M. Kahn, "Fading correlation and its effect on the capacity of multi-element antenna systems," *IEEE Transactions on Communications*, vol. 48, pp. 502–513, 2000.

[9] C. N. Chuah, D. N. C. Tse, J. M. Kahn, and R. A. Valenzuela, "Capacity scaling in MIMO wireless systems under correlated fading," *IEEE Transactions on Information Theory*, vol. 48, pp. 637–650, 2002.

[10] A. F. Molisch, M. Steinbauer, M. Toeltsch, E. Bonek, and R. S. Thoma, "Capacity of MIMO systems based on measured wireless channels," *IEEE Jour. on Sel. Areas in Commun.*, vol. 20, pp. 561–569, 2002.

[11] R. G. Vaughan, "Signals in Mobile Communications: A Review," *IEEE Trans. Veh. Technol*., vol. 35, pp. 133–145, 1986.

[12] www.zeland.com.

[13] D. Gesbert, H. Bölcskei, D. A. Gore, and A. J. Paulraj, "Mimo wireless channels: Capacity and performance prediction," in *Proc. GLOBECOM*, vol. 2, pp. 1083–1088, IEEE, 2000.

[14] D. Chizhik, G. J. Foschini, M. J. Gans, and R. A. Valenzuela, "Keyholes, correlations, and capacities of multielement transmit and receive antennas," *IEEE Transactions on Communications*, vol. 1, pp. 361–368, 2002.

[15] M. A. Jensen and J. W. Wallace, "A review of antennas and propagation for MIMO wireless communications," *IEEE Trans. Ant. propagat*, vol. 52 (11), pp 2810–2824, 2004.

[16] C. Oestges and A. Paulraj, "Beneficial impact of channel correlations on MIMO capacity," *Electron. Lett.,* vol. 40, pp. 606–608, 2004.

[17] L. Schumacher, K. I. Pedersen, and P. E. Mogensen, "From antenna spacings to theoretical capacities - guidelines for simulating MIMO systems," *The 13th IEEE International Symposium on Personal, Indoor and Mobile Radio Communications*, vol. 2, pp. 587–592, 2002.

[18] D. Chizhik, F. Rashid-Farrokhi, J. Ling, and A. Lozano, "Effect of antenna separation on the capacity of BLAST in correlated channels," *IEEE Commun. Lett.* vol. 4 (11), pp. 337–339, 2000.

[19] A. Derneryd and G. Kristensson, "Signal correlation including antenna coupling," *Electron. Lett.,* vol. 40 (3), pp. 157–158, 2004.

[20] M. Karaboikis, C. Soras, G. Tsachtsiris, and V. Makios, "Compact dual-printed inverted-F antenna diversity systems for portable wireless devices," *IEEE Ant. Wireless Propagat. Lett*, vol. 3, pp. 9–14, 2004.

[21] B. Clerckx, D. Vanhoenacker-Janvier, C. Oestges, and L. Vandendorpe, "Mutual coupling effects on the channel capacity and the space-time processing of MIMO communication systems," *Commun., ICC '03. IEEE Int. Conf. on,* vol. 4, pp. 2638–2642, 2003.

[22] J. W. Wallace and M. A. Jensen, "The Capacity of MIMO wireless systems with mutual coupling," *IEEE VTC' 03*, pp. 696–700, 2002.

[23] *O. Edvardsson,* "Can two antennas be smaller than one?" *Proc*. *ICAP 2001*, pp. 533–536, 2001.

[24] J. Thaysen, "Mutual Coupling Between Two Identical Planar Inverted-F Antennas," *Proc. IEEE Antennas and Propagation Society International Symposium,* vol. 4, pp. 504–507, 2002.

[25] www.satimo.com.

[26] R. G. Vaughan and J. Bach Andersen, *Channels, Propagation and Antennas for Mobile Communications*, The IEE, UK, ISBN 0 85296 084 0, 2003.

[27] J. Blanch, J. Romeu, and I. Corbella, "Exact representation of antenna system diversity performance from input parameter description," *Electron. Lett*., vol. 39, pp. 705–707, 2003.

[28] R. H. Clarke, "A statistical theory of mobile reception," *Bell Syst. Tech. J*., pp. 957–1000, 1968.

[29] K. Boyle, "Radiation Pattern and Correlation of Closely Spaces Linear Antennas" ," *IEEE Trans. Ant. Propagat,* vol. 50*,* pp. 1162–1165, 2002.

[30] H. T. Hui; W. T OwYong, and K. B. Toh, "Signal Correlation Between Two Normal-Mode Helical Antennas for Diversity Reception in a Multipath Environment," *IEEE Trans. Ant. Propagat,* pp. 572–577, 2004.

[31] P. S. H. Leather and D. Parson, "Antenna diversity for UHF handportable radio," *Electron. Lett.,* vol 39 (13), pp. 946–948, 2003.

[32] A. Derneryd and G. Kristensson, "Antenna signal correlation and its relation to the impedance matrix," *Electron. Lett.,* vol. 40 (7), pp. 401–402, 2004.

[33] I. Salonen and P. Vainikainen, "Estimation of signal correlation in antenna array," *Jina'02 – 12éme Journées. Internationales de Nice sur les Antennas*, pp. 383–386, 2002.

[34] S. Stein, "On cross coupling in multiple-beam antennas" *IRE Trans. Ant. Propagat*, pp 548–557, 1962.

[35] K. Sulonen, P. Suvikunnas, J. Kivinen, L. Vuokko, and P. Vainikainen, "Study of different mechanisms providing gain in MIMO systems," *Proc. IEEE 58th Veh. Technol. Conf.*, 2003.

[36] K. Kalliola, H. Laitinen, K. Sulonen, L. Vuokko, and P. Vainikainen, "Directional Radio Channel Measurements as Mobile Station in Dirfferent Radio Environments at 2.15 GHz," *4th European Personal Mobile Communications 2001 -Conference*, Austria, 2001.

[37] J. Kivinen, P. Suvikunnas, D. Perez, C. Herrero, K. Kalliola, and P. Vainikainen, "Characterization system for MIMO channels," *Proc. 4th Int. Symp. Wireless Personal Multimedia Communications*, pp. 159−162, 2001.

[38] K. Kalliola, H. Laitinen, L. Vaskelainen, and P. Vainikainen, "Real−time 3−D spatial−temporal dual−polarised measurement of wideband radio channel at mobile station," *IEEE Trans. Instrum. Meas.*, vol. 49, pp. 439−448, 2000.

[39] K. Sulonen, P. Suvikunnas, L. Vuokko, J. Kivinen, and P. Vainikainen, "Comparison of MIMO antenna configurations in picocell and microcell environments," *IEEE J. Select Areas Commun., special issue on MIMO systems and Applications*, vol. 21 (5), pp. 703−712, 2003.

[40] P. Suvikunnas, K. Sulonen, J. Villanen, C. Icheln, J. Ollikainen, and P. Vainikainen, "Evaluation of Performance of Multi-antenna terminals using two approaches," *IMTC 2004*, p. 6, Italy, 2004.

[41] C. E. Shannon, "A mathematical theory of communications: Parts I and II," *Bell Syst. Tech. J.*, vol. 27, pp. 379–423, 623–656, 1948.

[42] A. F. Molisch and M. Z. Win, "MIMO systems with antenna selection," *Microwave Magazine, IEEE,* vol. 5 (1), pp. 46−56, 2004.

[43] G. Lebrun, S. Spiteri, and M. Falkner, "MIMO complexity reduction through antenna

selection," *ANNAC' 03*, pp. 5, 2003.

[44] J. Thaysen, K. B. Jakobsen, "MIMO channel capacity versus mutual coupling in multi antenna element system," *Antenna Measurement Techniques Association, 26th Annual Meeting & Symposium*, Atlanta, GA, USA, pp. 124–129, 2004.

3 Antenna and antenna system minimisation for mobile phones – an overview

3.1 Introduction

During the past 20 years one of the trends in cellular-phone technology has been a dramatical decrease in the size and the weight of the handset. A reduction by a factor of ten or more in weight and volume has necessitated a rapid evolution of the antennas used for the handsets. This hampers the design of antennas that could maintain their performance unchanged, even though the antenna size became smaller, a degradation of the gain and bandwidth is inherently observed in small antennas. In view of the progress of small mobile terminals, the design of antennas is acquiring large importance. The antennas are required to be small, and yet to have prescribed characteristics and performance, such as wide bandwidth, operation in dual, triple or quad frequency bands, diversity, Multi-Input Multi-Output (MIMO) and so forth.

Several ways to reduce the antenna size exist. However, they are all at the expense of lower antenna gain and bandwidth [1]. This follows from the fact that an antenna is used to transform a bounded wave into a radiated wave [2]. An antenna performs this transformation, however, only with a poor efficiency when it is much smaller than the wavelength [3]. The loss in antenna gain can, to some extent, be compensated for by amplification. This is obviously not the case for the bandwidth. If the impedance match is much better than required in part of the required bandwidth, broadbanding techniques could be used to increase the bandwidth [4]. Parasitic elements have been used to enhance the bandwidth of PIFAs for many years (see, e.g., Sanad [5]). These techniques are also expected to be valid with the PIFA designs proposed by the author of this thesis, but will not be discussed further in this work. For a given cellular configuration, the design of the antenna should use the total volume available [6], [7]. There exist an upper theoretically limit of the antenna performance for a fixed volume occupied by the antenna. This limit, however, is seldom reached, and the design of small antennas is thus a trade-off between bandwidth and gain for the antenna chosen for a given application [8], [9]. Many authors have dealt with the issues regarding the minimisation of antennas suitable for cellular applications, recently published by, e.g., Skrivervik et al. [10].

A challenging task in minimising the antenna system is that the distance between the antenna and the other components, such as the loudspeaker and the camera, decreases as well. This motivates the need for information regarding how the antenna should be placed on the ground plane as well as the placement of other components with respect to the antenna and the ground plane. Reano et al. [68] uses phase-less near-field mapping of the electric and magnetic field distribution for diagnostic purposes and for overall understanding of operational behaviour of microwave/millimetre-wave circuits and radiating structures. It is found that field mapping of the electric field yields information regarding the resonant mode whereas magnetic field data provides insight into the location of large currents. Phase-less planar near-field antenna measurements could also be used to retrieve the near-field phase and subsequently perform near-field to far-field transformation [15], [16]. We propose the use of the raw unprocessed amplitude for diagnostic purposes [V], [17].

It is expected that high isolation between two or more frequency bands is essential in many future applications. The job is also motivated by the fact that applications such as, e.g., the separation into separate receiver and transmitter antenna, diversity and Multiple-Input Multiple-Output (MIMO) systems require extra antennas inside the mobile phone. Edvardsson

[18] has discussed the issues regarding the advantages and disadvantages regarding separate RX and TX antennas.

The task is complicated by the fact that the overall size of the mobile phone and the frequency separation between the different bands continues to decrease. In order to meet these demands, physically small antenna elements with low coupling are required. Therefore, information regarding how these antennas should be oriented in order to minimise the coupling is also needed [19], [VI]. Lui et al. [20] uses an LC resonator for multi-band purposes on a PIFA, Thaysen et al. [VII] suggest the use of a LC resonator for suppressing the mutual coupling.

For dipole, monopole, PIFA etc., size reduction can be accomplished, simply by shortening the antenna, however, at lengths shorter than the resonant length, the radiation resistance changes, and the impedance at the terminals of the antenna become reactive as well. The latter can be compensated for by the use of one or more inductors connected in series with the antenna for cancellation of the capacitance, and thus improve the impedance match [11], [61], and hence the efficiency [12]. Another method is top loading, which in practice means replacing the missing height by some sort of electrical circuit that has the same electrical characteristic as the missing part of the antenna [9]. The idea of using a lumped inductor or capacitor in conjunction with an antenna has often been used in connection with low frequency antennas where the physical size might be several hundred meters [9], but up to date it has found very little relevance in mobile telephony [13]. Capacitive load reduces the resonance length of the PIFA [14], [70] however at the expense of reduced radiation efficiency. In combination with capacitive loading by a distributed capacitor at the open end of the antenna arm the resonant length is decreased from $\lambda/4$ to less than $\lambda/8$ is reported by Rowell et al. [14]. This reduction demonstrates that compact antennas for mobile telephone handsets can be constructed using these approaches.

Diversity is a technique to overcome the effects of multipath fading and has been a topic of considerable interest to designers in the personal wireless communications industry for many years (see, e.g., Vaughan et al. [25]). For two antennas on a single receiver, the diversity performance is most commonly evaluated by investigating the correlation coefficient; a statistical value indicating the similarity in the signals received by the antennas. Because a great deal of literature exists that contains a statistical description of multipath fading fields as well as relations for the correlation coefficient [21], [25], [60], diversity will be treated as part of the MIMO system in this work.

Multiple-input multiple-output (MIMO) systems are very attractive in order to boost the capacity of a wireless communication system that operates in a rich multipath environment. The last few years, MIMO systems have received considerable attention due to the potential increase in capacity (see e.g., Foschini [22]). The theoretical capacity increases linearly with the number of antenna elements N in a (N, N) MIMO system [22]. However, in a more practical MIMO system the capacity is reduced due to correlation between the signals in the receiver [23]. Therefore, the correlation between the signals that are received from the different antenna elements is an important parameter in a MIMO system, due to the increased capacity for decreased correlation [75]. Vaughan et al. [25] has shown that the diversity gain of the mobile phone is not particularly sensitive to the envelope correlation, as long as the envelope correlation is less than 0.5. Even though, this motivates for low correlation it is not a guarantee for high capacity, since in some special cases, denoted “keyholes” lead to a drop in the capacity [26]. Imagine that the receiver and transmitter antennas are located in two clusters of buildings, in between almost line-of-sight properties. This gives rise to significant local scattering around both the transmitter and the receiver unit, causing uncorrelated fading at

each end of the MIMO link but the channels still have poor rank properties and hence low capacity; see, e.g., Jensen et al. [27] for a more thorough description of the "keyholes".

The expected linear capacity enhancement when the numbers of antennas are increasing motivates the use of more antenna elements. However, mutual coupling between the antenna elements affects the correlation [28] – [33]. For a mobile phone this inevitably causes higher mutual coupling due to the smaller distances between the antennas [19], [34]. The increased mutual coupling results in higher spatial correlation, which leads to a lower MIMO gain as compared to fully uncorrelated antenna signals [27]. Thus, information regarding how these antennas should be oriented in order to minimise the envelope correlation is needed [III].

The prototypes that are shown in all the papers by the author of this thesis [I] - [X] are simulated using the IE3D electromagnetic computer program [35]. The measured antenna characteristics are measured through a coaxial cable [36], [37]. The inner conductor is soldered directly to the feed point of the antennas; the outer conductor is connected to the back of the ground plane and attached via the centre of the long edge of the ground plane. In this way the coaxial cable affects the measurement results the least.

The Planar Inverted-F Antenna (PIFA) is widely used in cellular phones due to the compactness and size [38]. Therefore, the investigations presented here are primarily based on Planar Inverted-F Antennas (PIFA). The next section deals with size reduction techniques for mobile phone antennas, first using lumped inductors [VIII], secondly utilizing capacitive top loading [IX], both with respect to the PIFA. Thirdly, a proposal for using a one turn stub loaded loop patch antenna on a small ground plane is discussed [X]. Section 3.3 contains issues for reducing the mutual coupling between two PIFAs, first regarding the optimum distance and mutual orientation of the antennas [VI], secondly, by the use of a lumped LC filter circuit for a fixed distance between two antennas with different resonant frequency [VII]. A discussion regarding minimisation of the envelope correlation by proper distance and mutual orientation between the antennas is provided in Section 3.4 [III]. In section 3.5 the proposal of using the raw unprocessed electrical near field distribution to estimate the optimal location of metallic objects inside a mobile phone, objects such as cameras and loudspeakers, is discussed [V]. Section 3.6 covers the antenna performance when affected by artificial hand and head [IV]. The conclusions are drawn in Section 3.7.

3.2 Size reduction techniques for mobile phone antennas

The demand for smaller communication devices for personal communication systems has led to a constant search for methods to reduce the cellular phone dimensions. However, the wavelength does not decrease, due to the higher frequency bands used, with the same speed as the size of the mobile phones. Even a quarter wavelength antenna, such as the Planar Inverted-F Antenna (PIFA) tends to become too large, and thus a demand exists in order to decrease the volume of the PIFA. The loop antenna is an element that has often been used in pager devices, but up to date it has found very little use in mobile telephony. However, as the operational frequency of wireless communication devices moves into higher frequency bands, the size of the loop antenna decreases and the loop antenna becomes a viable antenna element for these applications. The simplicity in the analysis and construction of the simple planar one-turn loop antenna adds to its appeal.

Wong et al. [39] have proposed a modified PIFA, the PIFA arm is bend into a meandering structure for minimizing the occupied volume for a fixed antenna arm length. The result is a compact PIFA with a size that is half of the traditional, not meandered PIFA, i.e., $\lambda/8$.

However, the antenna arm length is still λ/4. The drawback in that design is the rather narrow frequency band performance that is obtained. The PIFAs proposed by Thaysen et al. [I - IX], [17], [19], [33], [61], [70] are long and thin, by meandering the structure it could be made more compact as well. Such volume optimisation is not discussed in further details in this thesis.

This section is divided into three subsections. In the first two subsections the results of the numerical and experimental investigations of the size reduction of a PIFA by the use of a lumped inductor [VIII] and by the use of a top loaded distributed capacitor [IX] are discussed. The third subsection deals with a one turn loop antenna loaded with a quarter wavelength matching line [X].

Antenna size reduction using lumped inductors

For monopole antennas, Hall et al. [9] has demonstrated that the highest advantage is obtained by placing the inductor at the centre of each antenna arm, instead of at the input, such discussions are also provided by Collin [13]. In this subsection, the discussion related to the results obtained by Thaysen et al. [VIII], [61] regarding both the location of the inductor as well as the inductance is presented. For many practical applications, it is more suitable to place the inductor almost at the input. In this way no inductors are located on the antenna element itself, but rather on the supporting structure or on the ground plane.

Thaysen et al. [VIII] provides two different tests, first, for a fixed location of the inductor, the inductance is varied between 5 nH and 100 nH. Then, the optimal location is found for a fixed inductance value. The results are based on numerical and experimental investigation of a 40 mm long, 1.5 mm wide and 5 mm high PIFA located on a 40 mm × 100 mm ground plan as illustrated in Figure 1. Low permittivity material ($\varepsilon_r = 1.06$) is used as the supporting structures of the antenna.

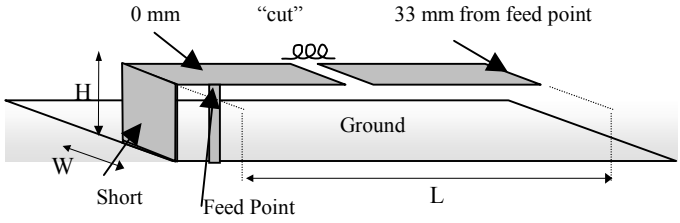

Figure 1. Illustration of the PIFA located above a ground plane, the cut illustrates the location of the lumped inductor.

Changing the inductor value between 5 nH and 100 nH for a fixed location 10 mm from the feed point, the centre frequency (min. $|S_{11}|$) drops from 1.8 GHz, towards 0.87 GHz for inductor values above 70 nH. However, for values above 35 nH the bandwidth is lower than the unloaded PIFA. This motivates for choosing an inductor value below 35 nH. Using a 5 nH inductor, the bandwidth is 2.3 times the bandwidth for the unloaded PIFA, this is due to the improved impedance match. Between 5 nH and 35 nH, the optimal inductor value is a trade-off between the decrease in centre frequency (min. $|S_{11}|$) and the actual bandwidth. Immediately, the optimal value is 20 nH. Here, the centre frequency (min. $|S_{11}|$) is lowered 30%, and the bandwidth is almost twice the bandwidth obtained for the unloaded 40 mm case.

The simulated results from the centre frequency, relative bandwidth, min. $|S_{11}|$, and the radiation efficiency versus the inductor location are shown in Figure 2 [VIII]. For a fixed inductor value of 20 nH an almost linear increase in the centre frequency (min. $|S_{11}|$) increases

from 1.2 GHz to 1.8 GHz, when the inductor is moved towards the open-end, from a position at 0.5 mm to 33 mm from the feed point. Locating the inductor at the very end of the antenna arm, i.e., 1 mm from the open end the reflection coefficient follows the same curve as the no-inductor-case. In addition, the peak efficiency is unchanged 85%. This was expected, since the current is zero at the end of the antenna arm, hence this validates the model. This motivates for locations as close to the feed point as possible. The peak radiation efficiency supports this as well.

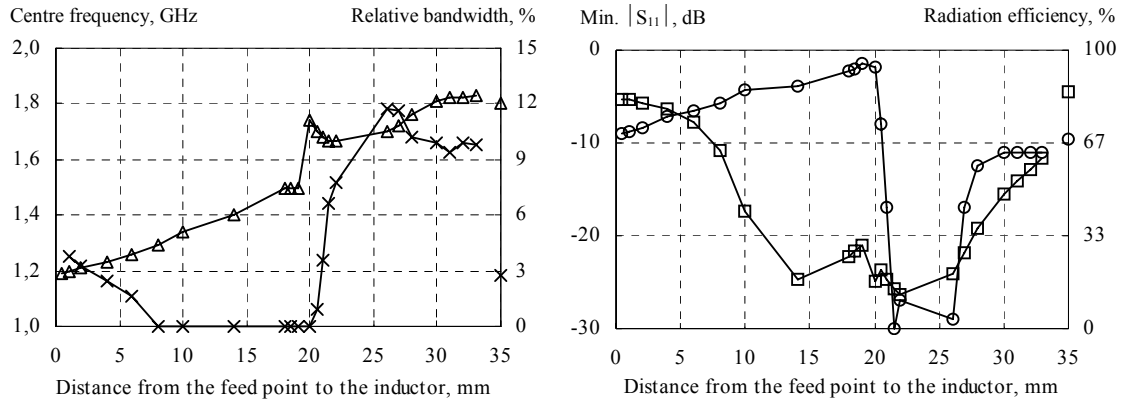

Figure 2. Simulated centre frequency (min. |S11|) (Δ), relative bandwidth (×), min. |S11| (°), and radiation efficiency (□) versus the inductor location. The values located on the 35 mm position referees to the unloaded 40 long PIFA.

The PIFA is basically an inverted-L antenna, that actually originates from a bended monopole; with the bend located such that most of the antenna arm is parallel to the ground plane. This means that the feed point is moved by a certain distance from the ground connection, here 5 mm from the bend and an additional 5 mm due to the antenna height. Meaning that the optimum location of the inductor is between 10.5 mm and 15 mm from the ground connection, i.e., almost one third the total length of 45 mm (length + height). Collin [13] argues that the optimum location of an inductor is at the centre of the arm of the monopole; of course, we cannot compare that directly to the PIFA. Nevertheless, this actually holds for the impedance match. If the inductor is located between 21 and 26 mm a rather good simulated impedance match is observed, below –25 dB, in this case the decrease in the frequency, with the lowest reflection coefficient, is not overwhelming, a reduction from 1.8 GHz to 1.7 GHz. Moreover, the radiation efficiency is below 25%. Despite the improved impedance, this could indicate that the optimum location for an inductor in the PIFA is closer to the feed point. Above 21 mm no significant frequency reduction is obtained, however at 30 mm the bandwidth is 200 MHz (13%), which is higher than the case of no inductor (50 MHz or 3%). However, locations near the open-end of the PIFA yield no size reduction. Thus, the higher bandwidth is at the expense of an inductor in terms of reduced efficiency and the cost of the inductor.

Antenna size reduction using capacitive top loading

By proper design, capacitive loading reduces the resonance length of the PIFA [14], [70], [IX]. A general degrade in the performance must be expected, especially in terms of a reduced radiation efficiency [14] and a decreased impedance match and hence a lower relative bandwidth [IX]. Collin [13] discusses the idea in connection to monopoles and dipoles, but here the use of top loading by a capacitor is adapted to the PIFA. For many practical applications, a lumped capacitor as well as a distributed capacitor could be used for top loading the antenna. Thaysen et al. [IX] proposes a distributed plate capacitor where the open

end of the PIFA forms one of the plates as illustrated in Figure 3. With both reduction techniques it is a trade-off between the actual requirement to the antenna performance and the cost of the antenna including the lumped or distributed components.

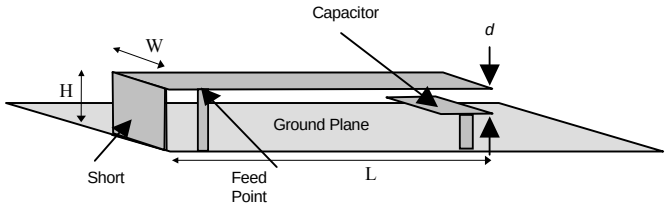

Figure 3. Illustration of the capacitor loaded PIFA located above a ground plane. The open end of the PIFA together with the plate forms the distributed capacitor.

The results presented by Thaysen et al. [IX] (the simulated ones shown in Figure 4) could be divided into two groups, the first for capacitances of values below 1.1 pF, second above 1.1 pF. For capacitances below 1.1 pF, the results are continuous and the best case with respect to the centre frequency (min. $|S_{11}|$) reduction, bandwidth and efficiency are obtained for a capacitance of approximately 1.1 pF. Here the simulated centre frequency (min. $|S_{11}|$) is decreased by 32% from 1.80 GHz to 1.22 GHz, the reflection coefficient is –12 dB, the bandwidth is 9% and the radiation peak efficiency is 91%. Measurements has verified the trends, however at somewhat lower values, most likely due to loss in the plate capacitor. Above 1.1 pF, the simulated as well as the measured results show rather decreasing performance in terms of poor impedance match, hence lower bandwidth and lower radiation efficiency. Therefore, capacitances close to 1.1 pF should be used.

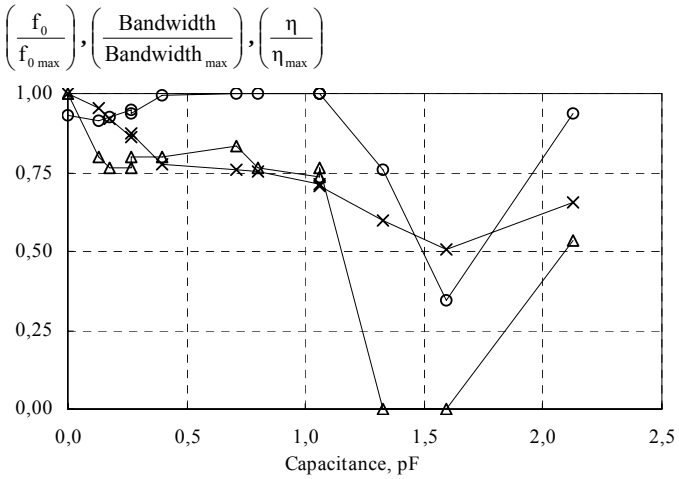

Figure 4. Simulated resonant frequency (×), bandwidth (Δ), and radiation efficiency (○). Data are normalised with the highest value in each data set value, respectively.

Capacitive loading by a 1.1 pF distributed capacitor at the open end of the antenna arm the resonant length is decreased from λ/4 to approximately λ/6 [IX]. In combination with capacitive loading by a distributed capacitor at the open end of the antenna arm the resonant length is decreased from λ/4 to less than λ/8 as demonstrated by Rowell et al. [14]. These results demonstrate that compact antennas for mobile telephone handsets can be constructed using capacitive top loading. Rowell et al. [14] has found that an optimal value of the distributed loading capacitor is approximately 1.4 pF; this is a slightly higher capacitance as compared to the optimal value found by Thaysen et al. [IX], being 1.1 pF. However, the capacitance found by Thaysen et al. [IX] is calculated under the assumption that the relative

permittivity ε_r is set to one, even though that sticky tape is used as the spacer in the prototype. This assumption means the actual capacitance values are somewhat higher than the capacitance values stated by Thaysen et al. [IX].

The key results from the capacitor-loaded antenna [IX] and from the 40 mm long inductor loaded antenna [VIII] could be compared in Table 1 with a 60 mm long unloaded PIFA that has the same centre frequency as the two 40 mm long loaded PIFAs.

Table 1. Major specifications and key results of the three different antennas.

Principle		Unloaded PIFA 60 mm long	Top loaded with a capacitor	Inductor loaded near feed point
Centre frequency (min. $\|S_{11}\|$)		1.20 GHz, sim. 1.07 GHz, meas.	1.22 GHz, sim. 0.99 GHz, meas.	1.20 GHz, sim. 1.08 GHz, meas.
Loading value			1.1 pF	20 nH
PIFA element length		60 mm	40 mm	40 mm
PIFA element height		5 mm	5 mm	5 mm
PIFA element wide		1.5 mm	1.5 mm	1.5 mm
Efficiency, within BW where $\|S_{11}\|$ <-6 dB, meas.		>55%	>65%	>65%
Size ground plane			40 mm × 100 mm	
BW S_{11}>-6 dB	Measured	7.3% (78 MHz)	none	6.7% (71 MHz)
	Simulated	9% (150 MHz)	9% (110 MHz)	3.9% (45 MHz)
Radiation Pattern		Almost identical for all three prototypes		
Max gain		3.9 dBi	2.1 dBi	3.3 dBi
Size or centre frequency reduction, as compared to the unloaded 40 mm long PIFA			32%, sim. 39%, meas.	33%, sim. 34%, meas.

Comparing the 60 mm long unloaded PIFA with the two 40 mm long loaded antennas, it could be seen (in Table 1) that the advantages by reducing the size is a trade-off to the decreased bandwidth. The 18 nH inductor yields the same frequency reduction as the 1.1 pF capacitor, however with a higher gain. This might be due to the sticky tape used as a separator in the capacitor.

A measured 39% reduction of the centre frequency (min. $|S_{11}|$) is accomplished by using an 1.1 pF distributed capacitor, that is formed by a 4 mm × 1.5 mm plate located 0.1 mm below the open end of the PIFA, in between the ground plane and the PIFA. The 1.1 pF distributed capacitor is used in addition to a 5 mm high 0.3 cm^3 PIFA located on a 40 mm × 100 mm ground plane. One drawback is the increased complexity and hence the price of the antenna system.

For the 60 mm long PIFA without any inductor the measured centre frequency (min. $|S_{11}|$) is 1.06 GHz having a peak return loss of 16.5 dB. The bandwidth is 7.3% (78 MHz). The measured efficiency is above 65% within this frequency range of interest. The best case with respect to centre frequency (min. $|S_{11}|$) reduction is obtained when a 20 nH lumped inductor is placed within the first few millimetres from the feed point. Here the measured frequency point with the lowest reflection coefficient is decreased by 33% from 1.60 to 1.06 GHz, the reflection coefficient is –16.5 dB, the measured –6 dB bandwidth is 6.7% (71 MHz), within which the efficiency is above 60%. The major benefit is the reduced size for a fixed centre

frequency (min. $|S_{11}|$), however it is at expense of reduced efficiency and reduced bandwidth. By the use of inductor or capacitor loading it is shown that for a fixed size the centre frequency (min. $|S_{11}|$) can be decreased. The principle could also be used for a fixed frequency and hence a 30% to 40% size reduction is expected. Collin [13] shows that from a theoretical point of view the inductor loading principle yields better antenna performance as compared to the capacitive top loading principle when applied to small antennas with triangular current distribution.

Combining the antenna loading techniques with the meander principle might lead to a further reduction in the occupied volume for the antenna. The proposed meandered PIFA [39] has a length that is half the resonant length. Applying the same meandering technique, the size of the proposed inductor loaded PIFA [VIII] and the top-loaded PIFA [IX] might be reduced to $\lambda/12$.

One turn stub loaded loop patch antenna on a small ground plane

The loop antenna is an element that has often been used in pager devices, but up to date it has found very little use in mobile telephony. However, as the operational frequency of wireless communication devices moves into higher frequency bands, the loop becomes a viable antenna element for these applications, since its physical size becomes small enough for modern mobile phones [X]. The simplicity in the analysis and construction of the simple planar one-turn loop antenna adds to its appeal. Proposals for using loop antennas for mobile phones are discussed by, e.g., Li et al. [40] and Katsibas et al. [41]. A size comparable one turn loop antenna proposal is shown by Li et al. [40], it provides a 24% bandwidth. However, since it is an external antenna, and without any ground plane it is not suitable for the purpose of this research. Morishita et al. [42] relates the influence of the body effect to the antenna performance. It is shown that the degradation of gain at the talk position could be reduced by use of the balanced antenna structure as compared with an unbalanced antenna structure.

The technique of incorporating a ground plane on a one-turn loop for improvement of performance has been published by Balanis [43]. It is demonstrated that the size of the reflector, the distance between the loop and the reflector is a factor, which can significantly change the performance of the loop antenna. The parameters that are mostly affected are the pattern, directivity, input impedance, and antenna efficiency. Adding a reflector makes the loop into a microstrip patch antenna, which lowers the resonant frequency of the loop, and thus reduces the required antenna size for a fixed operating frequency. However, owing to the antenna size reduction, the antenna bandwidth is also decreased.

Altshuler [44] has shown some tests on a monopole loaded with a loop antenna. This idea is used opposite by Thaysen et al. [X], [45], i.e., a loop loaded with an open-ended quarter wavelength matching line, as illustrated in Figure 5. Dielectric loading of antennas reduces the resonant frequency of a patch antenna [46]. Both the permittivity and the thickness of the substrate affect the performance. The loss in the material will alter the performance as well, and substrate materials with low loss are to be preferred. Another disadvantages are that higher permittivity substrates tend to be heavier. By adding a ground plane to the loop, and thus transforming the loop antenna into a patch antenna, the bandwidth could be improved by adding a quarter wavelength open matching line.

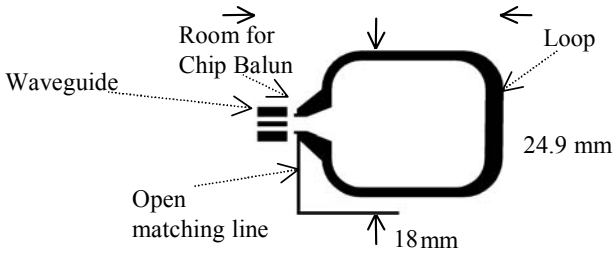

Figure 5. The loop antenna including the coplanar waveguide connection for the balun.

Thaysen et al. [X] have demonstrated that a wideband, small microstrip loop antenna with near omni directional radiation patterns can easily be implemented by loading the antenna with a quarter wavelength open matching line in addition to the high permittivity substrate layer [44], [46]. Almost symmetrically radiation in both front and back direction is obtained, meaning that the ground plane actually is a part of the structure and does not act as a reflector. Due to limitations in the simulation program, infinite extent of the dielectrically layer is the only option [35]. Hence, no radiation is obtained in the $\theta = 90°$ direction. In practice radiation will occur in this direction as well. The loop antenna is a balanced structure, thus a balanced feed is required. This could be accomplished by the use of chip balun, however various other types could be used, e.g., [47] – [56].

The best case with respect to bandwidth is obtained when the matching line is 18.5 mm. Here the resonant frequency is 2.04 GHz, the return loss is 14 dB and the relative bandwidth is 14.5% [X]. At the resonant frequency, the matching line acts as a quarter wavelength line. A proposal for a loop antenna located 2.5 mm above a ground plane, separated by a dielectric loaded substrate with a resonant frequency of 1.45 GHz is presented by Thaysen et al. [45]. The antenna is simulated and the results are very promising, simulated bandwidth of 9.6% being obtained.

The antenna is designed with size as one of the driving parameters; therefore, the obtained bandwidth is compared to the theoretical obtainable bandwidth calculated using the Q values for the antenna. Many authors have dealt with minimum Q values for small antennas, recently reviewed by Thiele [57]. The simulated relationship between the bandwidth versus Return Loss differs with a few percent from the theoretical result, but follows a somewhat similar decreasing trend see Figure 6. One reason for the deviation obtained is due to the simple RLC circuit model used, as well as the loss less environments that are assumed. The simulated results include dielectric and conductor loss. However, the obtained result indicates that the suggested antenna has a performance that is close to the highest possible expected from the RLC circuit model principle.

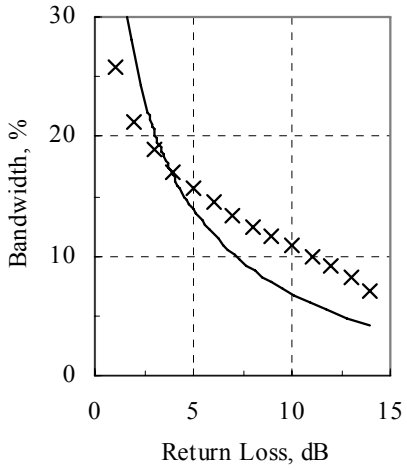

Figure 6. Theoretical (solid) and simulated (×) bandwidth versus the Return Loss.

The shape of the loop antenna element is optimised and the matching line is bend in order to minimise the occupied area. This, also, increases the conducting material inside the minimum sphere, which lowers the Q value and thus optimises the bandwidth. For practical use both the shape of the loop and the length of the matching line should be carefully chosen in order to get the best frequency (bandwidth) performance for a given application.

3.3 Reduction of mutual coupling between Planar Inverted-F Antennas

The mutual coupling between two antennas could be reduced simply by increasing the distance between the antennas [74]. This is, however, not possible due to the rather small volume of a modern mobile phone. However, their mutual orientation and localisation on the ground plane might be topics that could be optimised [VI]. Thaysen et al. [VII] has shown that an LC resonator could also reduce the coupling between antennas. However, this approach requires that the antennas have sufficiently different resonant frequencies.

Optimum distance and mutual orientation

The main objective of the work presented by Thaysen et al. [VI] is to explain the coupling between two identical PIFA antennas. Symmetrical as well as unsymmetrical coupling scenarios using two identical PIFAs located close to each other is investigated, in order to determine the mutual coupling versus distance for fixed orientations (see illustration in Figure 7), and mutual coupling versus rotation of the antennas for fixed distance. The results illustrate how to orientate and locate the antennas in order to minimise the coupling. The effect on mutual coupling between two identical antennas is recently published by Carrasco et al. [58], the results are in accordance with previous work by the authors of this work [19].

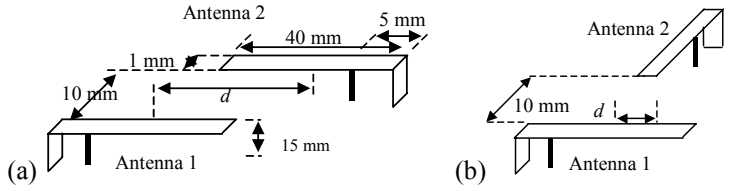

Figure 7. Illustration of the different configurations that are investigated (with a horizontal distance, d, defined so that d is positive in the case illustrated in (a).

To analyse the performance of the PIFA located above an infinite plane conductor, the image theory will be introduced to account for the reflections. The PIFA could be assumed to consist of two radiating components, namely the feed line (and the shorting pin) and the patch itself, the feed line being vertical, the patch horizontal. For an incident electric field with vertical polarisation, the polarisation of the reflected waves must also be vertical and with a polarity in the same direction as that of the actual source to satisfy the boundary conditions. For the radiating element in a horizontal orientation, it follows that the image is placed at a separation equal to the antenna height below the interface with a 180° phase difference relative to the actual source. The radiation from the horizontal element and its image cancels in the plane of the ground plane; thus major parts of the radiated field originate from the feed line.

This explains the rather low change in the field as a function of the mutual orientation, as illustrated by Thaysen et al. [VI]. This is also in accordance with the fact that the strongest coupling is found when the PIFAs are orientated such that the shorting pins are located in the opposite ends, i.e., maximum separation. For the setup of mutual rotation of the PIFAs the expected inverse proportionality between the coupling and the separation is not easily identified. However, the results indicate that it is most likely the distance between the open ends of the PIFAs that dictates the coupling, as shown in Figure 8. Thus, minimum coupling between two identical PIFAs is obtained when they are oriented such that the separation between the open ends are maximised. Thus, it was found that choosing configurations that maximise the separation between the open-end of the PIFAs could reduce the mutual coupling [VI]. The difference between the highest and lowest coupling is 5 dB in the case where the antennas are separated by 50 mm. This difference is reduced for increased distance; at 200 mm separation the mutual coupling differs by 1.5 dB, only. Hence, by proper orientation of the antennas the mutual coupling could be reduced.

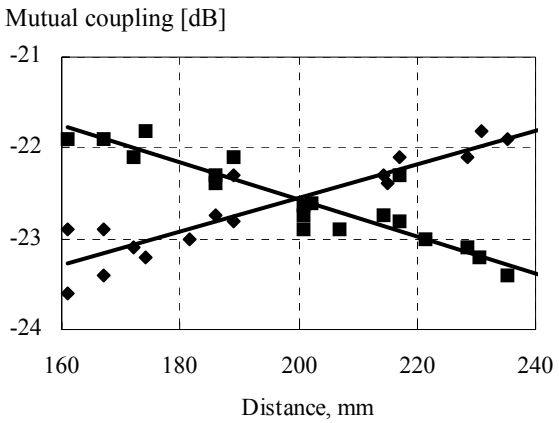

Figure 8. Simulated coupling as a function of the separation between the open ends (■) and short pins (♦) of the two PIFAs.

It is found that the coupling is generally a few dB lower for the orthogonal than for the parallel cases. The lower coupling might be due to the increased separation between the feed lines. This may be because the orthogonal cases yield larger separations between the feed lines as compared with the distances obtained in the parallel cases. In addition, the polarisation of the PIFAs affects the coupling as above mentioned. The lowest coupling is obtained for the configuration where the open end of antenna 1 is closest to antenna 2, which is orthogonal located with respect to antenna 1 (c.f. Figure 7a). The overall conclusion is that both (the) orientations as well as the separation are important factors regarding coupling.

Mutual coupling reduction using a lumped LC circuit

In Thaysen et al. [VII] the antenna system consists of two separate antennas, one for each of two frequency bands, that is denoted LB (low band) and HB (high band), see Figure 9. For an antenna system consisting of more than one antenna, mutual coupling occurs. Here, a resonant LC circuit, consisting of a capacitor and an inductor, is used to reduce the mutual coupling. Hall ed. [9] describes a resonant circuit useful for multi-band performances. By using tuned circuits of appropriate design strategically placed in a dipole, the antenna can be made to show what are essentially fundamental resonances at a number of frequencies. More recently, e.g., Lui et al. [20] has investigated a distributed LC circuit for single feed dual frequency PIFA designs. The same principle could be used to minimize unwanted coupling between two antennas. For example, if an LC circuit, that is placed at the feed end of antenna 1, is chosen to be resonant at the frequency where antenna 2 is resonant, then antenna 2 is effectively isolated from antenna 1, thus the coupling is minimised, it was verified by Thaysen et al. [VII]. The second function of the LC circuit is electrical loading, which is obtained when the frequency of operation is not at the resonant frequency of the LC circuit. If the operating frequency is below that of the LC circuit resonance, which is the case here, the LC circuit behaves as an inductor. If the operation frequency is above the resonant frequency, it acts as a capacitor. Inductive loading will electrically lengthen the antenna, and capacitive loading electrically shorten the antenna.

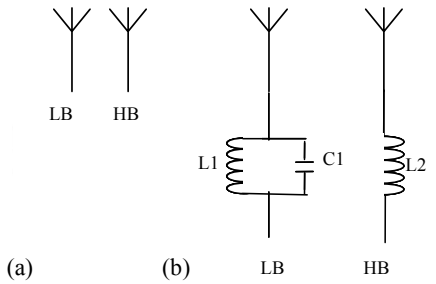

Figure 9. The unloaded PIFA (a) and LC loaded PIFA and the inductor matched PIFA (b).

Thaysen et al. [VII] use a lumped resonant LC circuit for decreasing the mutual coupling by 14.4 dB, and increasing the radiation efficiency by 16.4%. The drawback that has to be taken into account is the increased complexity and hence the price of the antenna system.

In the low frequency band, no significant changes occur by adding a LC circuit. It should be noted that the observed improved coupling and peak reflection coefficient do not lead to higher radiation efficiency. This is due to the insertion loss in the components used for the LC circuit.

By the use of the LC circuit, and hence lower the coupling between the antennas, it is possible to reduce the overall volume necessary for two antennas, since they can be spaced closer and still have a high radiation efficiency.

3.4 Reduction of the envelope correlation

In Thaysen et al. [III] the relation between the mutual orientations, the location, the mutual coupling and the envelope correlation between two identical antennas are investigated (see illustration in Figure 7). The calculation of the antenna correlation can be approached in different ways, one is based on the far-field pattern [25], and another is based directly on the scattering parameters at the antenna terminals [59]. The envelope correlation is determined

from the distribution of the external sources and the radiation pattern from the antennas. Only by assuming omni-directional source distribution one can relate the mutual impedances (or scattering parameters) to the correlation [60]. This means that the envelope correlations estimated based on S-parameters [59] corresponds to that based on the radiation pattern [25] if a uniform distribution of the sources is assumed. Given that the investigation is to design practical antenna system for MIMO (e.g. on a mobile phone), the uniform distribution of the sources assumed in the envelope correlation expression may be inadequate. Therefore, it should be clearly pointed out, that this formulation could not replace completely the pattern correlation (as a quality criterion) in the case of small terminal antennas. This is mainly due to the reason, that the mutual coupling is a near-field effect whereas the pattern correlation is a pure far-field effect. The radiation pattern based method gives us the possibility to include a better description of the radio channel in the evaluation, although it makes the evaluation more cumbersome. Thaysen et al. [III] use the scattering parameters method for calculating the envelope correlation since this is a time saving methods. Further discussions related to the envelope correlation could be found in Chapter 2 of this Thesis (i.e., [XI]).

Symmetrical as well as unsymmetrical coupling scenarios using two identical PIFAs located close to each other are investigated (see Figure 7), in order to determine the complex envelope correlation squared versus distance for fixed orientations, and mutual coupling versus rotation of the antennas for fixed distance. The results illustrate how to orientate and locate the antennas in order to minimise the complex envelope correlation squared.

An almost exponential relation between the mutual coupling and the envelope correlation is found [III]. The envelope correlation versus mutual coupling for the orthogonal scenario is shown in Figure 10, more examples could be seen in [III]. A certain limit of the mutual coupling of –10 dB is found, below the limit the envelope correlation is almost constant, being ρ_e = 0.15, and therefore effort in decreasing the mutual coupling should be limited to this level. As long as the envelope correlation is less than $\rho_e < 0.5$ diversity gain could be obtained in a mobile phone [25].

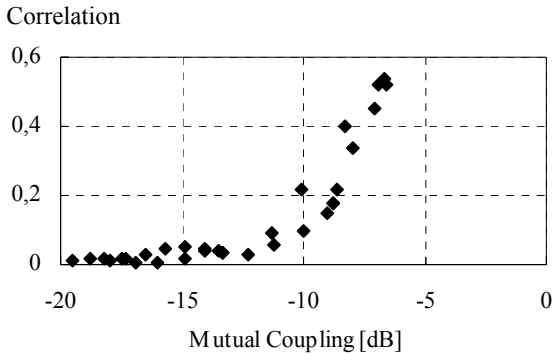

Figure 10. Envelope correlation versus mutual coupling for the orthogonal scenario. Antenna 2 is fed at the bottom, i.e., closest to antenna 1 (c.f. Figure 7).

Two different cases are investigated; one with parallel PIFAs another with orthogonal orientation. For the parallel case with 10 mm separation, it is found that the envelope correlation is ρ_e = 0.8 and simply by rotation one of the antennas 180 degrees, the envelope correlation decreases to ρ_e = 0.4. Similar to orthogonal antennas set-up, here the envelope correlation decreases. A decrease from ρ_e = 0.5 to ρ_e = 0.25 is observed. For the orthogonal set-ups the highest envelope correlation is obtained when the open end and the feed line are vertically on line.

3.5 Antenna location inside a mobile phone

One of the challenging task in minimising the mobile phone, and hence the antenna system is that the distance between the antenna and the other components, such as the loudspeaker and the camera, decreases as well. This motivates the need for information regarding how the antenna should be placed on the ground plane as well as the placement of other components with respect to the antenna and the ground plane. Another important factor that also motivates to the investigation of the near-field from cellular phones is the specific absorption rate (SAR), which is a measure of the energy absorbed by the human tissue. With the increase in the current distribution on the ground plane inside the handsets, the radiation toward the human head may increase, and so would the SAR. To reduce the undesired radiation toward the human head, and thus the SAR value in the head, the appropriate selection of antenna type, the method of feeding it, and the place and method of mounting the antenna element on the equipment, should all be seriously considered, see, e.g., Sager et al. [71]. The SAR issue is not discussed in further details in this thesis.

Thaysen et al. [V] investigate the location of small metallic objects with respect to the antennas on the ground plane using the raw unprocessed electric near-field distribution.

One way to obtain this kind of information is with planar near-field measurements [17], [62]–[65]. Usually the electric near-field is transformed to far-field data, nevertheless it is the raw unprocessed near-field data that is presented and used in Thaysen et al. [V]. The electric field distribution is measured in a measurement plane that is λ/61 [66], [67] from the radiating structure it is the same distance used by Reano et al. [68]. The purpose of Thaysen et al. [V] was to determine whether the raw unprocessed near-field data could be used as a design parameter. Visualising the results using the raw data of the electric near field gives rise to a rather subjective evaluation. Nevertheless, this information could be used when one has to place two or more antennas within the same phone. The result could also be used to explain, and thus indicate how to minimise the mutual coupling between the antenna elements. In Figure 11 the simulated reflection coefficient of antenna 2 is shown and could be compared in a more objective manner. The results for antenna 2 is chosen instead of that from antenna 1 since the largest deviation in the reflection coefficient is observed for antenna 2. Minor change in the resonant frequency are observed when locating the metallic cube nearest to the shorting pin of the PIFA, i.e., at (x, y) = (27, 7) the resonant frequency is 1945 MHz, as compared to the resonant frequency of antenna A2 in the original case (1940 MHz). A decrease in resonant frequency to 1920 MHz is observed when the metallic cube is moved towards (x, y) = (0, 7).

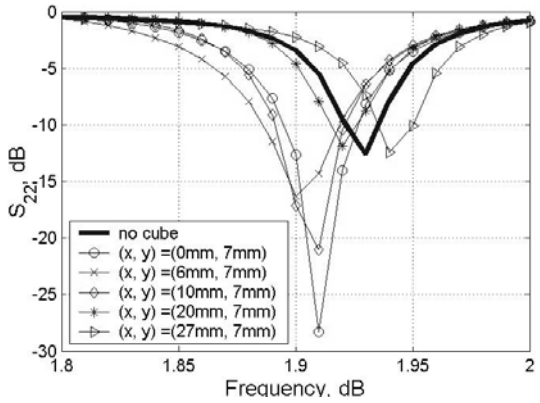

Figure 11. Simulated reflection coefficient for antenna 2 for different location of the metallic cube compared to the case of no metallic cube (wide line).

Thaysen et al. [V] have shown that metallic objects that are placed in the regions above the ground plane where the field intensity is the lowest affect the antenna performance the least. Hence, the optimal location of a metallic object, which might be a camera or a loudspeaker, could be determined directly from the raw unprocessed electric near-field distribution. From the shape and colour (amplitude) of the total electric field it is concluded by Thaysen et al. [V] that locating the metallic cube close to the feed point affects the near-field the least. Most affected is the case where the metallic cube is located nearest the open end of the PIFA arms. Thus, from Thaysen et al. [V] it is concluded that metallic objects should be located in areas having a local minima in the electric field amplitude of the total field, and one should maximise the distance between the metallic object and the open end of the radiating element.

3.6 Antenna performance when affected by artificial hand and head

A three-antenna configuration that is mounted in a realistic mobile phone consists of three PIFAs is proposed in Thaysen et al. [IV]. Placing the phone in talk position, i.e., beside an artificial hand and head, the free space antenna performance is affected. The total electrical field components of the measured radiation patterns at a frequency of 1.8 GHz are shown in Figure 12 in a conventional (r, θ, ϕ) spherical coordinate system. It could clearly be observed that the artificial head as well as the artificial hand affects the radiation performance in terms of reduced amplitude these directions. The reflection coefficients are degraded and the mutual coupling is improved due to the mismatch attached to the hand and head. In addition, the radiation efficiency is affected: Antenna 1 and antenna 2 have free space efficiencies above 15% between 1.7 GHz and 1.9 GHz and peak efficiencies around 37% around 1.75 GHz. Antenna 3 peaks at 1.8 GHz with an efficiency of 30%. The results for radiation efficiency have shown that close to half of the energy is absorbed by hand and head, Morishita et al. [42] has reported similar tendencies.

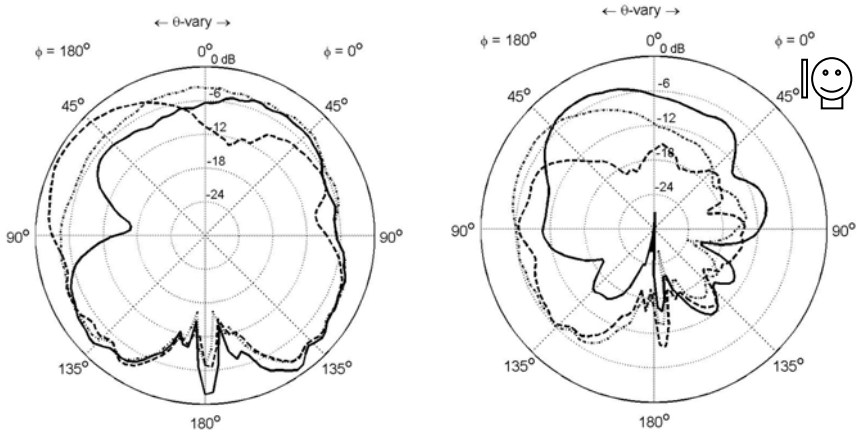

(a) (b)

Figure 12. Measured free-space θ-cuts for ϕ = 0° (a), and beside hand and head (b). Antenna 1 (solid), antenna 2 (dotted), and antenna 3 (dashed), The vignettes illustrate the orientation of the three-antenna configuration with respect to the artificial head.

Morishita et al. [72] report that more than 6 dB gain degradation has been observed in the talk position of mobile phones, mainly due to the effect of a user's hand. A hand holding a handset varies the currents on the ground plane, and thus the impedance and frequency, so that antenna gain and efficiency deteriorate. The human head, when the handset is in a talk position, also

varies antenna performance in the same way, as the hand does. Both the hand and the head, which absorb radiation power, also cause a decrease in the antenna's gain. Even though the results obtained by Morishita et al. [72] are based on simulations and a rather simple model is used for both the hand and head, the gain degradation is comparable to the gain reduction stated by Thaysen et al. [IV]. However, the results provided by Thaysen et al. [IV] are based on talk position measurement on a prototype, i.e., measured beside an artificial hand and head. Many authors (for example, Jensen et al. [73]) have reported comparable human body effects on mobile phone handset antenna performance as well.

The calculated envelope correlation is lowered considerably due to the changed scattering parameters. Placing the antennas next to the hand and head affects the radiation pattern, especially in the $\theta = 90°$ plane for $\phi = 0°$ and $\phi = 90°$. The radiation in the direction of the artificial hand are most affected, especially the radiation from the antenna that is mounted in the bottom of the phone, here the artificial hand covers the antenna fully. These tendencies are valid at other mobile frequency bands as well see, e.g., Toftgard et al. [69]. Despite the rather large degradation of the antenna performance when the phone is mounted in talk position, the capacity is only affected by 2.8%; a drop from 7.1 bit/s/Hz to 6.9 bit/s/Hz is accomplished; see Thaysen et al. [IV] for further details.

3.7 Conclusion

This Chapter has provided an overview of different techniques to reduce the size of mobile phone antennas and mobile phone antenna systems that consist of more than one antenna. Issues regarding size reduction of a PIFA accomplished by inductive or by capacitive loading is discussed. Proposal for using a balanced dielectric loaded loop antenna loaded with a quarter wavelength open stub microstrip line is given.

Furthermore, guidelines for reducing the mutual coupling and the envelope correlation between identical PIFAs with completely frequency overlap are discussed in terms of separation and mutual orientation. This overview has shown that a LC resonator could be used for multi-band performance as well as a filter for reducing the mutual coupling between two antennas with different resonant frequency.

The advantages and disadvantages for estimating the optimal location of small metallic objects with respect to the antennas on the ground plane that is investigated using the raw unprocessed electrical near field distribution are given.

Numerical and experimental techniques have been applied to the situation where a mobile phone is close to an artificial hand and head. The influence on radiation pattern, input impedance, radiation efficiency, and far-field radiation pattern has been discussed. It should be noted that the capacity could be almost unaffected even though a rather large degradation of the antenna performance when the phone is mounted in talk position is observed.

3.8 References

The references referred to in the text by their Roman numerals are found on page v in the beginning of this thesis.

[1] R. F. Harrington, "Effect of antenna size on gain, bandwidth and efficiency," Journal of research of national bureau of standards, D-radio Propagation, vol. 64D, pp. 1–12, 1960.

[2] "The IEEE standard definitions of terms for antennas," *IEEE Trans. Antennas and Propagat*., vol. 17, 1969.

[3] R. C. Hansen, "Fundamental limitations in antennas," *Proc. IEEE*, vol. 69, 1981.

[4] H. A. Wheeler, "The wide-band matching area for a small antenna," *IEEE Trans. Antennas and Propagat*., vol. 31, pp. 364–367, 1983.

[5] M. Sanad, "A wide band microstrip antenna for portable cordless telephones," *Proc. of Antennas and Propagat*., 1995., vol. 2 , pp. 18–23, 1995.

[6] L. J. Chu, "Physical limitations of omnidirectional antennas," *J. App. Phys*., vol. 19, pp. 1163–1175, 1948.

[7] J. S. McLean, "A re-examination of the fundamental limits on radiation Q of electrically small antennas," *IEEE Trans. Antennas Propagat.,* vol. 44, pp. 672–675, 1996.

[8] H. A. Wheeler, "Fundamental limitations of small antennas," *Proc. IRE*, vol. 35, pp. 1163-1175, 1947.

[9] G. Hall (ed.), "*The ARRL antenna book*," 15th Edition, Third printing, Chap. 7, ISBN 0-87259-206-5, 1990.

[10] A. K. Skrivervik, J-F Zürcher, O. Staub, and J. R. Mosig, "PCS antenna design: The challenge of miniaturization," *IEEE Trans. Antennas Propagat.*, vol. 43, pp. 12–27, 2001.

[11] C. W. Harrington, " Monopole with Inductive Loading," *IEEE Trans. Antennas Propagation*, pp. 394–400, 1963.

[12] G. S. Smith, "Efficiency of electrically small antennas combined with matching networks," *IEEE Trans. Antennas Propagation*, vol. 25, pp. 369–373, 1977.

[13] R. E. Collin, "*Antennas and radiowave propagation*," McGraw-Hill, ISBN 0-07-011808-6, pp. 97–104, 1985.

[14] C. R. Rowell and R. D. Murch, "A compact PIFA suitable for dual-frequency 900/1800-MHz Operation," *IEEE Trans. Antennas Propagat.*, vol. 46, pp. 596–598, 1998.

[15] R. G. Yaccarino and Y. Rahmat-Samii, "A comparison of conventional and phaseless planar near-field antenna measurements: The effect of probe position errors," *Proc. 2000 IEEE International Conference on Phased Array Systems and Technology*, pp. 525–528, 2000.

[16] S. Costanzo and G. D. Mossa, "An integrated probe for planar near-field only intensity measurements," *Proc. IEEE Antennas and Propagat. Symposium*, pp. 614–617, 2001.

[17] J. Thaysen, K. B. Jakobsen, "Near field Distribution from a Planar Inverted-F Antenna," *Proc. of Twelfth International Conf. on Antennas & Propagation*, Univ. of Exeter, UK, pp. 4, 2003.

[18] O. Edvardsson, "Will active antenna modules revolutionize mobile phones antennas?" *Proc. 11th International Conf. on Antennas & Propagation*, pp. 236–240, 2001.

[19] J. Thaysen, "Mutual Coupling Between Two Identical Planar Inverted-F Antennas," *Proc. IEEE Antennas and Propagation Society International Symposium,* pp. 504–507, vol. 4, 2002.

[20] K. H. Lui and R. D. Murch, "Compact dual-frequency PIFA designs using LC resonators" IEEE Trans. AP, vol. 49, pp. 1016–1019, 2001.

[21] M. A. Jensen and Y. Rahmat-Samii, "Performance analysis of antennas for hand-held transceivers using FDTD," *IEEE Trans. Antennas Propagat.,* vol. 42, pp. 1106–1113, 1994.

[22] G. J. Foschini and M. J. Gans, "On limits of wireless communications in a fading environment when using multiple antennas," *Wireless Pers. Commun.*, vol. 6, pp. 311–335, 1998.

[23] R. Janaswamy, “Effect of Element Mutual Coupling on the Capacity of Fixed Length Linear Arrays,” *IEEE Antennas and Wireless Propagat. Lett*, vol. 1, pp. 157–160, 2002.

[24] R. G. Vaughan, “Signals in Mobile Communications: A Review,” *IEEE Trans. Veh. Technol*., 35, pp. 133–145, 1986.

[25] R. G. Vaughan and J. Bach Andersen, “Antenna diversity in mobile communication,” *IEEE Trans. Veh. Technol*., 36, pp. 149–172, 1987.

[26] D. Chizhik, F. Rashid-Farrokhi, J. Ling, and A. Lozano, “Keyholes, correlations, and capacities of multielement transmit and receive antennas,” *IEEE Ant. Trans. Wireless Commun.*, pp. 361–368, 2002.

[27] M. A. Jensen and J. W. Wallace, “A review of antennas and propagation for MIMO wireless communications,” *IEEE Trans. Antennas propagat*., vol. 52 (11), pp. 2810–2824, 2004.

[28] D. Chizhik, F. Rashid-Farrokhi, J. Ling, and A. Lozano, “Effect of antenna separation on the capacity of BLAST in correlated channels,” *IEEE Commun. Lett.,* vol. 4 (11), pp. 337–339, 2000.

[29] A. Derneryd, and G. Kristensson, “Signal correlation including antenna coupling,” *Electron. Lett.,* Vol. 40 (3), pp. 157–158, 2004.

[30] M. Karaboikis, C. Soras, G. Tsachtsiris, and V. Makios, “Compact dual-printed inverted-F antenna diversity systems for portable wireless devices,” *IEEE Ant. Wireless Propagat. Lett*, pp. 9–14, 2004.

[31] B. Clerckx, D. Vanhoenacker-Janvier, C. Oestges, and L. Vandendorpe, “Mutual coupling effects on the channel capacity and the space-time processing of MIMO communication systems,” *Commun., ICC '03. IEEE Int. Conf. on,* vol. 4, pp. 2638–2642, 2003.

[32] J. W. Wallace and M. A. Jensen, “The Capacity of MIMO wireless systems with mutual coupling,” *IEEE VTC’ 03*, pp. 696–700, 2002.

[33] J. Thaysen, K. B. Jakobsen, “MIMO channel capacity versus mutual coupling in multi antenna element system,” *Antenna Measurement Techniques Association, 26th Annual Meeting & Symposium*, Atlanta, GA, USA, pp. 124–129, 2004.

[34] O. Edvardsson, “Can two antennas be smaller than one?” *Proc*. *ICAP 2001*, pp. 533–536, 2001.

[35] “IE3D User’s Manual, Release 8,” Zeland Software, Inc., Fremont, CA, 2001.

[36] www.hp.com.

[37] www.satimo.com.

[38] K. Hirasawa and M. Haneishi, “Analysis, design, and measurement of small and low profile antennas,” Artech House, ISBN 0-89006-486-5, 1991.

[39] K.-L. Wong, K.-P. Yang, “Modified planar inverted F antenna,” *Electron. Lett.*, vol. 34 (1), pp. 7–8, 1998.

[40] R. L. Li, E. M. Tentzeris, J. Laskar, V. F. Fusco, and R. Cahill, “Broadband loop antenna for DCS-1800/IMT-2000 Mobile Phone Handsets,” *IEEE Micro. Wire. Comp.,* vol. 12 (8), pp. 305–307, 2002.

[41] K. D. Katsibas, C. A. Balanis, P. A. Tirkas, and C. R. Birtcher, “Folded loop antenna for mobile hand-held units,” *IEEE Trans. Antennas Propagat*., vol. 46 (2), pp. 260–266, 1998.

[42] H. Morishita, H. Furuuchi, K. Fujimoto, “Performance of balance-fed antenna system for handsets in the vicinity of human head or hand,” *IEE Proc.-Microw. Antennas Propag*., vol. 149 (2), 2002.

[43] C. A. Balinis, "*Antenna theory analysis and design,*" John Wiley & Sons inc., Second edition, ISBN 0–471–59268–4, 1997.

[44] E. E. Altshuler, "A monopole loaded with a loop antenna," *IEEE Trans. Antennas Propagat*., vol. 44 (6), pp. 787–791, 1996.

[45] J. Thaysen and K. B. Jakobsen, "One turn stub loaded loop patch antenna on a small ground plane," *URSI International Symposium on Electromagnetic Theory*, vol. 2, pp. 763–765, 2004.

[46] J.-F. Zurcher and F. E. Gardiol, "Broadband patch antennas," *Artech House Publishers*, 1995.

[47] J. Thaysen, K. B. Jakobsen, and J. Appel-Hansen, "A wideband balun - how does it work?," More *Practical Filters and Couplers: A Collection from Applied Microwave & Wireless*, ISBN 1-884932-31-2, pp. 77–82, 2002.

[48] J. Thaysen, K. B Jakobsen, and J. Appel-Hansen, "A Logarithmic Spiral Antenna for 0.4 to 3.8 GHz," *Applied Microwave & Wireless, Norcross, GA, USA*, vol. 13 (2), pp. 32–45, 2001.

[49] J. Thaysen, K. B. Jakobsen, and J. Appel-Hansen, "Characterisation and optimisation of a coplanar waveguide fed logarithmic spiral antenna". *Proc. IEEE AP-S Conf. Antennas and Propagation for Wireless Communication*, Waltham, Mass., USA, pp. 25–28, 2000.

[50] H. Shuhao, "The balun family," *Microwave Journal*, Technical notes, vol. 30, pp. 227–229, 1987.

[51] M.-Y. Li, K. Tilley, J. McCleary, and K. Chang, "Broadband coplanar waveguide-coplanar strip-fed spiral antenna," *Electron. Lett*., vol. 30, pp. 176–177, 1995.

[52] Y.-D. Lin and S-N. Tsai, "Coplanar waveguide-fed uniplanar bow-tie antenna," *IEEE, Trans. Antennas Propagat*, vol. 45, pp. 305–306, 1997.

[53] R. N. Simons and S. R. Taub, "Coplanar waveguide radial line stub," *Electron. Lett*., vol. 29, pp. 412–414, 1993.

[54] V. Trifunovic and B. Jokanovic, "Four decade Bandwidth Uniplanar Balun," *Electron. Lett*., vol. 28, pp. 534–535, 1992.

[55] A. T. Kolsrud, M-Y. Li, and K. Chang, "Dual-frequency electronically tunable CPW-fed CPS dipole antenna," *Electron. Lett*., vol. 34, pp. 609–611, 1998.

[56] K. Tilley, X. D. Wu, and K. Chang, "Coplanar waveguide fed coplanar strip dipole antenna," *Electron. Lett*., vol. 30, pp. 176–177, 1994.

[57] G. A. Thiele, P. L, Detweiler, and P. P. Penno, "On the lower bound of the radiation Q for electrically small antennas," *IEEE, Trans. Antennas Propagat*., vol. 51, pp. 1263–1269, 2003.

[58] H. Carrasco, H. D. Hristov, R. Freick, and D. Cofre, "Mutual coupling between planar inverted-F antennas," *Microwave and optical Tech. Lett.,* vol. 42, pp. 224–227, 2004.

[59] J. Blanch, J. Romeu, and I. Corbella, "Exact representation of antenna system diversity performance from input parameter description," *Electron. Lett*., 39, pp. 705–707, 2003.

[60] R. G. Vaughan and J. Bach Andersen, *Channels, Propagation and Antennas for Mobile Communications*, The IEE, UK, ISBN 0 85296 084 0, 2003.

[61] J. Thaysen and K. B. Jakobsen, "Small inductor Loaded mobile phone Antenna," *JINA* 2004, *International Symposium on Antennas*, pp. 4, 2004.

[62] J. Appel-Hansen, "*Antenna measurements*," Ch. 8 in A.W. Rudge (Ed.) "*The handbook of antenna design,*" Peter Pelegrinus Ltd, 1982.

[63] R. C. Baird, A. C. Newell, and C. F. Stubenrauch, "A brief History of near-field measurements of antennas at the national bureau of standards," *IEEE Trans. Antennas Propagation*, vol. 36 (6), 1988.

[64] Y. Gau and I. Wolff, "A new miniature magnetic field probe for measuring three-dimensional fields in planar high-frequency circuits," *IEEE Trans. Microwave Theory and Techniques*., vol. 44, pp. 911–918, 1996.

[65] Y. Gau and I. Wolff, "Miniature electric near-field probe for measuring 3-D fields in planar microwave circuits," *IEEE Trans. On Microwave theory and Techniques*, vol. 46, pp. 907–913, 1998.

[66] www.semcad.com.

[67] www.speag.com.

[68] R. M. Reano, W. Thiel, J. F. Whitaker, and L. P. B. Katehi, "Measured and simulated electric, magnetic, and thermal field distributions of a patch antenna operation at high power," *Proc. IEEE Antennas and Propagat. Symposium*, pp. 886–889, 2002.

[69] J. Toftgard, S. N. Hornsleth, J. Bach Andersen, "Effects on portable antennas of the presence of a person," *IEEE Trans. Antennas and Propagat*., vol. 41 , pp. 739–746, 1993.

[70] J. Thaysen and K. B. Jakobsen, "Capacitive top-loading of a mobile phone antenna for size reduction*," JINA 2004*, *International Symposium on Antennas*, pp. 4, 2004.

[71] M. Sager, M. Forcucci, and T. Kristensen, "A novel technique to increase the realized efficiency of a mobile phone antenna placed beside a head-phantom," IEEE Antennas and Propagation Society International Symposium, 2003, vol. 2, pp. 1013–1016, 2003.

[72] H. Morishita, Y. Kim, and K. Fujimoto, "Design concept of antennas for small mobile terminals and the future perspective," IEEE Antennas and Propagation Magazine, vol. 44 (5), pp. 30–43, 2002.

[73] M. A. Jensen and Y. Rhamat-Samii, "EM Interaction of Handset Antennas and a Human in Personal Communications," *Proceedings IEEE,* vol. 83 (1), pp. 7–17, 1995.

[74] W. Jakes, "*Microwave mobile communications,*" IEEE press, 1974.

[75] A. Goldsmith, S. Jafar, N. Jindal, and S. Vishwanath, "Capacity limis of MIMO channels," *IEEE J. Select. Areas Commun.*, vol. 21, no. 5, pp. 684−702, 2003.

4 Conclusion and further work

In this study, the potential of using multiple antennas inside a mobile phone was investigated. The work has beenconcentrated on the following applications: Different techniques to reduce the size of mobile phone antennas and mobile phone antenna systems that consist of more than one antenna [XI, XII], and performance evaluation of the antennas [XII] as well as the MIMO system performance [XI].

Different aspects related to the antenna design and performance as well as issues related to the practical implementation of the proposed antennas on a ground plane that has a size which is comparable to modern mobile phones, have been discussed.

From the results presented in this thesis it could be concluded that:

LC circuit could lower the coupling between the antennas and hence it is possible to reduce the overall volume necessary for two antennas, since they can be spaced closer and still have a high radiation efficiency [VII].

It is likely that the separation between the open ends of the PIFAs dictates the mutual coupling. Choosing configurations that maximise the separation between the open-end of two PIFAs reduces the mutual coupling. The overall conclusion is that both the orientation as well as the separation are important factors regarding coupling [VI].

Inductor loading of a fixed sized PIFA could reduce the centre frequency (min. $|S_{11}|$) by 33% when a lumped inductor is placed within the first few millimetres from the feed point. The principle could also be used for a fixed frequency and hence a 30% to 40% size reduction is expected [VIII]. Similar results are obtained for the top-loaded PIFA [IX]. For both proposals the drawbacks are the increased complexity and hence the price of the antenna system.

The bandwidth of a loop antenna could be improved by adding a ground plane to the loop, and thus transforming the loop antenna into a patch antenna. Further improvement in the antenna performance is accomplished by adding a matching line that acts as a quarter wavelength line [X].

Antenna configurations that consist of orthogonal located PIFAs yield the lowest envelope correlation. In some particular configurations it is found that the envelope correlation could be reduced by 50%, simply by rotating one of the antennas 180 degrees. For the orthogonal set-ups the highest envelope correlation is obtained when the open end and the feed line are vertically on line. An almost exponential relation between the mutual coupling and the envelope correlation is found. A certain limit of the mutual coupling of –10 dB is found, below this limit the envelope correlation is almost constant, being 0.15, and therefore effort in decreasing the mutual coupling should be limited to this level [III].

The envelope correlation coefficient could be calculated directly from the scattering parameters between any two antennas in a MIMO antenna array system with an arbitrary number of antennas [II]. The proposed formula gives a knowledge of where the effort could be placed doing design and optimisation of the antennas in a diversity system or in a MIMO system. For a MIMO application, where low envelope correlation is essential, one should bear in mind that the location and orientation of the antennas should be optimised not only with respect to envelope correlation but also with respect to the bandwidth [I].

Low mutual coupling leads to low envelope correlation [I]. However, low envelope correlation does not necessarily come from low mutual coupling. Also, it is observed that low mutual coupling leads to low bandwidth. This is primary caused by poor impedance match (high

reflection coefficient) of the antennas in these particular configurations. A high bandwidth occurs in the configurations that also yield a high mutual coupling. The conclusion is that high mutual coupling reduces the freedom in choosing an optimal configuration [I].

Metallic objects that are placed in the regions above the ground plane where the electric field intensity is the lowest affect the antenna performance the least. Hence, the optimal location of a metallic object, which might be a camera or a loudspeaker, could be determined directly from the raw unprocessed electric near-field distribution. In the cases where the metallic object is located closest to the open end of the radiating element, the antenna performance is affected the most. Placing the metallic object close to the shorting pin and the feed point of the antennas affects the antenna performance least. Thus, the conclusion is that metallic objects should be located in areas having a local minima in the electric field amplitude of the total field, and one should maximise the distance between the metallic object and the open end of the radiating element [V].

The capacity increases with increased signal to noise ratio (*SNR*). It is shown that the capacity of a SISO system yields approximately half the (2, 2) capacity and a third of that obtained using a (3, 3) MIMO system for large signal to noise ratio.

Adding more elements at the TX antenna configuration increases the capacity. For the three-antenna configuration mounted inside a mobile phone the talk position capacity increases from 4.7 bit/s/Hz to 8.2 bit/s/Hz. When increasing the numbers of TX elements from one to seven. Above four TX elements the capacity increase is less per TX element as the capacity increase per TX element below three. From one to four the talk position capacity increases from 4.7 bit/s/Hz to 7.4 bit/s/Hz, as compared to an increase of 0.8 bit/s/Hz for the last three antennas.

From a capacity point of view it is advantageous to have three antennas instead of two antennas, despite that the talk position radiation efficiency of the third antenna is a few percent, only. Nevertheless, it is a trade-off between increased capacity and the increased complexity the extra antenna brings. Also, from a capacity point of view, it is better to have a full (2, 2) MIMO system ($C_{0.5}$ of 4.9 bit/s/Hz) than a RX diversity system of (1, 3) ($C_{0.5}$ of 4.7 bit/s/Hz). Also, with the same amount of antennas (3, 2) versus (2, 3) it yields an extra capacity of 0.6 bit/s/Hz. This means that in this case, it is better to have an extra RX antenna, i.e., the three-antenna configuration (2, 3) rather than an extra TX antenna, the (3, 2) configuration [IV]. Antenna selection could be used as a simple method to increase the capacity of a MIMO antenna configuration with minimal added hardware complexity.

From the study and overview of MIMO principle, it is clear that MIMO systems offer significant gains in performance over traditional wireless communication systems. Measurements were presented to show the capability for several potential MIMO antenna configurations [XI].

A three-antenna MIMO array incorporated in a commercial available mobile phone has verified the MIMO gain. The fact that the measured free-space radiation efficiency is approximately 20 percent point lower when incorporating the antennas into a commercial mobile phone only has a minor affect the free-space capacity, which is unchanged 7.1 bit/s/Hz. Placed beside an artificial hand and head, the capacity is 6.9 bit/s/Hz [IV]. This comes from the rather unchanged ratio between the peak total efficiencies measured in free space.

The work presented in this thesis can be extended in many ways. Firstly, the different techniques for minimising the size of the antennas and the volume of the antenna system should be combined for optimal performance. Secondly, the antennas and the MIMO

evaluation should be elaborated to the ultra-wideband (UWB) transmission system. UWB transmission has recently received increased attention in both academia and industry for applications in wireless communications. UWB has many benefits, including high data rate, availability of low-cost transceivers, low transmit power, and low interference. It operates in the unlicensed frequency band between 3.1 to 10.6 GHz (7.5 GHz). For instance, industrial standards such as IEEE 802.15.3a (high data rate) and IEEE 802.15.4a (very low data rate) have been introduced based on UWB technology. Although R&D efforts in recent years have demonstrated that UWB radio is a promising solution for high-rate short-range wireless communications, further extensive investigation, experimentation and development are necessary towards developing effective and efficient UWB communication system antennas.

Paper I

Reduction of Antenna Correlation and Bandwidth Optimisation for Increased Mobile Phone MIMO Antenna System Performance

Authors

Jesper Thaysen

Nokia Denmark, DK-1790 København, DENMARK
Technical University of Denmark DK-2800 Kgs. Lyngby, DENMARK

Kaj B. Jakobsen

Technical University of Denmark DK-2800 Kgs. Lyngby, DENMARK

Paper submitted to

IEEE Transaction on Antennas and Propagation

J. Thaysen and K.B. Jakobsen, "Reduction of Antenna Correlation and Bandwidth Optimisation for Increased Mobile Phone MIMO Antenna System Performance", submitted 2005.

1 Reduction of Antenna Correlation and Bandwidth Optimisation for Improved MIMO Performance

Jesper Thaysen
Nokia Denmark, www.nokia.com, DK-1790 Kbh V, DENMARK
Email: jesper.thaysen@nokia.com

Kaj B. Jakobsen

Technical University of Denmark, www.dtu.dk, DK-2800 Kgs. Lyngby, DENMARK
Email: kbj@oersted.dtu.dk

A novel simple closed form formulation based on the scattering parameters to calculate the envelope correlation between any two antennas in a (3, 3) Multi-Input Multi-Output (MIMO) system is derived. This approach has the advantage that it does not require knowledge of the antenna radiation pattern. Based on simulations and measurements of different two- or three-PIFA (Planar Inverted F-Antenna) configurations, it is found that high mutual coupling reduces the freedom in choosing an optimal configuration with respect to a high bandwidth and low envelope correlation. Even though being essential for high MIMO capacity, configurations with the lowest envelope correlations are not necessarily the most suitable for a MIMO system. Some additional selection criteria, one being the bandwidth, must be satisfied in the choice of the configuration as well. Simulations and measurements on small multi element prototypes yield envelope correlations ρ_e below 0.24 between 1.7 GHz and 1.9 GHz. As long as the envelope correlation is less than $\rho_e < 0.5$ diversity gain could be obtained in a mobile phone.

Keywords: Correlation, Mutual Coupling, Bandwidth, Mobile Phones, MIMO.

1.1 Introduction

Multiple-input multiple-output (MIMO) systems are very attractive in order to boost the capacity of wireless communication systems that operate in a rich multipath environment. During the last few years, MIMO systems have received considerable attention due to the potential increase in capacity (see e.g., [1]). The idea behind MIMO is that the signals on the transmitter (TX) antennas at one end and the receiver (RX) antennas at the other end are "combined" in such a way that the quality in terms of the bit-error rate (BER) or the data rate (bits/sec) for each of the MIMO user is increased [2].

In a rich multipath environment the theoretical capacity increases linearly with the number of antenna elements N in a (N, N) MIMO system [1]. However, in a more practical MIMO system the capacity is reduced due to correlation between the signals in the receiver [3]. Therefore, the correlation between the signals that are received from the different antenna elements is an important parameter in a MIMO system [4]. As long as the envelope correlation is less than $\rho_e < 0.5$ diversity gain could be obtained in a mobile phone [5]. Even though this motivates the need for low correlation it is not a guarantee for high capacity, since it has been predicted theoretically and has been confirmed by measurements as well that for some environments, the capacity of MIMO systems can become very low even for uncorrelated signals; this effect has been termed keyholes [7, 35].

In [8] a beneficial impact of channel correlations on MIMO capacity is described. The result shows that high correlation does not necessarily result in low capacity. In [9] the physical channel is related to the observed correlations. In both cases it is the cross correlation between the receiving and transmitting antennas that is investigated, and not as in this paper, which concerns the correlation between the elements. The results obtained in [8, 9] are therefore not directly comparable to the results in this paper.

The expected linear capacity enhancement when the number of antennas are increased motivates to increase the number of antenna elements. However, mutual coupling between the antenna elements affects the correlation [10-14]. For a fixed sized mobile phone an increase in the number of antenna elements causes inevitably higher mutual coupling due to the smaller distances between the antennas [15], [16]. The increased mutual coupling often results in higher spatial correlation which again leads to a lower MIMO gain as compared to the case of fully uncorrelated antenna signals [13].

Adding an extra antenna could increase the capacity, however, it is expected that the extra antenna causes a decrease in the element performance due to the reduced space between the antenna elements. Thus, the benefit of the extra antenna might be reduced compared to the theoretically expected capacity increase. Therefore, a trade-off between the capacity and the increased complexity/capacity when an extra antenna element has been added exists. Taking the increased complexity into account it might be that careful optimisation of a given number of antenna elements is preferred as compared to the scenario when an extra antenna element has been added. In this paper, the evaluation of the MIMO system is based on some performance metrics, such as envelope correlation, mutual coupling, and total efficiency of the elements. However, the capacity should be evaluated in a multipath environment in order to determine this trade-off between the capacity and the increased complexity/capacity fully.

The calculation of the antenna correlation can be approached in different ways. One is based on the radiation pattern [17], and another is based on the scattering parameters obtained at the antenna terminals [18]. A third method, based on Clarke's formula [19], has recently been used in [20] and [21]. Correlation calculation using the radiation pattern principle is a time consuming process, no matter whether it is done using simulated or experimental data. Nevertheless, the method is often used (see e.g., [22]). A proposal for calculating the correlation between antennas in a two antenna system using the scattering parameters is found in [18]. The correlation between two antennas can also be calculated using the impedance matrix [23].

In this paper, a (3, 3) MIMO system is investigated, thus the correlation between any two antennas in this three-antenna system is required. The formula has been derived using the law of energy conservation [24], which is also the case in [18] and [25]. Simulated and experimental data have validated the approach [34].

The scattering parameters and the radiation patterns of the antennas that are located on a finite ground plane were simulated using the IE3D software (method of moment) [26], and the radiation patterns of the experimental prototypes were measured in an anechoic chamber at the Nokia premises in Copenhagen [27]. The experimental data have verified the simulation results.

In this paper several array configurations are investigated, each including a number of identical antennas; some performance metrics are applied (correlation and bandwidth) to choose the best antenna configuration. In the design of the MIMO antennas each of the antennas are optimised in terms of the input impedance and bandwidth of the Planar Inverted

F-Antenna (PIFA) (e.g., by changing the distance between the feed and the ground contact) dependent on the location of the PIFA on the ground plane. However, the proximity effects of mobile phone cover, the artificial hand and head should be included. Hence, the results concerning the optimal configurations might differ somewhat when such cover, hand and head effects are taking into account.

1.2 MIMO model

The principle of a (3, 3) MIMO system is illustrated in Figure 1. Three different signals $x_{Ai}(t)$ are transmitted simultaneously from antenna elements A1, A2, and A3. At the receiver each of the antenna elements B1, B2, and B3 receives a signal $r_{Bi}(t)$ from each of the transmitting antennas.

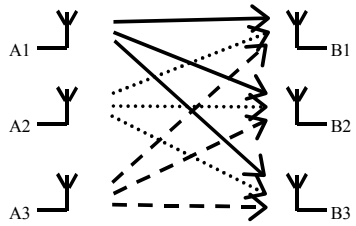

Figure 1. Model of a (3, 3) MIMO channel environment.

If the received signals at each of the antenna elements B1, B2, and B3 are sufficiently independent, as is typically the case in the presence of a rich multipath environment, it is possible to regenerate the original transmitted signal. The relationship between $A=[x_{A1}(t)\ x_{A2}(t)\ x_{A3}(t)]^T$ and $B=[\ r_{B1}(t)\ r_{B2}(t)\ r_{B3}(t)]^T$ is $B=\mathbf{H}(t)A$. Each matrix $\mathbf{H}$ is the 3×3 matrix whose *(i, j)*th element denotes the complex channel gain between the *j*th transmit and the *i*th receive antennas, at a certain time *t* and the spatial location of the antennas in the multipath environment.

To calculate the capacity in a MIMO system knowledge about both the propagation environment and the antenna configurations is required [28-30]. This paper focuses on the design of the mobile phone antennas. Hence, the envelope correlation treated here is the envelope correlation between the elements in the mobile phone.

Theory

The envelope correlation for a two-antenna system can be calculated using Equation (1) [5, 18, 31], where $\vec{\mathbf{F}}_i(\theta,\phi)$ is the radiation pattern of the antenna system when port *i* is excited (all other ports are terminated in a 50 ohm match), and $\bullet$ denotes the Hermitian product.

$$\rho_e = \frac{\left| \iint_{4\pi} \vec{\mathbf{F}}_1(\theta,\phi) \bullet \vec{\mathbf{F}}_2^*(\theta,\phi)\, d\Omega \right|^2}{\iint_{4\pi} \left|\vec{\mathbf{F}}_1(\theta,\phi)\right|^2 d\Omega \iint_{4\pi} \left|\vec{\mathbf{F}}_2(\theta,\phi)\right|^2 d\Omega} \qquad (1)$$

The envelope correlation between antenna $i=1$ and $j=2$ is derived in the Appendix for an array with $N=3$ antennas to

$$\rho_e(1,2,3) = \frac{\left|S_{11}^* S_{12} + S_{21}^* S_{22} + S_{31}^* S_{32}\right|^2}{\left(1-\left(\left|S_{11}\right|^2+\left|S_{21}\right|^2+\left|S_{31}\right|^2\right)\right)\left(1-\left(\left|S_{12}\right|^2+\left|S_{22}\right|^2+\left|S_{32}\right|^2\right)\right)} \quad (2).$$

The envelope correlation is determined from the distribution of the external sources and the radiation patterns. Only by assuming an omni-directional source distribution one can relate the mutual impedances (or scattering parameters) to the correlation [31]. This means that the envelope correlations estimated based on S-parameters (as in Equation 2) correspond to that given by Equation 1 if a uniform distribution of the sources is assumed, which might be a good approximation in some indoor environments [31]. When calculating the envelope correlation by the use of the scattering parameters the radiation efficiencies of the two antennas are not included, as in the case when the radiation pattern formula are used. Given that the investigation is to design a practical antenna system for MIMO (e.g. on a mobile phone), where radiation efficiencies can be low, due to the compressed electrical size of the terminals, the assumed energy conservation in the envelope correlation expression may be inadequate. Therefore, it should be pointed out clearly that this formulation cannot completely replace the pattern correlation (as a quality criterion) in the case of small terminal antennas. The radiation pattern based method gives us the possibility to include a better description of the radio channel in the evaluation, although it makes the evaluation more complicated.

1.3 Results and discussion

The presented antenna configurations consist of either two or three 40 mm long, 1.5 mm wide and 5 mm high PIFA located on a 40 mm × 100 mm ground plane. The feed point is located 5 mm from the edge where a 90-degree bend forms the short to the ground plane. The ground connection point is denoted with dots in the figures. In all the cases, the antennas are located parallel to the edge of the ground plane, as illustrated in Figure 2, and have a simulated centre frequency of 1810 MHz ±1.1%. Simulated as well as measured results are shown; three different two-antenna configurations and one three-antenna configuration are fabricated.

This Section is divided into two subsections: one treating the two-antenna configurations, and one treating the three-antenna configurations.

Two-antenna configurations

The current section treats the two-antenna configurations and has two subsections. In the first subsection fifteen different two-antenna configurations are investigated with respect to simulated reflection coefficient, mutual coupling, bandwidth, and envelope correlation. The second subsection elaborates on three selected configurations. These investigations are both based on simulated results as well as measurements on fabricated prototypes.

Comparison of 15 two-antenna configuretions

Fifteen different two-antenna configurations, i.e., B1-B15 are investigated in this subsection. The different layouts are shown in Figure 2.

For each configuration, the simulated highest envelope correlation calculated between 1.7 GHz and 1.9 GHz, is shown in Figure 3. In Table 1 the simulated values of the envelope correlation (ρ_{12}), the reflection coefficients ($|S_{ii}|$), the mutual coupling ($|S_{ij}|$ (i~=j)), and the –6 dB bandwidth (within which the reflection coefficients are below –6 dB) are shown.

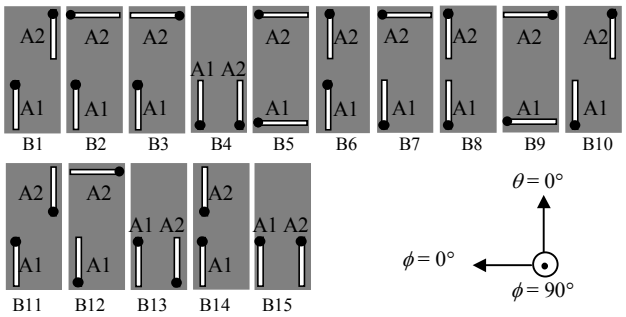

Figure 2. Layouts of the fifteen different two-antenna configurations located on the same finite ground plane, the grey area illustrates the 40 mm × 100 mm ground plane. The matchsticks symbolise the PIFAs, and the dot on the matchstick denotes the location of the shorting pin. The antenna orientation in the spherical coordinate system is shown in the lower right part of the figure.

The lowest envelope correlation is ρ_e = 0.02, which is obtained using configuration B1. For configuration B15 the envelope correlation is ρ_e = 0.48.

In a MIMO system, a high capacity dictates a low envelope correlation, which motivates the choice of a configuration that has a low envelope correlation. Nevertheless, configuration B1 with the lowest envelope correlation has low bandwidth, within which the reflection coefficients are below –6 dB (see Table 1), and thus has no practical interest. Therefore, some additional selection criteria, one being the bandwidth, must be satisfied in the choice of the configuration.

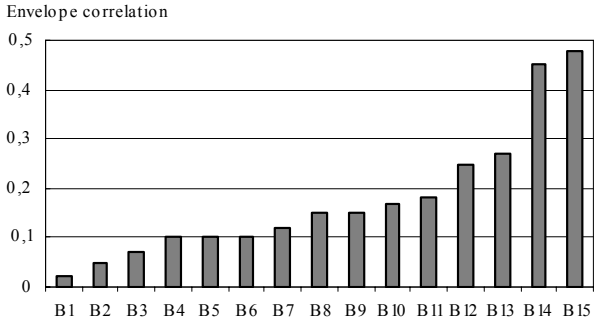

Figure 3. Simulated envelope correlations for configuration B1-B15.

Configuration B14 and B15 are discarded due to the rather high envelope correlation. Among the remaining 13 configurations there are eight configurations where both antennas (◊ and × in Figure 4) have a bandwidth of above 6% and an envelope correlation below 0.3; these are B4, B5, B7, B8, B9, B10, B12, and B13.

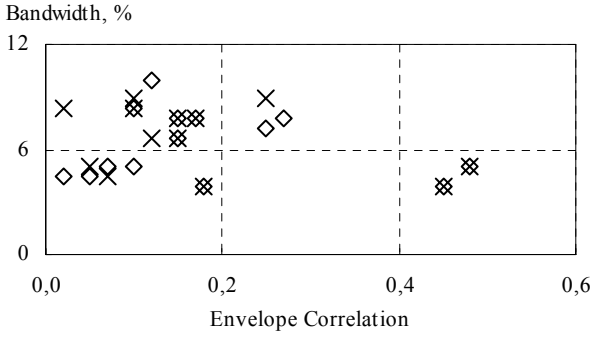

Figure 4. Simulated bandwidth versus envelope correlation for antenna A1(◊) and A2(×).

Also, the mutual coupling should be low, since this affects the correlation [10–14]. Low mutual coupling results in high total efficiency, which is the ratio of the power radiated to the total power supplied to the antenna as compared to that obtained for high mutual coupling. The relation between the envelope correlation and the mutual coupling (see Figure 5) indicates that low mutual coupling leads to low envelope correlation. However, low envelope correlation is not necessarily associated with low mutual coupling.

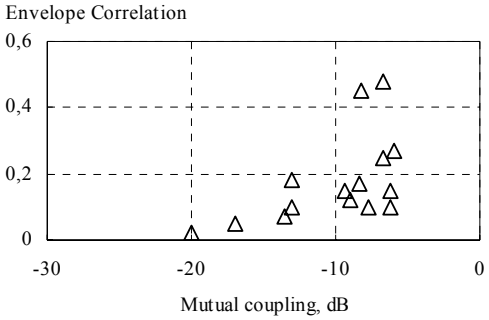

Figure 5. Simulated envelope correlation versus mutual coupling between antenna A1 and A2.

TABLE 1. Simulated values of the envelope correlation (highest value calculated between 1.7 GHz and 1.9 GHz), the reflection coefficients, S_{11}, S_{22}, (lowest value calculated between 1.7 GHz and 1.9 GHz), the mutual coupling, S_{21} (highest value calculated between 1.7 GHz and 1.9 GHz), and the –6 dB bandwidth (within which the reflection coefficients are below –6 dB).

	Correlation	S_{21}, dB	S_{11}. A1, dB	S_{22}. A2, dB	BW A1, %	BW A2, %
B1	0.02	-20.0	-14.8	-14.8	4.4	8.3
B2	0.05	-17.0	-15.0	-15.0	4.4	5.0
B3	0.07	-13.6	-16.0	-18.0	5.0	4.4
B4	0.10	-7.7	-15.8	-15.8	12.2	12.2
B5	0.10	-6.2	-14.2	-14.2	8.3	8.3
B6	0.10	-13.0	-16.0	-16.0	5.0	8.9
B7	0.12	-9.0	-15.5	-15.5	10.0	6.7
B8	0.15	-9.4	-15.8	-15.8	6.7	6.7
B9	0.15	-6.2	-16.4	-16.4	7.8	7.8
B10	0.17	-8.4	-14.8	-14.8	7.8	7.8
B11	0.18	-13.0	-18.3	-18.3	3.9	3.9
B12	0.25	-6.7	-16.8	-16.8	7.2	8.9
B13	0.27	-5.9	-15.7	-16.2	7.8	12.5
B14	0.45	-8.2	-15.5	-15.5	3.9	3.9
B15	0.48	-6.7	-16.5	-16.5	5.0	5.0

Based on the results presented in Figure 4 and Figure 5, it is concluded that high mutual coupling reduces the freedom in choosing an optimal configuration. Only a few of the configurations shown in Figure 2 should be used in a (2, 2) MIMO system. Obviously, configuration B4 yields the best performance in terms of bandwidth (12.2%) and still has a rather low envelope correlation of $\rho_e = 0.1$.

Adding an extra antenna yields the possibility of diversity gain in combination to the (2, 2) MIMO system [33]. Alternatively, the extra antenna can be used in a full (3, 3) MIMO system. Several three-antenna solutions can be constructed by combining some of the two-antenna configurations shown in Figure 2, i.e., by using identical antenna elements and located them parallel to the edge of the ground plane. There appear to be three criteria: Bandwidth, envelope correlation, and impedance match (reflection coefficient). Motivated by the fact that configuration B4 yields the best performances, the design of a three-antenna configuration

should contain configuration B4 in a combination with one or two more configurations. This gives the following two three-antenna combinations, namely one combining configurations B4, B7, and B8 and one combining configuration B4, B7, and B12. The two configurations are expected to have more or less the same performance. Design reasons motivate the three-antenna configuration that is formed by configuration B4, B7, and B12. The following subsection elaborates on the three selected configurations, i.e., configuration B4, B7 and B12.

Thorough two-antenna investigations

The investigations presented in this subsection are based on both simulated results as well as measurements on fabricated prototypes. Three different prototypes have been fabricated, i.e., configuration B4, B7 and B12. For each configuration the simulation results are compared to the measurement results. This is followed by a discussion of the key parameters when changing the position of one of the antennas while the position of second antenna are fixed.

Configuration B4 and variations

Good agreements between the simulation and measurement results for the scattering parameters are obtained as seen from Figure 6. The measured mutual coupling, $|S_{21}|$, almost coincides with the simulated result.

Both the simulated and the measured resonant frequencies of antenna A1 are 1.79 GHz, the measured reflection coefficient yields somewhat better impedance match as compared to the simulated results. For antenna A1, the measured resonant frequency is 1.80 GHz, which is higher as compared to the simulated resonant frequency.

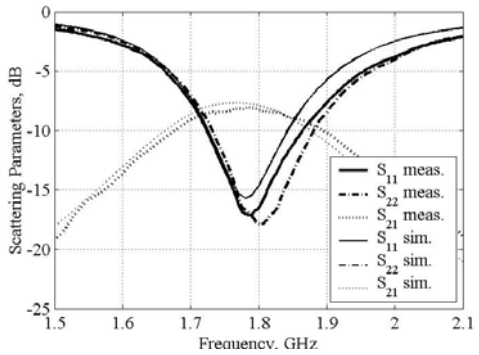

Figure 6. Simulated and measured scattering parameters for configuration B4.

The simulated envelope correlation shown in Figure 7a deviates from the measured envelope correlation curve. The agreement is best between 1.7 GHz and 1.9 GHz. However, both the simulated as well as the measured envelope correlations are below $\rho_e = 0.4$. The primary reason for this difference is that the two antennas are hand made, i.e., made using a scalpel, and therefore not completely identical.

Both antennas yield a measured total efficiency above 60% between 1.7 GHz and 1.9 GHz (Figure 7b) [27]. Due to the symmetry in this configuration, the total efficiency should be equal, which also is the case in the simulated model. Again the deviation is believed to be attributed to the physical difference of the two antennas on the prototype.

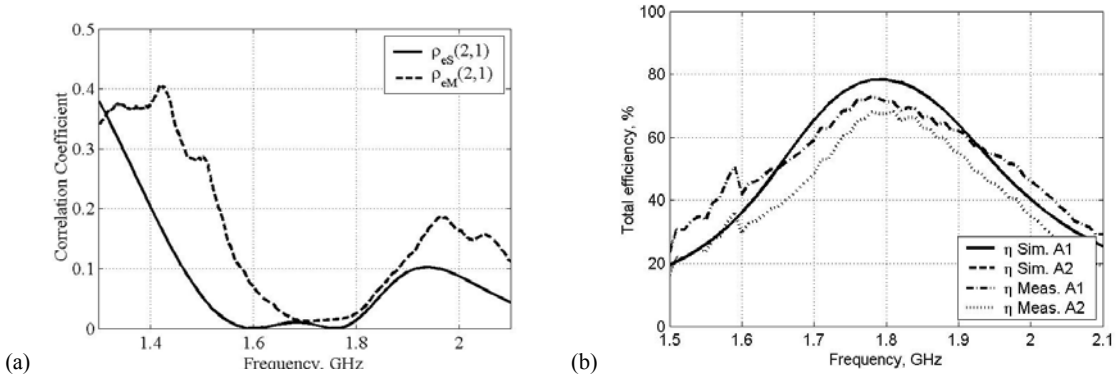

Figure 7. Simulated (solid) and measured envelope correlation (a). Simulated and measured total efficiency for antenna A1 (solid), A2 (dashed) (b).

Good agreement between the simulated and measured radiation patterns for configuration B4 is observed (see Figure 8).

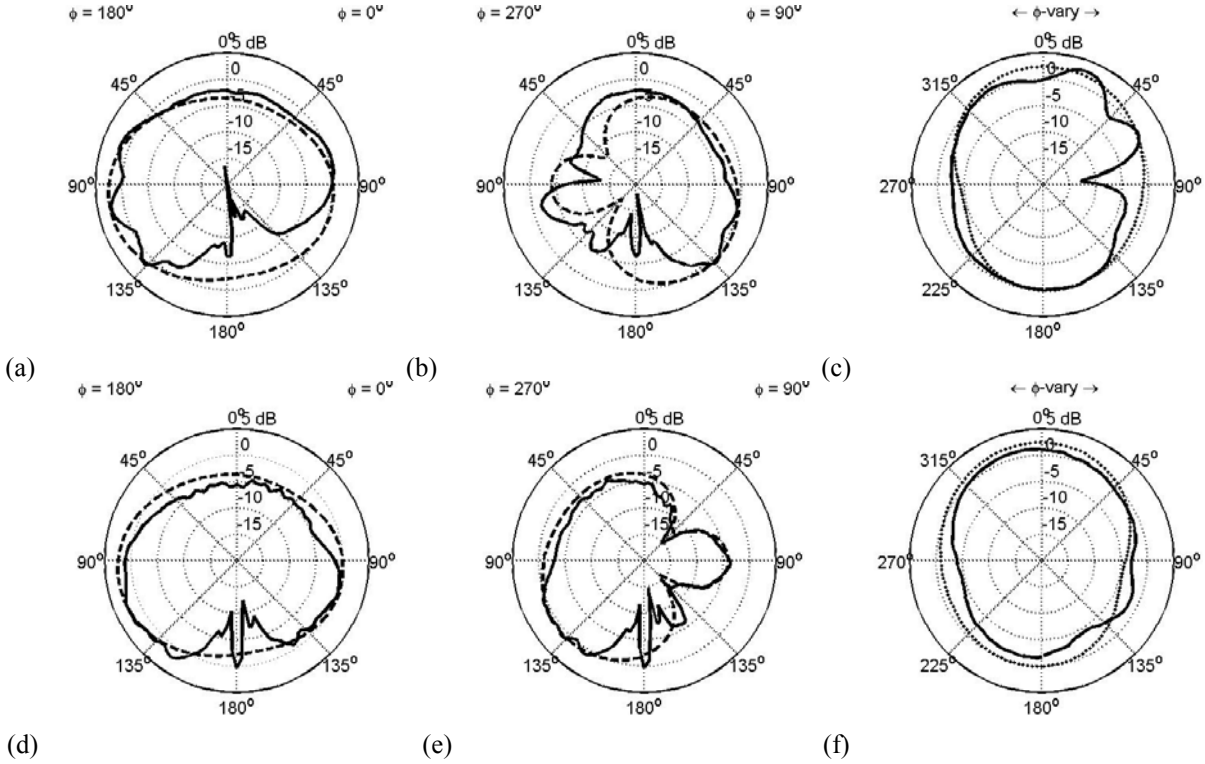

Figure 8. Simulated (dashed) and measured (solid) radiation pattern cuts at 1.8 GHz for configuration B4, A1 (a, b, c) and A2 (d, e, f). θ-cuts for ϕ = 0° (a, d) and for ϕ = 90° (b, e). ϕ-cut for θ = 90° (c, f) and B4-A2 (d). Configuration B4 is oriented as illustrated in Figure 2. The dips in the measured θ-cuts for $\phi = 180° \pm 12°$ are due to the antenna mounting and positioning system [27].

For the θ-cuts the agreement is better in the upper hemisphere ($\theta < 90°$) primarily due to the dips in the $\phi = 180° \pm 12°$, which are caused by the antenna mounting and positioning system [27]. In theory, the symmetry in configuration B4 should lead to identical ϕ-cuts for $\theta = 0°$ and symmetrical properties for the ϕ-cuts ($\theta = 90°$) and θ-cuts for $\phi = 90°$ around the vertical centre

of the ground plane. This is verified by the simulated results. The symmetry is also found for the measured results, though it is not that clear due to the difference between the two antennas on the prototype. For both antennas the simulated maximum gain is 3.9 dBi. The measured gain is lower, 3.2 dBi and 2.9 dBi for antennas A1 and A2, respectively. The difference is mainly caused by conductor loss and loss in the supporting material (between the ground plane and the radiating element) in the prototype.

In order to investigate the optimum location of the antennas on the ground plane, 10 different models were simulated. As a starting point configuration B4 is used (see Figure 9), hereafter the distance between antenna A1 and A2 is increased. With a maximum horizontal distance between the two antennas short pin being 60 mm, B4 degenerates to configuration B1 (see Figure 9).

The key parameters when changing the position of antenna A1 are shown in Figure 9. The position 0 mm corresponds to configuration B4 where the envelope correlation is $\rho_e = 0.1$. Moving antenna A2 by 60 mm configuration B1 is reached, and the envelope correlation decreases to $\rho_e = 0.02$. The mutual coupling decreases to $|S_{21}| = -20$ dB. However, the decrease is at the expense of a decreased –6 dB bandwidth.

For optimum trade-off of low correlation and high bandwidth, the configurations where antenna A2 is moved less than 30 mm, should be used. Here the bandwidth is above 8.8%, and the correlation is below 0.1. However, the mutual coupling is the highest, but below –6 dB. If antenna A2 is separated more than 30 mm the –6 dB bandwidth degrades considerably for antenna A1.

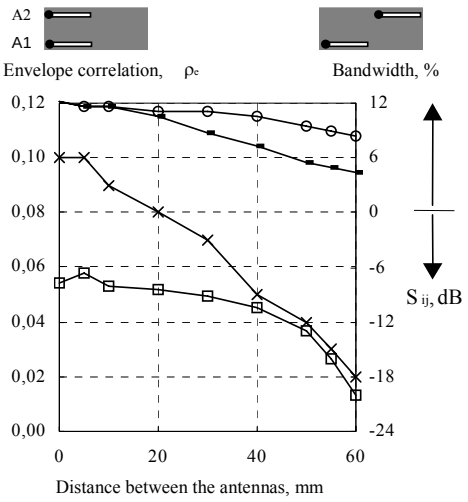

Figure 9. Simulated S-parameters of antenna A1 and A2. Mutual coupling (□), –6 dB bandwidth A1 (○), A2 (-), and envelope correlation (×) versus position of antenna A2.

Configuration B7 and variations

For the antenna configuration B7 that consists of two orthogonal PIFAs as indicated in Figure 2, the scattering parameters are shown in Figure 10.

The simulated and measured resonant frequencies of antenna A1 are 1.8 GHz, the measured reflection coefficient of antenna A1 ($|S_{11}|$) yields somewhat better impedance match as compared to the simulated results. For antenna A2, the measured resonant frequency is 1.77

GHz, i.e., 60 MHz below the simulation result. The measured mutual coupling $|S_{21}|$ is –15 dB, which is 5 dB better than the simulated value of –10 dB.

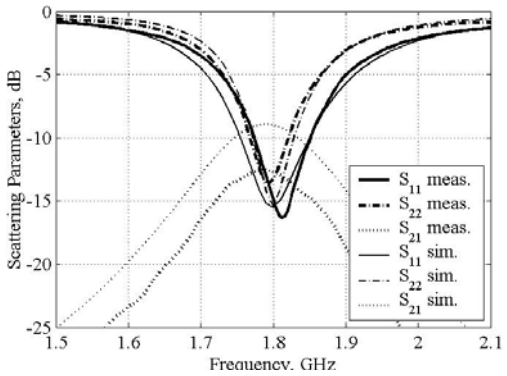

Figure 10. Simulated and measured scattering parameters for configuration B7.

Even though there are some discrepancies in the scattering parameters, the envelope correlation coincides between 1.5 GHz and 2.1 GHz, with the highest value of $\rho_e = 0.24$ at 1.5 GHz (see Figure 11a).

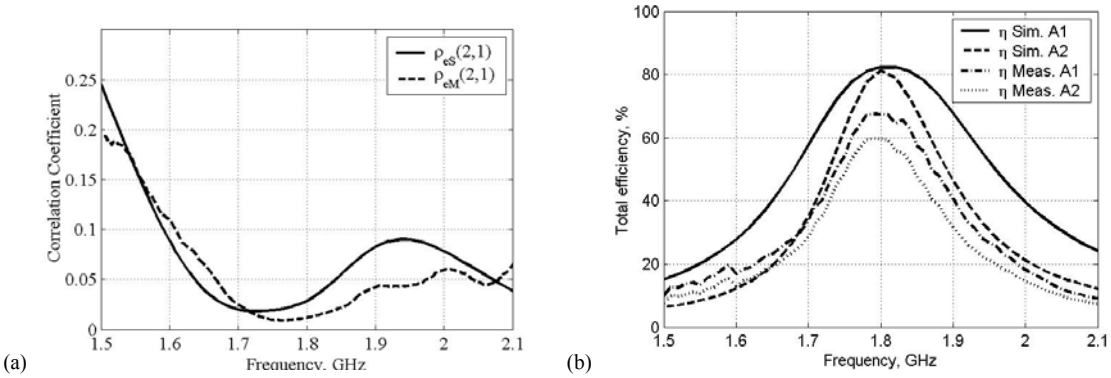

Figure 11. Simulated and measured envelope correlation (a). Measured total efficiency for antenna A1 and A2 (b).

The measured total efficiency for antenna A1 is higher than 40% between 1.7 GHz and 1.9 GHz. This result is comparable to that obtained for antenna A1 from configuration B4 (see Figure 7b). This seems reasonable due to the fact that they are located in the same position on the ground plane. Antenna A2 yields a measured total efficiency higher than 30%, as shown in Figure 11b. For both antennas the simulated values are somewhat higher.

The radiation patterns for configuration B7 are shown in Figure 12. Again the agreement between the simulated and measured θ-cuts is better in the upper hemisphere, primarily due to the dips in the $\phi = 180° \pm 12°$, which again are caused by the antenna mounting and positioning system [27]. The agreement is better for antenna A1 which is also the case for the reflection coefficient (see Figure 10). The measured maximum gain is 2.6 dBi for antenna A1 (2.9 dBi simulated), and 1.8 dBi for antenna A2 (2.5 dBi simulated). The radiation patterns obtained from antenna A1 are almost identical to those obtained from antenna A2 from configuration B4, due to the fact that they are placed at the same location on the ground plane; the difference arises from the interaction with the second antenna.

Eleven different simulations for various vertical distance between the open ends of antenna A1 and A2 are shown in Figure 13. At a separation between the short pin of antenna A2 and the

open end of antenna A1 being 0.5 mm the envelope correlation is $\rho_e = 0.31$, and decreases to 0.12 for the B7 configuration (at a separation of 58.5 mm). Again it is seen that the decrease in the envelope correlation is at the expense of decreased –6 dB bandwidth, especially for antenna A2.

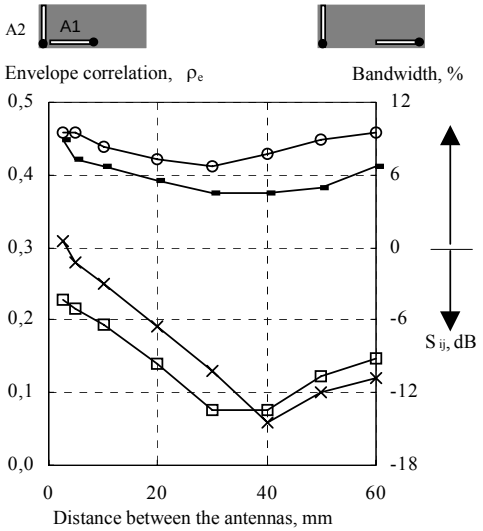

Figure 13. Simulated S-parameters of antenna A1 and A2. Mutual coupling (□), –6 dB bandwidth A1 (○), A2 (-), and envelope correlation (×) versus vertical distance between the antennas.

1.3.1.1 Configuration B12 and variations

For optimum trade-off of low correlation and high bandwidth, the configurations with distances between 18 mm and 55 mm should be avoided. At a distance of 2.5 mm a local minimum of $\rho_e = 0.32$ and 9% bandwidth is achieved simultaneously.

Good agreements between the simulation and measurement results are seen in Figure 14. Both antennas have resonant frequency at 1.82 GHz. The measured mutual coupling is somewhat lower as compared to the simulated.

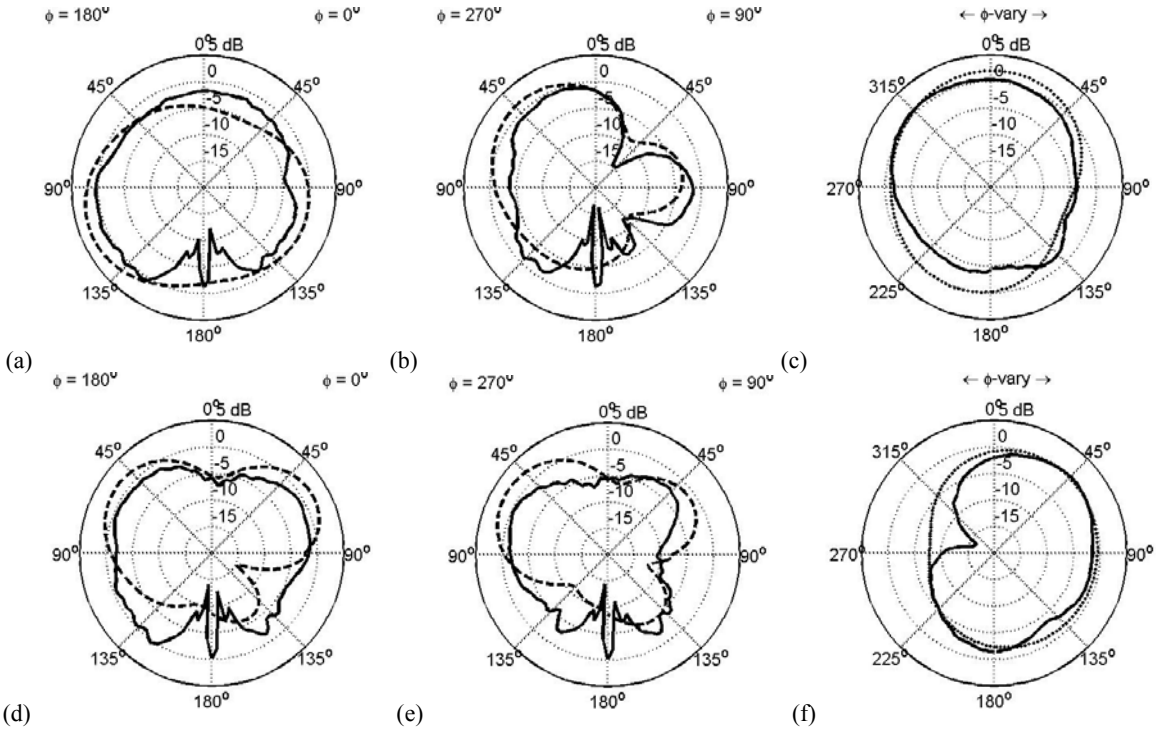

Figure 12. Simulated (dashed) and measured (solid) radiation pattern cuts at 1.8 GHz for configuration B7, antenna A1 (a, b, c) and A2 (d, e, f). θ-cuts for ϕ = 0° (a, d) and for ϕ = 90° (b, e). ϕ-cut for θ = 90° (c, f). Configuration B7 is oriented as illustrated in Figure 2. The dips in the measured θ-cuts for ϕ = 180° ± 12° are due to the antenna mounting and positioning system [27].

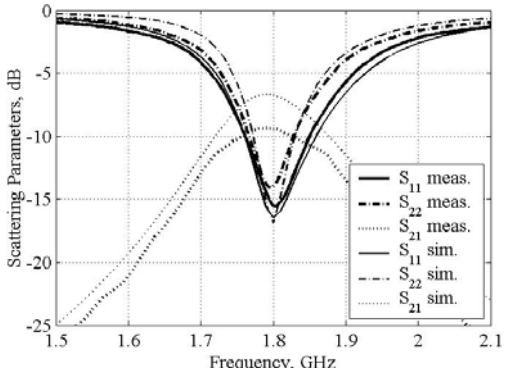

Figure 14. Simulated and measured scattering parameters for configuration B12.

Agreement between the simulated and measured envelope correlation is obtained see Figure 15. The agreement is best around the resonant frequency. Again the difference in the simulated and measured envelope correlations could be explained by the difference between the two antennas, which are hand made, i.e., made by using a scalpel, and therefore not completely identical.

The measured total efficiency of antenna A1 in configuration B12 is higher than 40% between 1.7 GHz and 1.9 GHz. Antenna A2 yields a total efficiency higher than 35%, as shown in Figure 15b. There are good agreement between the simulation and measurement results for antenna A2.

Good agreement between the simulated and measured radiation patterns is obtained for configuration B12 see Figure 16. The measured maximum gain is 2.6 dBi for antenna A1 (3.2 dBi simulated), and 1.5 dBi for antenna A2 (1.7 dBi simulated). In the main direction of antenna A2 ($\theta = 0°$) just below the feed and short pins of antenna A1 a null is observed. A somewhat similar effect is observed for configuration B7 see Figure 12.

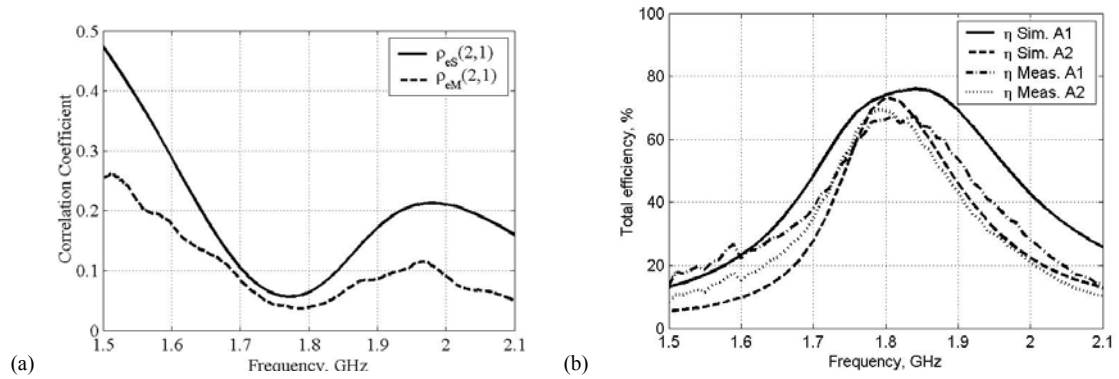

Figure 15. Simulated and measured envelope correlations (a). Measured total efficiency for antenna A1 and A2 (b).

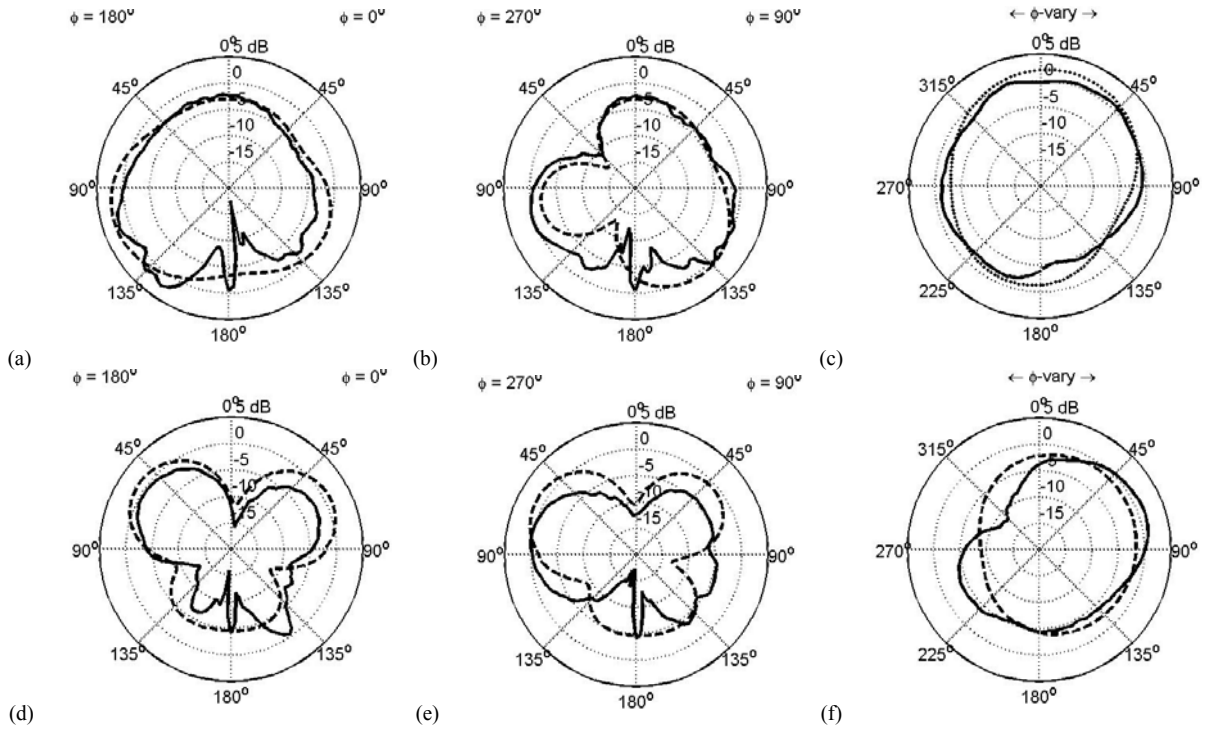

Figure 16. Simulated (dashed) and measured (solid) radiation pattern cuts at 1.8 GHz for configuration B12, antenna A1 (a, b, c) and A2 (d, e, f). θ-cuts for ϕ = 0° (a, d) and for ϕ = 90° (b, e). ϕ-cut for θ = 90° (c, f). Configuration B12 is oriented as illustrated in Figure 2. The dips in the measured θ-cuts for ϕ = 180° ± 12° are due to the antenna mounting and positioning system [27].

The optimum location of the antennas on the ground plane is found among 10 different configurations that were simulated. The results from the vertical variation of the distance between antenna A1 and A2 in configuration B12 are shown in Figure 17. Configuration B12 and B7 differ only in the orientation of Antenna A2.

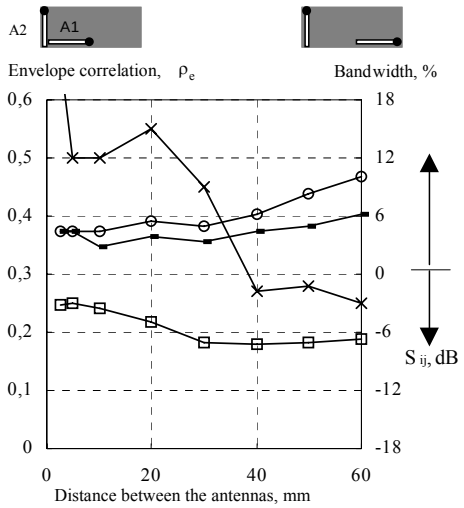

Figure 17. Simulated S-parameters of antenna A1 and A2. Mutual coupling (□), -6 dB bandwidth A1 (○), A2 (-),and envelope correlation (×) versus distance between the antennas.

The closer antenna A1 and A2 are located the lower bandwidth and higher envelope correlation is obtained. It is the original B4 configuration (60 mm in Figure 17) that yields the best performance.

Three-antenna configuration

In this section we study a three-antenna configuration: It is created by combining configuration B4, B7 and B12. The first two subsections include a parameter study with the location of two of the antennas fixed and the location of the third is varied. The third subsection includes investigations both based on simulated results as well as measurements on fabricated prototypes.

Optimum location of antenna element A2

The envelope correlation presented in this subsection is calculated for each position of antenna A2, with respect to the distance between the open end of antenna A2 and the shorted position of antenna A3, as shown in Figure 18.

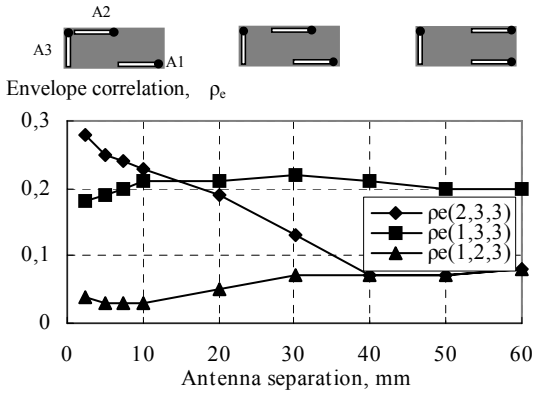

Figure 18. Simulated worst case envelope correlation between 1.7 GHz and 1.9 GHz versus distance for A2 moved away from A3.

The poorest envelope correlation within the frequency band of interest, i.e., from 1.7 GHz to 1.9 GHz is $\rho_e = 0.28$ which is obtained between antenna elements A2 and A3 at a distance of 2.5 mm. This correlation decreases to 0.07 for distances above 40 mm.

Above 15 mm a maximum envelope correlation between any antennas is less than 0.21, thus the optimum location for this configuration should not be found based on the envelope correlations, but rather based on other design parameters such that total efficiency and bandwidth, or simply where the antenna fits the best with respect to the remaining design parameters.

Optimum location of antenna element A1

In this subsection the envelope correlation is calculated for each position of antenna A1, with respect to the distance between the open end of antenna element A1 and the open end of antenna A3, as shown in Figure 19.

In this case, the worse envelope correlation $\rho_e = 0.62$ is obtained between antenna elements A1 and A3 at a distance of 15 mm (0.09 λ), as shown in Figure 19. As the distance between antenna elements A1 and A3 is increased the envelope correlations decreases monotonously. To obtain lowest envelope correlation, the optimum location of antenna element A1 is when the distance from A3 is as large as possible, i.e., 58.5 mm.

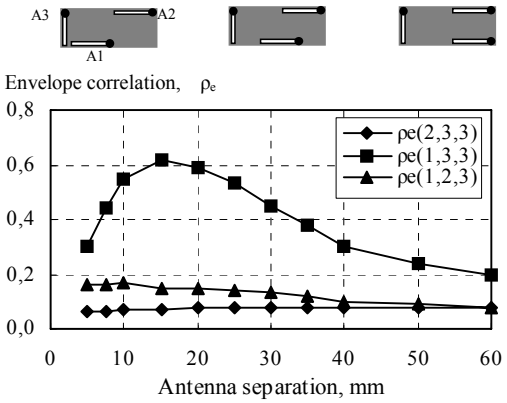

Figure 19. Simulated worst case envelope correlation between 1.7 and 1.9 GHz versus distance for A1 moved away from A3.

Comparing the envelope correlation curves for the two investigations shown in Figure 18 and 19, the envelope correlation between antenna elements A1 and A2 $\rho_e(2,1,3)$ is approximately identical. At distances above 50 mm the envelope correlations approach the same asymptote in both configurations. In general, the envelope correlations shown in Figure 18 are lower than those in Figure 19. This motivates the selection of this configuration in the following work.

Thorough three-antenna investigations

Based on the previous results, a prototype, as shown in Figure 20 with a distance of 45 mm between antenna elements A2 and A3, had been fabricated.

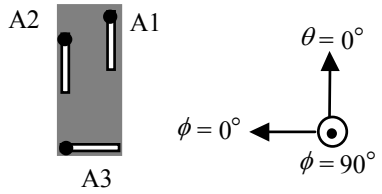

Figure 20. Three-antenna configuration, and orientation in the spherical coordinate system.

For this configuration, good agreement between the measured and the simulated resonant frequencies exist (see Figure 21); the agreement is best for antenna A2. For all three antennas the measured reflection coefficients are generally better than the simulated results. Also, the measured mutual coupling is lower than the simulated, especially the coupling between antenna elements A1 and A3.

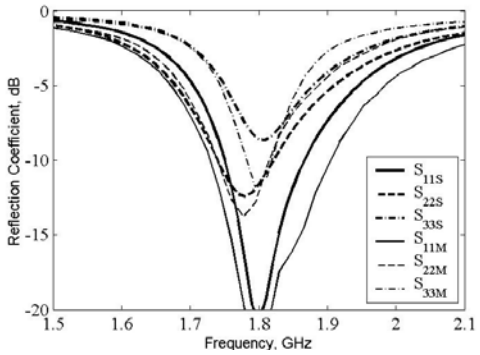

Figure 21. Simulated and measured reflection coefficient.

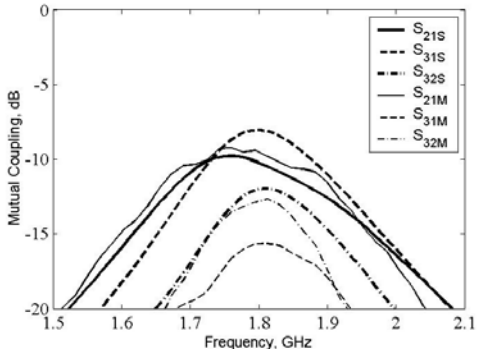

Figure 22. Simulated and measured reflection coefficient (a) and mutual coupling S_{21}.

The key measurement and simulation results are given in Table 2.

Table 2. Simulation and measurement key results.

Antenna	A1 sim./meas.	A2 sim./meas.	A3 sim./meas.
f_0, GHz	1.80/1.80	1.78/1.78	1.80/1.81
RL, dB	25/31	13/14	8/12
BW, %	13/15	12/10	5.8/5.2
Peak efficiency, %	75/75	70/64	50/54
Max. Gain, dBi	2.5/2.3	2.5/2.3	1.7/2.0

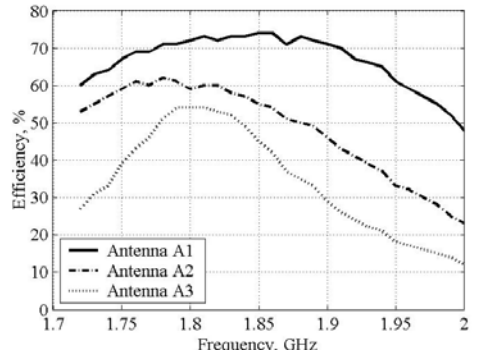

Figure 23. Measured total efficiency.

For all three antennas, the measured total efficiency is above 20% between 1.7 GHz and 1.9 GHz (see Figure 23).

For the three antenna configuration mounted as indicated in Figure 20, the simulated and measured radiation patterns are compared in Figure 24. The agreement between the simulated and measured θ-cuts is better in the upper hemisphere, primarily due to the dips in the $\phi = 180° \pm 12°$, which are caused by the antenna mounting and positioning system [27].

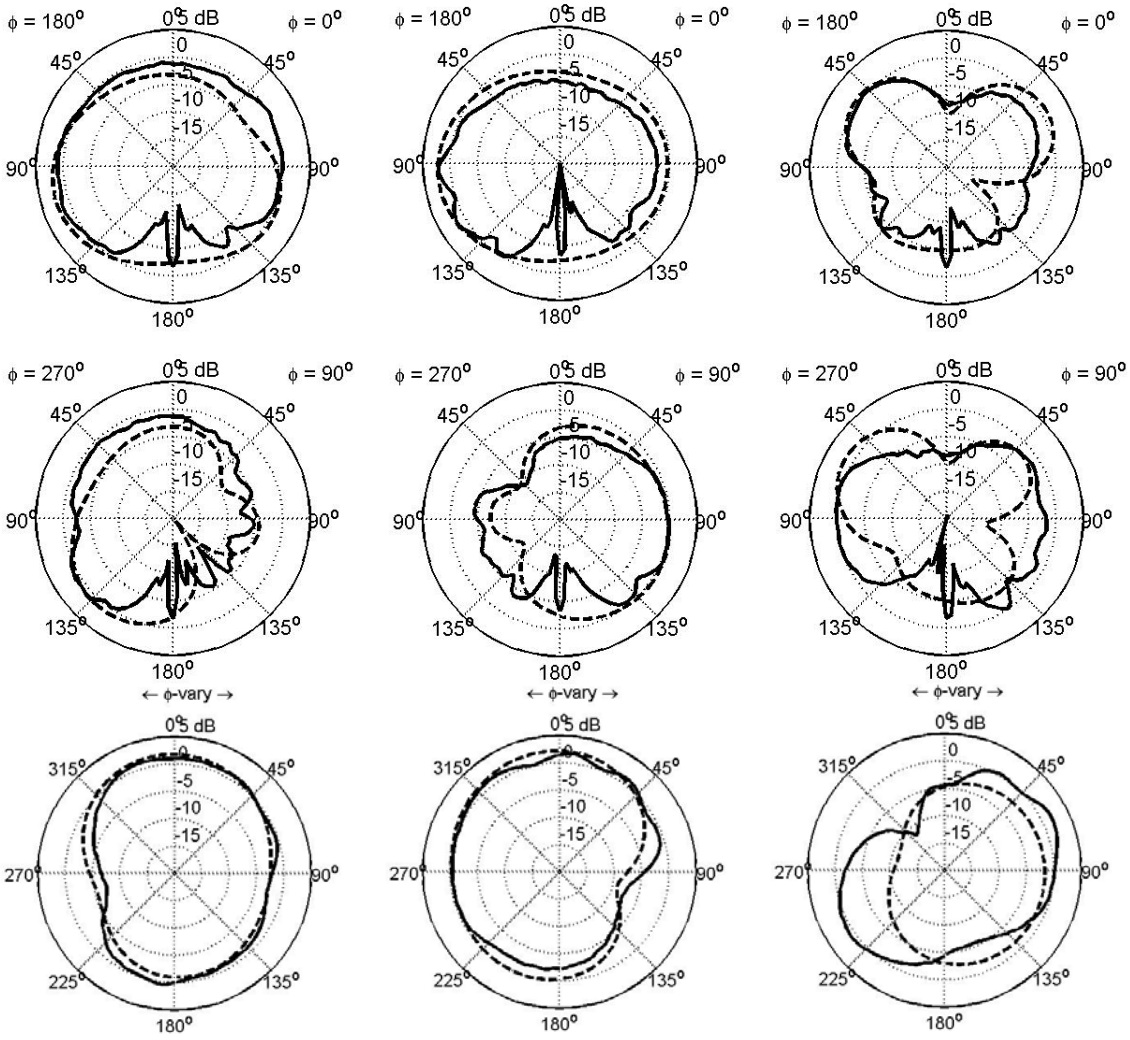

Figure 24. Simulated (dashed) and measured (solid) θ-cuts for $\phi = 0°$ (1. row) and for $\phi = 90°$ (2. row), and measured ϕ-cut for $\theta = 90°$ (3. row) for the three-antenna configuration for antenna A1 (1. column), A2 (2. column), and A3 (3. column). The distance between A2 and A3 is 45 mm. The dips in the measured θ-cuts for $\phi = 180° \pm 12°$ are due to the antenna mounting and positioning system [27]. The orientation is as shown in Figure 20.

The agreement is best for antennas A1 and A2, which also agreed best for the reflection coefficient (see Figure 21).

The radiation patterns obtained from antenna A1 (in this three-antenna configuration) are almost similar to those obtained from antenna A2 from configuration B4, due to the same

location on the ground plane; the difference comes from the interaction with the third antenna, A3.

The measured and simulated envelope correlations are shown in Figure 25. The discrepancy between the simulated and measured scattering parameters leads to the observed deviations of the envelope correlations.

Nonetheless, the simulated and measured curves have the same shapes, e.g., $\rho_e(2,3,3)$ has a local minimum and a maximum at 1.7 GHz and 1.95 GHz, respectively and visa versa for $\rho_e(3,1,3)$ and $\rho_e(1,2,3)$. Between 1.7 GHz and 1.9 GHz the worst case envelope correlation ρ_e = 0.24, which is much lower than the "rule of thumb" number ($\rho_e < 0.5$) for diversity gain stated in [5].

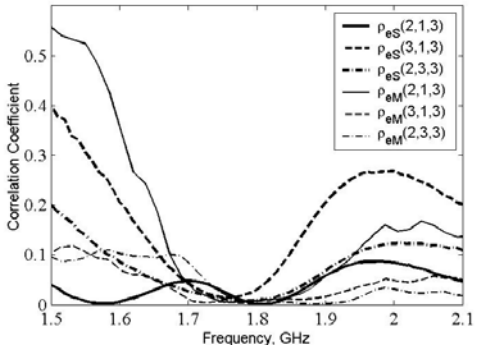

Figure 25. Simulated and measured envelope correlation vs. frequency 45 mm between antenna A2 and A3.

1.4 Conclusion

A novel closed formed expression has been proposed that can be used to calculate the envelope correlation from the scattering parameters between any two antennas in a (*3, 3*) MIMO antenna array system. When the knowledge of the envelope correlation for each of the configurations, the configuration with the best, i.e., the lowest envelope correlation can be chosen for further design optimisation in order to obtain the optimal antenna configuration for a diversity or MIMO system. The formula can be applied to space, polarisation and pattern diversity as well.

Good agreement has been obtained for the envelope correlations that have been calculated from the simulated and measured scattering parameters.

For MIMO application, where low envelope correlation is essential, one should bear in mind that the location and orientation of the antennas should be optimised not only with respect to envelope correlation but also with respect to bandwidth.

For the two-antenna configuration optimal locations and orientation with respect to the MIMO performance are not necessarily the configurations with the lowest envelope correlation. A certain bandwidth is required as well. Here, it is found that configurations B4 and B7 yield the best performance when taking the envelope correlation and bandwidth into account.

From the 15 different two-antenna configurations it could be concluded that high mutual coupling reduces the freedom in choosing an optimal configuration.

In this paper, the evaluation of the MIMO system is based on the performance, such as envelope correlation, mutual coupling, and total efficiency of the elements. However, the capacity should be evaluated in a multipath environment in order to determine this fully.

The worst case envelope correlation in the proposed three-antenna configuration is 0.24 in the frequency band of interest, i.e., from 1.7 GHz to 1.9 GHz. This number is approximately half of the "rule of thumb" number (ρ_e <0.5) for diversity gain stated in [5].

Future work could include the proximity effect by the mobile phone cover and by artificial hand and head should be included.

1.5 Appendix

Consider three antennas which are driven by three generators operating at the same frequency. The antennas are not necessarily well matched and have non-zero mutual coupling. In the far-field region, in a usual spherical co-ordinate system, the total radiated electrical field is the sum of the contributions from each of the three antennas:

$$\vec{\mathrm{E}} = \vec{E}_1 + \vec{E}_2 + \vec{E}_3 = a_1\sqrt{\eta_0}\sqrt{\frac{D_1}{4\pi}}\,\vec{\mathrm{F}}_1(\theta,\phi)\frac{e^{-jkr}}{r} + a_2\sqrt{\eta_0}\sqrt{\frac{D_2}{4\pi}}\,\vec{\mathrm{F}}_2(\theta,\phi)\frac{e^{-jkr}}{r} + a_3\sqrt{\eta_0}\sqrt{\frac{D_3}{4\pi}}\,\vec{\mathrm{F}}_3(\theta,\phi)\frac{e^{-jkr}}{r}, \tag{3}$$

Where a_i is the incident wave to antenna i, η_0 the free-space wave impedance, k the wave number, D_i the maximum directivity of antenna i and $\vec{\mathrm{F}}_i(\theta,\phi)$ its complex radiation pattern, which includes the influence from the other antennas [32].

In the far-field, the total power radiated by the three antennas is the integral of the power density over a full sphere, that is:

$$P = \frac{1}{\eta_0}\iint_{4\pi}\left|\vec{E}\right|^2 dS = \frac{1}{\eta_0}\iint_{4\pi}\left|\vec{E}_1+\vec{E}_2+\vec{E}_3\right|^2 dS = \frac{1}{\eta_0}\iint_{4\pi}\left(\begin{array}{l}\left|\vec{E}_1\right|^2+\left|\vec{E}_2\right|^2+\left|\vec{E}_3\right|^2+\\ \vec{E}_1\bullet\vec{E}_2+\vec{E}_1\bullet\vec{E}_3+\vec{E}_2\bullet\vec{E}_1+\\ \vec{E}_2\bullet\vec{E}_3+\vec{E}_3\bullet\vec{E}_1+\vec{E}_3\bullet\vec{E}_2\end{array}\right) dS\,. \tag{4}$$

Using (3) and (4) we get

$$\mathrm{P} = |a_1|^2 C_{11} + |a_2|^2 C_{22} + |a_3|^2 C_{33} + C_{12}a_1a_2^* + C_{13}a_1a_3^* + C_{21}a_2a_1^* + C_{23}a_2a_3^* + C_{31}a_3a_1^* + C_{32}a_3a_2^*, \tag{5}$$

where C_{ij} is given by

$$\mathbf{C}_{ij} = \begin{cases} \dfrac{D_i}{4\pi}\displaystyle\iint_{4\pi}\left|\vec{\mathbf{F}}_i(\theta,\phi)\right|^2 d\Omega & i = j \\ \sqrt{\dfrac{D_iD_j}{4\pi}}\displaystyle\iint_{4\pi}\left(\vec{\mathbf{F}}_i(\theta,\phi)\bullet\vec{\mathbf{F}}_j(\theta,\phi)\right)d\Omega & i \neq j \end{cases} \tag{6}$$

and $d\Omega = dS/r^2$. From the definition of the scalar product, and having a reciprocal network, it follows that $\mathbf{C}_{ij} = \mathbf{C}_{ji}^*$.

Equation (4) can be written as

$$\mathrm{P} = \mathbf{a}^+\mathbf{C}\mathbf{a}, \tag{7*}$$

Where '+' denotes the hermitian transpose operation, and

$$\mathbf{a} = \begin{bmatrix} a_1 \\ a_2 \\ a_3 \end{bmatrix}. \tag{8}$$

C can be written as a 3 × 3 correlation matrix:

$$\mathbf{C} = \begin{bmatrix} C_{11} & C_{12} & C_{13} \\ C_{21} & C_{22} & C_{23} \\ C_{31} & C_{32} & C_{33} \end{bmatrix} \tag{9}$$

where the elements C_{ij} are obtained from (6).

Using the law of energy conservation, the total radiated power is equal to the power incident *(a_1, a_2*, and *a_3*) in the antenna minus the sum of the reflected power *(b_1, b_2*, and b_3). Expressed using the S-parameter, this is

$$\mathrm{P} = \sum_{i=1}^{3} |a_i|^2 - \sum_{i=1}^{3} |b_i|^2 = \mathbf{a}^+\mathbf{a} - \mathbf{b}^+\mathbf{b} = \mathbf{a}^+\left(\mathbf{I} - \mathbf{S}^+\mathbf{S}\right)\mathbf{a} \tag{10}$$

where **I** is the identity matrix and **S** the S-parameters defined at the input ports of the antennas. It is seen from (7) and (10) that

$$\mathbf{C} = \mathbf{I} - \mathbf{S}^+\mathbf{S}, \tag{11}$$

where

$$\mathrm{S}^+\mathrm{S} = \begin{bmatrix} S_{11}^* & S_{21}^* & S_{31}^* \\ S_{12}^* & S_{22}^* & S_{32}^* \\ S_{13}^* & S_{23}^* & S_{33}^* \end{bmatrix} \begin{bmatrix} S_{11} & S_{12} & S_{13} \\ S_{21} & S_{22} & S_{23} \\ S_{31} & S_{32} & S_{33} \end{bmatrix} = \begin{bmatrix} S_{11}^*S_{11} + S_{21}^*S_{21} + S_{31}^*S_{31} & S_{11}^*S_{12} + S_{21}^*S_{22} + S_{31}^*S_{32} & S_{11}^*S_{13} + S_{21}^*S_{23} + S_{31}^*S_{33} \\ S_{12}^*S_{11} + S_{22}^*S_{21} + S_{32}^*S_{31} & S_{12}^*S_{12} + S_{22}^*S_{22} + S_{32}^*S_{32} & S_{12}^*S_{13} + S_{22}^*S_{23} + S_{32}^*S_{33} \\ S_{13}^*S_{11} + S_{23}^*S_{21} + S_{33}^*S_{31} & S_{13}^*S_{12} + S_{23}^*S_{22} + S_{33}^*S_{32} & S_{13}^*S_{13} + S_{23}^*S_{23} + S_{33}^*S_{33} \end{bmatrix} \tag{12}$$

Using (11) in (5) it follows that

$$\frac{D_1}{4\pi} \iint_{4\pi} \left|\vec{F}_1(\theta,\phi)\right|^2 d\Omega = 1 - \left(|S_{11}|^2 + |S_{21}|^2 + |S_{31}|^2\right) \tag{13}$$

and

$$\frac{\sqrt{D_1 D_2}}{4\pi} \iint_{4\pi} \left(\vec{\mathrm{F}}_1(\theta,\phi) \bullet \vec{\mathrm{F}}_2(\theta,\phi)\right) d\Omega = -\left(S_{12}^*S_{12} + S_{22}^*S_{22} + S_{32}^*S_{32}\right) \tag{14},$$

which leads to the envelope correlation as given by Equation 2, which is valid in the case of a (3, 3) MIMO system. With *N*=3 antennas at both ends, the envelope correlation between antenna *i*=1 and *j*=2 could be calculated as.

$$\rho_e(1,2,3) = \frac{\left|S_{11}^*S_{12} + S_{21}^*S_{22} + S_{31}^*S_{32}\right|^2}{\left(1 - \left(|S_{11}|^2 + |S_{21}|^2 + |S_{31}|^2\right)\right)\left(1 - \left(|S_{12}|^2 + |S_{22}|^2 + |S_{32}|^2\right)\right)} \tag{15}$$

1.6 Acknowledgement

This work has been supported by Nokia Denmark. Thanks to Elna Sørensen from Technical University of Denmark for proof reading.

1.7 References

[1] G. J. Foschini and M. J. Gans, "On limits of wireless communications in a fading environment when using multiple antennas," *Wireless Personal Communications*, vol. 6, pp. 311–335, 1998.

[2] A. Goldsmith, S. A. Jafar, N. Jindal, and S. Vishwanath, "Capacity limits of MIMO channels," *IEEE Journal on Selected Areas in Communications*, vol. 21, no. 5, pp. 684–702, 2003.

[3] R. Janaswamy, "Effect of element mutual coupling on the capacity of fixed length linear arrays," *IEEE Antennas and Wireless Propagation Lett*, vol. 1, pp. 157–160, 2002.

[4] R. G. Vaughan, "Signals in Mobile Communications: A Review," *IEEE Trans. Vehicular Technology*, vol. 35, pp. 133–145, 1986.

[5] R. G. Vaughan and J. Bach Andersen, "Antenna diversity in mobile communication," *IEEE Trans. Vehicular Technology*, vol. 36, pp. 149–172, 1987.

[6] D. Chizhik, F. Rashid-Farrokhi, J. Ling, and A. Lozano, "Keyholes, correlations, and capacities of multielement transmit and receive antennas," *IEEE Trans. Wireless Communications*, pp. 361–368, 2002.

[7] M. A. Jensen and J. W. Wallace, "A review of antennas and propagation for MIMO wireless communications," *IEEE Trans. Antennas propagation*, vol. 52 (11), pp. 2810–2824, 2004.

[8] C. Oestges and A. Paulraj, "Beneficial impact of channel correlations on MIMO capacity," *Electronics Letters*, vol. 40, pp. 606–608, 2004.

[9] L. Schumacher, K. I. Pedersen, and P. E. Mogensen, "From antenna spacings to theoretical capacities - guidelines for simulating MIMO systems," *Proc. The 13th IEEE International Symposium on Personal, Indoor and Mobile Radio Communications*, vol. 2, pp. 587–592, 2002.

[10] D. Chizhik, F. Rashid-Farrokhi, J. Ling, and A. Lozano, "Effect of antenna separation on the capacity of BLAST in correlated channels," *IEEE Communications Letters,* vol. 4 (11), pp. 337–339, 2000.

[11] A. Derneryd and G. Kristensson, "Signal correlation including antenna coupling," *Electronics Letters,* vol. 40 (3), pp. 157–158, 2004.

[12] M. Karaboikis, C. Soras, G. Tsachtsiris, and V. Makios, "Compact dual-printed inverted-F antenna diversity systems for portable wireless devices," *IEEE Antennas and Wireless Propagation Lett*, pp. 9–14, 2004.

[13] B. Clerckx, D. Vanhoenacker-Janvier, C. Oestges, and L. Vandendorpe, "Mutual coupling effects on the channel capacity and the space-time processing of MIMO communication systems," *Proc. IEEE International Conference on Communication, ICC '03. Int. Conf,* vol. 4, pp. 2638–2642, 2003.

[14] J. W. Wallace and M. A. Jensen, "The Capacity of MIMO wireless systems with mutual coupling," *Proc. IEEE Vehicular Technology Conf.*, pp. 696–700, 2002.

[15] *O. Edvardsson,* "Can two antennas be smaller than one?" *Proc. ICAP 2001*, pp. 533–536, 2001.

[16] J. Thaysen, "Mutual Coupling Between Two Identical Planar Inverted-F Antennas," *Proc. IEEE Antennas and Propagation Society International Symp.,* vol. 4, pp. 504–507, 2002.

[17] G. Lebrun; S. Spiteri, and M. Falkner, "MIMO complexity reduction through antenna selection," *Proc. Australian Telecommunication Cooperative Research Center, ANNAC' 03*, pp. 5, 2003.

[18] J. Blanch, J. Romeu, and I. Corbella, "Exact representation of antenna system diversity performance from input parameter description," *Electronics Letters*, vol. 39, pp. 705–707, 2003.

[19] R. H. Clarke, "A statistical theory of mobile reception," *Journal Bell System Tech.*, pp. 957-1000, 1968.

[20] K. Boyle, "Radiation pattern and correlation of closely spaces linear antennas" *IEEE Trans. Antennas Propagation, vol. 50,* pp. 1162–1165, 2002.

[21] H. T. Hui; W. T OwYong, and K. B. Toh, "Signal Correlation Between Two Normal-Mode Helical Antennas for Diversity Reception in a Multipath Environment," *IEEE Trans. Antennas Propagation,* pp. 572–577, 2004.

[22] P. S. H. Leather and D. Parson, "Antenna diversity for UHF handportable radio," *Electronics Letters* vol. 39 (13), pp. 946–948, 2003.

[23] A. Derneryd and G. Kristensson, "Antenna signal correlation and its relation to the impedance matrix," *Electronics Letters,* vol. 40 (7), pp. 401–402, 2004.

[24] S. Stein, "On cross coupling in multiple-beam antennas" *IRE Trans. Antennas Propagation*, pp. 548–557, 1962.

[25] I. Salonen and P. Vainikainen, "Estimation of signal correlation in antenna array," *Proc. Jina'02 – 12éme Journées. Internationales de Nice sur les Antennas*, pp. 383–386, 2002.

[26] www.zeland.com.

[27] www.satimo.com.

[28] K. Sulonen, P. Suvikunnas, J. Kivinen, L. Vuokko, and P. Vainikainen, "Study of different mechanisms providing gain in MIMO systems," *Proc. IEEE Vehicular Technology (VTC-2003)*, p. 4. 2003.

[29] P. Suvikunnas, K. Sulonen, J. Villanen, C. Icheln, J. Ollikainen, and P. Vainikainen, "Evaluation of performance of multi-antenna terminals using two approaches," *Proc. IEEE Instrumentation and Measurement Technology, IMTC 2004*, pp. 6, Italy, 2004.

[30] J. Thaysen and K. B. Jakobsen, "An experimental evaluation of the capacity, correlation, efficiency, and mutual coupling of three MIMO designs for mobile phones," accepted *IEEE Trans. Vehicular Technology* 2005.

[31] R. G. Vaughan and J. B. Andersen, *Channels, Propagation and Antennas for Mobile Communications*, The IEE, UK, 2003.

[32] J. E. Hansen (Ed.), *Spherical Near-field Antenna Mea-surements*, Peter Peregrinus Ltd, London, UK, 1988.

[33] A. F. Molisch and M. Z. Win, "MIMO systems with antenna selection," *IEEE Microwave Magazine,* vol. 5, pp. 46–56, 2004.

[34] J. Thaysen and K. B. Jakobsen, "Envelope correlation in N×N MIMO antenna array from scattering parameters," submitted 2005.

[35] P. Almers et al, "Measurement of keyhole effect in a wireless MIMO channel," IEEE Commun. Lett., vol. 7, pp. 373-375, Aug. 2003.

Paper II

Envelope Correlation in infinite MIMO antenna Array from scattering parameters

Authors

Jesper Thaysen

Nokia Denmark, DK-1790 København, DENMARK
Technical University of Denmark DK-2800 Kgs. Lyngby, DENMARK

Kaj B. Jakobsen

Technical University of Denmark DK-2800 Kgs. Lyngby, DENMARK

Paper Accepted in

Microwave and optical technology letters

J. Thaysen and K.B. Jakobsen, "Envelope Correlation in infinite MIMO antenna Array from scattering parameters", Accepted 2005.

1 Envelope Correlation in (N, N) MIMO antenna Array from scattering parameters

Jesper Thaysen
Nokia Denmark, www.nokia.com, DK-1790 Kbh V, DENMARK
Email: jesper.thaysen@nokia.com

Kaj B. Jakobsen

Technical University of Denmark, www.dtu.dk, DK-2800 Kgs. Lyngby, DENMARK
Email: kbj@oersted.dtu.dk

A simple closed formed equation to calculate the envelope correlation between any two receiver or transmitter antennas in a Multi-Input Multi-Output (MIMO) system of an arbitrary number of elements is derived. The equation uses the scattering parameters obtained at the antenna feed point to calculate the envelope correlation coefficient. This approach has the advantages that it does not require knowledge of the antenna radiation pattern. Numerical data that includes conductor and permittivity loss are shown to validate the approach. Using the scattering parameters for calculating the envelope correlation is less laborious and relatively cheaper as compared to the radiation pattern approach.

1.1 Introduction

In a rich multipath environment the theoretical capacity of a MIMO system increases linearly with the number of antenna elements N in a (N, N) MIMO system [1]. However, in a more practical MIMO system the capacity is reduced due to correlation between the signals in the receiver [2]. Therefore, the correlation between the signals that are received from the different antenna elements is an important parameter in a MIMO system [3]. As long as the envelope correlation is less than $\rho_e < 0.5$ diversity gain could be obtained in a mobile phone [4].

In [5] a beneficial impact of channel correlations on MIMO capacity is described. The result shows that high correlation does not necessarily result in low capacity. In [6] the physical channel is related to the observed correlations. In both cases it is the cross correlation between the receiving and transmitting antennas that is investigated, and not as in this paper, which concerns the correlation between the elements. The results obtained in [5, 6] are therefore not directly comparable to the results in this paper.

The calculation of the antenna correlation can be approached in different ways. One is based on the far-field pattern [7], and another is based on the scattering parameters obtained at the antenna terminals [8]. A third method, based on Clarke's formula [9], has recently been used in [10] and [11]. Correlation calculation using the radiation pattern principle is a time consuming process, no matter whether it is done using simulated or experimental data. Nevertheless, the method is often used (see e.g., [12]). A proposal for calculating the correlation between antennas in a two antenna system using the scattering parameters is found in [8]. The correlation between two antennas can also be calculated using the impedance matrix [13].

In MIMO systems more than two antennas often are required, thus the correlation between any two antennas in an antenna array system of arbitrary size is required. The equation has been derived using the law of energy conservation [14], which is also the case in [8] and [15]. We demonstrate its suitability in the special case of a (3, 3) MIMO system. The result obtained through the radiation pattern agrees with that obtained using the scattering parameters.

1.2 Theory

The envelope correlation for a two-antenna system could be calculated using (1), where $\vec{F}_i(\theta,\phi)$ is the field radiation pattern of the antenna system when port *i* is excited [4, 8], all other ports are terminated in Z_0 = 50 ohm match, and • denotes the Hermitian product.

$$\rho_e = \frac{\left| \iint_{4\pi} \left[\vec{F}_1(\theta,\phi) \bullet \vec{F}_2^*(\theta,\phi) \right] d\Omega \right|^2}{\iint_{4\pi} \left| \vec{F}_1(\theta,\phi) \right|^2 d\Omega \iint_{4\pi} \left| \vec{F}_2(\theta,\phi) \right|^2 d\Omega} \qquad (1)$$

Here, a closed formed equation for the envelope correlation between any two antennas is derived. Using the law of energy conservation the relation between the scattering parameters and the element radiation pattern is [14]:

$$\vec{I} - \vec{S}^H \vec{S} = \vec{F}^H \vec{F}\,, \qquad (2)$$

where *I* is the identity matrix and *H* is the complex conjugate transpose

The envelope correlation ρ_e for the correlation between antenna *i* and *j* in a MIMO system consisting of *N* antennas is given by:

$$\rho_e(i,j,N) = \frac{\left| C_{i,j}(N) \right|^2}{\prod_{k=i,j} \left[1 - C_{k,k}(N) \right]} \qquad (3)$$

where $C_{i,j}(N)$ is given by:

$$C_{i,j}(N) = \sum_{n=1}^{N} S_{i,n}^* S_{n,j} \qquad (4)$$

Using (3) with (4) the envelope correlation ρ_e expressed in scattering parameters can be calculated from:

$$\rho_e(i,j,N) = \frac{\left| \sum_{n=1}^{N} S_{i,n}^* S_{n,j} \right|^2}{\prod_{k=i,j} \left[1 - \sum_{n=1}^{N} S_{k,n}^* S_{n,k} \right]} \qquad (5)$$

Using Eq. 5 the envelope correlation between antenna *i* and *j* in and (*N*, *N*) MIMO antenna system can be calculated. For the correlation in a two-antenna diversity scheme, i.e., *N*=2, see [8]. In the case of a (3, 3) MIMO system, with *N*=3 antennas in both ends, the envelope correlation between antenna *i=1* and *j=2* could be calculated using Eq. 6.

$$\rho_e(1,2,3)=\frac{\left|S_{11}^*S_{12}+S_{12}^*S_{22}+S_{13}^*S_{32}\right|^2}{\left(1-\left(\left|S_{11}\right|^2+\left|S_{21}\right|^2+\left|S_{31}\right|^2\right)\right)\left(1-\left(\left|S_{12}\right|^2+\left|S_{22}\right|^2+\left|S_{32}\right|^2\right)\right)} \quad (6)$$

The envelope correlation is determined from the distribution of the external sources and the radiation patterns from the antennas. Only by assuming omni-directional source distribution one can relate the mutual impedances (or scattering parameters) to the correlation [4]. This means that the envelope correlations estimated based on S-parameters (as in Equation 5) correspond to that given by Equation 1 if a uniform distribution of the sources is assumed, which might be a good approximation in some indoor environments [4]. When calculating the envelope correlation by the use of the scattering parameters the radiation efficiencies of the two antennas are not included, as in the case when the radiation pattern formula are used. Given that the investigation is to design a practical antenna system for MIMO (e.g. on a mobile phone), where radiation efficiencies can be low, due to the compressed electrical size of the terminals, the assumed energy conservation in the envelope correlation expression may be inadequate. Therefore, it should be pointed out clearly that this formulation cannot completely replace the pattern correlation (as a quality criterion) in the case of small terminal antennas. The radiation pattern based method gives us the possibility to include a better description of the radio channel in the evaluation, although it makes the evaluation more complicated. However, it is found that the envelope correlation calculated using the scattering parameters yields sufficiently accurate results, and thus could be used in many practical cases.

1.3 Example

A system of three 40 mm long, 1.5 mm wide and 5 mm high Planar Inverted F-Antenna's (PIFA's) located on a 40 mm × 100 mm ground plane is considered. The antennas are located at the edge, as illustrated in Fig. 1. The feed point is located 5 mm from the edge where a 90-degree bend forms the short to the ground plane, the ground connection is denoted with dots. The distance between antenna 2 and antenna 3 is 47 mm. Conductor loss as well as loss in the permittivity is included for more realistic results.

The antenna system is simulated in terms of Scattering parameters and radiation pattern. For the scattering parameters, the measurement results validates the simulation results, see Table 1.

Fig. 1. Layout of the three-antenna configuration located on the same finite ground plane, the grey area illustrates the 40 mm × 100 mm ground plane. The matchsticks symbolise the PIFAs, and the dot on the matchstick denotes the location of the shorting pin.

Table 1. Simulation and measurement key results.

Antenna	1	2	3
f_0, sim./meas., GHz	1.80/1.80	1.80/1.81	1.83/1.84
RL, sim./meas., dB	12/19	11/11	7/8
BW, sim./meas., %	12/13	11/11	3/5
Peak radiation efficiency, sim., %	98	98	96
	S_{12}	S_{23}	S_{31}
Mutual coupling, sim./meas.,dB	-10/-11	-13/-13	-9/-15

The envelope correlation obtained using Eq. 1 is compared to that from Eq. 6 in Fig. 2.

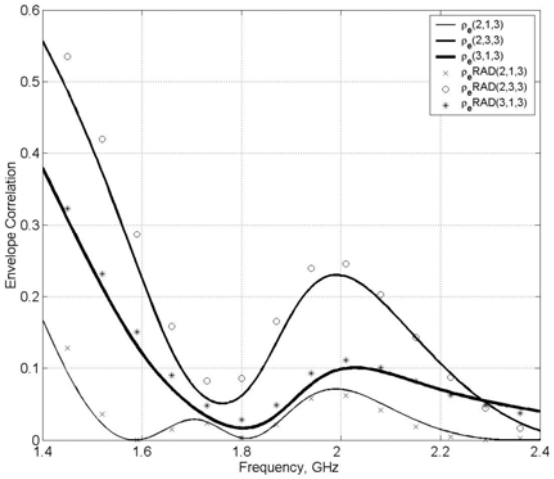

Fig. 2. Simulated envelope correlation versus frequency for a three-antenna configuration. Calculated using the scattering parameter formula (Equation 6) (solid lines) and the radiation pattern formula (Equation 1) (○, *, ×).

In the frequency range from 1.4 GHz to 2.4 GHz the envelope correlation that is based on the scattering parameter formula given by Eq. 6, yields slightly lower values as compared to the radiation pattern based method given by Eq. 1. Parts of the difference could be caused by the measurement facility, primary due to the measured dips in the $\phi = 180° \pm 12°$, which are caused by the antenna mounting and positioning system [16]. The discrepancies are probably also attributed to the fact that the scattering parameters are measured in the laboratory, a scattering environment, whereas the radiation patterns are measured in an anechoic environment. Finally, the scattering parameters do not contain any information of the radiation efficiency. The radiation efficiencies for the three antennas vary between 80% for antenna 3 at 1.4 GHz to 98% for antenna 1 and antenna 2 at 2.0 GHz as shown in Fig. 3.

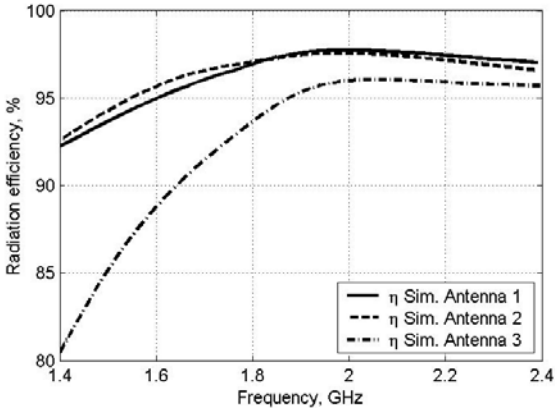

Fig. 3. Simulated radiation efficiency.

The maximum absolute difference between the envelope correlations calculated using Eq. 1 and that based on Eq. 6 are 0.04. An error of 0.04 is small compared to the 0.5 diversity rule of thumb. 0.04/0.5*100%=8%, i.e., less than 10% error. Even though that the radiation efficiency is as low as 80% for Antenna 3 the discrepancies is still very low, this means that the proposed formula could be used in many practical example though the loss is not included in the scattering parameter formula.

The worst correlation within the frequency band of interest, i.e., 1.7 GHz-1.9 GHz is $\rho_e = 0.2$ obtained between Antenna 2 and Antenna 3.

1.4 Conclusion

A closed formed expression have been presented that can be used to calculate the envelope correlation coefficient from the scattering parameters between any two antennas in a MIMO antenna array system with arbitrary number of antennas, *N*.

The expression gives a knowledge of where the effort could be placed doing design and optimisation of the antennas in a diversity or MIMO system. The equation can be applied to space, polarisation and pattern diversity as well.

Using the scattering parameters for calculating the envelope correlation is less laborious and relatively cheaper as compared to radiation pattern approach.

The shown example indicates that the formula could be used with high accuracy, even if the radiation efficiency is rather low.

1.5 Acknowledgements

Jørgen Bach-Andersen is gratefully acknowledged for valuable comments. This work has been supported by Nokia Denmark A/S.

1.6 References

[1] G. J. Foschini and M. J. Gans, “On limits of wireless communications in a fading environment when using multiple antennas,” *Wireless Personal Communications*, vol. 6, pp. 311–335, 1998.

[2] R. Janaswamy, “Effect of element mutual coupling on the capacity of fixed length linear arrays,” *IEEE Antennas and Wireless Propagation Lett*, vol. 1, pp. 157–160, 2002.

[3] R. G. Vaughan, “Signals in Mobile Communications: A Review,” *IEEE Trans. Vehicular Technology*, vol. 35, pp. 133–145, 1986.

[4] R. G. Vaughan and J. Bach Andersen, "Antenna diversity in mobile communication," *IEEE Trans. Vehicular Technology*, vol. 36, pp. 149–172, 1987.

[5] C. Oestges and A. Paulraj, "Beneficial impact of channel correlations on MIMO capacity," *Electronics Letters*, vol. 40, pp. 606–608, 2004.

[6] L. Schumacher, K. I. Pedersen, and P. E. Mogensen, "From antenna spacings to theoretical capacities - guidelines for simulating MIMO systems," *Proc. The 13th IEEE International Symposium on Personal, Indoor and Mobile Radio Communications*, vol. 2, pp. 587–592, 2002.

[7] G. Lebrun; S. Spiteri, and M. Falkner, "MIMO complexity reduction through antenna selection," *Proc. Australian Telecommunication Cooperative Research Center, ANNAC' 03*, pp. 5, 2003.

[8] J. Blanch, J. Romeu, and I. Corbella, "Exact representation of antenna system diversity performance from input parameter description," *Electronics Letters*, vol. 39, pp. 705–707, 2003.

[9] R. H. Clarke, "A statistical theory of mobile reception," *Journal Bell System Tech.*, pp. 957-1000, 1968.

[10] K. Boyle, "Radiation pattern and correlation of closely spaces linear antennas" *IEEE Trans. Antennas Propagation, vol. 50,* pp. 1162–1165, 2002.

[11] H. T. Hui; W. T OwYong, and K. B. Toh, "Signal Correlation Between Two Normal-Mode Helical Antennas for Diversity Reception in a Multipath Environment," *IEEE Trans. Antennas Propagation,* pp. 572–577, 2004.

[12] P. S. H. Leather and D. Parson, "Antenna diversity for UHF handportable radio," *Electronics Letters* vol. 39 (13), pp. 946–948, 2003.

[13] A. Derneryd and G. Kristensson, "Antenna signal correlation and its relation to the impedance matrix," *Electronics Letters,* vol. 40 (7), pp. 401–402, 2004.

[14] S. Stein, "On cross coupling in multiple-beam antennas" *IRE Trans. Antennas Propagation*, pp. 548–557, 1962.

[15] I. Salonen and P. Vainikainen, "Estimation of signal correlation in antenna array," *Proc. Jina'02 – 12éme Journées. Internationales de Nice sur les Antennas*, pp. 383–386, 2002.

[16] www.satimo.com

Paper III

Design considerations for low antenna correlation and mutual coupling reduction in multi antenna terminals

Authors

Jesper Thaysen

Nokia Denmark, DK-1790 København, DENMARK
Technical University of Denmark DK-2800 Kgs. Lyngby, DENMARK

Kaj B. Jakobsen

Technical University of Denmark DK-2800 Kgs. Lyngby, DENMARK

Paper Accepted in

ETT-European Transactions on Telecommunications

J. Thaysen and K.B. Jakobsen, "Design considerations for low antenna correlation and mutual coupling reduction in multi antenna terminals", Accepted 2005.

1 Design considerations for low antenna correlation and mutual coupling reduction in multi antenna terminals

Jesper Thaysen
Nokia Denmark, www.nokia.com, DK-1790 København, DENMARK
Email: jesper.thaysen@nokia.com

Kaj B. Jakobsen
Technical University of Denmark, www.dtu.dk, DK-2800 Kgs. Lyngby, DENMARK
Email: kbj@oersted.dtu.dk

The influence of mutual coupling on the envelope correlation between two identical planar inverted F-antennas (PIFA) are investigated. The capacity of a multiple-input multiple-output (MIMO) antenna system strongly depends on the correlation between the antennas. By placing two antennas in a fixed area it is found that the envelope correlation could be halved simply by proper mutual orientation. The set-ups that maximise the distances between the open ends of the PIFAs yield the lowest mutual coupling as well as the lowest envelope correlations. It is found that the envelope correlation is 0.8 when the PIFAs are oriented in parallel. The envelope correlation can be decreased to 0.4 by rotating one of the PIFAs by 180 degrees.

Key-Words: - Envelope correlation, mutual coupling, MIMO, PIFA

1.1 Introduction

The Planar Inverted-F Antenna (PIFA) is widely used in cellular phones primarily due to the compactness and size [1]. The demand for smaller communication devices for personal communication systems has led to a constant search for ways to reduce the cellular phone dimensions. However, the wavelength does not decrease, due to the higher frequency bands used, with the same speed as the size of the mobile phones. Even the widely used PIFA tends to become too large, and thus a demand for decreasing the volume of the antenna exists. At the same time new applications such as Multiple-input multiple-output (MIMO) systems are emerging.

MIMO requires several antennas each covering the same frequency band, and thus the complexity and the requirements to the antenna system continue to increase. MIMO systems are very attractive in order to boost the capacity of a wireless communication system that operates in a rich multipath environment. The theoretical capacity increases linearly with the number of antenna elements N in a (N, N) MIMO system [2].

When the MIMO system is to be implemented the capacity will be reduced due to correlation between the signals in the receiver [3]. Thus the correlation between signals that are received from different antenna elements is an important parameter in a MIMO system [4]. The requirement is that the envelope correlation should be less than $\rho_e < 0.5$ in order to obtain diversity gain in a mobile phone [5]. A low envelope correlation is on the other hand not always a guarantee for high capacity. A drop in the capacity can occur in special cases denoted “keyholes”. See [6, 7] for a more throughout description of the keyholes.

Mutual coupling between the antenna elements might also affects the correlation [8-12]. Cramming more antennas into a mobile phone causes inevitably higher mutual coupling due to the smaller distances between the antennas [13, 14]. The increased mutual coupling results in higher spatial correlation which again leads to a lower MIMO gain as compared to the case of fully uncorrelated antenna signals [13, 15]. Therefore, knowledge regarding how these antennas should be oriented in order to minimise the coupling [14] and the correlation is needed.

Calculation of the antenna correlation can be done in different ways. One way is to use the far-field radiation pattern [5], and another is to use the scattering parameters obtained at the PIFA terminals [16]. Using the radiation pattern, the envelope correlation for a two-antenna system can be calculated using Equation (1) [5, 16], where $\vec{\mathbf{F}}_i(\theta,\phi)$ is the far-field pattern of the antenna system when port *i* is excited (all other ports are terminated in a 50 ohm match), and • denotes the Hermitian product.

$$\rho_e = \frac{\left| \iint_{4\pi} \vec{\mathbf{F}}_1(\theta,\phi) \bullet \vec{\mathbf{F}}_2^*(\theta,\phi)\, d\Omega \right|^2}{\iint_{4\pi} \left| \vec{\mathbf{F}}_1(\theta,\phi) \right|^2 d\Omega \iint_{4\pi} \left| \vec{\mathbf{F}}_2(\theta,\phi) \right|^2 d\Omega} \qquad (1)$$

In this paper the envelope correlation are calculated using Equation (2), which is the formula proposed by Blanch et al. [17].

$$\rho_e = \frac{\left| S_{11}^* S_{12} + S_{21}^* S_{22} \right|^2}{\left(1 - \left(\left|S_{11}\right|^2 + \left|S_{21}\right|^2\right)\right)\left(1 - \left(\left|S_{12}\right|^2 + \left|S_{22}\right|^2\right)\right)} \qquad (2).$$

The envelope correlation is determined from the distribution of the external sources and the radiation patterns from the antennas, thus the envelope correlations estimated based on S-parameters (as in Equation 2) correspond to that given by Equation 1 if a uniform distribution of the sources is assumed, which might be a good approximation in, e.g., some indoor environments [16].

A drawback when calculating the envelope correlation by the use of the scattering parameters is the lacking radiation efficiencies of the two antennas which are not included, as in the case when the radiation pattern formula are used. In the design of small antennas on a mobile phone, the radiation efficiencies can be low, due to the compressed electrical size of the terminals, thus the assumed energy conservation in the envelope correlation expression may be inadequate. Therefore, it should be pointed out clearly that this formulation cannot completely replace the pattern correlation (as a quality criterion) in the case of small terminal antennas. The radiation pattern based method gives us the possibility to include a better description of the radio channel in the evaluation, although it makes the evaluation more complicated, no matter whether it is done using numerical or experimental data. Nevertheless, this method is often used see e.g. [18]. However, in many practical cases the envelope correlation calculated using the scattering parameters yields sufficiently accurate results and hence it is used in the remaining part of this paper [17].

The scattering parameters are found by the use of the method-of-moment simulation program IE3D [19]. There are good agreement between the experimental and the simulation results.

In this paper it is the PIFAs, which are small radiators, well known and well suited for handheld or the like terminals that are considered. A systematic comparison between the various relevant quantities like return loss, isolation and correlation are provided. Also, the effect of the relative distance and orientation of the radiators are systematic investigated.

An almost exponential relation between the mutual coupling and the envelope correlation is found. Below this limit the envelope correlation is almost constant, and therefore effort in decreasing the mutual coupling should be limited to this level.

1.2 Results and discussion

This section is divided into two subsections. In the first subsection a two-antenna configuration are investigated with respect to the reflection coefficient, mutual coupling, bandwidth, and envelope correlation of the two antennas located on the same finite ground plane. These investigations are both based on simulated results as well as measurements on a fabricated prototype. The second subsection elaborates on the two-antenna configuration located on an infinite ground plane. Here, symmetrical as well as unsymmetrical coupling scenarios using two identical PIFAs located close to each other is investigated, in order to determine the correlation versus distance for fixed orientations. The results illustrate how to orientate and locate the antennas in order to minimise the correlation.

The infinite ground plane is chosen to determine the influence of the distance and mutual orientation and not the effect of the location on a finite ground plane. At a later stage in the design of the MIMO antennas one should optimise the input impedance and bandwidth of the PIFA (e.g., by changing the distance between the feed and the ground contact) on a finite ground plane. Also the proximity effect by mobile phone cover and by artificial hand and head should be included.

Two antennas on finite ground plane

The presented two-antenna configuration consists of two 40 mm long, 1.5 mm wide and 5 mm high PIFAs located on a 40 mm × 100 mm ground plane. The feed point is located 5 mm from the edge where a 90-degree bend forms the short to the ground plane denoted with dots in Figure 1.

Figure 1. Illustration of the antenna model and the orientation, the grey area illustrates the 40 mm × 100 mm ground plane. The matchsticks symbolises the PIFAs and the dots denote the location of the shorting pins.

Good agreements between the simulation and measurement are obtained as can be seen in Figure 2. Both antennas have resonant frequency at 1.82 GHz. The measured mutual coupling is somewhat lower as compared to the simulated.

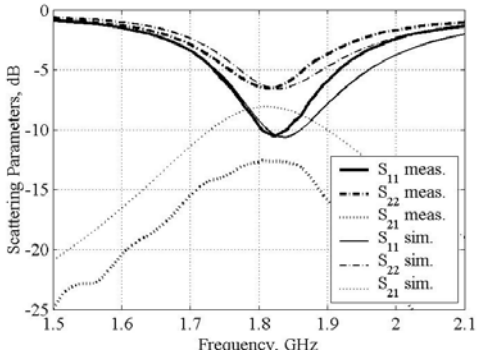

Figure 2. Simulated and measured scattering parameters for the two antenna configuration illustrated in Figure 1 above a 40 mm × 100 mm ground.

Agreement between the simulated and measured envelope correlation is obtained, see Figure 3. The agreement is best around the resonant frequency. Major parts of the difference in the simulated and measured envelope correlation could be explained by the difference between the two antennas, which are hand made, i.e., made by using a scalpel, and therefore not completely identical.

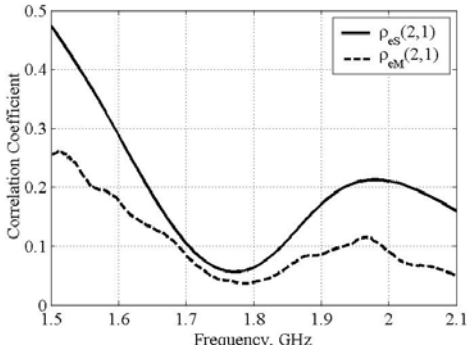

Figure 3. Simulated and measured envelope correlations.

Two antennas on infinite ground plane

The PIFA investigated consists of a 40 mm × 1 mm patch located 15 mm above an infinite perfect conducting ground plane. The feed line is located 13 mm from the edge where a 90° bend forms the short circuit to the ground plane see illustration in Figure 4.

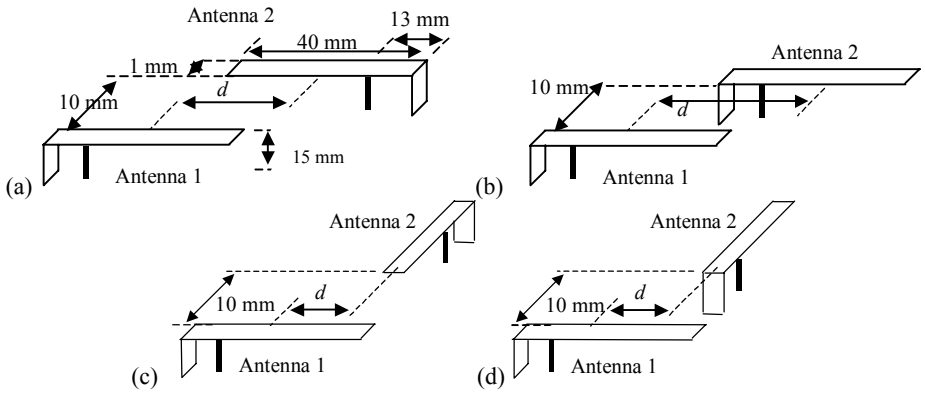

Figure 4. Illustration of the four different configurations that are investigated. Parallel antennas fed at the opposite ends (a), parallel antennas fed at the same end (b), orthogonal antennas with antenna 2 fed

at the top (c), and orthogonal antennas with antenna 2 fed at the bottom. The vertical distance is fixed 10 mm, whereas the horizontal distance, d, varies in the different scenarios.

This section is divided into three subsections: one treating parallel PIFA configurations (see Figure 4a and 4b), and one treating orthogonal PIFA configurations (see Figure 4c and 4d). In the third subsection the envelope correlation are investigated with respect to mutual coupling.

In all cases it is the geometrical centre that is used since it is a simple measure. Another measure could be the phase centre of the antenna; this point however, is not easy to identify for a PIFA [20].

Fixed parallel orientations:

Two parallel PIFAs separated by 10 mm, with a horizontal distance, *d,* that is defined so that *d* is positive in the case illustrated in Figure 4a are investigated. First both antennas are fed in the same end (Figure 4b), hereafter called (0, 0), and second they are fed in the opposite ends (0, 180), as illustrated in Figure 4a.

Figure 5 shows the simulated envelope coefficient and S-parameters as a function of the horizontal distance, *d*. Both the highest coupling, $|S_{21}| = -4.8$ dB and the highest envelope correlation $\rho_{21} = 0.8$ is obtained for $d = 0$. A symmetrical roll-off is observed for the correlation as well as for the coupling when the distance is increased; this seems reasonably due to the symmetry in the set-up. At d = ±13 mm where the shorting point is above the feed line the impedance match is worst.

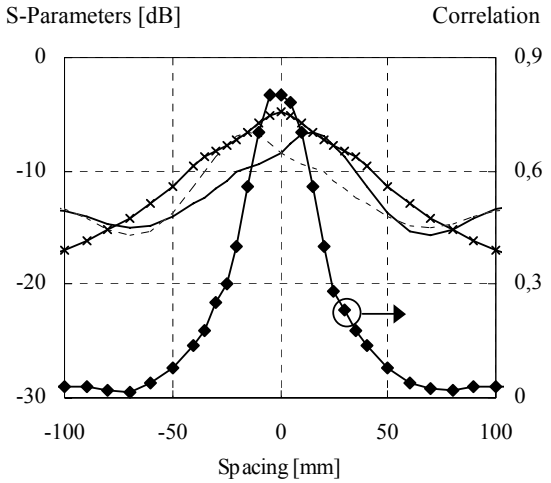

Figure 5. Simulated envelope coefficient ρ_{21} (♦), S-parameters S_{11} (solid), S_{22} (dashed) and S_{21} (×) at the simulated centre frequency (min. $|S_{11}|$) for two parallel PIFAs separated by 10 mm and fed at the same end, on infinite ground plane.

The centre frequency (min. $|S_{11}|$) of the two antennas is only altered slightly as a function of distance (data not shown). The largest deviation is obtained at zero horizontal distance between the open end of one of the antennas and the feed line of the other. Here the centre frequency (min. $|S_{11}|$) is shifted 30 MHz compared to the result that is obtained for a single antenna. At $d = 0$ mm the centre frequency (min. $|S_{11}|$) change from 1.94 to 1.96 GHz – a difference of 1.5% only.

Similar simulations are made for the configuration where the two antennas are fed in the opposite ends; the results are shown in Figure 6.

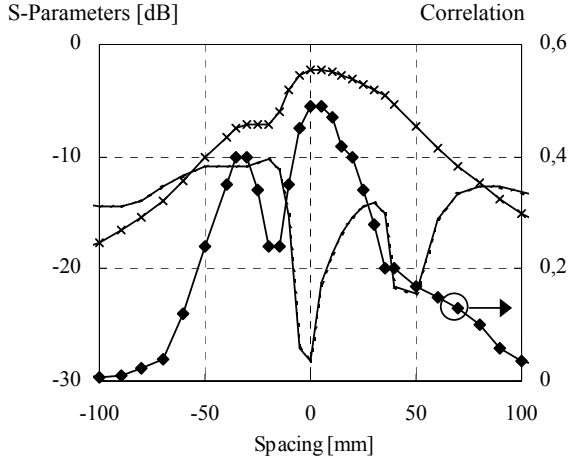

Figure 6. Simulated envelope coefficient ρ_{21} (♦), S-parameters S_{11} (solid), S_{22} (dashed) and S_{21} (×) at the simulated centre frequency (min. $|S_{11}|$) for two parallel PIFAs separated by 10 mm and fed at the opposite ends, on infinite ground plane.

Apart from the location of the peak correlation (ρ_{21}=0.52) and coupling (S_{21} = –2.3 dB) that are obtained for d = 0, the results are quite different from the results shown in Figure 5, a rather unsymmetrical decrease is observed for an increase in the distance. This seems reasonable due to asymmetry in the set-up. For positive values of d, similarities in the two parallel cases are observed, i.e., the correlation and the coupling decrease almost continuously. However, a rather different behaviour is observed for negative values of d. A steep flange is observed where the feed lines are closest, i.e., for d = –5 to –20 mm, followed by an almost horizontal curve section where the coupling remains constant at around –7 dB for d = –20 to –40 mm.

For the correlation a local minima of ρ_{21} = 0.25 is observed at d = –13 mm, here the vertical distance between the fed points is zero. Also, observed is the local maxima of ρ_{21} = 0.4, at d = –40 mm, here the vertical distance between the short pins is zero.

Changing the horizontal distance such that the feed line is moved towards the shorting point causes a rapid decrease in the coupling, whereas moving the feed line away from the shorting point, i.e. towards the open end does not seem to affect the coupling. The coupling starts to decrease again when the two PIFAs are emancipated horizontally from each other.

The two identical reflection coefficients shown in Figure 6 have two dips in the impedance match, the best at d = 0 mm and the other between d = +40 to +50 mm. The latter is when the vertical distance between the open ends is zero.

Comparing the simulated scattering parameters shown in Figure 5 with those shown in Figure 6 it can be seen that the coupling is 2.5 dB higher for (0, 180) than for (0, 0), this indicates lower coupling for the latter. A similar difference in the correlation from ρ = 0.8 to ρ = 0.52 is observed as well. However, making this comparison one should bear in mind that no corrections have been made regarding the different impedance match. This explains part of the difference. Nevertheless, it is still the set-up, corresponding to the results shown in Figure 5 that yields the lowest coupling and the lowest correlation.

The centre frequency (min. $|S_{11}|$), shown in Figure 7, is altered quite dramatically from 1.96 GHz to 1.75 GHz. The largest deviation is obtained when the open end of one of the antennas

is located above the feed line of the other; here the centre frequency (min. $|S_{11}|$) is decreased by 200 MHz.

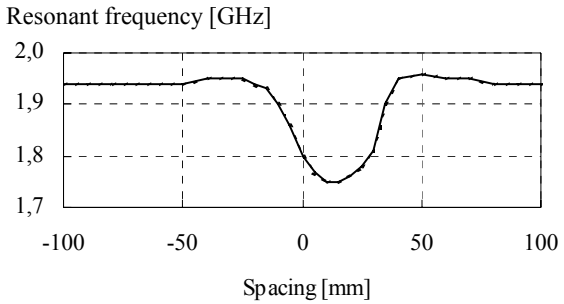

Figure 7. Simulated centre frequency (min. $|S_{11}|$) of both antennas for feeding at opposite ends. Due to symmetry in the configuration the two curves are identical.

Fixed Orthogonal Orientations:

This subsection covers the orthogonal cases. The two orthogonal PIFAs separated by 10 mm, with a horizontal distance, *d,* that is defined so that *d* is positive in the case illustrated in Figure 4c. First, antenna 2 are fed in the top (Figure 4c), hereafter called (0, 270), and secondly fed in the bottom (0, 90) (Figure 4d).

For the orthogonal cases the behaviour seems comparable with the parallel cases. However, they need some explanation which will be provided in the following.

For the curves showed in Figure 8, the reflection coefficient for the to antennas is rather fluctuating between –16 and –9 dB, no directly minima or maxima is easily identified. The lowest reflection coefficient of –16 dB is obtained at a distance of –40 mm, this is where the open end of antenna 2 is above the shorting pin of antenna 1. This is also the case for the parallel case showed in Figure 6 at +40 mm. The worst impedance match at –9 dB is obtained at a distance of –7 mm, when the open end of antenna 2 is above the feeding line of antenna 1.

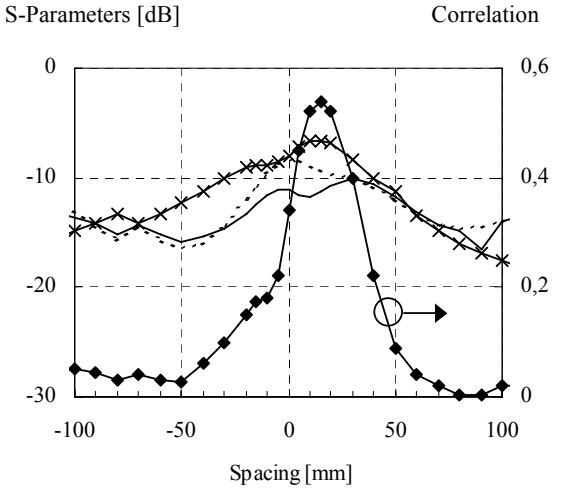

Figure 8. Simulated envelope coefficient ρ_{21} (♦), S-parameters S_{11} (solid), S_{22} (dashed) and S_{21} (×) at the simulated centre frequency (min. $|S_{11}|$) for the two orthogonal PIFAs separated by 10 mm, antenna 2 is fed at the top, on infinite ground plane.

The results shown in Figure 8 indicate a rather asymmetrical behaviour. For both the correlation and the coupling a local plateau is located at –7 mm when the open end of antenna 2 is located above the feeding line of antenna 1. The highest correlation of 0.54 and the strongest coupling of –6 dB occurs at +20 mm when the open end of antenna 2 is above the open end of antenna 1.

For the curves showed in Figure 9, the correlation, the coupling as well as the impedance match for the two antennas are rather symmetrical around –7 mm with a maxima that is easily identified, and a roll off as a function of distance. The worst correlation of 0.25, the best impedance match on –50 dB, and the strongest coupling of –6 dB is obtained at a distance of –7 mm, where the shorting pin of antenna 2 is above the feeding point of antenna 1.

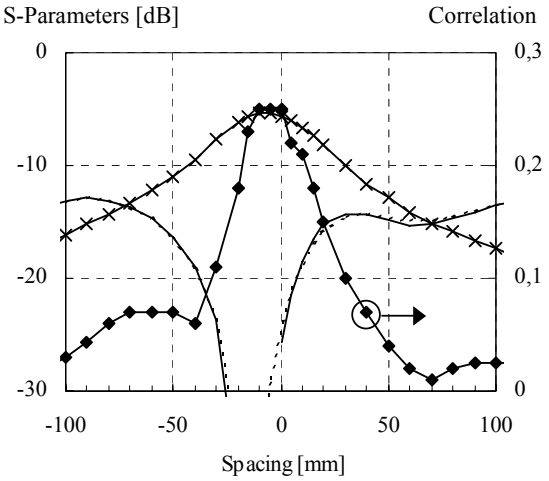

Figure 9. Simulated envelope coefficient ρ_{21} (♦), S-parameters S_{11} (solid), S_{22} (dashed) and S_{21} (×) at the simulated centre frequency (min. $|S_{11}|$) for two parallel PIFAs separated by 10 mm, antenna 2 is fed at the bottom, on infinite ground plane.

A minor change in the centre frequency (min. $|S_{11}|$) for the orthogonal cases is observed (data not shown) . For the case where antenna 2 is feed in the bottom (see illustration in Figure 4) the largest deviation is obtained at ±20 mm that is when the open end of antenna 2 is above the open end (20 mm) and the shorting pin (–20 mm) of antenna 1. Here the centre frequency (min. $|S_{11}|$) is shifted by 30 MHz, i.e., 1.5%.

For the case where antenna 2 is feed in the top, the largest deviation is obtained at –7 mm that is when the shorting pin of antenna 2 is above the feeding point of antenna 1. Here the centre frequency (min. $|S_{11}|$) is shifted by 50 MHz compared with the result obtained for a single antenna(data not shown).

Comparing the two simulated scattering parameters shown in Figure 8 and Figure 9, it can be seen that the coupling is 1.3 dB better for (180, 270) than for (180, 90), this indicates higher coupling for the latter. At the same time the correlation is decreased from 0.54 to 0.25. However, making this comparison again one should bear in mind that no corrections have been made regarding the different impedance match. Nevertheless, it is still the set-up, corresponding to the results shown in Figure 9 that yields the lowest coupling and the lowest correlation.

Correlation versus mutual coupling

The relation between the envelope correlation and the mutual coupling for the cases described in Figure 4 is indicated in Figures 10, 11, 12, and 13.

An almost exponential decrease of the correlation as a function of the mutual coupling could be observed from Figure 10 which corresponds to the parallel case with short pins in the same ends, as illustrated in Figure 4. The worst mutual coupling is –5 dB, here the correlation is 0.8.

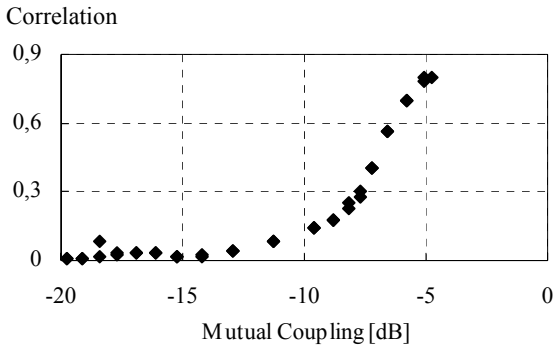

Figure 10. Envelope correlation versus mutual coupling for the parallel scenario. Both antennas are feed in the same end.

It can be observed that when the mutual coupling is lowered from –5 dB to –10 dB, the correlation decreases rapidly to 0.15. Further isolation, i.e., for mutual coupling below –10 dB, only a fractional decrease in the correlation is observed. For $S_{21} < -10$ dB, the correlation is somewhat below 0.15.

For the parallel case with opposite short-pin location, a decrease in the correlation could be observed for an improved mutual coupling, as shown in Figure 11. Here, the worst mutual coupling is –2.3 dB which is rather high as compared with the result shown in Figure 10. Even though, the rather high mutual coupling, the correlation is 0.5 as compared to 0.8 in the previous case.

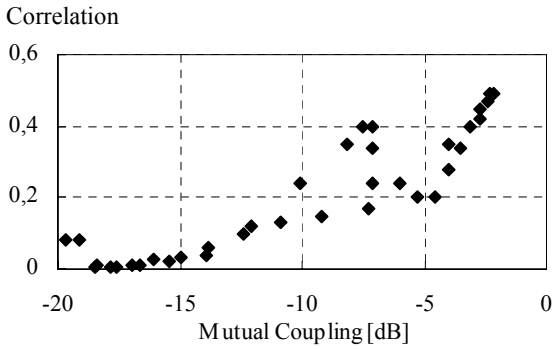

Figure 11. Envelope correlation versus mutual coupling for the parallel scenario. The antennas are feed in opposite ends.

Again, for $S_{21} < -10$ dB, the correlation is somewhat below 0.15. Above –10 dB no direct relation between the envelope correlation and the mutual coupling is found. It can be observed

that when the mutual coupling is lowered from –2.3 dB to –5 dB, the correlation decreases rapidly to 0.2. For $S_{21} < -10$ dB, the correlation is somewhat below 0.15. In between, i.e. $-5 < S_{21} < -10$ dB, the correlation is rather fluctuating between $0.15 < \rho_{21} < 0.40$.

For both the orthogonal cases the correlation is below 0.1 for $S_{21} < -10$ dB as shown in Figure 12 and Figure 13. In Figure 12, the results from the orthogonal case having antenna 2 is fed at the top that is shown. Here, the worst correlation is 0.25.

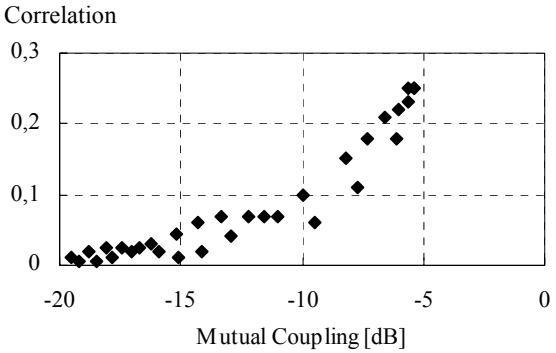

Figure 12. Envelope correlation versus mutual coupling for the orthogonal scenario. Antenna 2 is fed at the top.

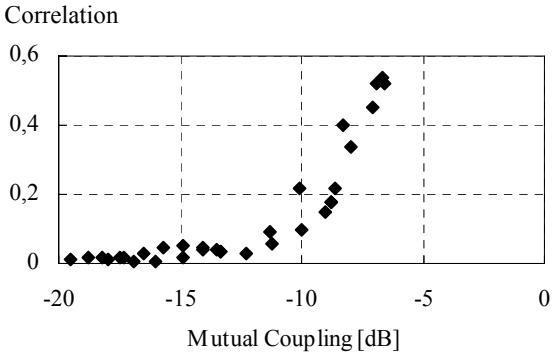

Figure 13. Envelope correlation versus mutual coupling for the orthogonal scenario. Antenna 2 is fed at the bottom.

The correlation shown in Figure 13 has an almost exponential behaviour; the set-up is illustrated in Figure 4. The highest correlation is 0.5 obtained for a mutual coupling of –8 dB.

1.3 Conclusions

The correlation and the coupling between two identical Planar Inverted F-Antenna (PIFA) has been investigated using IE3D.

It is found that two identical PIFAs closely spaced affect each other, the deviation in the centre frequency (min. $|S_{11}|$) is most affected in the case of parallel antennas, each having the feed point in the same end, here a change of 12% is observed. In the three other scenarios the change is below 2%, as compared to a single PIFA.

Maximum envelope correlation of 0.8 is obtained for the parallel set-up, when the antennas are overlapping each other, and highest for the set-up having the feed point in same ends.

Two different cases are investigated; one with parallel PIFAs another with orthogonal orientation. For the parallel case with 10 mm separation it is found that the envelope correlation is 0.8 and simply by rotation one of the antennas 180 degrees the envelope correlation decreases to 0.4. Similarly for the orthogonal antennas set-up, here the envelope correlation decreases from 0.5 to 0.25. For the orthogonal set-ups the highest envelope correlation is obtained when the shorting pin and the feed line are vertically on line.

An almost exponential relation between the mutual coupling and the envelope correlation is found. A certain limit of the mutual coupling of –10 dB is found, below this limit the envelope correlation is almost constant, being below 0.15, and therefore effort in decreasing the mutual coupling should be limited to this level.

In this paper an infinite ground plane is chosen to determine the influence of the distance and mutual orientation, and not the effect of the location which would be the case if a finite ground plane. At a later stage in the design of the MIMO antennas one should optimise the input impedance and bandwidth of the PIFA (e.g., by changing the distance between the feed and the ground contact) on a finite ground plane. Also the proximity effect by mobile phone cover and by artificial hand and head should be included.

1.4 Acknowledgements:

This work has been supported by Nokia Denmark.

2 References

[1] Hirasawa K, and Haneishi M, “Analysis, design, and measurement of small and low profile antennas,” *Artech House*, ISBN 0-89006-486-5, 1991.

[2] Foschini G.J, and Gans M.J, “On limits of wireless communications in a fading environment when using multiple antennas,” *Wireless Personal Communications*, vol. 6, pp. 311–335, 1998.

[3] Janaswamy R, “Effect of Element Mutual Coupling on the Capacity of Fixed Length Linear Arrays”, *IEEE Antennas and Wireless Propagation Lett*, vol. 1, pp. 157-160, 2002.

[4] Vaughan R.G, “Signals in Mobile Communications: A Review”, *IEEE Trans. Vehicular Technology*,vol. 35, pp. 133-145, 1986.

[5] Vaughan, R.G and Bach Andersen J, “Antenna diversity in mobile communication”, *IEEE Trans. Vehicular Technology*, vol. 36, pp. 149–172, 1987.

[6] Chizhik D, Rashid-Farrokhi F, Ling J, and Lozano A, “Keyholes, correlations, and capacities of multielement transmit and receive antennas”, *IEEE Trans. Wireless Communications*, pp. 361-368, 2002.

[7] Jensen M.A and Wallace J.W, “A review of antennas and propagation for MIMO wireless communications”, *IEEE Trans. Antennas propagation*, vol. 52 (11), pp. 2810–2824, 2004.

[8] Derneryd A, Kristensson G, “Signal correlation including antenna coupling”, *Electronics Letters,* vol. 40 (3), pp. 157-158, 2004.

[9] Wallace J.W, Jensen M.A, “The Capacity of MIMO wireless systems with mutual coupling”, Proc. *IEEE VTC’ 03*, pp. 696-700, 2002.

[10] Chizhik D, Rashid-Farrokhi F, Ling J, and Lozano A, “Effect of antenna separation on the capacity of BLAST in correlated channels”, *IEEE Communication Lett.* vol. 4 (11), pp. 337–339, 2000.

[11] Karaboikis M, Soras C, Tsachtsiris G., and Makios V, "Compact dual-printed inverted-F antenna diversity systems for portable wireless devices", *IEEE Antennas Wireless Propagation Lett*, pp. 9–14, 2004.

[12] Clerckx B, Vanhoenacker-Janvier D, Oestges C, and Vandendorpe L, "Mutual coupling effects on the channel capacity and the space-time processing of MIMO communication systems", *Proc. ICC '03. IEEE Int. Conf. on Communication,* vol. 4, pp. 2638–2642, 2003.

[13] Edvardsson O, "Can two antennas be smaller than one?" *Proc. ICAP 2001*, pp. 533 – 536, 2001.

[14] Thaysen J, "Mutual Coupling Between Two Identical Planar Inverted-F Antennas", *Proc. IEEE Antennas and Propagation Society International Symp.,* pp 504–507, 2002 Digest, vol. 4, 2002.

[15] Thaysen J and Jakobsen K.B, "MIMO channel capacity versus mutual coupling in multi antenna element system", Proc. *AMTA 2004, Antenna Measurement Techniques Association, 26th Annual Meeting & Symposium*, Atlanta, GA, USA, pp. 124-129, 2004.

[16] Vaughan, R.G and Bach Andersen J, "*Channels, Propagation and Antennas for Mobile Communications"*, The IEE, UK, 2003.

[17] Blanch J, Romeu J, and Corbella I, "Exact representation of antenna system diversity performance from input parameter description", *Electronics Letters*, vol. 39, pp. 705–707, 2003.

[18] Leather P.S.H and Parson D, "Antenna diversity for UHF handportable radio", *Electronics Letters,* vol. 39 (13), pp. 946–948, 2003.

[19] IE3D, www.zeland.com.

[20] Appel-Hansen J, "Centres of structures in electromagnetism – a critical analysis," *IEEE Transaction on antennas and propagatio*n, pp. 606–610, 1982

.

Paper IV

An experimental evaluation of the capacity, correlation, efficiency, and mutual coupling of three MIMO designs for mobile phones

Authors

Jesper Thaysen

Nokia Denmark, DK-1790 København, DENMARK
Technical University of Denmark DK-2800 Kgs. Lyngby, DENMARK

Kaj B. Jakobsen

Technical University of Denmark DK-2800 Kgs. Lyngby, DENMARK

Paper accepted in

IEEE Transactions on Vehicular Technology

J. Thaysen and K.B. Jakobsen, "An experimental evaluation of the capacity, correlation, efficiency, and mutual coupling of three MIMO designs for mobile phones", Accepted 2005.

1 An experimental evaluation of the capacity, correlation, efficiency, and mutual coupling of three MIMO designs for mobile phones

Jesper Thaysen
Nokia Denmark, www.nokia.com, DK-1790 Kbh V, DENMARK
Email: jesper.thaysen@nokia.com

Kaj B. Jakobsen

Technical University of Denmark, www.dtu.dk, DK-2800 Kgs. Lyngby, DENMARK
Email: kbj@oersted.dtu.dk

Multiple-input multiple-output (MIMO) wireless systems use multiple antenna elements to transmit and receive to offer higher capacity over single antenna topologies in multipath environments. In such systems, the antenna properties as well as the multipath channel characteristics play a key role in evaluation of the performance. The proposed simple yet realistic three-antenna configuration (3, 3) has a 50% outage talk position capacity $C_{0.5}$ of 6.4 bit/s/Hz in small macro cell environment, measured in downtown Helsinki. The maximum ratio combining (MRC) gain of using two extra antennas is 5.5 dB as compared to the branch power (Br) of antenna A3. Though a low efficiency (below 2%) of one of the three antennas, this extra antenna results in a 1.5 bit/s/Hz improvement over the (2, 2) MIMO configuration. It is also shown that the gain of using a (3, 3) system as compared to a (2, 2) system is increasing for improved signal to noise ratio (*SNR*). At zero *SNR* the difference is 0.5 bit/s/Hz increasing to 14 bit/s/Hz at a *SNR* of 50 dB. Here, the talk position capacity of the (3, 3) configuration is 43 bit/s/Hz. Simply by adding more elements at the Tx antennas the capacity of the (3, 3) configuration increases. From one to four Tx antennas the talk position capacity increases from 4.7 bit/s/Hz to 7.4 bit/s/Hz, as compared to the increase of 0.8 bit/s/Hz for the last three antennas. Taking the increased hardware complexity into account, the (4, 3) MIMO system is the optimal with respect to the obtained capacity. It is found that a (2, 3) yields an extra capacity of 0.6 bit/s/Hz as compared to a (3, 2) though having the same amount of antennas.

Keywords: Channel capacity, Correlation, Mutual Coupling, Multi-Input Multi-Output (MIMO) measurements.

1.1 Introduction

When a mobile and wireless terminal is moved in multipath environments, strong fading inevitable occurs due to multipath propagation. Diversity is a technique to overcome the effects of multipath fading [1]. In a receiver diversity system, the basic concept is that the receiver should have more than one version of the transmitted signal available, each received through a distinct channel. In the channel the fading indented to be mostly independent, i.e., simultaneously deep fade in all channel are seldom [1]. The hole idea behind MIMO is that the signals on the transmitter (TX) antennas at one end and the receiver (RX) antennas at the other end are "combined" in such a way that the quality in terms of the bit-error rate (*BER*) or the data rate (bits/sec) for each of the MIMO user can be improved [3]. A MIMO-system transmits data over a matrix channel rather than just over single radio channels. This requires signal processing over both time and space.

Since the early pioneering work by Winters [4], Foschini [5], and Telatar [6], MIMO systems have received considerable attention due to the potential increase in capacity. It has been shown that MIMO systems have the potential for large capacities, since the system can provide several independent communication channels between transmitter and receiver [5]. In an ideal multipath channel, the theoretical MIMO capacity increases linearly by *m* times the capacity of a single-antenna system SISO (Single-Input Single-Output), where *m* is the smaller of the number of transmit or receive antenna elements [5].

However, in a more practically MIMO system the capacity is reduced due to correlation between the signals in the receiver [7], this effect has been investigated both theoretically [8], [9], and experimentally [10].

Therefore the correlation between the signals that are received from the different antenna elements is an important parameter in a MIMO system, due to the increased capacity for decreased correlation [11]. However, for correlations below a certain value, only minor increase in the capacity is obtained [1].

Even though, this motivates for low correlation, it is not a guarantee for high capacity, since in some special propagation scenarios, the MIMO channel capacity can be low (i.e., comparable to the SISO capacity) even though the signals at the antenna elements are uncorrelated [12], [13]. This effect that has been denoted ”keyhole” leads to a drop in the capacity [14]. It is related to scenarios where rich scattering around the transmitter and receiver leads to low correlation of the signals, while other propagation effects, like diffraction or waveguiding, lead to a rank reduction of the transfer function matrix.

Moreover, in the case of non-richness of the scattering environment that could be line-of-sight properties the correlation at the receiver increases and causes a drop in the potential capacity.

Also, the effect of mutual coupling between the antenna elements affects the correlation [15-19]. High MIMO capacity is due to the fact that many antennas each cover the same frequencies in the link. Cramming many antennas on the same finite sized ground plane results in higher mutual coupling due to the smaller distances between the antennas [20]. Therefore, knowledge regarding how these antennas should be oriented in order to minimise the coupling [21] and the correlation is needed. In many cases, an increased mutual coupling results in higher spatial correlation [22], which in many case leads to a lower MIMO gain as compared to fully uncorrelated antenna signals.

The correlation between signals received with different antenna elements is an important parameter in a multi-input multi-output (MIMO) system, due to the increased capacity for decreased correlation

Traditionally, the calculation of the antenna correlation is based on the far-field pattern [23]. The radiation pattern based method gives the possibility to include a better description of the radio channel in the evaluation, although it makes the evaluation more complicated. This, however, is a time consuming process, whether it is done using numerically or experimentally data. Therefore it is the scattering parameter approach that is used in this paper to calculated the antenna correlation. The correlation between any two antennas in an infinite large MIMO system is calculated using the formula derived by in [24].

The envelope correlation is determined from the distribution of the external sources and the radiation pattern from the antennas. Only by assuming omni-directional source distribution one could relate the mutual impedances (or scattering parameters) to the correlation [34]. This

means that the envelope correlations estimated based on S-parameters corresponds to that based on the far-field pattern if a uniform distribution of the sources is assumed.

In order to calculate the capacity of MIMO systems information of both the propagation environment and the antenna configurations are required. In this study the used measured MIMO coupling matrix between the antenna elements have been measured by Vainikainens group at Helsinki University of Technologi, HUT. For further details see, e.g., [25, 26]. This coupling matrix is then combined with the complex radiation pattern of the antennas under test. Here, the complex radiation patterns are measured in a radio-anechoic chamber, where the antennas are mounted next to an artificial hand and head.

Recently, Molisch has shown that a MIMO system which take simple diversity into account, i.e., in either one or both of the link ends, the number of antenna elements L in the (N, N) MIMO system can be reduced [27]. In this way a reduced MIMO system is created which has a reduced complexity as compared to the full (N, N) MIMO system. Among others, Vaughan has shown that transmit or receive diversity can improve the link quality [11].

In this paper, experimental results of the capacity and the diversity gain for three simple yet realistic two- and three-antenna configurations are presented. The channel data used have been measured in small macro cell environment in downtown Helsinki. The provided results are for both free space radiation pattern as well as talk position radiation pattern, i.e., beside an artificial hand and head. The measured envelope correlation as well as the measured radiation efficiency and the scattering parameters are discussed.

The effects on the capacity by increasing the transmitting (Tx) elements from one to seven are studied. The effect of a reduced MIMO system with an unequal number of antennas in the receiver and transmitter are studied as well. In addition, the gain of using a (3, 3) as compared to a (2, 2) system for increased signal to noise ratio (SNR) is presented.

In Section 2.2 the measurement system and the environments used in the work are described. Section 3 presents the results and discussion of the results and Section 4 concludes the work.

1.2 Description of the experiments

Mimo model

The main idea behind MIMO is that the signals on the transmitter (TX) antennas at one end and the receiver (RX) antennas at the other end are “combined” in such a way that the quality in terms of the bit-error rate (BER) or the data rate (bits/sec) for each of the MIMO user can be improved [2]. A MIMO-system transmits data over a matrix channel rather than just over single radio channels. This requires signal processing over both time and space as illustrated in Figure 1.

The signal to be transmitted is fed to transmitting block. Hereafter, the three different signals are transmitted simultaneously from antenna element A1, A2, and A3. At the receiver each of the antenna element B1-B3 receive a signal from each of the transmitting antennas. If the received signal at each of the antenna element B1-B3 is sufficiently independent, as is typically the case in the presence of rich multipath, it is possible to re-establish the original transmitted signal. Hence, a (3, 3) MIMO system has a potential capacity increase of three as compared to the single element.

In theory this gives an upper speed limit that is limited only by the hardware cost and the requirement of a rich multi path environment.

MIMO system capacity

In a traditional channel with only one transmission channel used for data transmission the Single-Input Single-Output (SISO) system capacity is [35].

$$C = \log_2(1 + SNR) \quad [\text{bit/s/Hz}], \qquad (1)$$

where *SNR* is the signal to noise ratio. The capacity of a MIMO system with equal power distribution and unknown channel is defined as [4-6]

$$C = \log_2\left[\det\left(I + \frac{SNR}{m}\overline{H}\ \overline{H}^*\right)\right] \quad [\text{bit/s/Hz}] \quad (2)$$

with I as the identity matrix, (*) means transpose conjucate and H is the MIMO system channel matrix.

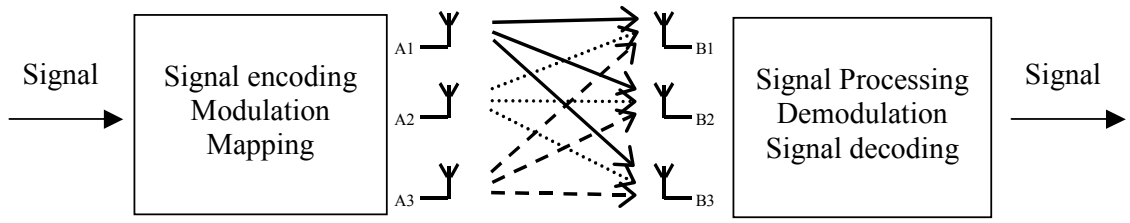

Figure 1. Illustration of the MIMO system with 3 transmitter and 3 receiver antennas.

It has been demonstrated that the capacity in Equation (2) grows linearly with $m = \min(M, N)$, rather than logarithmically as in the diversity case [5], [6].

Mimo channel

Realistic evaluation of MIMO antenna structures requires multielement propagation measurements with MIMO antenna configurations. One way to obtain these multielement propagation measurements is to combine the measured or simulated propagation paths with the radiation pattern of the antenna elements. This leads to a MIMO coupling matrix between the antenna elements. This requires the extraction of the full double-directional propagation channel parameters and can be done experimentally with proper measurement antenna arrays enabling unambiguous directional estimations with two polarisations [25, 28]. The results of the radio channel measurement system equipped with a channel sounder for measuring the spatial and temporal characteristics of the radiowave channel, a linear transmitting (Tx) antenna array, and a spherical receiving (Rx) antenna array both employing dual polarised patch antennas are used. The linear antenna array consists of eight directive and dual polarised antenna elements from which different number of elements were selected in the post processing of the measurement data [29, 30]. The spherical receiving antenna array is formed by 32 directive and dual-polarised elements, similar to the elements of the Tx array, located on the sphere, was used at the receiving mobile station (MS). One dual polarised element consists of two orthogonal channels, i.e., θ- and φ-polarised feeds [31].

A potential MIMO environment, i.e., a small macrocell in downtown Helsinki, is included in the study. See for example [25] for maps.

Channel transfer function

The signal at the basestation

$$y(t) = [y_1(t), y_2(t), \cdots, y_m(t)]^T \qquad (3)$$

is related to the signal at the receiving mobile station

$$s(t) = [s_1(t), s_2(t), \cdots, s_n(t)]^T, \qquad (4)$$

through the matrix H that represent the transmission at a certain time and spatial location of the antennas in the multipath environment. The MIMO system channel matrix is defined as

$$H = \begin{bmatrix} \alpha_{1,1} & \alpha_{1,2} & \cdots & \alpha_{1,n} \\ \alpha_{1,1} & \alpha_{1,1} & \cdots & \alpha_{1,n} \\ \vdots & \vdots & \ddots & \vdots \\ \alpha_{m,1} & \alpha_{m,1} & \cdots & \alpha_{m,n} \end{bmatrix}, \qquad (5)$$

where $\alpha_{i,j}$ is the complex transmission coefficient from antenna i to antenna j. The relationship between the signal at the basestation $y(t)$ and the signal at the receiving mobile station $s(t)$ is

$$y(t) = H(t)s(t). \qquad (6)$$

Antenna elements

The presented antenna configurations consist of either two or three 40 mm long, 1.5 mm wide and 5 mm high PIFAs located on a 40 mm × 100 mm ground plane. The feed point is located 5 mm from the edge where a 90-degree bend forms the short to the ground plane denoted with dots in the vignettes of the figure shown in Figure 2.

In total three different configurations are investigated. In all the cases, the antennas are located parallel to the edge of the ground plane, see the illustration in Figure 2, and have a simulated resonant frequency of 1810 MHz ±1.1% [32].

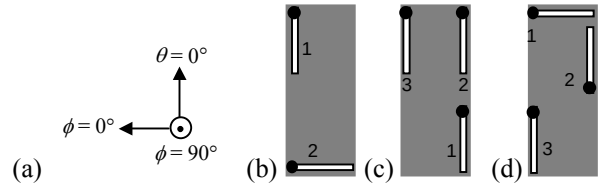

Figure 2. Antenna models (b) – (d) and orientation in the spherical coordinate system (a).

The radiation pattern from the antennas is measured in radio anechoic environments, firstly in free space, and secondly beside artificial hand and head as shown in Figure 3.

Different prototypes have been made. The three-antenna configuration illustrated in Figure 2 (d) has been mounted inside a realistic mobile phone. The phone has been modified such that it contains three PIFAs each having a centre frequency of 1.8 GHz. This phone is mounted next to the artificial hand and head. The artificial hand is fixed such that it represents the way a user might hold the phone in a typical talk position, see Figure 3.

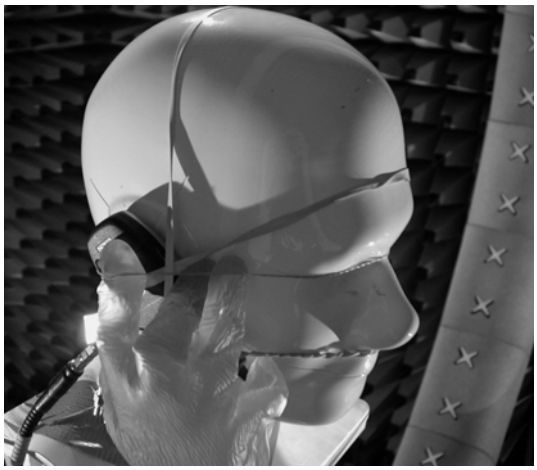

Figure 3. Illustration of the antenna mounted next to an artificial hand and head in the anechoic chamber [33].

The two remaining prototypes consist of a ground plane and the PIFAs only; they are mounted in the anechoic chamber as above-described.

For calculating the capacity it is the radiation pattern of a single element when all the other elements are present (but terminated with loads representing the source impedance on their ports) that must be measured.

1.3 Results and discussion

This section is divided into two subsections: Section 3.1 treats the antenna performance, and Section treats the results related to the MIMO system.

Antenna performance

The first section that treats the antenna performance has three subsections. The first subsection deals with the two-antenna configuration. The performance of the three-antenna configuration on a ground plane is discussed in the second subsection. The third subsection treats the three-antenna configuration that is mounted in a mobile phone.

The two-antenna configuration on a ground plane

For the two-antenna configuration that consists of two orthogonal PIFAs as indicated in Figure 2, the measured scattering parameters, the envelope correlation and the measured radiation efficiency are shown in Figure 4.

Antenna 1 has a relative bandwidth ($|S_{11}|$<–6dB) of 8.3% at a centre frequency of 1.83 GHz, and 3.3% around 1.82 GHz for antenna 2. The mutual coupling is measured to –12.6 dB. The highest envelope correlation within the frequency band of interest (between 1.7 GHz and 1.9 GHz) is $\rho_e = 0.09$.

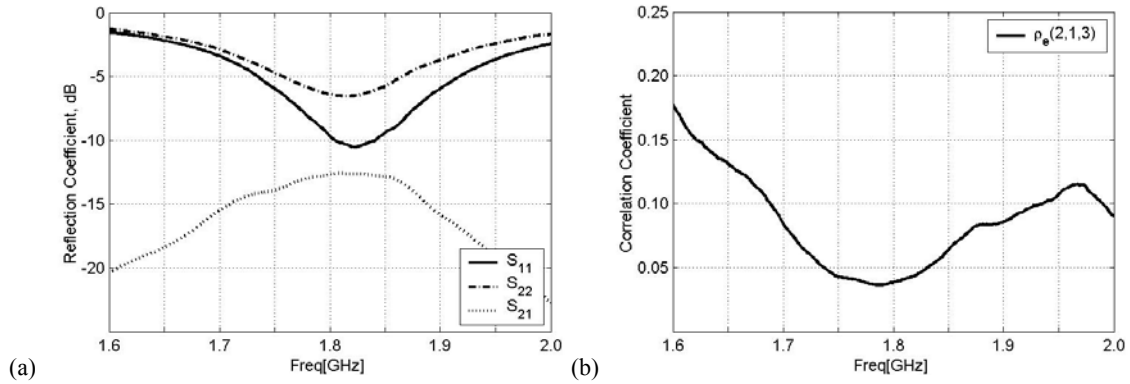

Figure 4. Measured scattering parameters (a), and envelope correlation (b).

Antenna 1 and antenna 2 yield a measured free space radiation efficiency above 50% and 30% (see Figure 5), respectively, within the frequency band of interests, i.e., between 1.7 GHz and 1.9 GHz [32]. Placing the antennas next to an artificial hand and head as illustrated in Figure 3, the peak radiation efficiency is 12% and 7% for antenna 1 and antenna 2, respectively.

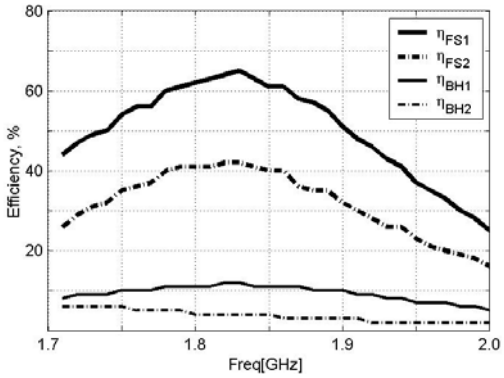

Figure 5. Measured free-space (FS) and beside hand and head (BH) radiation efficiency for antenna 1 and antenna 2.

The measured maximum free space gain is 3.8 dB and 1.5 dB for antenna 1 and antenna 2, respectively. In talk position the gain is –3.1 dB and –5.6 dB. The reduction in the gain is mainly due to the way that the artificial hand holds the antenna configuration; some fingers have direct contact to the PIFA arm. If the antennas were placed inside a mobile phone, no direct contact between the hand and the PIFA, and thus a somewhat lower decrease could be expected.

The three-antenna configuration on a ground plane

The three-antenna configuration consists of three PIFAs (see Figure 2 c). The scattering parameters, the envelope correlation and the radiation efficiency are shown in Figure 6 and Figure 7. Antenna 1 has a bandwidth of 3.9% centred at the resonant frequency of 1.80 GHz, 11.2% at 1.78 GHz for antenna 2 and 14.8% at 1.76 GHz for antenna 3. The strongest mutual coupling is measured to –8.2 dB between antenna 2 and antenna 3, between antenna 1 and antenna 2 a –12.2 dB coupling is observed.

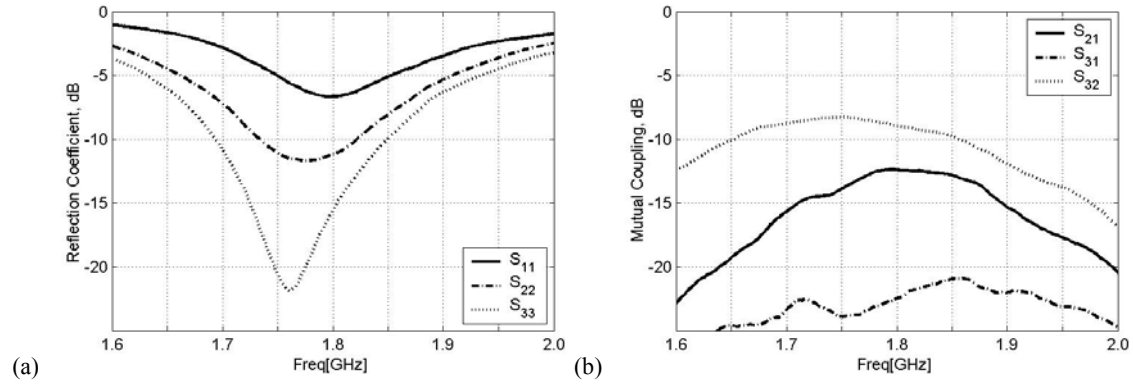

(a) (b)

Figure 6. Measured reflection coefficient (a), and mutual coupling (b).

The measured envelope correlations are shown in Figure 7. Here, the highest value of $\rho_e = 0.19$ at 1.95 GHz is between antenna 2 and antenna 3, between antenna 1 and antenna 2 the envelope correlation is 0.15.

Antenna 1, 2 and 3 yield measured free space radiation efficiency above 52%, 45%, and 38% between 1.7 GHz and 1.9 GHz, respectively, as can be seen in Figure 7. Again the peak radiation efficiency drops when the antennas are placed next to the artificial hand and head.

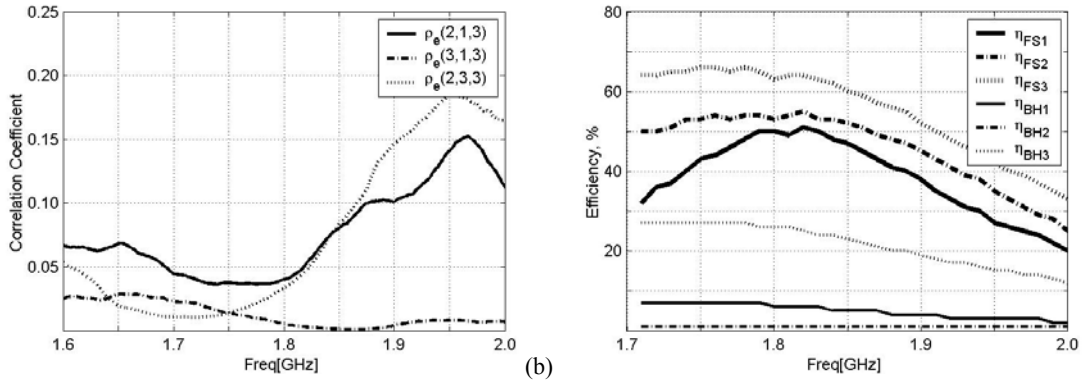

(a) (b)

Figure 7. Measured envelope correlation (a). Measured free-space (FS) and beside hand and head (BH) radiation efficiency (b).

When placing the artificial hand and head next to the antennas, the measured maximum gain for antenna 1 drops from 0.3 dB to -5.9 dB, and a decrease from 1.3 dB to -14.4 dB and from 3.4 dB to 0.2 dB for antenna 2 and antenna 3, respectively.

The three-antenna configuration in a mobile phone

The three-antenna configuration that is mounted in a realistic mobile phone that consists of three PIFAs can be seen in Figure 2d and Figure 3. In Figure 3 the modified mobile phone mounted beside artificial hand and head in the anechoic chamber is shown. The measured scattering parameters, the envelope correlation and the radiation efficiency are shown in Figure 8. The centre frequency is 1.76 GHz for antenna 1 and antenna 3; they have a relative bandwidth of 6.3% and 9.1%, respectively. Antenna 2 has a 4.5% bandwidth at a centre frequency of 1.79 GHz. The strongest mutual coupling is measured to -6.3 dB between antenna 1 and antenna 3.

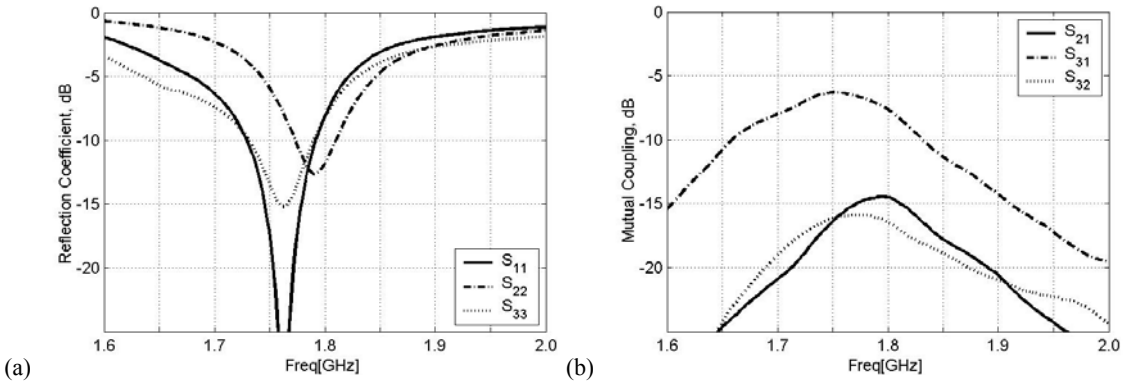

Figure 8. Measured reflection coefficient (a), and measured mutual coupling (b).

The envelope correlation is calculated at frequencies between 1.6 GHz and 2.0 GHz; the results are shown in Figure 9. Here, the worst value of the envelope correlation is $\rho_e = 0.26$ at 1.66 GHz obtained between antenna 1 and antenna 3. The remaining correlation coefficients are all well below $\rho_e < 0.05$.

The antennas are inside a full mounted mobile phone with a real cover. These things decrease the free space efficiency. Antenna 1 and antenna 2 have free space efficiencies above 15% between 1.7 GHz and 1.9 GHz, and peak efficiencies around 37% around 1.75 GHz. The radiation efficiency of antenna 3 peaks at 1.8 GHz with 30%. For all three antennas the measured radiation efficiency, when placed next to an artificial hand and head, is between 4% to 14% in the frequency range from 1.7 GHz to 1.9 GHz.

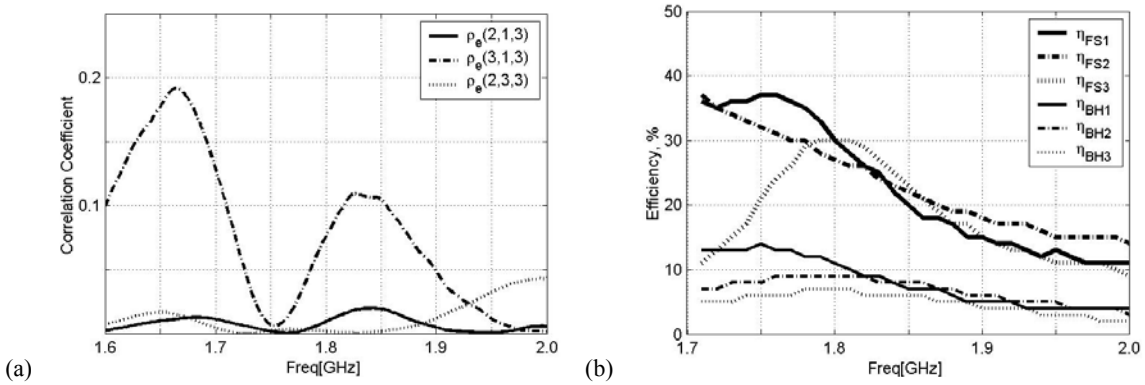

Figure 9. Measured envelope correlation (a). Measured free-space and beside hand and head radiation efficiency for antenna 1 and antenna 2 (b).

The measured free space radiation patterns are shown in Figure 10. Placing the antennas next to the artificial hand and head affects the radiation pattern, especially in the $\theta = 90°$ plane for ϕ=0° and ϕ= 90°. The dips in the ϕ-cuts for $\theta = 180° \pm 12°$ is due to the antenna mounting and positioning system [23]. The maximum free space gain is 1.6 dBi for antenna element 1, being 5 dB higher than the beside hand and head gain. A decrease in the free-space from -1.2 dB to -4.2 dB and from 3.4 dB to –3.9 dB for antenna 2 and antenna 3 is observed, respectively.

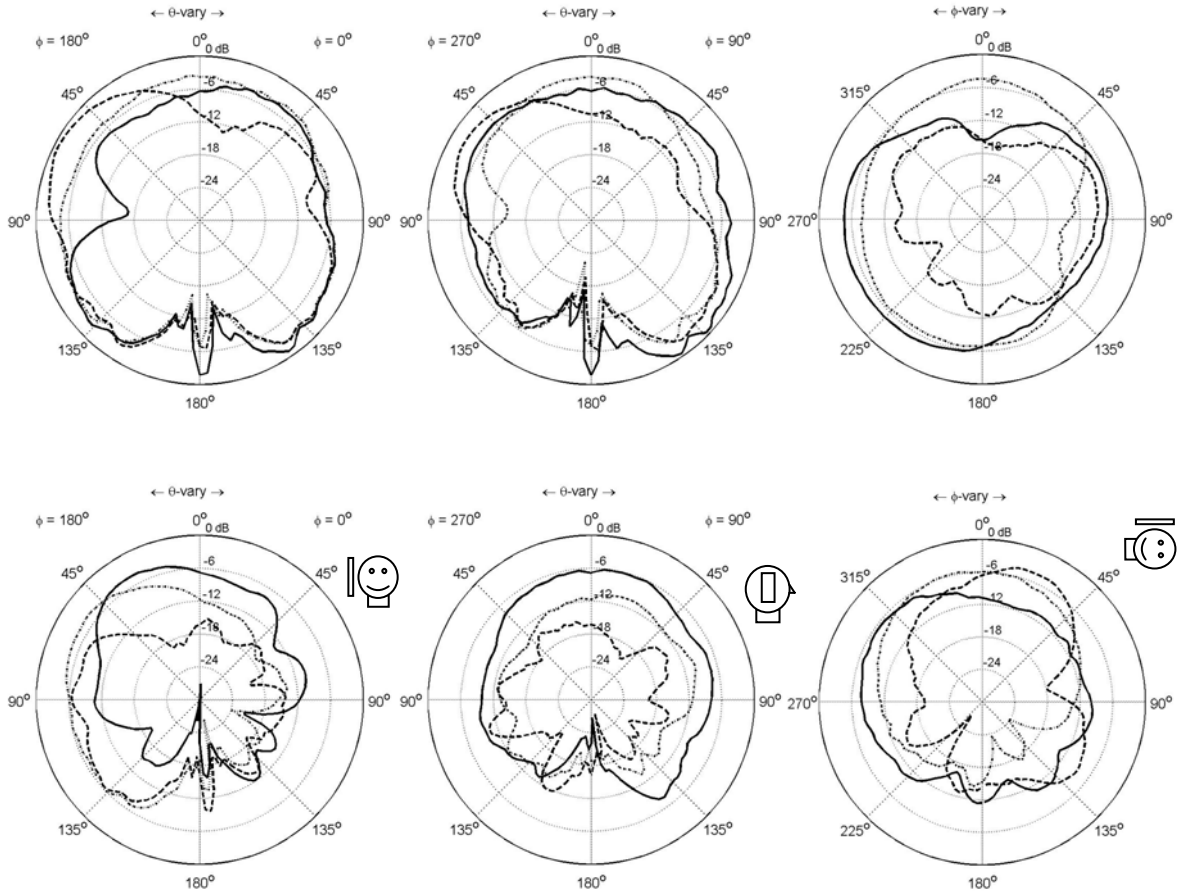

Figure 10. Measured free-space radiation pattern cuts (upper), and beside hand and head (lower). θ-cuts for $\phi = 0°$ (left) and for $\phi = 90°$ (centre) and ϕ-cut for $\theta = 90°$ (right). Antenna 1 (solid), antenna 2 (dotted) and antenna 3 (dashed), with respect to the orientation as shown in Figure 2 at 1.8 GHz. The vignettes illustrate the orientation of the three-antenna configuration with respect to the artificial head, cf. Figure 2.

Mimo results

This section that treats the MIMO results has six subsections. The results from the two-antenna configuration on a ground plane, the three-antenna configuration on a ground plane, and the three-antenna configuration that is mounted in a mobile phone are discussed in the first three subsections. The fourth and fifth subsections deal with the frequency dependency on the capacity and the capacity versus signal to noise ration (*SNR*), respectively. A subsection regarding MIMO with antenna selection follows this.

Two antennas on a ground plane

In Figure 11 the instantaneous capacity of the (2, 2) MIMO configuration in the small macro multipath environment is shown as a function at the actual position, i.e., each sample represents a measurement point. A variation in both the actual location and in time is then observed, since the antenna is moved from point A to point B.

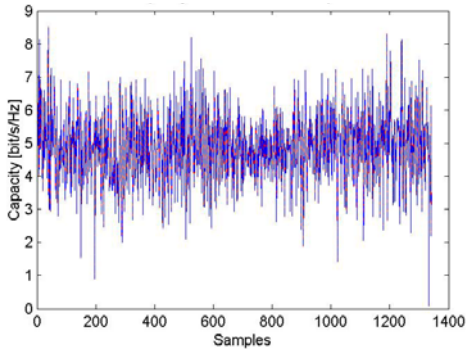

Figure 11. Instantaneous capacity versus samples of the two-antenna configuration when the spherical receiving antenna array is moved in a macro environment. The capacity is calculated using the measured talk position radiation patterns of the two-antenna configuration, i.e., measured beside an artificial hand and head.

The cumulative distribution functions (cdf) of the instantaneous capacity (Equation 2) are presented in Figure 12. The capacities are calculated both using the free-space radiation patterns and the radiation patterns obtained in talk position beside an artificial hand and head.

The average received *SNR* is chosen to be 10 dB. The 50% outage channel capacity $C_{0.5}$ in the (2, 2) system is 5.0 bit/s/Hz calculated using the free-space radiation patterns. A slight decrease of 0.1 bit/s/Hz for the radiation patterns obtained in talk position beside an artificial hand and head is seen. This is in accordance with the measured radiation efficiency, see Figure 5. Here, the peak radiation efficiency for antenna 1 and antenna 2 is somewhat lower as compared to the free space results.

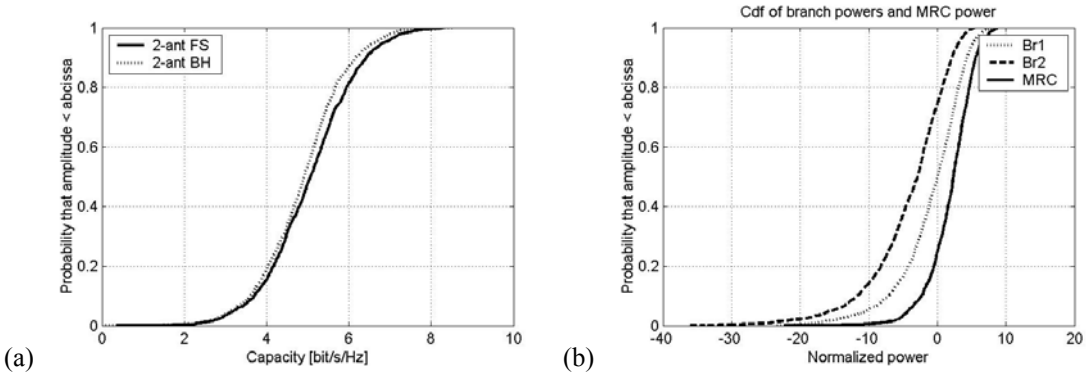

Figure 12. Capacity results for the two-antenna configuration in the macro environment. The antenna patterns are measured in free space (FS) and beside head (BH) (a). Cumulative distribution functions of the branch power (Br) Br1, Br2, and MRC power (b).

For the two-antenna configuration the cumulative distribution function of the power received by both the branches (Br1 are related to antenna 1and Br2 are related to antenna 2) and the power after maximum ratio combining (MRC) is shown in Figure 12.

The gain of using more than one antenna is calculated as the difference between the MRC power and the strongest branch power at 10% probability level. This result is strongly affected by the branch power difference and the envelope correlation. The MRC is 4.8 dB higher than Br1. At the probability level *p* of 50% the difference between Br1 and Br2, $\Delta_{Br2\text{-}Br1}$ is 2.8 dB.

The fact that the branch power of antenna 1 is the highest seems reasonably when taking the measured radiation efficiency into account, see Figure 5.

Three antennas on a ground plane

Observed in Figure 13, the 50% outage channel capacity $C_{0.5}$ in the (3, 3) system is 7.1 bit/s/Hz and 6.4 bit/s/Hz using the free-space and beside head radiation patterns, respectively. As for the (2, 2) configuration, the reduced radiation efficiency explains the difference. Recalling the capacity from the (2, 2) configuration the capacity is improved by 1.5 bit/s/Hz (beside hand and head) by adding the extra antenna.

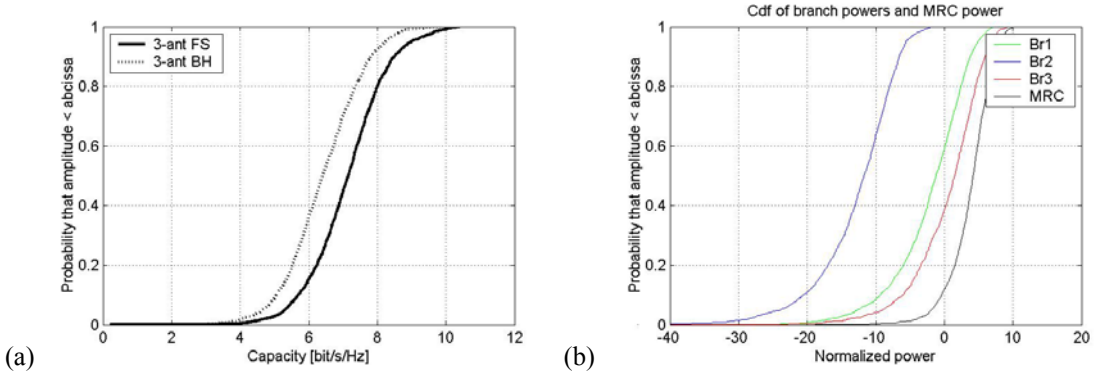

Figure 13. Capacity results for the three-antenna configuration in macro environment. The antenna patterns are measured in free space (FS) and beside head (BH) (a). Cdf of Br1, Br2, Br3 powers, and MRC power (b).

The MRC is 5.5 dB higher than Br3. At the probability level p of 50% the $\Delta_{Br3\text{-}Br1}$ is 2.7 dB, and $\Delta_{Br3\text{-}Br2}$ is 11.3 dB. Indicating that antenna 2 contributes the least the total capacity. From Figure 7 it is seen that antenna 2 has a very low radiation efficiency, when placed beside the artificial hand and head. This low value is due to the fact that one of the artificial fingers has direct contact to the radiating element of antenna 2.

Three antennas in a mobile phone

Placing the three-antenna configuration that is mounted in a realistic mobile phone cover, beside the artificial hand and head, has a minor effect on the capacity. A drop from 7.1 bit/s/Hz to 6.9 bit/s/Hz is accomplished as seen in Figure 14. This comes from the rather unchanged ratio between the peak total efficiencies measured in free space.

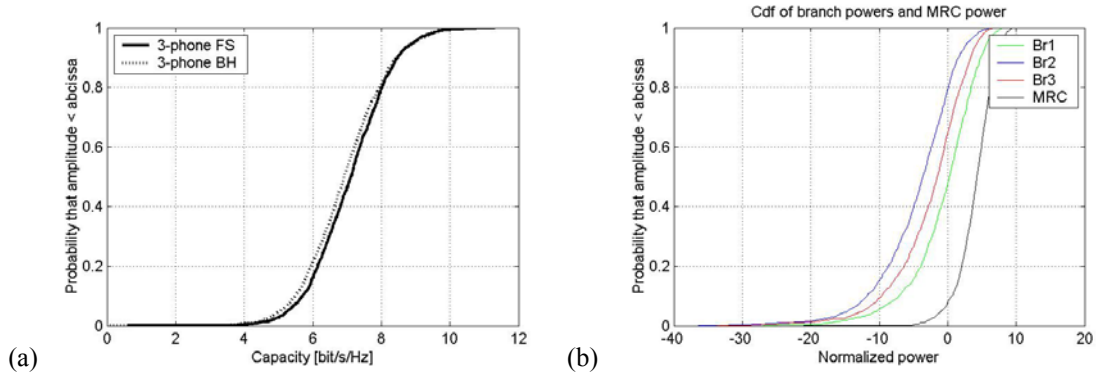

Figure 14. Capacity results for the mobile phone mounted three-antenna configuration in macro environment. The antenna patterns are measured in free space (FS) and beside head (BH) (a). Cdf of Br1, Br2, Br3 powers, and MRC power (BH) (b).

In the free-space the capacity is equal to the capacity obtained in the three-antenna configuration mounted on a ground plane. Beside the artificial hand and head, the capacity is reduced by 0.5 bit/s/Hz. A reason for the reduction is that in this case no finger has direct contact to any of the radiating elements due to the mobile phone cover. Compared to the (2, 2)

configuration the capacity is improved by 2 bit/s/Hz (beside hand and head) by adding the extra antenna.

For the there antennas in a mobile phone configuration the gain of using more antennas is easily visible from Figure 14. Here, the MRC is 7.9 dB higher than Br3. At the probability level *p* of 50% the $\Delta_{Br1\text{-}Br3}$ is 1.7 dB, and $\Delta_{Br1\text{-}Br2}$ is 3.7 dB.

The branch power difference between the two extra antennas, antenna 2 and antenna 3, $\Delta_{Br1\text{-}Br2}$ is 2 dB. This indicates that both antenna 2 and antenna 3 contributes to the total capacity.

Capacity versus signal to noise ratio (SNR)

The capacities presented so far are based on an average *SNR* of 10 dB. The capacity at varying the *SNR* for the three configurations described previously is presented in Figure 15. For comparison the SISO capacity is plotted as well. Notice that the capacity for the SISO is based on the Shannon limit, and therefore not calculated using the channel data *H(t)* obtained in the macro environment as for the remaining capacities.

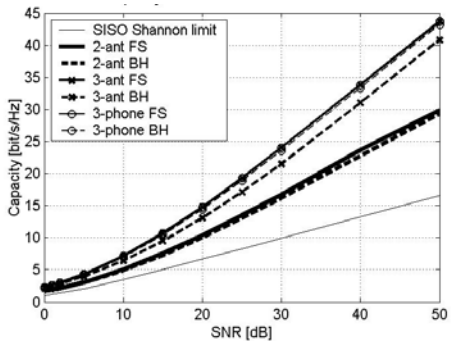

Figure 15. Mean capacity, with the outage rate of 50% at varying *SNR* for the three configurations. The antenna patterns are measured in free space (FS) and beside head (BH). Notice that the SISO capacity is based on the Shannon limit.

For increasing *SNR* the difference between the capacity of the (2, 2) and the (3, 3) configurations differs. The capacity of the three antennas configuration on a ground plane (3-ant BH), in talk position, differs from the remaining three-antenna examples, most likely due to the very low branch power obtained with antenna 2.

At low *SNR*, i.e., below 5 dB the difference in using 3 antennas instead of 2 antennas is low. At *SNR*=0 dB the difference is 0.5 bit/s/Hz, the talk position capacity of 1.6 bit/s/Hz being the lowest. The gain by using an extra antenna having a *SNR* of 50 dB is a talk position capacity of 43 bit/s/Hz, being 14 bit/s/Hz higher that the capacity obtained using the two-antenna configuration. The Shannon limit of the capacity of the SISO system at a signal to noise ration of 50 dB is 16.6 bit/s/Hz. This is approximately half the (2, 2) capacity and a third of that obtained using a (3, 3) MIMO system.

MIMO with antenna selection

The MIMO system is based on two or more subchannels transferring data simultaneously in the same bandwidth. The effect of increasing the number of Tx elements on the average capacity for the three different configuration used here are shown in Figure 16.

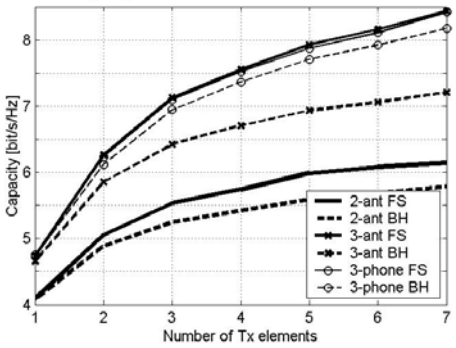

Figure 16. Mean Capacity, with the outage rate of 50% as a function of number of antenna element at the sphere in macro environment. The number of elements is two and three for the respectively configurations.

In the macro environment studied, the capacity from the three antenna configurations increases the most as the number of Tx elements increases from one to four. Here, the talk position capacity increases from 4.7 bit/s/Hz to 7.4 bit/s/Hz. Similarly a talk position capacity increases from 4.1 bit/s/Hz to 5.2 bit/s/Hz, when increasing the number of Tx elements for the two-antenna configuration from one to three. Even though the number of Tx antennas exceeds the number of Rx antennas, an increase in the capacity is observed, this is due to the increased antenna array gain. Adding additional three Tx elements, the 3-phone the talk position capacity increases from 7.4 bit/s/Hz to 8.2 bit/s/Hz. This corresponds to an increase of 0.8 bit/s/Hz for the last three antennas, as compared to 2.7 bit/s/Hz for the first three antennas. Sulonen et al. has obtained similar results [31].

For both of the three-antenna configurations the free-space capacity is approximately the same, however, the capacity obtained with the antennas in talk position a difference is observed. This is in accordance with the difference in the radiation efficiency in talk position presented previous in this paper.

The advantages by chancing the number of Tx elements for two and three antenna configuration are shown in Figure 17. Here, the first three bars are for the two-antenna configuration, showing an increase of the talk position capacity from 4.1 bit/s/Hz for the simple diversity setup (1, 2) to 4.9 bit/s/Hz for the full (2, 2) MIMO system, reaching 5.2 bit/s/Hz in the case of three Tx elements and two Rx elements. Meaning that the extra Tx antenna yields an extra 0.3 bit/s/Hz.

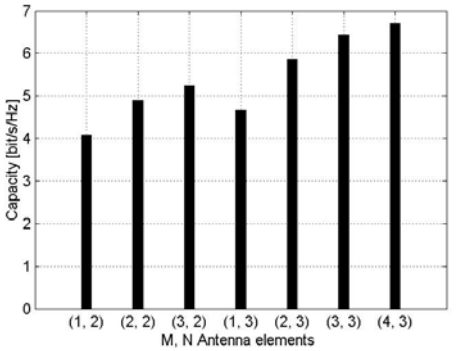

Figure 17. Mean capacity, with the outage rate of 50% as a function of number of antenna element at the sphere in macro environment. The antenna patterns are measured beside head (BH).

Similar trends are observed for the talk position capacity of the three-antenna configuration illustrated by the four last bars. Here the most significant improvement is for an increase from one to two Tx elements.

Comparing (1, 2) with (1, 3) yields capacity improvement of 0.6 bit/s/Hz, which is a smaller improvement when compared to an extra Rx antenna (2, 2). With the same amount of antennas, i.e., 3 antennas in one end and 2 antennas in the other end, t is found that it is better to have an extra Rx antenna, i.e., (Tx, Rx) = (2, 3) rather than an extra Tx antenna (3, 2). The Rx diversity setup has a capacity of 5.8 bit/s/Hz, which is 0.6 bit/s/Hz higher than the Tx diversity setup.

1.4 Conclusion

The increasing demand for wireless communication systems having high data rate transmission could to some extent be accomplished using MIMO. The basic idea behind MIMO system architecture is that the signals on the transmitter (TX) antennas at one end and the receiver (RX) antennas at the other end are "combined" in such a way that the quality in terms of the bit-error rate (BER) or the data rate (bits/sec) for each of the MIMO user can be improved. A MIMO-system transmits data over a matrix channel rather than just over single radio channel, with significant increased capacity or higher link reliability using the same bandwidth and transmit power as today.

The MIMO capacity formula was briefly explained which showed the increased capacity as compared to conventional SISO systems.

Realistic evaluation of MIMO antenna structures requires multi-element propagation measurements with MIMO antenna configurations. Here, a potential MIMO environment, i.e., a small macro cell in downtown Helsinki, is used.

Three different realistic prototypes have been made. Two simple yet realistic configurations, consisting of either two or three 40 mm long, 1.5 mm wide and 5 mm high PIFAs located on a 40 mm × 100 mm ground plane. Furthermore, a matured three-antenna MIMO prototype based on a commercial available mobile phone is presented. In all three prototypes the PIFAs have a centre frequency of 1.8 GHz. In order to use as realistic data as possible for the MIMO evaluation, the radiation pattern from the antennas are measured in talk-position, i.e., beside an artificial hand and head.

For the two-antenna configuration, the 50% outage channel capacity $C_{0.5}$ in the (2, 2) system is 4.9 bit/s/Hz in talk position. This is a decrease of 0.1 bit/s/Hz as compared to the capacity obtained using the free-space radiation patterns. Even though this rather small difference in the capacity, the measured talk position radiation efficiency is reduced to a fourth of the corresponding free-space radiation efficiency. For the (2, 2) MIMO system, the (MRC) gain of using the extra antenna is 4.8 dB as compared to the branch power of antenna 1, Br1. The difference between Br1 and Br2, $\Delta_{Br2\text{-}Br1}$ is 2.8 dB.

The three antenna configuration has a 50% outage channel capacity $C_{0.5}$ of 7.1 bit/s/Hz and 6.4 bit/s/Hz using the free-space and beside head radiation patterns, respectively. In spite of the fact that the capacity is decreased in talk position, the third antenna still results in a 1.5 bit/s/Hz improvement in the capacity as compared to the (2, 2) MIMO configuration.

Bearing in mind that the talk position radiation efficiency of antenna 2 is a few percent, only, primarily due to the fact that one of the artificial fingers has direct contact to the radiating element of antenna 2, it is an advantage to have three antennas instead of two, seen from a capacity point of view.

The fact that the measured free-space radiation efficiency is approximately 20 percent point lower when incorporating the antennas into a commercial mobile phone does not affect the

free-space capacity which is unchanged 7.1 bit/s/Hz. Placed beside an artificial hand and head, the capacity is 6.9 bit/s/Hz. This is 0.5 bit/s/Hz above the three-antenna configuration which is not incorporated into a phone. For all three antennas the measured radiation efficiency, when placed next to an artificial hand and head, is between 4% and 14% in the frequency range from 1.7 GHz to 1.9 GHz. In average this is lower than the three-antenna in a ground plane configuration, however, the high radiation efficiency (above 20%) of antenna A3 can not make it up for the extremely low radiation efficiency of antenna 2 (below 2%). The measured gain lowered with 3 dB to 5 dB in the talk-position as compared to the free space gain..

Obviously the capacity increases with increased signal to noise ratio (SNR). At low *SNR*, i.e., below 5 dB the difference in using three antennas instead of two antennas is low. At *SNR*=0 dB the difference is 0.5 bit/s/Hz, the talk position capacity of 1.6 bit/s/Hz being the lowest. The gain by using an extra antenna having a *SNR* of 50 dB is a talk position capacity of 43 bit/s/Hz, being 14 bit/s/Hz higher that the capacity obtained using the two-antenna configuration.

Simply by adding more elements at the Tx antenna configuration the capacity could be increased. For the three-antenna configuration mounted inside a mobile phone the talk position capacity increases from 4.7 bit/s/Hz to 8.2 bit/s/Hz when increasing the numbers of Tx elements from one to seven. Above four Tx elements the capacity increase is less per Tx element as the capacity increase per Tx element below three. From one to four the talk position capacity increases from 4.7 bit/s/Hz to 7.4 bit/s/Hz, as compared to an increase of 0.8 bit/s/Hz for the last three antennas. Bearing in mind the capacity grows linearly with $m = \min(M, N)$ and logarithmically in the diversity case this is in accordance with theory [5], [6].

Making some simple considerations, it could be concluded that, from a capacity point of view, it is better to have a full (2, 2) MIMO system ($C_{0.5}$ of 4.9 bit/s/Hz) than a Tx diversity system of (1, 3) ($C_{0.5}$ of 4.7 bit/s/Hz).

It is found that it is better to have an extra Rx antenna, i.e., (Tx, Rx) = (2, 3) rather than an extra Tx antenna (3, 2). The Rx diversity setup has a capacity of 5.8 bit/s/Hz, which is 0.6 bit/s/Hz higher than the Tx diversity setup.

Bearing in mind that the hardware complexity of a MIMO system increased with the number of antennas. Antenna selection could be used as a simple method to increase the capacity of a MIMO antenna configuration with minimal added hardware complexity.

From our study and overview of the MIMO principle, it is clear that MIMO systems offer significant gains in performance over traditional wireless communication systems. Measurements were presented to show the capability for several potential MIMO antenna configurations.

1.5 Acknowledgements

This work has been supported by Nokia Denmark. Helsinki University of Technologi, HUT especially Pasi Sivikunnas and Nokia Research Centre, NRC especially Kimmo Killola are gratefully acknowledged for technical support with the MIMO evaluation.

1.6 References

[1] R. G. Vaughan and J. Bach Andersen, “Antenna diversity in mobile communication”, *IEEE Trans. Veh. J1 Technol.*, vol. 36, pp. 149−172, 1987.

[2] D. Gesbert, M. Shafi, D. S. Shiu, P. J. Smith, and A. Naguib, “From theory to practice: An

overview of MIMO space-time coded wireless systems,"*IEEE J. Select. Areas in Commun.,* vol. 21 (3), 2003.

[3] A. Goldsmith, S. Jafar, N. Jindal, and S. Vishwanath, "Capacity limis of MIMO channels", *IEEE J. Select. Areas Commun.*, vol. 21 (5), pp. 684−702, 2003.

[4] J. H. Winters, "On the capacity of radio communication systems with diversity in a Rayleigh fading environment," *IEEE J. Select Areas Commun.*, vol. SAC-5, pp. 871–878, June 1987.

[5] G. J. Foschini and M. J. Gans, "On limits of wireless communications in a fading environment when using multiple antennas," *Wireless Pers. Commun.*, vol. 6, pp. 311–335, 1998.

[6] I. E. Telatar, "Capacity of multi-antenna Gaussian channels," *Eur. Trans.Telecommun. Related Technol.*, vol. 10, pp. 585–595, 1999.

[7] R. Janaswamy, "Effect of Element Mutual Coupling on the Capacity of Fixed Length Linear Arrays", *IEEE Antennas and Wireless Propagat. Lett*, vol. 1, pp. 157−160, 2002.

[8] D. Shiu, G. J. Foschini, M. J. Gans, and J. M. Kahn, "Fading correlation and its effect on the capacity of multi-element antenna systems," *IEEE Transactions on Communications*, vol. 48, pp. 502–513, March 2000.

[9] C. N. Chuah, D. N. C. Tse, J.M. Kahn, and R. A. Valenzuela, "Capacity scaling in MIMO wireless systems under correlated fading," *IEEE Transactions on Information Theory*, vol. 48, pp. 637 – 650, 2002.

[10] A. F. Molisch, M. Steinbauer, M. Toeltsch, E. Bonek, and R. S. Thoma, "Capacity of MIMO systems based on measured wireless channels," *IEEE Journal on Selected Areas in Communications*, vol. 20, pp. 561– 569, 2002.

[11] Vaughan, R. G., "Signals in Mobile Communications: A Review", *IEEE Trans. Veh. Technol.*, vol. 35, pp. 133−145, 1986.

[12] D. Gesbert, H. Bölcskei, D. A. Gore, and A. J. Paulraj, "Mimo wireless channels: Capacity and performance prediction," in *Proc. GLOBECOM*, vol. 2, pp. 1083–1088, IEEE, 2000.

[13] D. Chizhik, G. J. Foschini, M. J. Gans, and R. A. Valenzuela, "Keyholes, correlations, and capacities of multielement transmit and receive antennas," *IEEE Transactions on Communications*, vol. 1, pp. 361–368, 2002.

[14] D. Chizhik, F. Rashid-Farrokhi, J. Ling, and A. Lozano, "Keyholes, correlations, and capacities of multielement transmit and receive antennas", *IEEE Ant. Trans. Wireless Commun.*, pp. 361− 368, 2002.

[15] D. Chizhik, F. Rashid-Farrokhi, J. Ling, and A. Lozano, "Effect of antenna separation on the capacity of BLAST in correlated channels", *IEEE Commun. Lett.* vol. 4 (11), pp. 337−339, 2000.

[16] A. Derneryd, and G. Kristensson, "Signal correlation including antenna coupling", *Electron. Lett.,* vol. 40 (3), pp. 157−158, 2004.

[17] M. Karaboikis, C. Soras, G. Tsachtsiris, and V. Makios, "Compact dual-printed inverted-F antenna diversity systems for portable wireless devices", *IEEE Ant. Wireless Propagat. Lett*, pp. 9−14, 2004.

[18] B. Clerckx, D. Vanhoenacker-Janvier, C. Oestges, and L. Vandendorpe, "Mutual coupling effects on the channel capacity and the space-time processing of MIMO communication systems", *Commun., ICC '03. IEEE Int. Conf. on,* vol. 4, pp. 2638−2642, 2003.

[19] J. W. Wallace and M. A. Jensen, "The Capacity of MIMO wireless systems with mutual coupling", *IEEE VTC' 03*, pp. 696−700, 2002.

[20] O. Edvardsson, “Can two antennas be smaller than one?” *Proc*. *ICAP 2001*, pp. 533–536, 2001.

[21] J. Thaysen and K. B. Jakobsen “Mutual Coupling between Identical Planar Inverted-F Antennas”, submitted, 2005.

[22] J. Thaysen and K. B. Jakobsen “Correlation and Coupling Reduction Between Cellular MIMO Antennas”, submitted, 2005.

[23] G. Lebrun, S. Spiteri, and M. Falkner, “MIMO complexity reduction through antenna selection”, *ANNAC’ 03*, pp. 5, 2003.

[24] J. Thaysen and K. B. Jakobsen,“Reduction of Antenna Correlation and Bandwidth Optimisation for Increased Mobile Phone MIMO Antenna System Performance,” submitted 2004.

[25] K. Sulonen, P. Suvikunnas, J. Kivinen, L. Vuokko, and P. Vainikainen, “Study of different mechanisms providing gain in MIMO systems,” *Proc. IEEE 58th Veh. Technol. Conf.*, 2003.

[26] P. Suvikunnas, K. Sulonen, J. Villanen, C. Icheln, J. Ollikainen, and P. Vainikainen, “Evaluation of Performance of Multi-antenna terminals using two approaches”, *IMTC 2004*, p. 6, Italy, 2004.

[27] A. F. Molisch and M. Z. Win, “MIMO systems with antenna selection”, *Microwave Magazine, IEEE,* vol. 5 (1), pp. 46−56, 2004.

[28] K. Kalliola, H. Laitinen, K. Sulonen, L. Vuokko, and P. Vainikainen, ”Directional Radio Channel Measurements as Mobile Station in Dirfferent Radio Environments at 2.15 GHz,” *4th European Personal Mobile Communications 2001 -Conference*, Austria, 2001.

[29] K. Kalliola, H. Laitinen, L. Vaskelainen, and P. Vainikainen, “Real-time 3-D spatial-temporal dual-polarised measurement of wideband radio channel at mobile station,” *IEEE Trans. Instrum. Meas.*, vol. 49, pp. 439−448, 2000.

[30] J. Kivinen, P. Suvikunnas, D. Perez, C. Herrero, K. Kalliola, and P. Vainikainen, “Characterization system for MIMO channels,” *Proc. 4th Int. Symp. Wireless Personal Multimedia Communications*, pp. 159−162, 2001.

[31] K. Sulonen, P. Suvikunnas, L. Vuokko, J. Kivinen, and P. Vainikainen, ”Comparison of MIMO antenna configurations in picocell and microcell environments”, *IEEE Journal on Selected Areas in Communications, special issue on MIMO systems and Applications*, vol. 21 (5), pp. 703−712, 2003.

[32] www.zeland.com.

[33] www.satimo.com.

[34] R. G. Vaughan and J. Bach Andersen, *Channels, Propagation and Antennas for Mobile Communications*, The IEE, UK, 2003.

[35] C. E. Shannon, “A mathematical theory of communications: Parts I and II,” Bell Syst. Tech. J., vol. 27, pp. 379–423, 623–656, 1948.

Paper V

Estimation of the Optimal Location of Metallic Objects Inside a Mobile Phone

Authors

Jesper Thaysen

Nokia Denmark, DK-1790 København, DENMARK
Technical University of Denmark DK-2800 Kgs. Lyngby, DENMARK

Kaj B. Jakobsen

Technical University of Denmark DK-2800 Kgs. Lyngby, DENMARK

Published in

Microwave journal

J. Thaysen and K.B. Jakobsen, "Estimation of the Optimal Location of Metallic Objects Inside a Mobile Phone", *Microwave journal,* 2005.

1 Estimation of the Optimal Location of Metallic Objects Inside a Mobile Phone

Jesper Thaysen
Nokia Denmark, www.nokia.com, DK-1790 Kbh V, DENMARK
Email: jesper.thaysen@nokia.com

Kaj B. Jakobsen

Technical University of Denmark, www.dtu.dk, DK-2800 Kgs. Lyngby, DENMARK
Email: kbj@oersted.dtu.dk

Planar near-field measurements of the electric field components are used to determine where to place external components, i.e., loudspeaker, camera, etc. without affecting the radiated field significantly. The location of the peak value of the electric field is discussed. The three principal electric field components are simulated, in order to illustrate which of the individual components that contributes the most to the total field. The measured and simulated results are compared and discussed in terms of the radiation from the Planar Inverted-F Antenna (PIFA) element itself and from the ground plane of the antenna. We show that the optimal location of a camera or a loudspeaker could be determined directly from the raw unprocessed electric near-field distribution. The result is that metallic objects should be located in areas below local minima in the electric field amplitude of the total field.

1.1 Introduction

The Planar Inverted-F Antenna (PIFA) is widely used in cellular phones primarily due to the compactness and size [1]. The demand for communication devices for personal communication systems has led to a constant search for ways to reduce the cellular phone dimensions. Applications such as loudspeakers, cameras, etc. are emerging and thus the complexity and the requirements to the antenna system continue to increase. It is expected that the volume available for the antenna decrease, since the overall size of the mobile phone continue to decrease. However, antenna size reduction is done at the expense of antenna gain and bandwidth [2]. This follows from the fact that an antenna is used to transform a bounded wave into a radiating wave [3]. An antenna performs this transformation, however, only with a poor efficiency when it is much smaller than the wavelength [4]. The loss in antenna gain can to some extent be compensated for by amplification. This is obviously not the case for the bandwidth. If the impedance match is much better than required, broad banding techniques could be used [5]. For a given configuration, the design of the antenna should be done in order to use the total volume available [6-7]. The upper theoretically limit are never reached, and the design of small antennas is thus a trade-off between bandwidth and gain for the antenna chosen to the given application [2, 8]. Many authors have dealt with the issues regarding the minimisation of antennas suitable for cellular applications, recently published is, e.g., Skrivervik [9].

Another challenging task in minimising the antenna is that the distance between the antenna and the other components, such as the loudspeaker and the camera decreases as well. This motivates the need for information regarding how the antenna should be placed on the ground

plane as well as the placement of other components with respect to the antenna and the ground plane. The job is also motivated by the fact that applications such as, e.g., Bluetooth, Diversity and Multi-Input Multi-Output (MIMO) may require an extra antenna inside the mobile phone, hence information regarding how these antenna could be oriented in order to minimise the coupling is needed [10]. Another important factor that also motivates to investigate the near-field from cellular phones is the specific absorption rate (SAR), which is a measure of the energy absorbed by the human tissue.

One way to obtain this kind of information is through the use of planar near-field measurements [11-14]. Usually the near-field is transformed to far-field data, nevertheless it is the raw unprocessed near-field data that is presented and used in this paper. The purpose of this research is to determine whether the raw unprocessed near-field data could be used as a design parameter.

The main objective of this research is to investigate how the near-field is distributed at small distances from the ground plane of the PIFA antenna. The results show that at distances very close to the antenna structure it is the antenna element that dominates the field. However, at larger distances the dominant radiated field is due to the current that is induced on the ground plane and not the current on the antenna element itself. This information could be used when one has to place two or more antennas within the same phone. The result could also be used to explain, and thus indicate how to minimise the mutual coupling between the antenna elements. The location of the peak value of the electric field is discussed. The three principal electric field components are simulated in order to illustrate how the individual component contributions to the total field. The measured results are compared to the simulated and discussed in terms of the radiation from the antenna element itself and from the ground plane of the antenna.

In order to analyse the antenna the IE3D computer program was used to predict the performance of the antennas in terms of the scattering parameters, the input impedance as well as the electric field distribution at short distances from the antenna [16]. The simulated results are compared with the corresponding experimental results to show the effectiveness of this approach. It turns out that the measured results are in good agreement with theory.

1.2 Materials and methods

The presented antenna configuration consists of two PIFA's with small differences in length and width. They are located on a 40 mm × 100 mm ground plane. Antenna A1 is 36 mm long, 1.2 mm wide and 7.5 mm high. The feed point is located 3.3 mm from the edge where a 90-degree bend forms the short to the ground plane, denoted with dots in the vignettes of the figures. Antenna A2 is oriented parallel to A1 and is 35 mm long, 0.9 mm wide, 7.5 mm high, and the feed point is located 1 mm from the shorting pin. The separation between the PIFA's is 2.5 mm. The layout is illustrated in Figure 1.

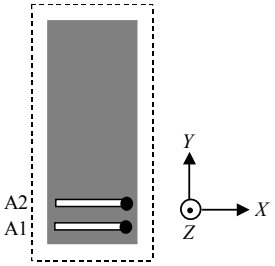

Figure 1. Illustration of the antenna model and the orientation, the grey area illustrates the 40 mm × 100 mm ground plane, the outer dashed frame illustrates the scan area that is mapped on all of the

following figures. The matchsticks symbolises the PIFA's and the dots denote the location of the shorting pins.

A planar scanner is used to perform the measurements. The step size is 4 mm leading to a total of 544 measurement points for a 64 mm × 124 mm area. This area covers the ground plane plus an additional 12 mm on each side of the ground plane [11]. The probe used for these measurements is a 3-dimensional E-field probe designed for electric near-field component measurements up to 3 GHz [15]. The measurements are carried out at 1950 MHz, i.e., the resonant frequency of antenna A2. The measurement facility gives the total amplitude of the electric field as well as the *x*, *y*, and *z* components. These measurements are compared to the results obtained from the IE3D computer program used [16].

In the planar scanning technique the probe is moved in a plane situated in front of the antenna and the received signal (amplitude) is recorded. The position of the probe is characterised by the coordinates (x, y, z_0) in the xyz coordinate system of the antenna as shown in Figure 1. During the scanning, z_0 is kept constant, while x and y is varied. The field is measured at two distances, e.g. z_0 = 2.5 mm and 22.5 mm, which corresponds to a free space distance of 0.016λ and 0.15λ, which are equivalent to an electric length of 6° and 52°, respectively. It should be noted that the distance between the ground plane and the measurement planes are 10 mm and 30 mm, since the antenna height is 7.5 mm.

1.3 Results and discussion

The simulated and measured field distribution shown in Figure 2 contains the electric field amplitude at 2.5 mm above the radiating element. In all sub-figures the highest field intensity (red) is attributed to the region where the PIFA elements are located, i.e., in the lower part of the figures.

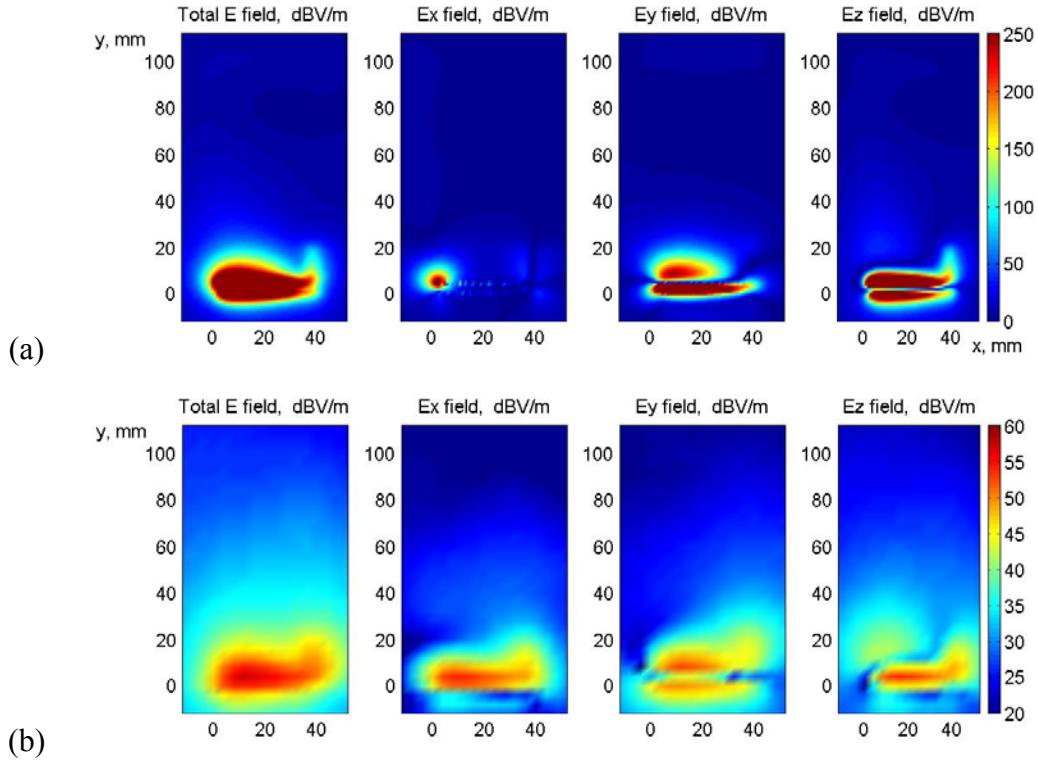

Figure 2. Simulated (a) and measured (b) electric field 2.5 mm above the radiating element at 1950 MHz.

The shape of the total electric field corresponds to the shape of the antenna elements. It is seen that the largest contribution is attributed to the open end of the radiating elements. Due to the very narrow elements in the *y* direction, the field contribution from the *x* component is expected to be low, as indicated by one major contribution. The peak radiation of the *x* component is attributed to the open end of the radiating element. The deviation observed when comparing the measured (Figure 2b) to the simulated (Figure 2a) *x* component could be caused by at least two things. First, the prototype is hand made using a scalpel and thus not perfectly rectangular as in the simulation model. And secondly, if the prototype is not fully aligned then the measured *x* component contains *y* component as well. The *y* component follows the shape of the elements, i.e., two major contributions, both two long and narrow plates as expected due to the shape of the antenna elements. For the *z* component one could observe two long and narrow plates as expected due to the shape of the antenna. The highest field amplitude is obtained above the antenna element itself. In both the simulated and measured case one also could observe a contribution from the *z* component that originates from the open end of the radiating element towards the centre of the ground plane.

Although, the higher resolution for the simulated results yields better visualisation of the trends the measured results agrees well.

One of the most obvious differences when looking at the total field and the *x* component of the electric field plot at 2.5 mm (Figure 2b) and 22.5 mm (Figure 3) above the ground plane is the different location of the maximum in the field intensity. In the lower cut (2.5 mm see Figure 2b), the field seems to originate from the open end of the radiating element, i.e., the PIFA elements itself. This fact changes when looking at the electric field obtained 20 mm further away (see Figure 3), here it is more likely that parts of the radiated field originate from the geometrical centre of the element. The maximum of the *z* component is at both distances located above the feed and short pin. However, observing in the 2.5 mm plane major part of the *z* component contribution originates from the open end of the radiating element, whereas a null is observed at the 22.5 mm plane. The maximum of the *y* component are located at (*x, y*) = (30, 20) this is not above the radiating element, which indicates that some kind of radiation from the ground plane exists.

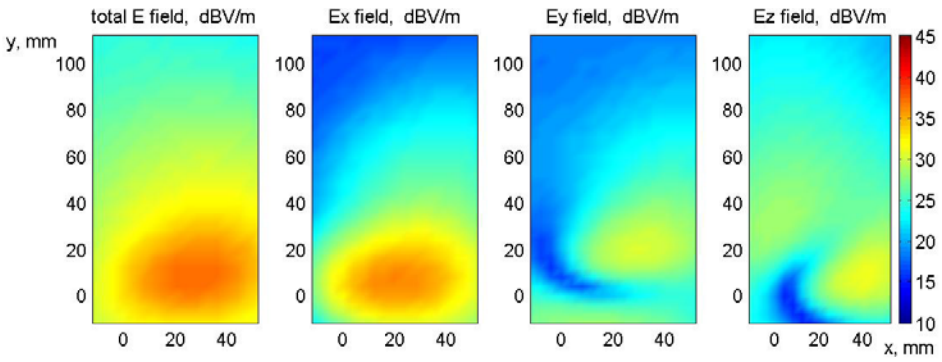

Figure 3. Measured electric field component 22.5 mm above the radiating element at 1950 MHz.

Optimisation of the location of a metallic object having a size of 7 mm × 7 mm × 7 mm.

Optimisation of the location of a metallic cube with a size of 7 mm × 7 mm × 7 mm. The cube is assumed to model a loudspeaker or a camera, by the size.

The simulated electric field component 2.5 mm above the antenna ground plane at 1950 MHz that is shown in Figure 4 could be compared with the corresponding simulations where the metallic cube is located at different locations. The location is varied from (x, y) = (0, 7) to (27, 7) in 5 steps, namely at x = 0 mm, 6 mm, 10 mm, 20mm, and 27 mm from the left edge of the ground plane.

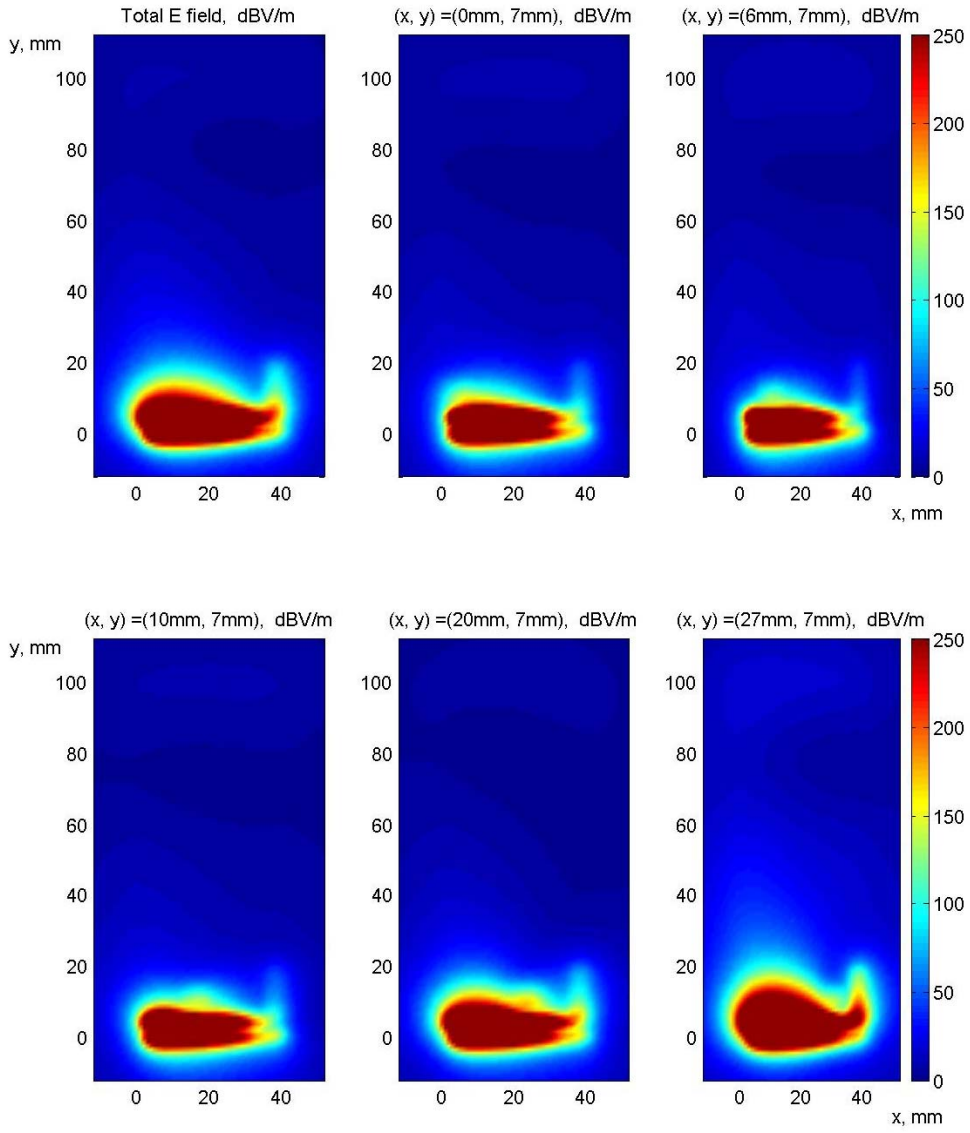

Figure 4. Simulated electric field component 2.5 mm above the antenna ground plane at 1950 MHz (upper left). With the metallic cube located as described above each subfigure.

Comparing the shape of the total electric field it can be seen that locating the metallic cube at either (x, y) = (20, 7) or (27, 7) affects the near field the least. Most affected is the (x, y) = (0, 7) case, here the metallic cube is located nearest the open end of the PIFA arms.

Visualising the results using the raw data of the electric near field give rise to a rather subjective evaluation. In Figure 5–7 the simulated reflection coefficient of antenna A1, A2 and the mutual coupling is shown and could be compared in a more objective manner.

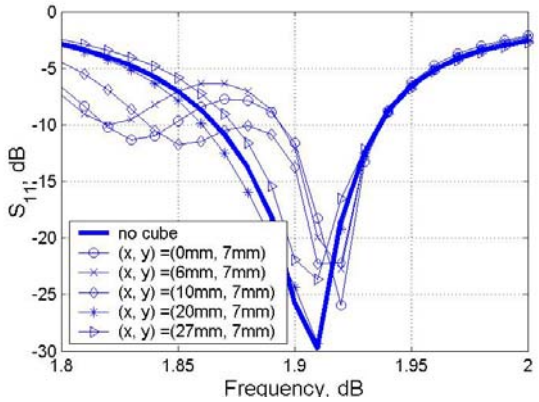

Figure 5. Simulated reflection coefficient for antenna A1 for different location of the metallic cube compared to the case of no metallic cube (wide line).

Chancing the location from 0 mm to 27 mm the resonant frequency of antenna A1 decreases from 1920 MHz to 1905 MHz. The original resonant frequency of antenna A1 is 1910 MHz. For cube locations of $(x, y) = (0, 7)$, (6, 7), and (10, 7) the bandwidth is increased significantly as compared to the original case. The wider bandwidth is caused by constructive interference between the metallic cube and the antenna arms.

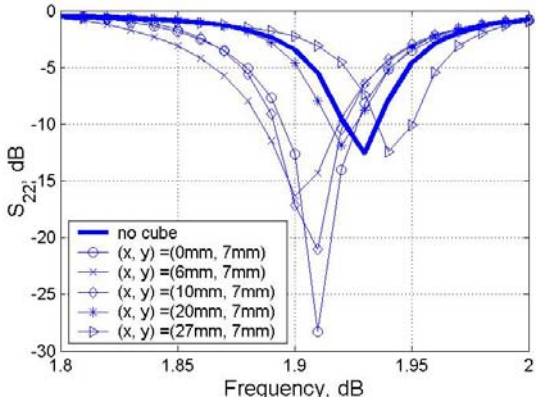

Figure 6. Simulated reflection coefficient for antenna A2 for different location of the metallic cube compared to the case of no metallic cube (wide line).

When locating the metallic cube nearest to the shorting pin of the PIFA, i.e., at $(x, y) = (27, 7)$ the resonant frequency is 1945 MHz. This is slightly higher than the resonant frequency of antenna A2 in the original case (1940 MHz). A decrease in resonant frequency to 1920 MHz is observed when the metallic cube is moved towards $(x, y) = (0, 7)$.

From the results shown in Figure 5 and Figure 6 it is observed that the resonant frequencies of the two antennas chances opposite. When chancing the location of the metallic cube from $(x, y) = (0, 7)$ to (27, 7) the resonant frequency of antenna A1 is decreased 1920 MHz to and 1905 MHz. Simultaneously the resonant frequency of antenna A2 is increased from 1905 MHz to 1945 MHz. This result explains the behaviour of the mutual coupling that is shown in Figure 7. The original case yields a mutual coupling of $S_{21} = -3$ dB. The strongest coupling of –1.6 dB is obtained at 1905 MHz, with the metallic cube located at $(x, y) = (0, 7)$. This is a 3.4 dB stronger coupling as compared to the –5 dB obtained at $(x, y) = (27, 7)$ case.

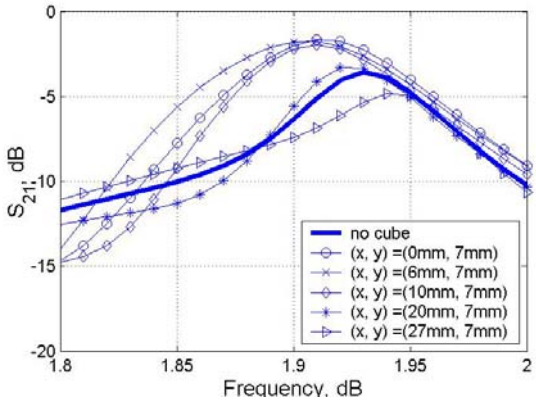

Figure 7. Simulated mutual coupling for different location of the metallic cube compared to the case of no metallic cube (thick line).

1.4 Conclusion

We have shown that metallic objects that are placed in the regions above the ground plane were the field intensity is the lowest affects the antenna performance the least. Hence, the optimal location of a metallic object, which might be a camera or a loudspeaker, could be determined directly from the raw unprocessed electric near-field distribution.

In the cases where the metallic object is located closest to the open end of the radiating element, the antenna performance is affected the most. Thus, the conclusion is that metallic objects should be located in areas having a local minima in the electric field amplitude of the total field, and one should maximise the distance between the metallic object and the open end of the radiating element.

1.5 References

1 K. Hirasawa and M. Haneishi, "Analysis, design, and measurement of small and low profile antennas," *Artech House*, ISBN 0-89006-486-5, 1991.

2 R. F. Harrington, "Effect of antenna size on gain, bandwidth and efficiency," *Journal of research of national bureau of standards, D-radio Propagation*, vol. 64D, pp. 1-12, 1960.

3 "The IEEE standard definitions of terms for antennas," *IEEE Trans. Antennas Propagat*., vol. 17, 1969.

4 R. C. Hansen, "Fundamental limitations in antennas," *Proc. IEEE*, vol. 69, Feb. 1981.

5 R. E. Collin, "Minimum Q of small antennas," *J. Elec. waves*, vol. 12, pp. 1369-1393, 1998.

6 L. J. Chu, "Physical limitations of omnidirectional antennas," *J. App. Phys*., Vol. 19, pp. 1163-1175, 1948.

7 G. A. Thiele, P. L Detweiler, and P. P. Penno, *"*On the lower bound of the radiation Q for electrically small antennas*", IEEE Trans. Antennas Propagat*., 51 (6), pp 1263-1269, 2003.

8 H. A. Wheeler, "Fundamental limitations of small antennas," *Proc. IRE*, vol. 35, pp. 1163-1175, 1947.

9 A. K. Skrivervik, J-F Zürcher, O. Staub, and J. R. Mosig, "PCS antenna design: The challenge of miniaturization," *IEEE Trans. Antennas Propagat*., vol. 43, pp. 12-27, 2001.

10 J. Thaysen, "Mutual Coupling Between Two Identical Planar Inverted-F Antennas," *IEEE AP-S International Symposium and USNC/URSI National Radio Science Meeting*, USA, pp. 504-507, 2002.

11 J. Appel-Hansen, "Antenna measurements," Ch. 8 in A.W. Rudge (Ed.) "The handbook of antenna design", *Peter Pelegrinus Ltd*, 1982.

12 R. C. Baird, A. C. Newell, and C. F. Stubenrauch, "A brief History of near-field measurements of antennas at the national bureau of standards," *IEEE Trans. Antennas Propagat*., vol. 36, no 6, June 1988.

13 J. Thaysen, K. B. Jakobsen, "Near field Distribution from a Planar Inverted-F Antenna", *Proceedings of Twelfth International Conference on Antennas & Propagation*, Univ. of Exeter, UK, pp 4, 2003.

14 Y. Gau and I. Wolff, "Miniature electric near-field probe for measuring 3-D fields in planar microwave circuits," *IEEE Trans. On Microwave theory and Techniques*, vol. 46, pp. 907-913, 1998.

15 www.speag.com, Data sheet, "3-Dimensional E-Field Probe for Small Band Applications," 2002.

16 "IE3D User's Manual, Release 8," Zeland Software, Inc., Fremont, CA, 2001.

Paper VI

Mutual Coupling between Identical Planar Inverted-F Antennas

Authors

Jesper Thaysen

Nokia Denmark, DK-1790 København, DENMARK
Technical University of Denmark DK-2800 Kgs. Lyngby, DENMARK

Kaj B. Jakobsen

Technical University of Denmark DK-2800 Kgs. Lyngby, DENMARK

Paper accepted in

International Journal of Electronics and Communications (AEU)

J. Thaysen and K.B. Jakobsen, "Mutual Coupling between Identical Planar Inverted-F Antennas", Accepted 2005.

1 Mutual Coupling Between Identical Planar Inverted-F Antennas

Jesper Thaysen
Nokia Denmark, www.nokia.com, DK-1790 Kbh V, DENMARK
Email: jesper.thaysen@nokia.com

Kaj B. Jakobsen

Technical University of Denmark, www.dtu.dk, DK-2800 Kgs. Lyngby, DENMARK
Email: kbj@oersted.dtu.dk

Mutual coupling between two identical planar inverted-F antennas (PIFA) located on an infinite ground plane is studied numerically. Several arrangements of side-by-side, collinear, parallel-in-echelon, and orthogonal PIFA antennas with element spacing varying from 0.06λ to 1.20λ are investigated at the design frequency of 1.9 GHz, and in the –6 dB bandwidth between 1.8 GHz and 2.0 GHz. It is found that choosing configurations that maximises the separation between the open-end of the PIFAs reduces the mutual coupling.

1.1 Introduction

The Planar Inverted-F Antenna (PIFA) has advantages of having small and multiband resonant properties. These characteristics make the PIFA a suitable antenna candidate to mobile phones.

Shrinking the size of the mobile phone also affects the distance between the antenna and the other components, such as the loudspeaker and the camera decrease in size as well. This motivates the need for information regarding how the antennas should be placed on the ground plane as well as the placement of other components with respect to the antenna and the ground plane. The job is also motivated by the fact that applications such as diversity and Multiple-input multiple-output (MIMO), e.g., may require an extra antenna inside the mobile phone, hence information regarding how these antennas should be oriented in order to minimise the coupling is also needed [1]. The effect on mutual coupling is recently published by Carrasco et al. [2], the results are in accordance with previous work by the authors of this paper [1].

Cramming many antennas on the same finite sized ground plane results in higher mutual coupling due to the smaller distances between the antennas [3]. The increased mutual coupling results in higher spatial correlation which leads to a lower MIMO gain as compared to fully uncorrelated antenna signals.

The main objective of this research is to explain the coupling between two identical PIFA antennas. Symmetrical as well as unsymmetrical coupling scenarios using two identical PIFAs located close to each other is investigated, in order to determine the mutual coupling versus separation for fixed orientations, and mutual coupling versus orientation of the antennas for fixed separation. The results illustrate how to orientate and locate the antennas in order to minimise the coupling. The scattering parameters are found by the use of the method-of-moment simulation program IE3D [4]. The experimental and the simulation results are in good agreement.

1.2 Materials and methods

This section is divided into two subsections. In the first subsection a two-antenna configuration is investigated both based on simulated results as well as measurements on a fabricated prototype. The second subsection describes the different scenario that is investigated.

Verification of the simulation results

The presented two-antenna configuration consists of two 40 mm long, 1.5 mm wide and 5 mm high PIFAs located orthogonal on a 40 mm × 100 mm ground plane. The feed point is located 5 mm from the edge where a 90-degree bend forms the short to the ground plane.

Good agreements between the simulation and measurement results are seen in Figure 1. Both antennas have resonant frequency at 1.8 GHz.

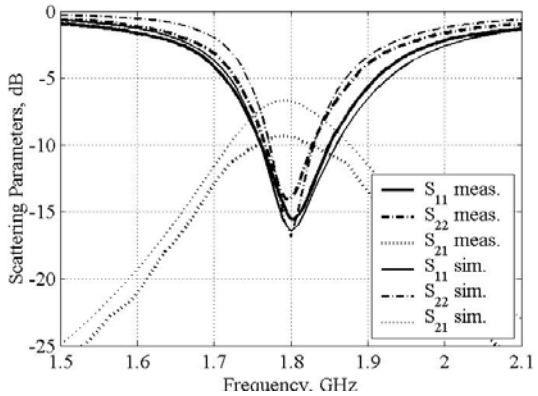

Figure 1. Simulated and measured scattering parameters.

The measured total efficiency of antenna A1 is higher than 40% between 1.7 GHz and 1.9 GHz. Antenna A2 yields a total efficiency higher than 25%, as shown in Figure 2.

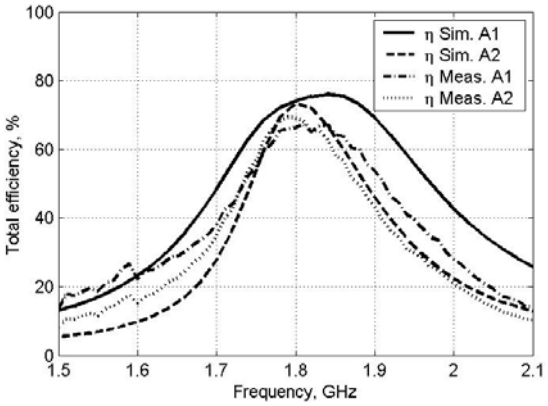

Figure 2. Total efficiency for antenna A1 and A2.

Good agreement between the simulated and measured radiation patterns is obtained see example in Figure 3. The measured maximum gain is 2.6 dBi for antenna A1 (3.2 dBi simulated), and 1.5 dBi for antenna A2 (1.7 dBi simulated).

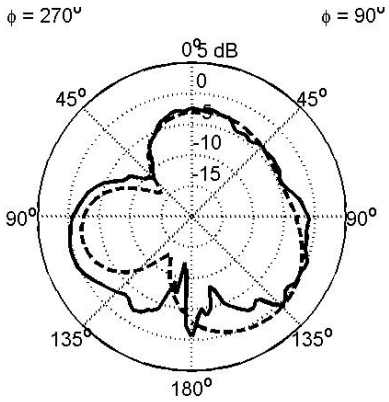

Figure 3. Simulated (dashed) and measured (solid) radiation patterns cut at 1.8 GHz for antenna A1 for $\phi = 90°$. The dips in the measured θ-cuts for $\phi = 180° \pm 12°$ are due to the antenna mounting and positioning system [5].

The difference in the simulated and measured results could be explained by the difference between the two antennas, which are hand made, i.e., made by using a scalpel, and therefore not completely identical. Also the effect from the coaxial cable used in the prototype affects the performance; especially the radiation pattern suffers from this.

Investigated scenario

The remaining investigations are based on a two-antenna configuration located on an infinite ground plane. The infinite ground plane is chosen to determine the influence of the distance and mutual orientation and not the effect of the location on a finite ground plane.

The investigated PIFA consists of a 40 mm × 1 mm patch located 15 mm above an infinite perfect conducting ground plane. The feed line is located 13 mm from the edge, where a 90° bend forms the short circuit to the ground plane, see illustration in Figure 4.

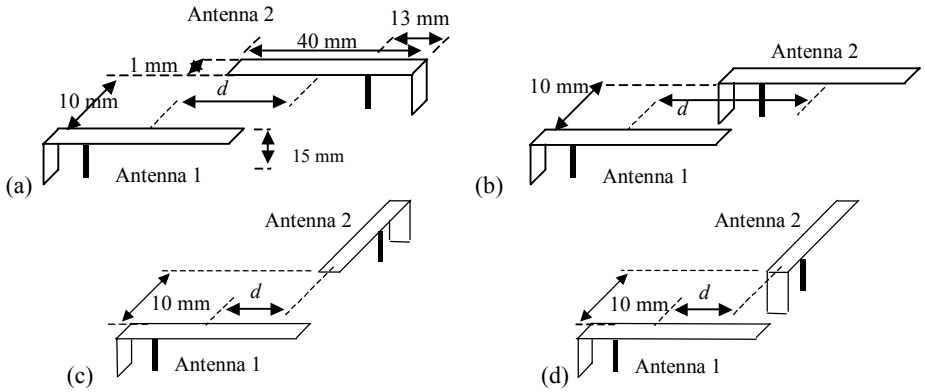

Figure 4. Illustration of the four different configurations that are investigated. Parallel antennas fed at the opposite ends (a), parallel antennas fed at the same end (b), orthogonal antennas with antenna 2 fed at the top (c), and orthogonal antennas with antenna 2 fed at the bottom. The vertical distance is fixed 10 mm, whereas the horizontal distance, *d*, varies in the different scenarios, *d* is positive in the case illustrated in the Figure.

1.3 Results

This section that treats the two-antenna configuration located on an infinite ground plane is divided into four subsections: One treating parallel PIFA configurations (see Figure 4a and 4b), and one treating orthogonal PIFA configurations (see Figure 4c and 4d). In the third subsection the bandwidth are investigated with respect to mutual coupling. The fourth subsection contains the mutual coupling for various orientations. In all cases it is the geometrical centre that is used since it is a simple measure.

Fixed Parallel Orientations:

Two parallel PIFAs are investigated. First both antennas are fed in the opposite ends (Figure 4a), hereafter called (0, 180), and second they are fed in the same end (0, 0), as illustrated in Figure 4b.

A rather unsymmetrical decrease is observed for an increased separation is seen from Figure 5. This seems reasonable due to asymmetry in the setup. The coupling decreases almost linearly for d = 0 to 150 mm, whereas a rather different behaviour is observed for a negative d. A steep slope is observed where the feed lines are closest, i.e., for d = –5 to –20 mm, followed by an almost horizontal curve section where the coupling remains constant at around –7 dB for d = –20 to –40 mm. Changing the horizontal separation such that the feed line is moved towards the shorting point causes a rapid decrease in the coupling, whereas moving the feed line away from the shorting point, i.e., towards the open end does not seem to affect the coupling. The coupling starts to decrease again when there is no overlap between the two PIFAs.

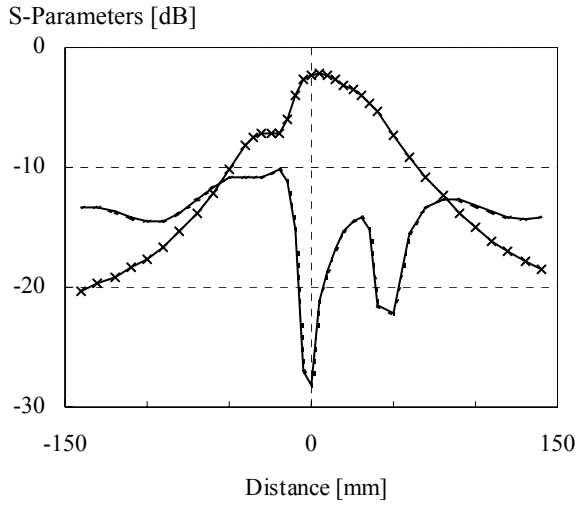

Figure 5. Simulated S-parameters $|S_{11}|$, $|S_{22}|$ and $|S_{21}|$ (×) for two parallel PIFA antennas separated 10 mm, feed in opposite end (0, 180) on an infinite ground plane (see Figure 4a). $|S_{11}|$ and $|S_{22}|$ are overlapping.

The reflection coefficients, $|S_{11}|$ and $|S_{22}|$ that are shown in Figure 5 are identical and have two dips in the impedance match. The best impedance match is obtained at d = 0 mm and the next best between d = +40 to +50 mm. The latter is when the horizontal separation between the open ends is zero.

Similar simulations are made for the configuration where the two antennas are fed in the same ends (0; 0) the data are not shown. Except from the highest coupling ($|S_{21}|$ = –4.8 dB) that is obtained for d = 0, the results are quite different from the (0; 180) case. A symmetrical roll-off

is observed when the separation is increased; this seems reasonably due to the symmetry, see Figure 4b. The $|S_{11}|$, $|S_{22}|$ also indicates symmetry around $d = \pm 13$ mm. Here, the shorting point of antenna A1 is above the feed line of A2, and visa versa. In these particular setups the reflection coefficient is the highest, being –6.6 dB.

Comparing the simulated scattering parameters for the two scenarios the coupling is 2.5 dB higher for (0, 180) than for (0, 0). This indicates lower coupling for the latter. However, making this comparison one should bear in mind that no corrections have been made regarding the different impedance match. This explains a part of the difference. In general, the (0; 0) case yields a coupling that is a few dB lower for a given separation.

Fixed Orthogonal Orientations

This subsection covers the orthogonal cases. First, antenna 2 is fed in the top (Figure 4c), hereafter called (0, 270), and secondly fed in the bottom (0, 90) (Figure 4d). For the orthogonal cases the behaviour seems comparable with the parallel cases. However, they need some explanation which will be provided in the following.

For the curves showed in figure 6, the reflection coefficients, for the to antennas are rather fluctuating between –16 and –9 dB, no direct minimum or maximum is easily identified. The lowest reflection coefficient of –16 dB is obtained at a separation of –40 mm, this is where the open end of antenna 2 is above the shorting pin of antenna A1. This is also the case for the parallel case at d=40 mm. The worst impedance match on –9 dB is obtained at a separation of –7 mm, which where the open end of antenna A2 is above the feeding line of antenna A1.

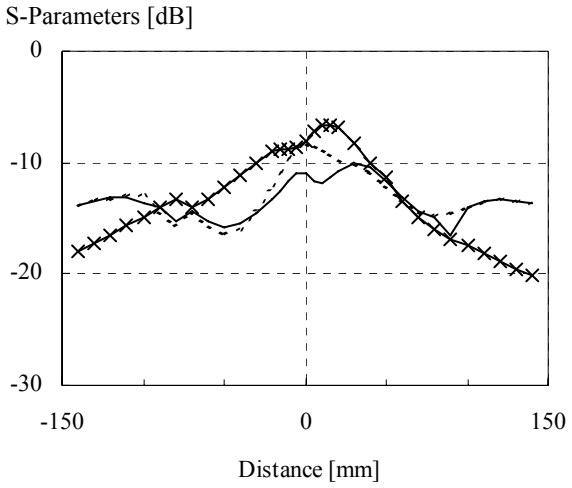

Figure 6. Simulated S-parameters $|S_{11}|$, $|S_{22}|$ (dash) and $|S_{21}|$ (×) for two orthogonal PIFA separated by 10 mm. Antenna 2 is fed at the top (0; 270).

For the coupling as showed in Figure 6 the curve behaviour is rather asymmetrical, a local plateau is located at –7 mm just next to the strongest coupling obtained at +20 mm. At a separation of –7 mm the open end of antenna 2 is located above the feeding line of antenna 1. The strongest coupling occurs at +20 mm where the open end of antenna 2 is above the open end of antenna 1.

For the (0, 90) case, illustrated in Figure 4b, the coupling as well as the impedance match for the two antennas are rather symmetrical around –7 mm with a maximum that is easily

identified, and a roll off as a function of separation. The best impedance match on –50 dB, and the strongest coupling of –6 dB is obtained at a separation of –7 mm, where the shorting pin of antenna 2 is above the feeding line of antenna 1, the data are not shown. In both orthogonal scenarios the distance variations affect the centre frequency negligible (<3%) the data are not shown.

For a given physical separation the setup, which is shown in Figure 6 (0, 270) yields a lower coupling as compared to the (0, 90) case. The worst case coupling is 1.3 dB lower. Again, no corrections have been made regarding the different impedance match. This explains some of the difference.

Bandwidth versus separation

From the simulated result showed in Figure 7 the bandwidth converges for an increase of the separation. Above a certain separation, 40 only minor changes are observed. Above 100 mm the coupling is well below –16 dB.

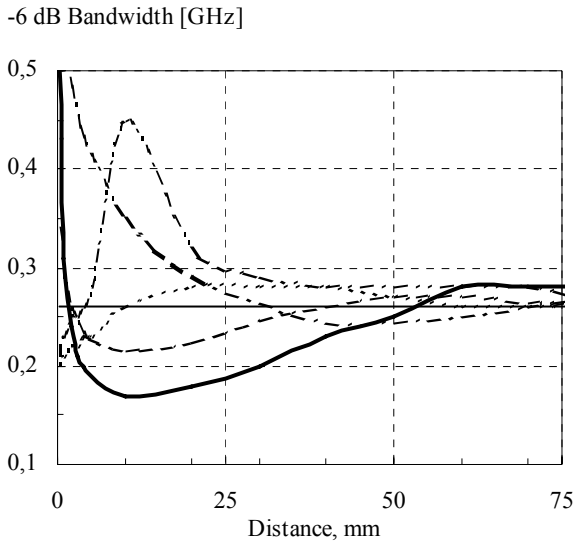

Figure 7. –6 dB bandwidth as a function of separation (0, 0) dot, (90, 90) wide solid, (90, 270) dash-dot-dot, (0, 180) dash-dash, (180, 0) dash-dot, compared to the bandwidth of a single antenna (solid).

Most interesting is the (180, 0) case, where the bandwidth increases for smaller separation. This is presumably due to a simultaneously increase in the coupling. The main reason for the changes is mainly due to mismatch from the original match.

Rotation of the Antennas

The third setup consists of two PIFAs located in line at a separation of 50 mm between the geometrical centres of the antennas. In order to determine the coupling in different setups the two antennas are rotated around the geometrical centre in eight equally steps of 45°. In the 20 setups that all together describe all the cases of the mutual orientation, the simulated S_{11} parameters show that the bandwidth, within which the reflection coefficient is better than –6 dB, is from 1.81 GHz to 2.07 GHz, which is unchanged compared to the bandwidth for the single PIFA, which indicates a rather weak coupling. Using the geometrical centre of the PIFA as the centre of rotation makes it possible to define the two separations that are used in

Figure 8. These are defined as the separation between the open ends of the two PIFAs and the separation between the shorting pins of the two PIFAs.

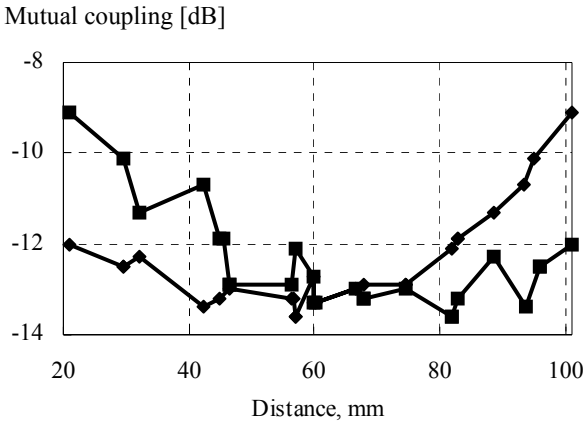

Figure 8. Simulated coupling as a function of the separation between the open ends (■), and the separation between the shorting pins (♦) of the two PIFAs.

The coupling, $|S_{21}|$ is found to −9 dB when the PIFAs are orientated such that the shorting pins are in the opposite ends, i.e., at the maximum separation between the open ends (0, 180). The coupling, $|S_{21}|$ are found to −12 dB when the shorting pins are located in the opposite ends, i.e., the minimum separation (180, 0). One would, however, expect that the largest difference would be between two orthogonal setups, as is the case for a dipole setup.

The results differ from the expectations since the simulated coupling indicates that only 4 dB separates the lowest from the highest coupling. The radiation patterns from the various PIFA setups are likely to have a slight tilt towards the open end of the PIFA, also the case shown in Figure 3. This explains the small derivation in the coupling for the various scenarios. In fact, there are no nulls in the direction of the end as for the dipole case.

From the theory it is expected that the coupling should decrease for an increase in the separation. In Figure 8 this is the case for the open-end distance, only. Thus, it is the open-end separation that yields a decrease in the coupling as a function of an increase in the separation.

1.4 Discussion

To analyse the performance of the PIFA located above an infinite plane conductor, the image theory will be introduced to account for the reflections. The PIFA could be assumed to consist of two radiating components, namely the feed line (and the shorting pin) and the patch itself, the feed line being vertical, the patch horizontal. For an incident electric field with vertical polarisation, the polarisation of the reflected waves must also be vertical and with a polarity in the same direction as that of the actual source to satisfy the boundary conditions. For the radiating element in a horizontal orientation, it follows that the image is placed at a separation equal to the antenna height below the interface with a 180° phase difference relative to the actual source. The radiation from the horizontal element and its image cancel in the plane at the ground plane; thus major parts of the radiated field originate from the feed line. This explains the rather low change in the field as a function of the mutual orientation, as illustrated in Figure 8. This is also in accordance with the fact that the strongest coupling is found when the PIFAs are orientated such that the shorting pins are located in the opposite ends, i.e., maximum separation. From a theoretical point of view a decrease in the field amplitude, hence

coupling, is expected when the separation is increased, thus it seems reasonable that the separation between the open-ends dictates the coupling.

1.5 Conclusions

It is found from the simulated scattering parameters that the coupling is generally a few dB lower for the orthogonal than for the parallel cases.

The resonant frequency is most affected at setups where the open end and the feed line are vertically in line. Maximum coupling is obtained when the antennas are overlapping and is strongest for the setup having the feed line in opposite ends, i.e., furthest apart.

For the setup of mutual rotation of the PIFAs the expected inverse proportionality between the coupling and the separation is not easily identified. However, the results indicate that it is most likely that it is the separation between the open ends of the PIFAs that dictates the coupling. Thus, it is found that choosing configurations that maximises the separation between the open-end of the PIFAs could reduce the mutual coupling.

1.6 Acknowledgement

This work has been supported by Nokia Denmark. Thanks to Elna Sørensen from Technical University of Denmark for proof reading.

1.7 References

1 Thaysen, J., "Mutual Coupling Between Two Identical Planar Inverted-F Antennas," IEEE AP-S International Symposium and USNC/URSI National Radio Science Meeting, USA, pp. 504-507, June 2002.

2 Carrasco H., Hristov H.D., Freick R., Cofre D., "Mutual coupling between planar inverted-F antennas", *Microwave and optical Tech. Lett.,* vol 42, pp. 224-227, Aug. 2004.

3 *Edvardsson, O.,* "Can two antennas be smaller than one?" *Proc*. *ICAP 2001*, pp. 533 – 536, 2001.

4 www.zeland.com.

5 www.satimo.com

Paper VII

Mutual coupling reduction using a lumped LC circuit

Authors

Jesper Thaysen

Nokia Denmark, DK-1790 København, DENMARK
Technical University of Denmark DK-2800 Kgs. Lyngby, DENMARK

Kaj B. Jakobsen

Technical University of Denmark DK-2800 Kgs. Lyngby, DENMARK

Conference paper published

JINA 2004, International Symposium on Antennas

J. Thaysen and K.B. Jakobsen, "Mutual coupling reduction using a lumped LC circuit", *JINA International Symposium on Antennas,* p. 4, 2004.

1 Mutual coupling reduction using a lumped LC circuit

Jesper Thaysen
Nokia Denmark, www.nokia.com, DK-1790 Kbh V, DENMARK
Email: jesper.thaysen@nokia.com

Kaj B. Jakobsen
Technical University of Denmark, www.dtu.dk, DK-2800 Kgs. Lyngby, DENMARK
Email: kbj@oersted.dtu.dk

Abstract: A technique to reduce the mutual coupling between two Planar Inverted-F Antennas (PIFA) is presented in this paper. By the use of a parallel LC circuit it is possible to reduce the mutual coupling between two antennas. This results in a 16 % improvement in the radiation efficiency.

1.1 Introduction

The Planar Inverted-F Antenna (PIFA) is widely used in cellular phones primarily due to the compactness and size [1]. The demand for smaller communication devices for personal communication systems has led to a constant search for ways to reduce the cellular phone dimensions. However, the wavelength does not decrease, due to the higher frequency bands used, with the same speed as the size of the mobile phones. Even the widely used PIFA tent to become too large, and thus a demand for decreasing the volume of the antenna exist.

Applications such as triple band antennas, Bluetooth antennas, and antennas for Global Position System (GPS) are emerging and thus the complexity and the requirements to the antenna system continue to increase. It is expected that high isolation between two or more frequency bands is essential in many future applications. The task is complicated by the fact that the overall size of the mobile phone and the frequency separation between the different bands continue to decrease. In order to meet these demands, physically small antenna elements with low coupling are required. Therefore, knowledge regarding how these antennas should be oriented in order to minimise the coupling is needed [2].

In this paper the antenna system consists of two separate antennas, one for each of two frequency bands, that is denoted LB (low band) and HB (high band). For an antenna system consisting of more than one antenna, mutual coupling occurs. Here, a resonant LC circuit, consisting of a capacitor and an inductor, is used to reduce the mutual coupling.

In Hall [3] a resonant circuit useful for multi-band performances is described. By using tuned circuits of appropriate design strategically placed in a dipole, the antenna can be made to show what are essentially fundamental resonances at a number of frequencies. More recently, e.g., Lui [4] has investigated a distributed LC circuit for single feed dual frequency PIFA designs. The same principle could be used to minimize unwanted coupling between two antennas. For example, if an LC circuit is placed at the feed end of Antenna 1 is chosen to be resonant at the frequency where Antenna 2 is resonant, then Antenna 2 is effectively isolated from Antenna 1, thus the coupling is minimized.

The objective of this paper is to present the results of numerical and experimental investigations of the coupling between two PIFA antennas. The coupling is improved using lumped inductors and capacitors. To analyse the antenna, the computer program, IE3D, was used to predict the performance of the antennas in terms of the radiated efficiency and reflection coefficients [5].

1.2 Materials and Methods

An LC circuit in an antenna system can perform either of two functions, depending on whether or not it is resonant at the operation frequency. The LC circuit shown in Figure 1c is resonant at the resonant frequency f_0 equal to 1.8 GHz. Hence at resonance, the LC circuit presents high impedance, and thus it behaves as an isolator. It simply serves to separate the antenna arm from the feed point, leading to a low band (LB) antenna that effectively is isolated from the high band (HB) frequencies.

The second function of the LC circuit is electrical loading, which is obtained when the frequency of operation is not at the resonant frequency of the LC circuit. If the operating frequency is below that of the LC circuit resonance, which is the case here, the LC circuit behaves as an inductor. If the operation frequency is above the resonant frequency, it acts as a capacitor. Inductive loading will electrically lengthen the antenna, and capacitive loading electrically shorten the antenna.

The presented antenna configuration consists of two different PIFA's with a similar long and thin shape. They are located on a 40×100 mm^2 ground plane. The HB PIFA is 40 mm long, 1.5 mm wide and 5 mm high. The feed point is located 5 mm from the edge where a 90-degree bend forms the short to the ground plane. The HB PIFA is oriented parallel to the LB PIFA that is 71 mm long, 1.5 mm wide, and the feed point is located 8 mm from the shorting pin. The separation between the PIFA's is 1.5 mm. The layout is illustrated in Figure 1(a).

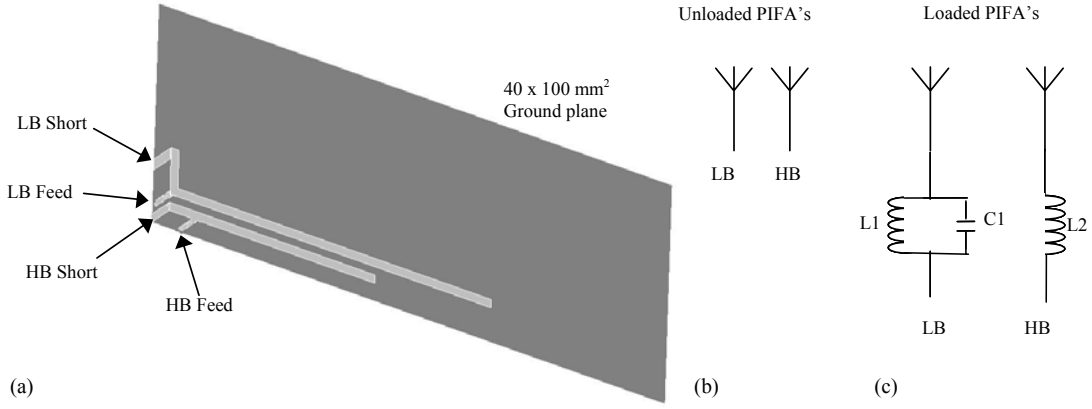

Figure 1. Illustration of the PIFA's located above a ground plane (a). The unloaded (b) and LC loaded PIFA and the inductor matched PIFA (c).

Two different scenarios are investigated. The unloaded case, and secondly the loaded case, i.e., an LC circuit and a matching inductor is placed just before the feed point, as shown in Figure 1 (b) and (c), respectively. With reference to Figure 1, two lumped 4.3 nH inductors [6] and one 1.8 pF capacitor are used in the simulations, and in the experiments. The component values are chosen such that the resonant frequency of the parallel circuit is 1.8 GHz, calculated from

$$f_0 = \frac{1}{2\pi\sqrt{LC}}. \quad (1)$$

The lumped components used are connected to the PIFA's such that it is possible to mount them on the ground plane; hence no extra complexity is added to the antenna element itself. Inductors with high Q values are chosen in order to decrease the insertion loss [6]. However, a high Q also tent to decrease the bandwidth, meaning that a trade of between insertion loss, efficiency and bandwidth must be made.

1.3 Results and discussions

The radiation efficiency and reflection coefficient for the unloaded as well as the loaded antenna system are simulated using IE3D and measured with a fabricated prototype. The simulated and measured reflection coefficients for the LB and the HB PIFA's, are shown in Figure 2. The isolation between the two PIFA's is shown in Figure 3. Figure 4 shows the efficiency curves. A summary of the results is given in Table 1.

The simulated resonant frequency of the LB PIFA without any loading components is 1.10 GHz with a –6 dB bandwidth of 6.1 % having a peak return loss of 9.0 dB. The mutual coupling at the resonant frequency (1.10 GHz) is 9.7 dB. Loading the antenna these parameters are slightly changed. Most affected is the reflection coefficient, which is improved to -23 dB in the loaded case. The isolation is increased by 3.3 dB to 13 dB, at the expense of a reduced bandwidth from 6.1 % to 4.6 %. The same trends are observed in the measured results. The measured resonant frequency is 1.04 GHz in both cases. A reduction in the bandwidth from 6.5 % to 5.2 % is observed and an improved peak reflection coefficient from –9.6 to –25 dB when loading the antenna. A 3 dB improvement in the isolation between the two antennas also occurs.

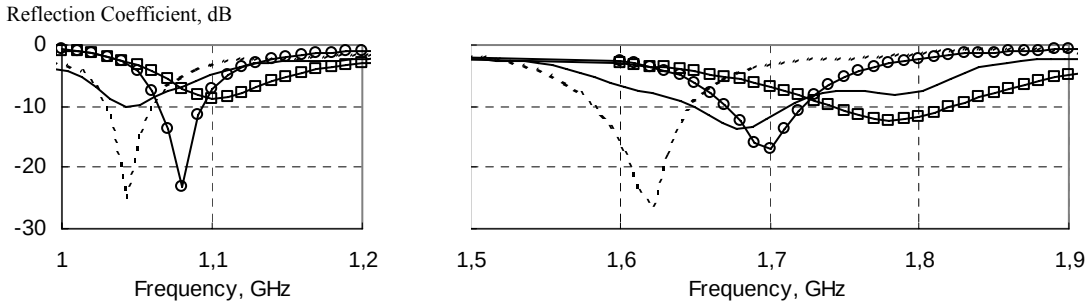

Figure 2. Simulated reflection coefficient for the unloaded (□) and LC loaded (○) case. Measured reflection coefficient for the unloaded (solid) and loaded (dashed) result.

The unloaded HB PIFA has a simulated bandwidth of 10.8 % around 1.77 GHz with a peak return loss of 12.1 dB. The loaded case yield a bandwidth of 5.6 % centred around 1.70 GHz. Loading the antenna yields better performance in especially the mutual coupling, which is lowered from –3.7 dB to –13.7 dB. A similar decrease in the resonant frequency as well as in the bandwidth is observed from the measured results. Also, a significant improvement in the mutual coupling from –6.6 dB to –21 dB is measured. The large improvement in the isolation is the result of adding the LC circuit. However, the LC circuit reduces the bandwidth. Also, the price and complexity is expected to be higher for the loaded case. This comes from the three lumped components that are needed. Two components, a capacitor and an inductor, are used for the resonant circuit, and one inductor is used for impedance match of the HB PIFA.

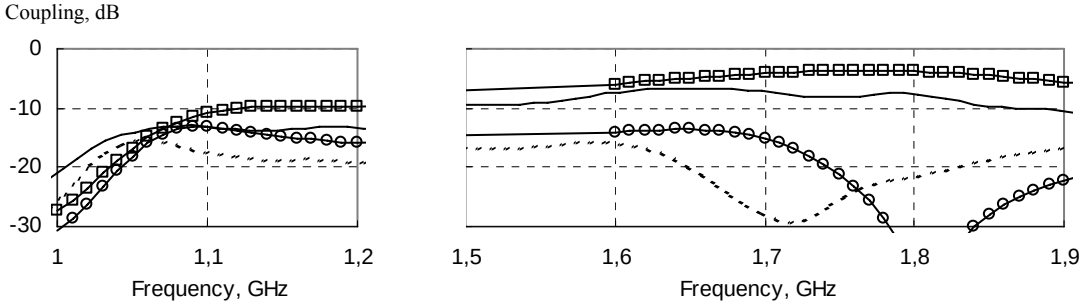

Figure 3. Simulated and measured isolation for the unloaded (□ sim., solid meas.) and LC loaded case (○ sim., dashed meas.).

As seen from Figure 4, the simulated peak efficiency is 53 % at 1.09 GHz and 7 % at 1.78 GHz. Loading with the LC circuit the simulated peak efficiency is 61 % at 1.09 GHz and 33 % at 1.71 GHz. For the unloaded set-up, the measured peak efficiency is 91 % at 1.06 GHz and 70 % at 1.69 GHz. Using the LC circuit, the measured peak efficiency is 78 % at 1.05 GHz and 94 % at 1.61 GHz.

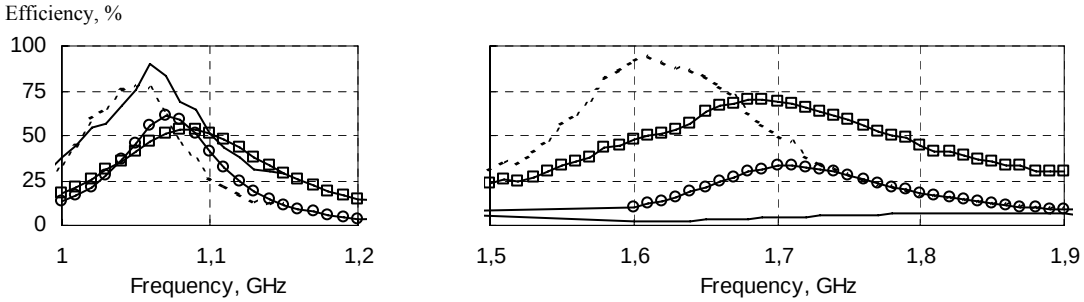

Figure 4. Simulated and measured radiation efficiency for the unloaded (□ sim., solid meas.) and LC loaded case (○ sim., dashed meas.).

In order to compare the results the minimum efficiency obtained over a fixed 50 MHz bandwidth is shown in Table 1. The improvement in the simulated HB efficiency of a factor four is at the expense of a slightly reduced LB efficiency, decreased by 7%. From the measurements the same are observed, however not as significant. The 16.4 % measured efficiency improvement in the high band comes with an 8.3 % decrease in the low band.

Table 1.
Simulated and measured results when adding a LC circuit on the low band antenna.

		Res. Frq., GHz	BW (-6 dB), MHz	Refl. Coeff., dB	Coupling, dB	Eff, %	Eff.(50 MHz BW), %
LB, Simulated		1.10	67 (6.1%)	-9	-9.7	53	47
	LC	1.08	50 (4.6%)	-23	-13	61	44
LB, Measured		1.04	68 (6.5%)	-9.6	-13	90.6	65
	LC	1.04	54 (5.2%)	-25	-16	77.7	60
HB, Simulated		1.77	192 (10.8%)	-12	-3.7	6.7	6.4
	LC	1.70	96 (5.6%)	-17	-13.7	33	25
HB, Measured		1.70	220 (12.9 %)	-12	-6.6	70	61
	LC	1.63	104 (6.4 %)	-26	-21	94	71

The observed deviation between the simulated and the measured results is mainly due to the cable used in the measurements, the simulated ideal assumptions, i.e., loss less and free space, as compared to the Rohacell material used for the prototype. In addition comes the deviation between the actual prototype and the model used in the simulation.

1.4 Conclusion

Measurements have verified that by the use of a lumped resonant LC circuit it is possible to decrease the mutual coupling by 14.4 dB, and thus to increase the radiation efficiency by 16.4 %. The drawback that has to be taken into account is the increased complexity and hence the price of the antenna system.

In the low frequency band, no significant changes occur by adding a LC circuit. It should be noted that the observed improved coupling and peak reflection coefficient do not lead to a higher radiation efficiency. This is due to the insertion loss in the components used for the LC circuit.

By the use of the LC circuit, and hence lower the coupling between the antennas, it is possible to reduce the overall volume necessary for two antennas, since they can be spaced closer and still have a high radiation efficiency. The shown PIFA's are not fully optimised with respect to the occupied volume or resonant frequency. Thus for practical use both the shape of the antenna and the location of the lumped inductor should be carefully chosen in order to get the best frequency bandwidth and efficiency performance for a given application.

1.5 References

1. K. Hirasawa and M. Haneishi, "Analysis, design, and measurement of small and low profile antennas," Artech House, ISBN 0-89006-486-5, 1991.
2. J. Thaysen, "Mutual Coupling Between Two Identical Planar Inverted-F Antennas," Proc. IEEE AP-S, USA, pp. 504-507, June 2002.
3. G. Hall (ed.), "The ARRL antenna book", 15th Edition, Third printing, chap. 7, ISBN 0-87259-206-5, 1990.
4. K.H. Lui, R.D. Murch, "Compact dual-frequency PIFA designs using LC resonators" IEEE Trans. AP, vol. 49, pp. 1016-19, July 2001.
5. "IE3D User's Manual, Release 8," Zeland Software, Inc., Fremont, CA, 2001.
6. Data sheet, www.coilcraft.com, Coilcraft inc., 2003.

Paper VIII

Reduction technique for mobile phone antennas using lumped inductors

Authors

Jesper Thaysen

Nokia Denmark, DK-1790 København, DENMARK
Technical University of Denmark DK-2800 Kgs. Lyngby, DENMARK

Kaj B. Jakobsen

Technical University of Denmark DK-2800 Kgs. Lyngby, DENMARK

Paper published in

Microwave Journal

J. Thaysen and K.B. Jakobsen, "Reduction technique for mobile phone antennas using lumped inductors", *Microwave journal*, 2005.

1 Reduction technique for mobile phone PIFA antennas using lumped inductors

Jesper Thaysen
Nokia Denmark, www.nokia.com, DK-1790 Kbh V, DENMARK
Email: jesper.thaysen@nokia.com

Kaj B. Jakobsen
Technical University of Denmark, www.dtu.dk, DK-2800 Kgs. Lyngby, DENMARK
Email: kbj@oersted.dtu.dk

Size reduction technique of the Planar Inverted-F Antenna (PIFA) is presented. A 18 nH lumped inductor is used in addition to a small 0.3 cm^3 PIFA. The PIFA is located on a dielectric foam 5 mm above a 40 mm × 100 mm ground plane. It is possible to reduce the centre frequency (min. $|S_{11}|$) by 33% for a fixed physical size. The measured –6 dB bandwidth is 6.7% with a peak radiation efficiency of 88%.

1.1 Introduction

The demand for smaller communication devices for personal communication systems has led to a constant search for methods to reduce the cellular phone dimensions. However, the wavelength does not decrease, due to the higher frequency bands used, with the same speed as the size of the mobile phones. Even a quarter wavelength antenna, such as the Planar Inverted-F Antenna (PIFA) tent to become too large, and thus a demand in order to decrease the volume of the antenna exist.

Size reduction can be accomplished, simply by shortening the antenna, however, at lengths shorter than the resonant length, the radiation resistance changes, and the impedance at the terminals of the antenna become reactive as well. The latter can be compensated for by the use of one or more inductors connected in series with the antenna for cancellation of the capacitance, and thus improve the impedance match [1], and hence the efficiency [2]. The idea of using a lumped inductor in conjunction with an antenna has often been used in connection with low frequency antennas where the physical size might be several hundred meters [3], but up to date it has found very little use in mobile telephony [4].

In [3, 4] it is demonstrated that the highest advantage is gained by placing the inductor at the centre of each antenna arm, instead of at the input. Here, the results from our investigations regarding both the location of the inductor as well as the inductance is presented. For many practical applications it is more suitable to place the inductor almost at the input. In this way no inductors is located on the antenna element itself, but rather on the supporting structure or on the ground plane.

In fact, the main objective of this paper is to present the results of numerical and experimental investigations of the size reduction of a PIFA by the use of a lumped inductor. As an intermediate target we aim to reduce the cebtre frequency by 33% for a fixed physical size of the antenna. The antenna performance in terms of the radiation properties, scattering parameters, electrical near-field distribution and current distribution is simulated and verified by measurements [5-8].

The evaluation of the antennas in terms of the electrical field distribution and current distribution on the antenna element as well as on the ground plane has been accomplished using planar near-field measurements [9-12]. Usually the near-field is transformed to far-field data, nevertheless it is the raw unprocessed near-field data that is presented and used in this paper.

1.2 Materials and Methods

The presented antenna configuration consists of a 40 mm long, 1.5 mm wide and 5 mm high PIFA located on a 40 mm × 100 mm ground plane. In all the prototypes, Rohacell material (ε_r=1.06) is used as the supporting structures of the antenna. The antenna is located at the edge and parallel to the 100 mm edge, as illustrated on Figure 1. The feed point is located 5 mm from the edge where a 90-degree bend forms the short to the ground plane. In the cases where the inductor is incorporated on the antenna element, a 0.5 mm wide gap is cut in the antenna arm. In order to determine the optimal setup, with respect to the antenna performance, the location of the inductor is varied. Hence, the cut is moved from almost at the feed point, the 0.5 mm case towards the open end, the 33 mm case.

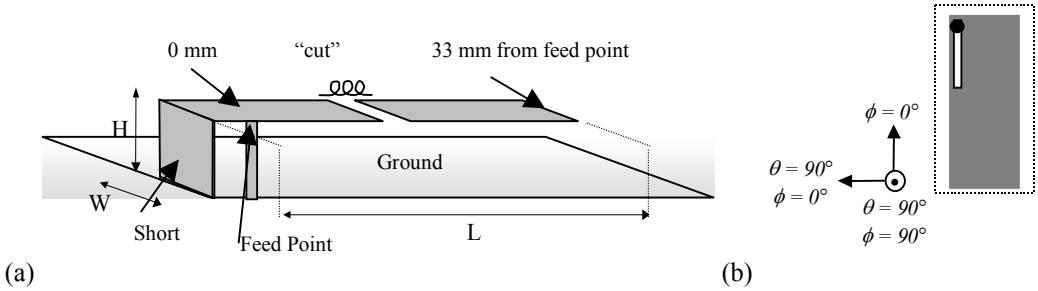

Figure 1. Illustration of the PIFA located above a ground plane, the cut illustrates the location of the lumped inductor(a). Antenna orientation in the spherical coordinate system, the outer dashed frame illustrates the scan area that is mapped on all of the following figures. The dots denote the short pin locations (b).

A planar scanner is used to perform the measurements [7]. The step size is 4 mm leading to a total of 496 measurement points for a 60 mm × 120 mm area. This area covers the ground plane plus an additional 10 mm on each side of the ground plane [9]. A 3-dimensional E-field probe are used for these measurements. The probe are designed for electrical near-field component measurements up to 3 GHz [8]. The measurements are carried out at 1.06 GHz, i.e., the measured centre frequency (min. $|S_{11}|$) of both the 40 mm loaded as well as for the 60 mm unloaded antenna. The measurement facility gives the total amplitude of the electrical fields. These measurements are compared to results obtained from the IE3D computer program used [6].

In the planar scanning technique the probe is moved in a plane situated in front of the antenna and the received signal (amplitude) is recorded. The position of the probe is characterised by the coordinates (x, y, z_0) in the *xyz* coordinate system of the antenna. During the scanning, z_0 is kept constant, while x and y is varied. The field is measured at a distance of z_0 = 3.2 mm, which corresponds to a free space distance of $\lambda_o/90$ equivalent to an electrical length of 4°. It should be noted that the distance between the ground plane and the measurement plane are 8.2 mm ($\lambda_o/35$), since the antenna height is 5 mm.

1.3 The Unloaded PIFA

In order to validate the performance of the loaded antennas, an unloaded prototype having the same dimension has been fabricated (L × W × H) = (40 mm × 1.5 mm × 5 mm). This antenna has a centre frequency, somewhat higher as compared to the loaded antennas. Therefore, a larger unloaded antenna that has the same centre frequency (min. $|S_{11}|$) as the loaded antenna is presented as well (60 mm × 1.5 mm × 5 mm). In this way a more realistic comparison can be made.

The simulated and measured reflection coefficient and radiation efficiency for two unloaded antennas, 40 mm and 60 mm, are shown in Figure 2. For the 60 mm PIFA the simulated centre frequency (min. $|S_{11}|$) is 1.2 GHz. Being 33% lower than the centre frequency (min. $|S_{11}|$) for the 40 mm long PIFA, which is 1.8 GHz.

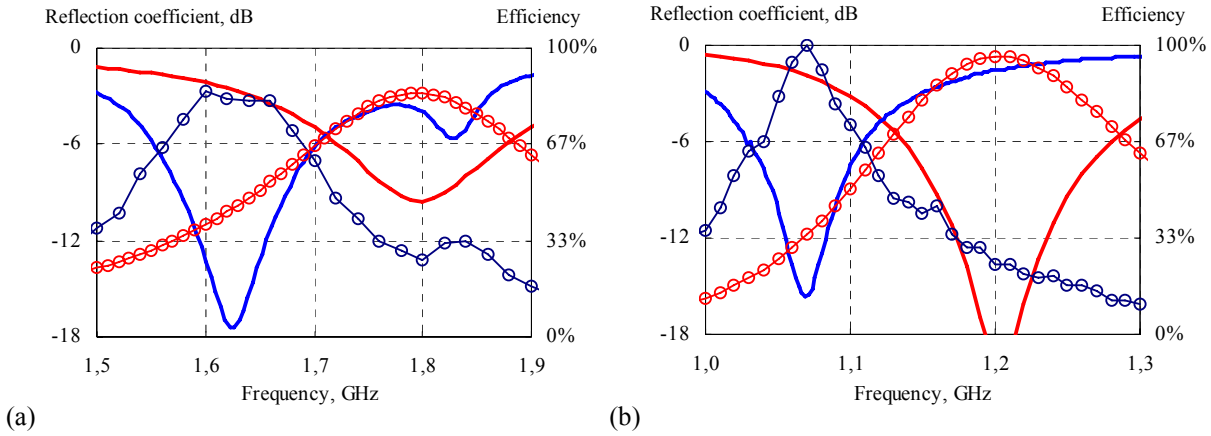

Figure 2. Simulated (red) and measured (blue) reflection coefficient (solid) and radiation efficiency (o) for the unloaded 40 mm (a) and the unloaded 60 mm (b) long PIFA.

For both antennas, the measured frequencies with the lowest reflection coefficient are approximately 10% lower than the simulated results. This difference could be caused by a slightly difference in the simulated model and the prototype. Also the resolution used in the simulation can cause some discrepancy. Here, converged results are obtained using 20 cells per wavelength and edge cells [6].

The measured total electrical field components of the radiation patterns shown in Figure 3 indicate good agreements between the simulated and the measured results. Notice the radiation patterns are obtained at the centre frequency (min. $|S_{11}|$); therefore the simulated patterns are at 1.23 GHz and the measured at 1.06 GHz. The measured maximum gain is 3.9 dBi, being slightly higher than the simulated gain.

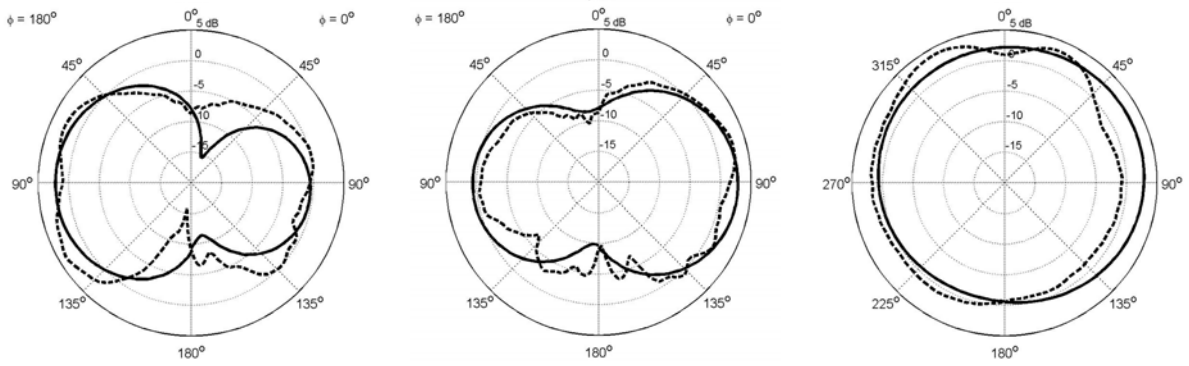

(a) (b) (c)

Figure 3. Simulated (solid) and measured (dashed) total electrical field components of the radiation pattern, θ-cuts for $\phi = 0°$ (a) and for $\phi = 90°$ (b), and ϕ-cut for $\theta = 90°$ (c) for the 60 mm unloaded PIFA. With respect to the orientation as shown in Figure 1 at 1.06 GHz and 1.23 GHz for the measured and simulated results, respectively.

The total electrical near-field distribution at a distance of Z_0 = 3.2 mm above the antenna element are shown in Figure 4. Good agreements in terms of peak amplitude and shape of the electrical near-field distribution between the simulated and the measured results are obtained, however more details could be observed from the simulated result. E.g., when observing just above the radiating element especially at (x, y) = (0, 40-70) a local minima is found and the edge peak radiation is higher above the ground when compared to that obtained at the side of the ground plane. This is also in accordance with the measured radiation pattern shown in Figure 3. In both cases the peak value are associated to the open end of the antenna, i.e., at (x, y) = (0, 40). Also, in both cases a minima is observed at (x, y) = (40, 40), i.e., the opposite edge of the PIFA.

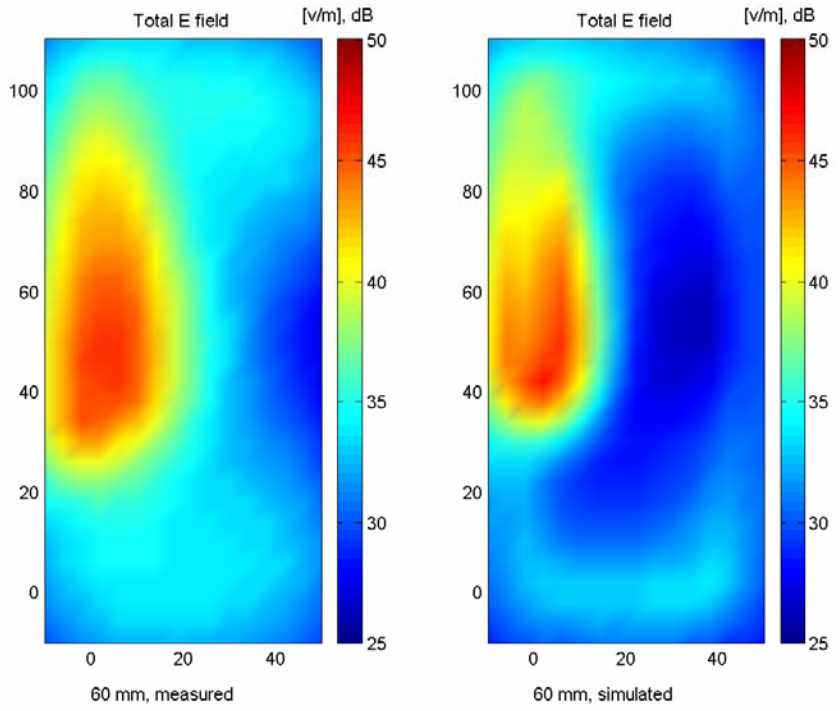

Figure 4. Measured (left) and simulated total electrical near-field distribution for the 60 mm long unloaded PIFA at 1.06 GHz.

In order to reduce the centre frequency (min. $|S_{11}|$) from 1.8 GHz as for the 40 mm long PIFA to 1.2 GHz either an inductor or a capacitor can be used. This frequency reduction corresponds to a size reduction of 33%, i.e., from 60 mm to 40 mm.

1.4 The inductor loaded PIFA

Two different test are made, first, for a fixed location of the inductor, the inductance is varied between 5 nH and 100 nH. Hereafter, the optimal location is found for a fixed inductance value.

Numerical results

Locating an inductor 10 mm from the feed point forms the inductor loading, see illustration in Figure 1. For this fixed location the simulation results for varying the inductor value between 5 nH and 100 nH is shown in Figure 5. Here the centre frequency (min. $|S_{11}|$) and the bandwidth are plotted with respect to the 40 mm unloaded case. The centre frequency (min. $|S_{11}|$) drops from 1.8 GHz, towards 0.87 GHz for inductor values above 70 nH. However, for values above 35 nH the bandwidth is lower than the unloaded. This motivates for choosing an inductor value below 35 nH. Using 5 nH, the bandwidth is 2.3 times the bandwidth for the unloaded PIFA, this is due to the improved impedance match. Between 5 nH and 35 nH, the optimal inductor value is a trade-off between the decrease in centre frequency (min. $|S_{11}|$) and the actual bandwidth. As a compromise, 20 nH is chosen for the rest of the work. Here, the centre frequency (min. $|S_{11}|$) is lowered 30%, and the bandwidth is almost twice the bandwidth obtained for the unloaded 40 mm case.

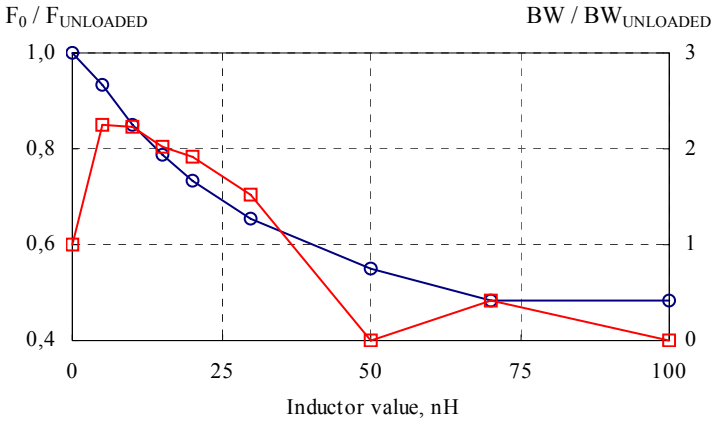

Figure 5. Centre frequency (min. $|S_{11}|$) (blue) and bandwidth (red) as a function of inductance variations for a fixed location on the PIFA.

For a fixed inductance of 20 nH, various locations of the inductor have been simulated, spanning from almost at the feed point (0.5 mm) toward the open end (33 mm). The simulated centre frequency (min. $|S_{11}|$) and relative bandwidth as a function of the location of the inductor, i.e., the distance from the feed point to the inductor, is shown in Figure 6. The lowest reflection coefficient and the peak efficiency as a function of the inductor location are shown in Figure 7.

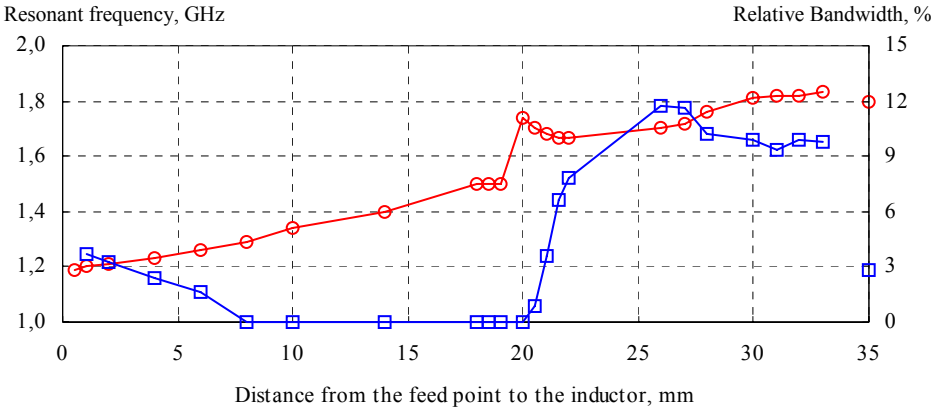

Figure 6. Simulated centre frequency (min. $|S_{11}|$) (red) and relative bandwidth (blue) versus the inductor location.

The centre frequency (min. $|S_{11}|$) increases almost linear from 1.2 to 1.8 GHz, when the inductor is moved towards the open-end, from a position at 0.5 mm to 33 mm from the feed point. Starting with a 45 MHz or 4% bandwidth at 1.2 GHz (0.5 mm) the bandwidth drops due to mismatch, for locations in the range from 8-20 mm, hence no –6 dB bandwidth occurs. The maximum bandwidth of 11.8% is obtained at 26 mm, and stabilises around 10% when the inductor is located at positions near the open end of the antenna (30 mm to 33 mm).

The peak efficiency starts at 75% and ends at 60% close to the feed point (0.5 mm) and the open end (33 mm), respectively. At locations below 5 mm the efficiency is higher than 75%. Above 5 mm a decrease in the efficiency is observed, and the efficiency is below 50% from 10 mm to 30 mm. Above 31 mm the reflection coefficient is –11 dB and the efficiency exceeds 50%, and reaches a peak of 60% at 33 mm. In between the efficiency has dropped to 17% at the 21 mm location.

The lowest reflection coefficient changes from –9 dB to –1.5 dB when the distance from the fed point to the inductor increases from 0.5 mm and 20 mm. From 21 mm to 26 mm the reflection coefficient peaks at –30 dB, ending at –11 dB for locations above 30 mm.

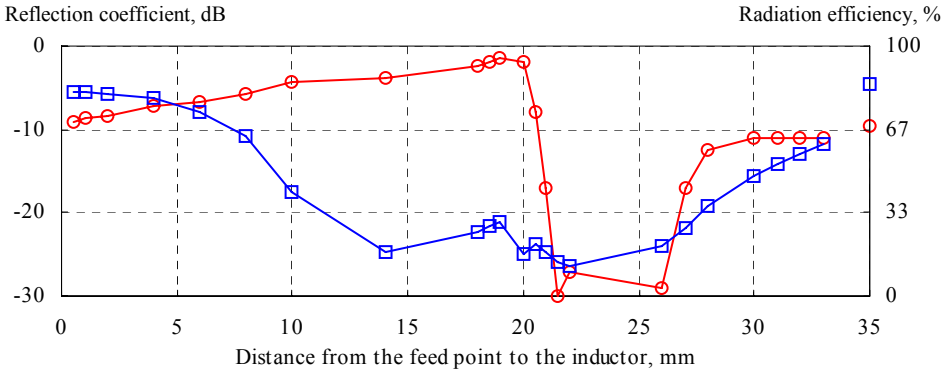

Figure 7. Simulated reflection coefficient (red) and radiation efficiency (blue) versus the inductor location.

Experimental results

Based on the results from the parameter study, a prototype has been measured with respect to radiation efficiency and reflection coefficient. A lumped 18 nH inductor is used in the measurements [13]. The inductor has an inductance of nearly 20 nH in the frequency range of interest. The results, that is compared to the unloaded 60 mm long PIFA, are shown in Figure 8.

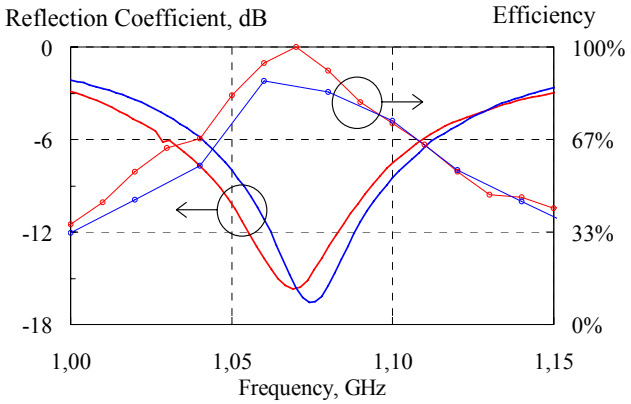

Figure 8. Measured reflection coefficient (solid) and radiation efficiency (o) versus frequency for the 60 mm unloaded (red) and for the 40 mm loaded with an 18 nH inductor located close to the feed point (blue).

For the PIFA without any inductor the centre frequency (min. $|S_{11}|$) is 1.06 GHz having a peak return loss of 16.5 dB. The bandwidth is 7.3% (78 MHz). The measured efficiency is above 65% within this frequency range of interest, having a peak efficiency of 85%. By loading this antenna with an 18 nH inductor soldered at the gab, just 0.5 mm from the feed point, the centre frequency (min. $|S_{11}|$) is 1.07 GHz, having a bandwidth of 6.7% (71 MHz)). The peak efficiency is 88%.

The total electrical field components of the radiation patterns shown in Figure 12 indicate almost omni-directional properties for the 40 mm long inductor loaded PIFA. Good resemblance between the simulation and measurement results. The measured maximum gain is 3.3 dBi, being slightly higher than the simulated gain.

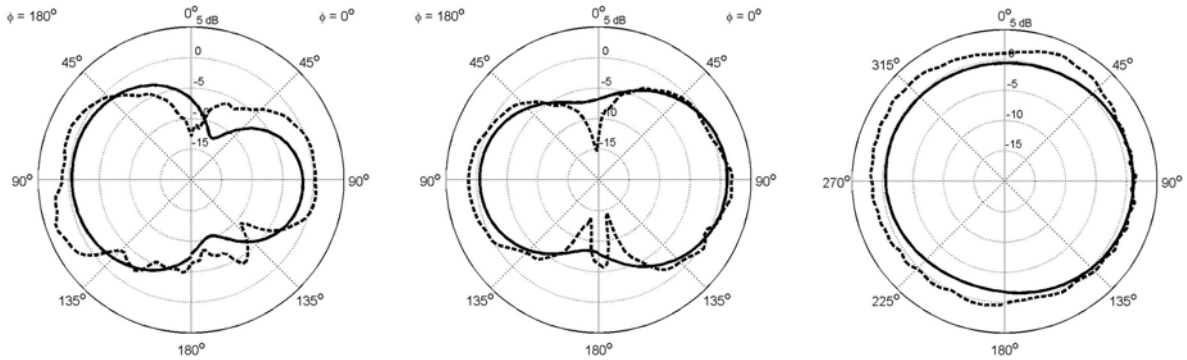

(a) (b) (c)

Figure 9. Simulated (solid) and measured (dashed) total electrical field components of the radiation pattern, θ-cuts for $\phi = 0°$ (a) and for $\phi = 90°$ (b), and ϕ-cut for $\theta = 90°$ (c) for 40 mm inductor loaded PIFA. With respect to the orientation as shown in Figure 1 at 1.06 and 1.23 GHz for the measured and simulated results, respectively.

For the 40 mm long 18 nH inductor loaded case, the measured total electrical field distribution is compared with the 60 mm unloaded (see discussion in addition to Figure 4) in Figure 10. It indicates higher amplitude above the inductor-loaded antenna as compared to the 60 mm case. This originates from the higher current distribution, that inevitable is present, and thus higher radiation from this area.

In the lower half of the pictures, the electrical field distribution behaves identical, however with slightly higher values for the 60 mm case. Also the null, that appears at the opposite side (x, y) = (40, 50) of the PIFA in the 60 mm case could be found in the 40 mm case.

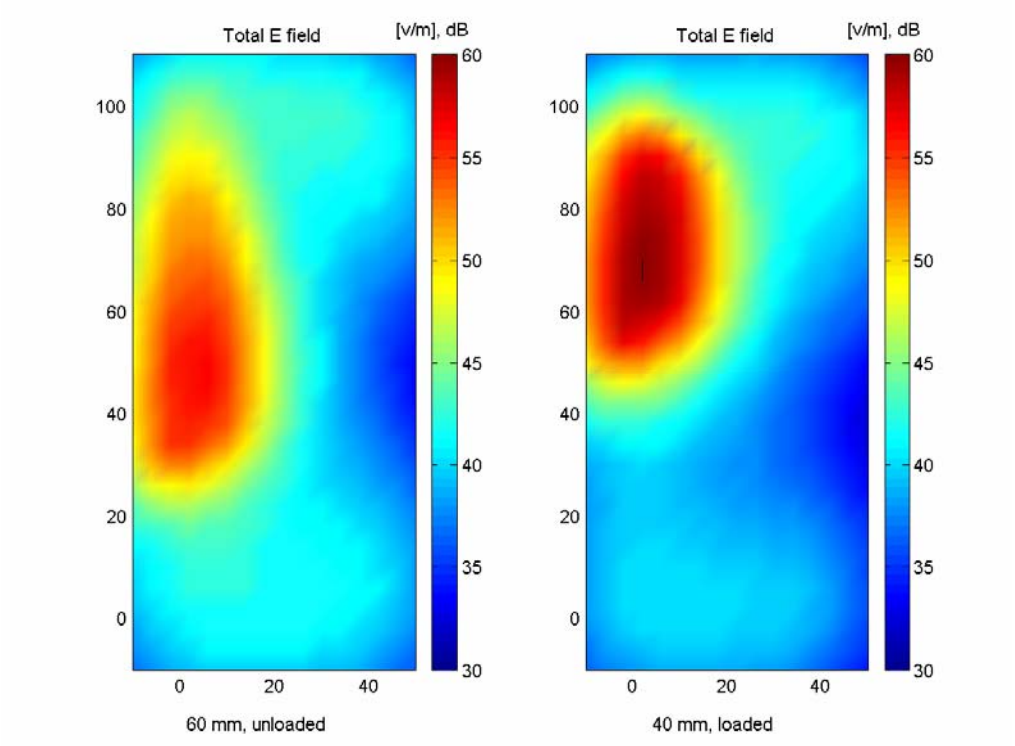

Figure 10. Measured current distribution for the inductor loaded versus unloaded PIFA

The PIFA is basically an inverted-L antenna, that actually comes from a monopole with a bend such that most of the arm is parallel to the ground plane. This means that the feed point is moved by a certain distance from the ground, here 5 mm from the bend and an additional 5 mm due to the antenna height. Meaning that the optimum location of the inductor is between 10.5 mm and 15 mm from the ground connection, i.e., almost one third the total length of 45 mm (length + height). Collin [4] argues that the optimum location of an inductor is at the centre of the arm of the monopole; of course we cannot compare that directly to the PIFA. Nevertheless, this actually holds for the impedance match. If the inductor is located between 21 and 26 mm a rather good simulated impedance match is observed, below –25 dB, in this case the decrease in the frequency, with the lowest reflection coefficient, is not overwhelming, a reduction from 1.8 GHz to 1.7 GHz, only. Moreover the radiation efficiency is below 25%. This could indicate that the optimum location for an inductor in the PIFA is closer to the feed point.

Above 21 mm no significant frequency reduction is obtained, however at 30 mm the bandwidth is 200 MHz (13%), which is higher than the case of no inductor (50 MHz or 3%).

Thus, the higher bandwidth is at the expense of an inductor in terms of reduced efficiency and the cost of the inductor.

1.5 Conclusion

A small 0.3 cm^3 PIFA located on a dielectric foam 5 mm above a 40 mm × 100 mm ground plane is investigated. Adding an inductor on the arm of the PIFA improves the performances for the shown PIFA. The best case with respect to centre frequency (min. $|S_{11}|$) reduction are obtained when an 18 nH lumped inductor is placed within the first few millimetres from the feed point, here the measured frequency point with the lowest reflection coefficient is decreased by 33% from 1.60 to 1.06 GHz, the reflection coefficient is –16.5 dB, the measured –6 dB bandwidth is 6.7% and the radiation peak efficiency is 88%.

When comparing the 40 mm inductor loaded antenna with the 60 mm unloaded antenna, the major benefit are the reduced size for a fixed centre frequency (min. $|S_{11}|$), however it is at expense of reduced efficiency and reduced bandwidth.

By the use of inductor loading it is shown that for a fixed size the centre frequency (min. $|S_{11}|$) can be decreased. The principle could also be used for a fixed frequency and hence a 30% to 40% size reduction is expected.

The shown PIFA are not fully optimised with respect to the occupied volume or frequency, nor is any other components or any cover included. Thus for practical use both the shape of the antenna and the shape of the distributed capacitor should be carefully chosen in order to get the best frequency bandwidth and efficiency performance for a given application.

1.6 Acknowledgements

This work has been supported by Nokia Denmark.

1.7 References

1. C. W. Harrington, " Monopole with Inductive Loading", *IEEE Trans. Antennas Propagation*, pp.394–400, Jul 1963.
2. G. S. Smith, "Efficiency of electrically small antennas combined with matching networks," *IEEE Trans. Antennas Propagation*, vol. AP-25, pp. 369–373, May 1977.
3. G. Hall (ed.), "The ARRL antenna book", 15th Edition, Third printing, Chap. 7, ISBN 0-87259-206-5, 1990.
4. R. E. Collin, "Antennas and radiowave propagation", McGraw-Hill, ISBN 0-07-011808-6, pp. 97-104, 1985.
5. www.satimo.com.
6. www.zeland.com.
7. www.semcad.com
8. www.speag.com
9. J. Appel-Hansen, "Antenna measurements," Ch. 8 in A.W. Rudge (Ed.) "The handbook of antenna design", *Peter Pelegrinus Ltd*, 1982.
10. R.C. Baird, A.C. Newell, and C.F. Stubenrauch, "A brief History of near-field measurements of antennas at the national bureau of standards," *IEEE Trans. Antennas Propagation*, vol. 36, no 6, 1988.

11. Y. Gau and I. Wolff, "A new miniature magnetic field probe for measuring three-dimensional fields in planar high-frequency circuits," *IEEE Trans. Microwave Theory and Techniques*, vol. 44, pp. 911-918, 1996.
12. Y. Gau and I. Wolff, "Miniature electric near-field probe for measuring 3-D fields in planar microwave circuits," *IEEE Trans. Microwave theory and Techniques*, vol. 46, pp. 907-913, 1998.
13. www.coilcraft.com.

Paper IX

Mobile phone antenna reduction techniques by capacitive top loading

Authors

Jesper Thaysen

Nokia Denmark, DK-1790 København, DENMARK
Technical University of Denmark DK-2800 Kgs. Lyngby, DENMARK

Kaj B. Jakobsen

Technical University of Denmark DK-2800 Kgs. Lyngby, DENMARK

Paper in press

Microwaves and RF

J. Thaysen and K.B. Jakobsen, "Mobile phone antenna reduction techniques by capacitive top loading", *Microwaves and RF,* 2005.

1 Mobile phone PIFA antenna size reduction using capacitive top loading

Jesper Thaysen
Nokia Denmark, www.nokia.com, DK-1790 Kbh V, DENMARK
Email: jesper.thaysen@nokia.com

Kaj B. Jakobsen

Technical University of Denmark, www.dtu.dk, DK-2800 Kgs. Lyngby, DENMARK
Email: kbj@oersted.dtu.dk

Size reduction technique of the Planar Inverted-F Antenna (PIFA) is presented. A measured 39% reduction in the centre frequency (min. $|S_{11}|$) from 1.8 GHz to 1.2 GHz is accomplished by top loading using a 1.1 pF distributed capacitor. The simulated –6 dB bandwidth is 9% with a peak radiation efficiency of 90%.

1.1 Introduction

Minimisation of the antenna is an essential part in reducing the size of a mobile phone. Several methods to reduce the antenna size exist. However, all are at the expense of lower antenna gain and bandwidth [1]. This follows from the fact that an antenna is used to transform a bounded wave into a radiated wave [3]. An antenna performs this transformation, however, only with a poor efficiency when it is much smaller than the wavelength [4]. The loss in antenna gain can to some extent be compensated for by amplification. This is obviously not the case for the bandwidth. If the impedance match is much better than required, broad-banding techniques could be used to increase the bandwidth [5]. For a given cellular configuration, the design of the antenna should be done in order to use the total volume available [6-7]. There exist an upper theoretically limit that are never reached, and for a fixed volume the design of small antennas is thus a trade off between bandwidth and the gain for the antenna chosen to the given application [2, 8].

A method of reducing the size is simply by shortening the antenna. However, this affects the impedance at the terminals of the antenna such that the radiation resistance becomes reactive as well. This can be compensated for by the use of capacitive top loading. In practice means replacing the missing height by some sort of electrical circuit that has the same electrical characteristic as the missing part of the antenna [2]. Practically, this improves the impedance match [9] and the efficiency [10]. The idea of using a capacitor in conjunction with an antenna has often been used in connection with low frequency antennas where the physical size might be several hundred meters [2], but up to date it has found very little use in mobile telephony [11].

Collin [11] discusses the idea in connection to monopoles and dipoles, but here the use of top loading by a capacitor is adapted to the PIFA. For many practical applications a lumped capacitor as well as a distributed capacitor could be used for top loading the antenna. Here, it is more suitable to use a distributed plate capacitor where the open end of the PIFA forms one of the plates.

The main objective of this paper is to present the results of numerical and experimental investigations of the size reduction of a PIFA by the use of a top loaded distributed capacitor. As an intermediate target we aim to reduce the centre frequency by 33% for a fixed physical size of the antenna. The antenna performance in terms of the radiation properties, scattering parameters, electrical near-field distribution and current distribution is simulated and verified by measurements [12, 13]. The results are also compared to an inductor loaded PIFA with the same size and a PIFA that is 60 mm long.

1.2 Materials and Methods

The presented antenna configuration consists of a 40 mm long, 1.5 mm wide and 5 mm high PIFA located on a 40 mm × 100 mm ground plane. In all the prototypes, Rohacell material (ε_r=1.06) is used as the supporting structures of the antenna. The antenna is located at the edge and parallel to the 100 mm edge, as illustrated on Figure 1. The feed point is located 5 mm from the edge where a 90-degree bend forms the short to the ground plane. A 1.5 mm wide piece of copper tape with different length is added in between the open end of the PIFA and the ground plane. The distance, *d*, between the two plates in the capacitor, i.e., the open end of the PIFA and the copper tape is illustrated in Figure 1. The copper tape makes up the lower plate of the capacitor; the upper is the PIFA.

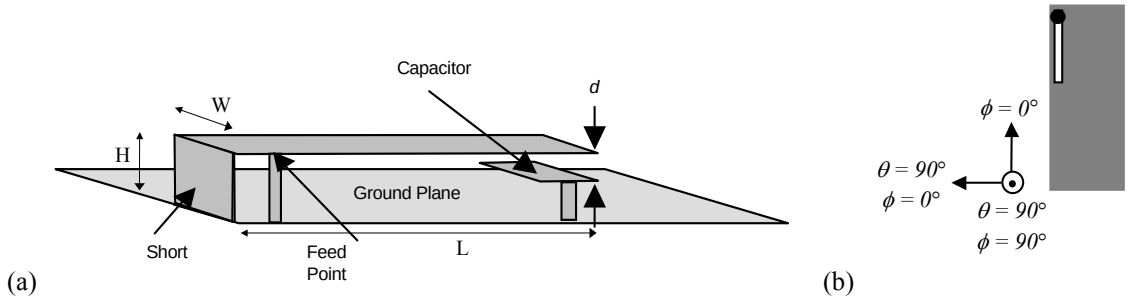

Figure 1. Illustration of the capacitor loaded PIFA located above a ground plane. The open end of the PIFA together with the plate that forms the distributed capacitor (a). Illustration of the antenna model, the dot denotes the short pin locations (b).

A 40 mm long unloaded PIFA's has a centre frequency, somewhat higher as compared to the loaded antennas. Therefore, a larger unloaded antenna that has the same centre frequency (min. $|S_{11}|$) as the loaded antenna is presented as well (60 mm × 1.5 mm × 5 mm). In this way a more realistic comparison can be made.

For the 60 mm PIFA the simulated centre frequency (min. $|S_{11}|$) is 1.2 GHz. Being 33% lower than the centre frequency (min. $|S_{11}|$) for the 40 mm long PIFA, which is 1.8 GHz. For both antennas, the measured frequencies with the lowest reflection coefficient are approximately 10% lower than the simulated results. This difference could be caused by a slightly difference in the simulated model and the prototype. Also the resolution used in the simulation can cause some discrepancy. Here, converged results are obtained using 20 cells per wavelength and edge cells [13].

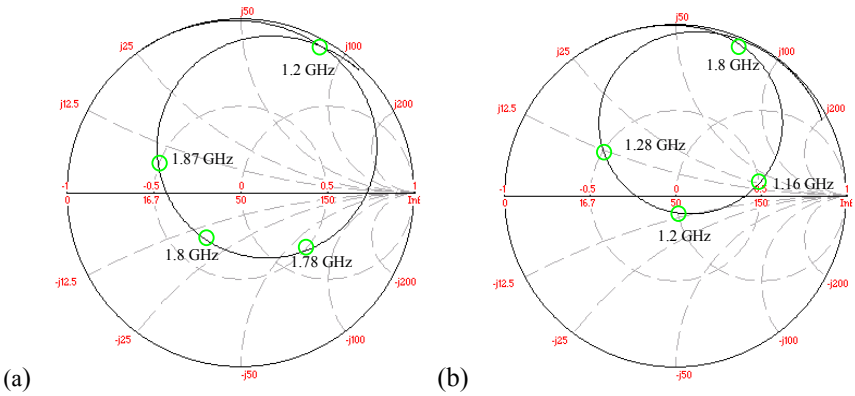

(a) (b)

Figure 2. Smith charts are illustrates the impedance of the unloaded 40 mm PIFA (a), and 60 mm PIFA (b).

The impedance curves for the 40 mm antenna that is illustrated on the smith charts in Figure 2 indicate the location of the centre frequency (min. $|S_{11}|$) (1.8 GHz), the points of which the return loss is 6 dB (1.78 GHz and 1.87 GHz), and also the centre frequency of the other antenna (1.2 GHz). Vice versa for the 60 mm antenna. In the 40 mm PIFA case, it is the 1.2 GHz point that must be shifted towards the 1.8 GHz point by proper loading of the antenna.

The reduction of the centre frequency (min. $|S_{11}|$) from 1.8 GHz as for the 40 mm long PIFA to 1.2 GHz is accomplished by the capacitor. This frequency reduction corresponds to a size reduction on 33% from 60 mm to 40 mm.

1.3 Results and Discussion

Two different simulation tests are carried out, in both cases the plate capacitor loading principle are utilized. First, with a fixed plate area of 4.0 mm × 1.5 mm the plate distance, d, is varied from 0.05 to 0.60 mm. Hereafter the distance is fixed at d = 0.1 mm and the area are chanced from 0.8 mm to 9.0 mm.

The areas, A of the two plates together with the plate distance, d gives the capacitances shown in Table 2 sorted with ascending capacitances. The capacitance is calculated as

$$C = \frac{A\varepsilon_0\varepsilon_r}{d}, \tag{1}$$

where ε_0 is the free space permittivity, $8.8542 \cdot 10^{-12}$ F/m . Even though that sticky tape is used as the spacer in the prototype the relative permittivity ε_r is set to one. This means the measurement values are somewhat higher than the simulation values. In this way overlapping capacitance values in the range from 0.13 pF to 2.13 pF are used. Prototypes have been fabricated with plate area and separation covering the simulated range.

Table 1.
The simulated and measured scenarios along with the associated capacitances.

	Area of each plate, mm × mm	Distance, mm	Capacitance, pF
Simulated	0.8 (0.5×1.5)	0.10	0.13
	6.0 (4.0×1.5)	0.60	0.18
	1.5 (1.0×1.5)	0.10	0.27
	6.0 (4.0×1.5)	0.10	0.27
	2.3 (1.5×1.5)	0.40	0.40
	6.0 (4.0×1.5)	0.15	0.71
	4.5 (3.0×1.5)	0.10	0.80
	6.0 (4.0×1.5)	0.10	1.06
	7.5 (5.0×1.5)	0.10	1.33
	9.0 (6.0×1.5)	0.10	1.59
	6.0 (4.0×1.5)	0.05	2.13
Measured	6.0 (4.0×1.5)	0.43	0.25
	9.0 (6.0×1.5)	0.58	0.28
	6.0 (4.0×1.5)	0.29	0.37
	6.0 (4.0×1.5)	0.14	0.74
	2.3 (1.5×1.5)	0.05	0.83
	6.0 (4.0×1.5)	0.10	1.11
	6.0 (4.0×1.5)	0.05	2.21

The simulated results for varying the plate capacitance, as described in Table 1, are shown in Figure 3 and 4,with a solid line, the measured results with crosses. Linear trend lines are added for easier visualisation of the behaviour of the results as a function of the capacitance.

The simulated centre frequency (min. $|S_{11}|$) decreases almost linearly from 1.8 GHz to 0.8 GHz for capacitances below 1.5 pF. The experimental results follow the same trend, at lower values, though. The simulated bandwidths are almost constant 120 MHz (9%) when adding a capacitor that is smaller than 1.1 pF. Above 1.1 pF the impedance match reduces to above –6 dB, hence no –6dB bandwidth are observed. The 2.1 pF case deviates from the remaining, since a –10 dB impedance match is obtained; the bandwidth is 7% (80 MHz). Also, the radiation efficiency is higher for this value compared to the 1.6 pF case. Again the measured results has lower values, due to the poor impedance match, i.e., between –8 dB and –2 dB for the unloaded and the 2.2 pF case.

The simulated and measured radiation efficiency is almost constant 80% for capacitances below 1.1 pF followed by a decrease for higher capacitances. The bandwidth in which the radiation efficiency are above 50% are shown, illustrating more or less the same trends, i.e., rather constant (a slight decrease) below 1.1 pF and rapidly decreasing above 1.1 pF.

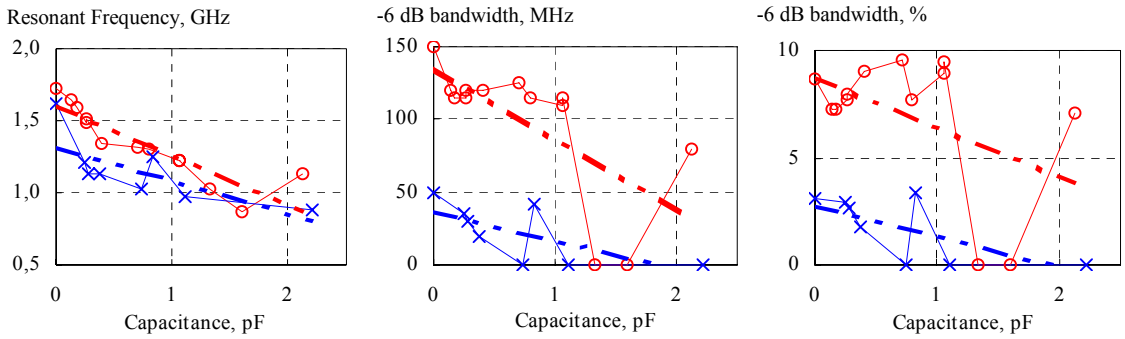

Figure 3. Simulated (red) and measured (blue) for the centre frequency (min. $|S_{11}|$) (a), the –6 dB bandwidth (b), the relative bandwidth (c). Trend lines (dash-dot-dot).

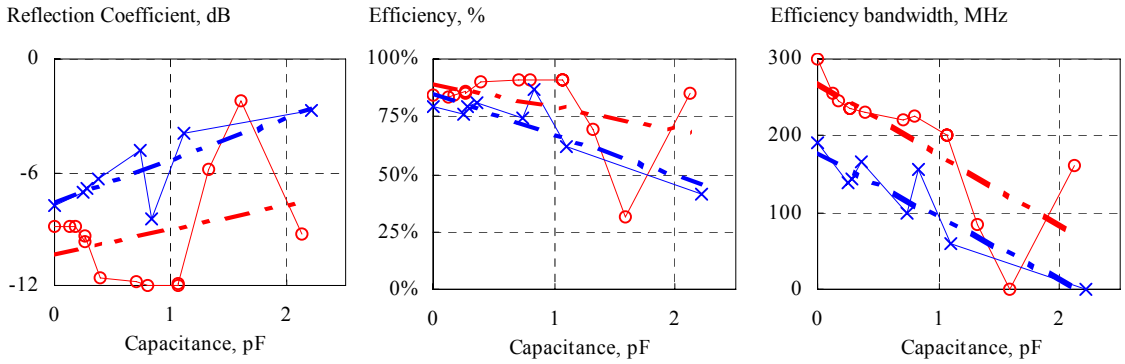

Figure 4. Simulated (red) and measured (blue) for the peak reflection coefficient, the peak radiation efficiency, and the bandwidth in which the radiation efficiency is higher than 50%. Trend lines (dash-dot-dot).

It is possible to improve the PIFA performance by adding a plate capacitor at the open end of the PIFA. Generally speaking, the results could be divided into to groups, the first for capacitances of values below 1.1 pF, secondly above 1.1 pF. In all six subfigures (in Figure 3 and 4) the added trend lines are almost parallel and hence illustrate that the experimental results perform as expected from the simulated results.

Below 1.1 pF, the results are continuous and the best case with respect to centre frequency (min. $|S_{11}|$) reduction and unchanged bandwidth and efficiency are obtained for a capacitance of approximately 1.1 pF. Here the simulated centre frequency (min. $|S_{11}|$) is decreased by 32% from 1.80 GHz to 1.22 GHz, the reflection coefficient is –12 dB, the bandwidth is 9% and the radiation peak efficiency is 91%. Measurements has verified the trends, however at somewhat lower values, most likely due to loss in the plate capacitor. Above 1.1 pF, the simulated as well as the measured results shows rather decreasing performance in terms of poor impedance match, hence lower bandwidth and lower radiation efficiency. Therefore, capacitances below 1.1 pF should be used, in the following the prototype that is loaded with a capacitance of 1.11 pF is investigated further.

The 40 mm capacitor loaded PIFA vs. the 40 mm unloaded PIFA

The simulated centre frequency (min. $|S_{11}|$) of the PIFA without a capacitor is 1.80 GHz, but it decreases to 1.22 GHz when a 1.06 pF plate capacitor is added. The unloaded configuration yield a peak efficiency of 91%, which is 6.5 percent point higher when compared to the

configuration with case 1.06 pF plate capacitor. For the prototype, the measured centre frequency (min. $|S_{11}|$) for the PIFA without any capacitor is 1.63 GHz, and 0.99 GHz with a 4.0 mm × 1.5 mm plate that is separated 0.1 mm. This corresponds to an added capacitance of 1.11 pF. Also shown in Figure 5 is the measured radiation efficiency. The peak efficiency decreases from 83% to 62% when the capacitor is added.

The deviation between the simulated and measured centre frequencies is mainly due to the cable used in the measurements, the simulated ideal assumptions, i.e., loss less and free space, as compared to the Rohacell material used for the prototype, and the deviation between the actual prototype and the model used in the simulation. The relative decrease in centre frequency (min. $|S_{11}|$) is approximately 39% for the experimental results and 32% in the simulated result. The reason for this deviation, and the lowered radiation efficiency, comes from the slightly higher value of the capacitance, and the fact that sticky tape is used as the spacer in the prototype. The loss and the relative permittivity of the tape are not taken into account in the calculation of the capacitance nor in the simulation where the space in between the plate is loss less and free space.

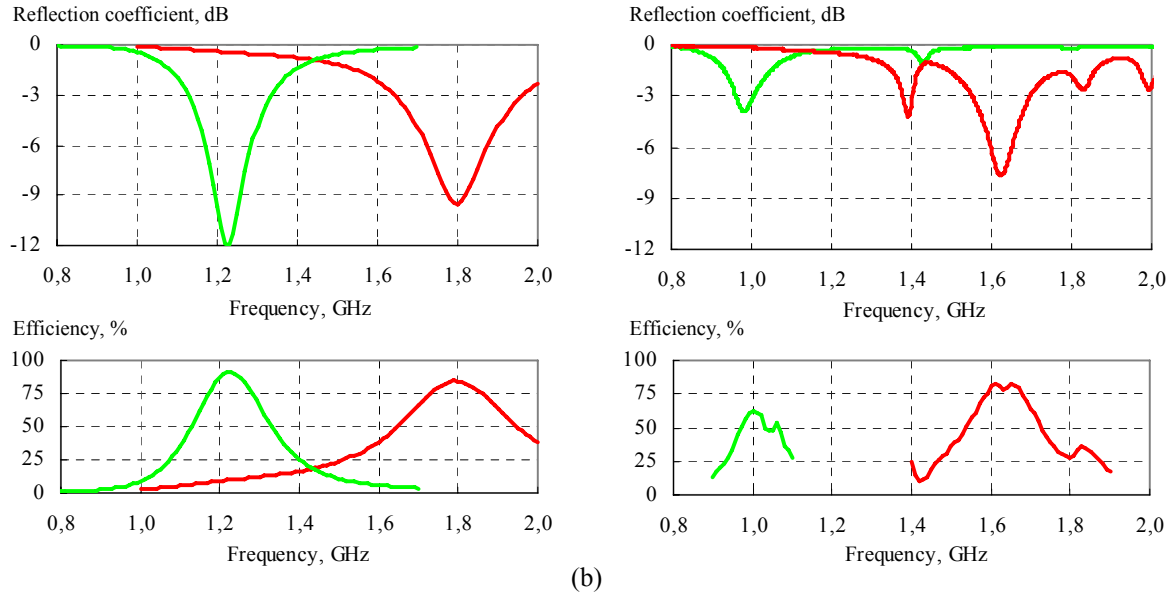

Figure 5. Simulated (a) and measured (b) reflection coefficient and radiation efficiency for the unloaded (red) and top loaded (green) cases.

The total electrical field components of the radiation patterns shown in Figure 6 indicate almost omni-directional properties for the 40 mm long top loaded PIFA. Good resemblances between the simulation and measurement results are obtained. The measured maximum gain is 2.1 dBi, being slightly lower than the simulated gain.

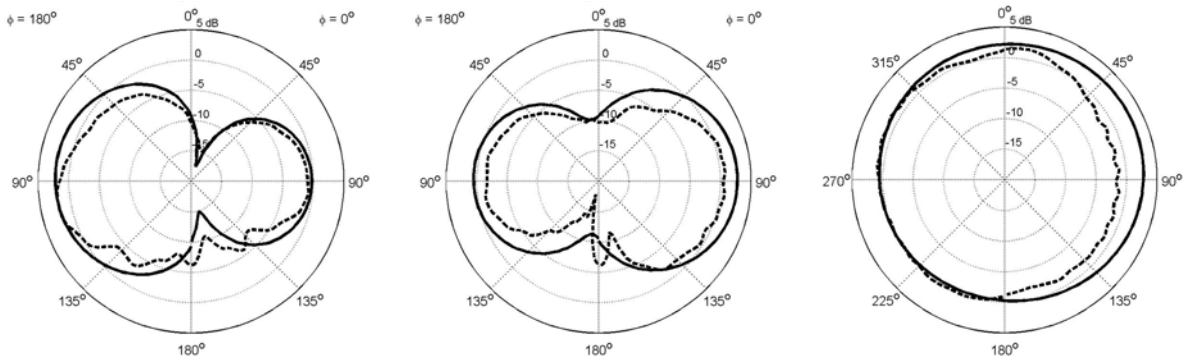

(a) (b) (c)

Figure 6. Simulated (solid) and measured (dashed) total electrical field components of the radiation pattern, θ-cuts for $\phi = 0°$ (a) and for $\phi = 90°$ (b), and ϕ-cut for $\theta = 90°$ (c) for the 40 mm long capacitor loaded PIFA. With respect to the orientation as shown in Figure 1 at 1.06 and 1.23 GHz for the measured and simulated results, respectively.

The simulated current distribution shown in Figure 7 illustrates the capacitive top loading principle. For both antennas, i.e., the unloaded 60 mm and the capacitive loaded 40 mm PIFA, the current density is highest near the feed point, and zero at the open end. The effect on the plate capacitor that is located at the open end is clearly visible in Figure 8. The ripple that is associated with the decrease of the current density as a function of the position on the antenna arm, is due to the model definition in IE3D, in practice it will be a continuously decreasing behaviour. The two curves are parallel until a location on the PIFA arm of 34 mm, which corresponds to the point where the plates are overlapping. Here, a discontinuity occurs and the current decreases to zero much faster than the unloaded 60 mm PIFA. Hence, using the top-loading principle one could remove fractions of the antenna arm. Here, the capacitor replaces the last 20 mm on the 60 mm PIFA for a fixed centre frequency.

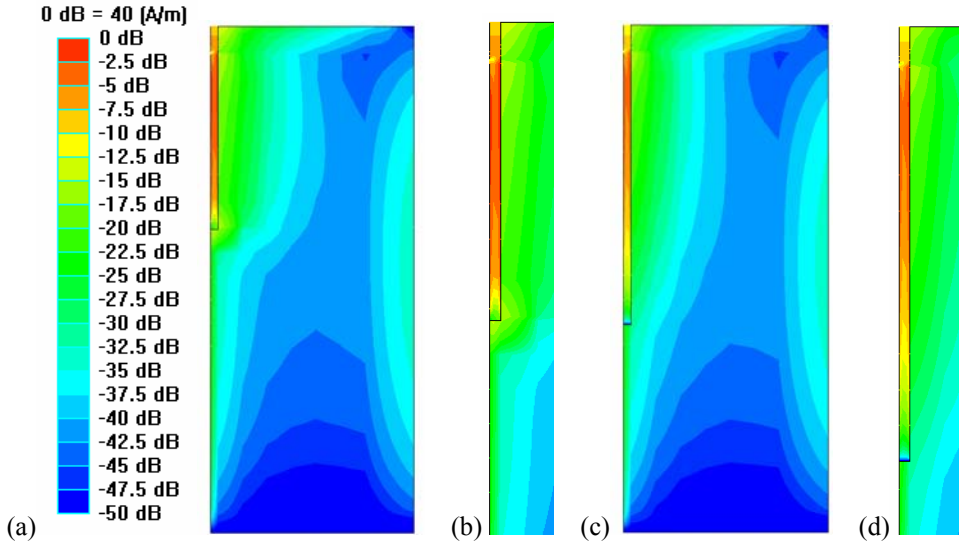

(a) (b) (c) (d)

Figure 7. Simulated current distribution for the 40 mm capacitor loaded (a), close up picture of the radiating element (b) versus the 60 mm unloaded PIFA (c) and close up picture of the radiating element (d).

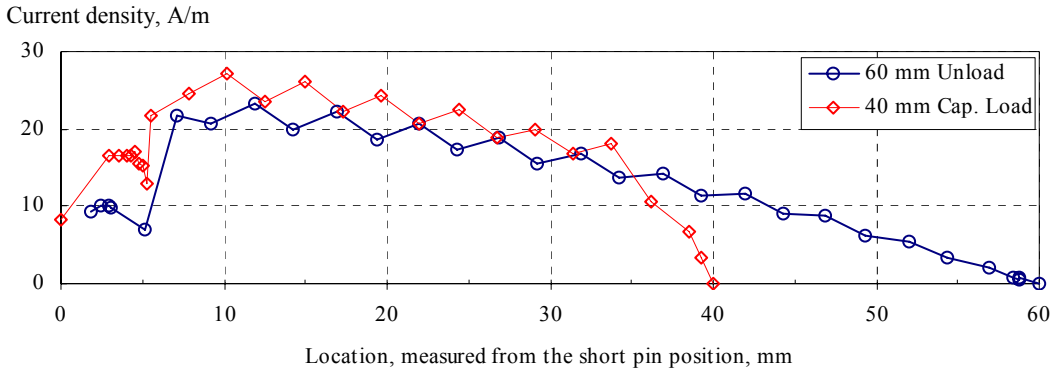

Figure 8. The average current distribution as a function of the location on the antenna arm.

The key results from the capacitor-loaded antenna could be compared in Table 2 with the 60 mm long unloaded antenna, and also with a 40 mm long inductor loaded antenna [15].

Table 2. Major specifications of the different antennas

Principle	Unloaded PIFA 60 mm long	Top loaded with a capacitor	Inductor loaded near feed point
Centre frequency (min. $\|S_{11}\|$)	1.20 GHz, sim. 1.07 GHz, meas.	1.22 GHz, sim. 0.99 GHz, meas.	1.20 GHz, sim. 1.08 GHz, meas.
Loading value		1.1 pF	18 nH
PIFA element lenght	60 mm	40 mm	40 mm
Efficiency, within BW where S_{11}>-6 dB, meas.	>55%	>65%	>65%
Size ground plane	40 mm × 100 mm	40 mm × 100 mm	40 mm × 100 mm
BW S_{11}>-6 dB	7.3% (78 MHz), meas. 9% (150 MHz), sim.	÷, meas. 9% (110 MHz), sim.	6.7% (71 MHz), meas. 3.9 % (45 MHz), sim.
Radiation Pattern	Omnidirectional	Omnidirectional	Omnidirectional
Max gain	3.9 dBi	2.1 dBi	3.3 dBi
Size or centre frequency reduction, as compared to the unloaded 40 mm long PIFA		32%, sim. 39%, meas.	33%, sim. 34%, meas.

Comparing the 60 mm long unloaded PIFA with the two 40 mm long loaded antennas, it could be seen that the advantages by reducing the size is a trade-off to the decreased bandwidth. A 18 nH inductor yields the same frequency reduction as the 1.1 pF capacitor, however with a higher gain. This might be due to sticky tape used as a separator in the capacitor.

1.4 Conclusion

A small 0.3 cm^3 PIFA located on a dielectric foam 5 mm above a 40 mm × 100 mm ground plane is investigated. When comparing the 40 mm top loaded antenna with the 60 mm unloaded antenna, the major benefit are the reduced size for a fixed centre frequency (min. $|S_{11}|$), however it is at expense of reduced efficiency and reduced bandwidth.

A measured 39% reduction of the centre frequency (min. $|S_{11}|$) is accomplished by using an 1.1 pF distributed capacitor, that is formed by a 4 mm × 1.5 mm plate located 0.1 mm below the open end of the PIFA, in between the ground plane and the PIFA. The 1.1 pF distributed capacitor is used in addition to a 5 mm high 0.3 cm^3 PIFA located on a 40 mm × 100 mm

ground plane. One drawback is the increased complexity and hence the price of the antenna system.

The shown PIFA are not fully optimised with respect to the occupied volume or frequency, nor is any other components or any cover included. Thus for practical use both the shape of the antenna and the shape of the distributed capacitor should be carefully chosen in order to get the best frequency bandwidth and efficiency performance for a given application.

1.5 Acknowledgements

This work has been supported by Nokia Denmark.

1.6 References

1. R.F. Harrington, "Effect of antenna size on gain, bandwidth and efficiency," *Journal of research of national bureau of standards, D-radio Propagation*, vol. 64D, pp. 1-12, Jan 1960.
2. G. Hall (ed.), "The ARRL antenna book", 15th Edition, Third printing, Chap. 7, ISBN 0-87259-206-5, 1990.
3. "The IEEE standard definitions of terms for antennas," *IEEE Trans. Antennas Propagation*, vol. 17, May 1969.
4. R.C. Hansen, "Fundamental limitations in antennas," *Proc. IEEE*, vol. 69, Feb. 1981.
5. H. A. Wheeler, "The wide-band matching area for a small antenna," *IEEE Trans. Antennas Propagation*, vol. 31, pp. 364–367, Mar. 1983.
6. L.J. Chu, "Physical limitations of omnidirectional antennas," *J. App. Phys*., vol. 19, pp. 1163-1175, Dec. 1948.
7. J.S. McLean, "A re-examination of the fundamental limits on radiation Q of electrically small antennas," *IEEE Trans. AP*, vol. 44, pp. 672-675, May 1996.
8. H.A. Wheeler, "Fundamental limitations of small antennas," *Proc. IRE*, vol. 35, pp. 1163-1175, Dec. 1947.
9. C. W. Harrington, " Monopole with Inductive Loading", *IEEE Trans. Antennas Propagation*, pp. 394–400, Jul 1963.
10. G. S. Smith, "Efficiency of electrically small antennas combined with matching networks," *IEEE Trans. Antennas Propagation*, vol. AP-25, pp. 369–373, May 1977.
11. R. E. Collin, "Antennas and radiowave propagation", McGraw-Hill, ISBN 0-07-011808-6, pp. 97-104, 1985.
12. www.satimo.com.
13. www.zeland.com.
14. J. Appel-Hansen, "Antenna measurements," Ch. 8 in A.W. Rudge (Ed.) "The handbook of antenna design", *Peter Pelegrinus Ltd*, 1982.
15. J. Thaysen and K.B. Jakobsen, "Size reduction technique for mobile phone PIFA antennas using lumped inductors", submitted 2005.

Paper X

One turn stub loaded loop patch antenna on a small ground plane

Authors

Jesper Thaysen

Nokia Denmark, DK-1790 København, DENMARK
Technical University of Denmark DK-2800 Kgs. Lyngby, DENMARK

Kaj B. Jakobsen

Technical University of Denmark DK-2800 Kgs. Lyngby, DENMARK

Paper published

Microwave and optical technology letters

J. Thaysen and K.B. Jakobsen, "One turn stub loaded loop patch antenna on a small ground plane",
Microwave Opt Technol Lett., vol. 45 (2), pp. 126-128, 2005.

1 One Turn Stub Loaded Loop Patch Antenna on a Small Ground Plane

Jesper Thaysen
Nokia Denmark, www.nokia.com, DK-1790 Kbh V, DENMARK
Email: jesper.thaysen@nokia.com

Kaj B. Jakobsen

Technical University of Denmark, www.dtu.dk, DK-2800 Kgs. Lyngby, DENMARK
Email: kbj@oersted.dtu.dk

A small 1.1 cm^3 one-turn loop patch antenna located 2.5 mm above an 18 mm × 25 mm ground plane separated by a dielectric substrate with a relative permittivity of 9.8 is presented. By length variation of a thin quarter of a wavelength matching line it is possible to chance the resonant frequency. An RLC circuit model is used to determine the minimum Q. It is shown, that the proposed loop yield bandwidth performance close to the theoretical limit. The antenna has a 14.5% bandwidth at the resonant frequency of 2.04 GHz.

Key Terms—Balanced, Loop, Ground plane.

1.1 Introduction

The technique of incorporating a ground plane on a one turn loop for improvement of performance has been published [1]. This makes the loop into a microstrip patch antenna, which lowers the resonant frequency of the loop, and thus reduces the required antenna size for a fixed operating frequency. However owing to the antenna size reduction, the antenna bandwidth is also decreased. In this Letter we demonstrate that a wideband, small microstrip antenna with omni directional radiation patterns can easily be implemented by loading the antenna with a quarter wavelength open matching line in addition to the high permittivity substrate layer [2,3]. The antenna is designed with size as one of the driving parameters; therefore the obtained bandwidth is compared to the theoretical obtainable based on the Q values for the antenna. Many authors have dealt with minimum Q values for small antennas, recently reviewed by Thiele [4].

1.2 Materials and methods

Fig. 1 shows the proposed configuration that consists of a single turn balanced loop antenna, i.e., a metallic conductor bent into the shape of a closed curve, with a gap in the conductor to form the terminals. The loop antenna is in its basic form an antenna element placed on a dielectric substrate. The substrate used is an 18 mm × 25 mm piece of ceramic material with a thickness of 2.5 mm, a relative permittivity of 9.8 and a loss tangent of 0.002. A metal layer to form a ground plane covers the back.

The layout that is illustrated in Fig. 1 also shows an open circuited matching line that is used to insure proper impedance match. The length of the 0.3 mm narrow matching line is a quarter of a wavelength and is placed almost at the feeding point of the loop antenna. The loop

antenna is a balanced structure, thus a balanced feed is required. This is accomplished by the use of chip balun, not shown, however various other types could be used, e.g., [5].

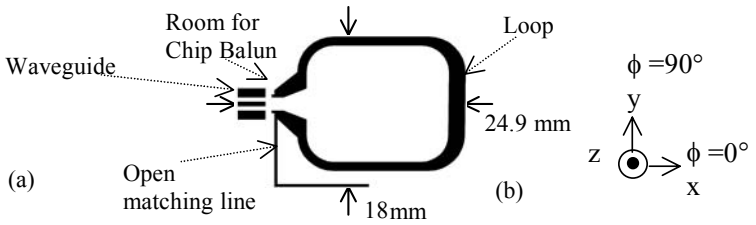

Fig. 1. The loop antenna including the coplanar waveguide connection for the balun (a) the used spherical coordinate system (b).

The perimeter of the one-wavelength loop placed on a substrate is found to approximately 63 mm at the design frequency of 2.05 GHz [3].

Using an RLC circuit model as in [4], the theoretical maximum bandwidth (BW) can be calculated as a function of the Return Loss (*RL*) and the Q of the antenna.

1.3 Results

The influence of changing the length of the matching line was simulated using IE3D [6] and the results are showed in Fig. 2. With a matching line length of 18.5 mm the resonant frequency is 2.04 GHz with a minimum in *RL* of 14 dB. The bandwidth within which the *RL* is better than 6 dB, hereafter just bandwidth, is 14.5 %. The impedance curve in the Smith chart is located around the centre of the chart, can be seen in Fig. 3 as the centre curve.

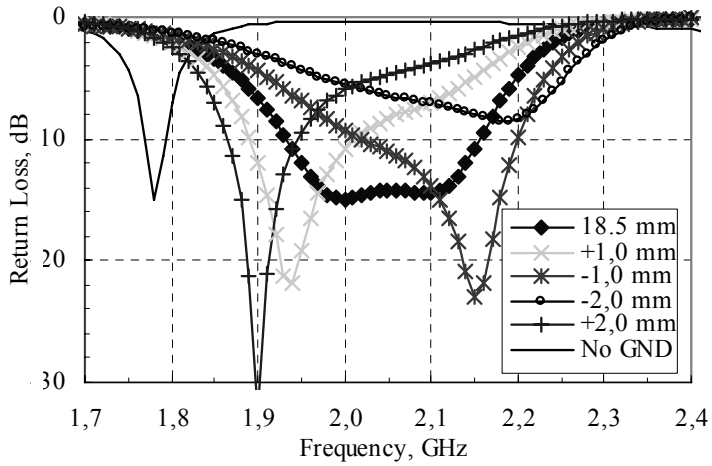

Fig. 2. Return Loss for a variation of the matching transmission line length of 0, ±1, and ±2 mm, around 18.5 mm.

Increasing the length of the matching line length by one millimetre decreases the resonant frequency to 2.0 GHz, with a *RL* = 21.7 dB and the *BW* =13.5%. A further increase by one

millimetre yields a resonant frequency of 1.92 GHz, a *RL* = 32.0 dB, and *BW* = 8.3 %, as also shown in the Smith chart (□).

By decreasing the matching line by one millimetre an increase of the resonant frequency to 2.08 GHz is observed from fig. 2., here, the *RL is* 23 dB and *BW*=14%. A further decrease of the length by one millimetre yields a resonant frequency of 2.13 GHz, the *RL*= 8.5 dB and the *BW*=10.3%, also shown as the lower loop in the Smith chart (◇).

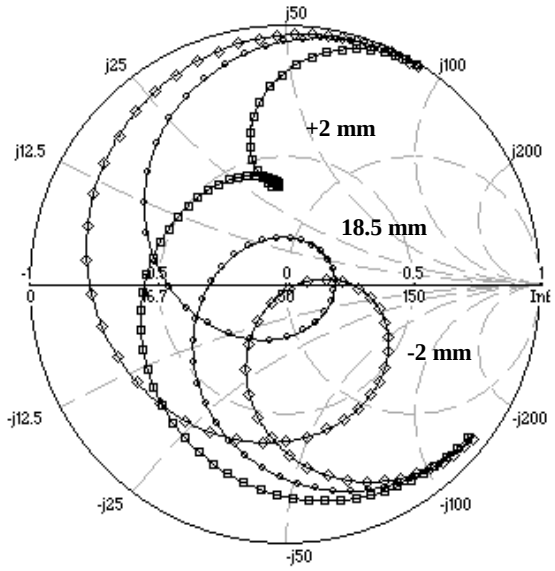

Fig. 3. Impedance curves for variation of the matching transmission line length by ±2 mm around 18.5 mm.

For comparison the bandwidth of the loop antenna without a ground plane is simulated to 2.6 % at a resonant frequency of 1.78 GHz with a minimum in Return Loss of 15 dB.

In Fig. 4, the simulated (×) and theoretical bandwidth as a function of the *RL* (solid line) are shown. The theoretical bandwidth at *RL* of 3dB is 20.6%, being two percent point higher than the simulated result. At *RL*=4dB the two curves intersect. The maximum deviation is obtained at *RL*=10 dB, where, the simulated bandwidth is 10.9%, i.e., 3.1% above the theoretical bandwidth limit.

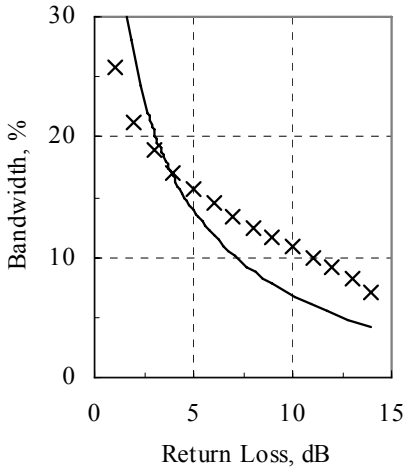

Fig. 4. Theoretical (solid) and simulated (×) bandwidth versus the Return Loss (b).

The total electrical field components of the simulated radiation patterns at a frequency of 2.05 GHz are shown in Fig. 4 in a conventional (r, θ, ϕ) spherical coordinate system. Fig. 5(a) shows θ-cuts for ϕ_0 = 0° and ϕ_0 = 90°, respectively. The patterns are almost rotationally symmetric around θ = 0° (180°). The ϕ-cut is shown in Fig. 5(b) for θ = 60° instead of θ = 90°, since there is no radiation in this plane.

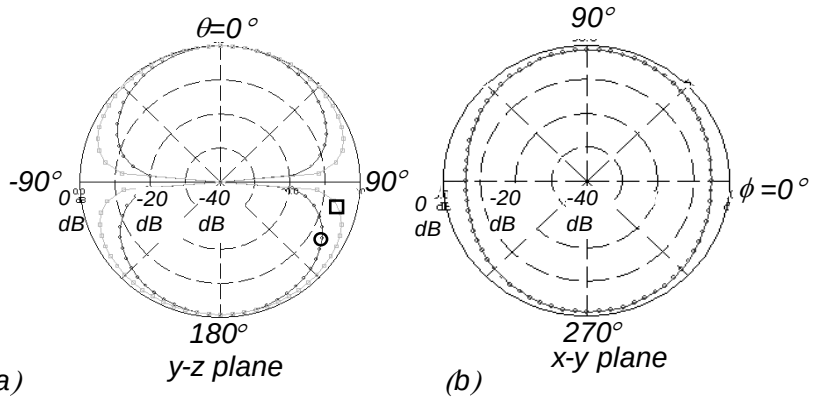

Fig. 5. Simulated θ-cuts for ϕ_0 = 0° (○) and 90° (□) at 2.05 GHz (a). Simulated ϕ-cut for θ = 60° at 2.05 GHz (b). Notice that since there is no radiation in the θ = 90° direction the direction θ = 60° is shown instead.

1.4 Discussion

By adding a ground plane to the loop, and thus transforming the loop antenna into a patch antenna, the bandwidth is improved. The best case with respect to bandwidth is obtained when the matching line is 18.5 mm. Here the resonant frequency is 2.04 GHz, the *RL*=14 dB and the *BW*=14.5 %. At the resonant frequency, the matching line acts as a quarter wavelength line. In order to minimise the influence from the matching line on the radiation pattern from the loop, the matching line was made very thin. Then the influence on the radiation pattern from the

matching line becomes insignificant, and the pattern predominantly originates from the loop, which means omni azimuth. Otherwise the matching line becomes an antenna itself.

The simulated relationship between the bandwidth versus Return Loss differs with a few percent from the theoretical result, but follows a somewhat similar decreasing trend. One reason for the deviation obtained is due to the simple RLC circuit model used, lossless environments are assumed. The simulated results include lossy dielectric material as well as metal loss. However, the obtained result indicates that the suggested antenna has a performance that is close to the highest possible expected from the RLC circuit model principle.

Almost symmetrically radiation in both front and back direction is obtained, meaning that the ground plane actually is a part of the structure and not acts as a reflector.

The shape of the loop antenna element is optimised and the matching line is bend in order to minimise the occupied area. This, also, increases the conducting material inside the minimum sphere, which lowers the Q value and thus optimises the bandwidth. For practical use both the shape of the loop and the length of the matching line should be carefully chosen in order to get the best frequency (bandwidth) performance for a given application.

1.5 Conclusion

A small 1.1 cm3 one-turn loop patch antenna located 2.5 mm above an 18 mm $\times$ 25 mm ground plane separated by a dielectric substrate with a relative permittivity of 9.8 is presented. The shown loop antenna has a 14.5 % bandwidth at a resonant frequency of 2.04 GHz. Using the RLC circuit theory it is shown that the proposed loop antenna has bandwidth performances that approaches the theoretical limit.

1.6 References

[1] C. A. Balinis, "*Antenna theory analysis and design,*" John Wiley & Sons inc., Second edition, 1997.

[2] E. E. Altshuler, "*A monopole loaded with a loop antenna,*" IEEE Trans. Antennas Propagat., 44 (6), pp. 787 -791, 1996 .

[3] J.-F Zurcher, and F. E. Gardiol, " *Broadband patch antennas,*" Artech House Publishers, 1995.

[4] G. A. Thiele, P. L Detweiler, and P. P. Penno, *"On the lower bound of the radiation Q for electrically small antennas",* IEEE, Trans. Antennas Propagat., 51 (6), pp 1263-1269, 2003.

[5] J.Thaysen, K. B Jakobsen, and J.Appel-Hansen, "*A wideband balun - how does it work?*", Applied microwave and wireless communication, Vol. 12, No 10, pp. 40-50, 2000.

[6] "*IE3D User's Manual, Release 8*", www.zeeland.com.